DISSERTATION

SPATIAL STATISTICAL ANALYSIS OF SOIL PROPERTIES AND CROP YIELDS FOR PRECISION AGRICULTURE APPLICATIONS

Submitted by

William J. Gangloff

Department of Soil and Crop Sciences

In partial fulfillment of the requirements

For the Degree of Doctor of Philosophy

Colorado State University

Fort Collins, Colorado

Spring 2004

COLORADO STATE UNIVERSITY

January 5, 2004

WE HEREBY RECOMMEND THAT THE DISSERTATION PREPARED UNDER OUR SUPERVISION BY WILLIAM J. GANGLOFF ENTITLED SPATIAL STATISTICAL ANALYSIS OF SOIL PROPERTIES AND CROP YIELDS FOR PRECISION AGRICULTURE APPLICATIONS BE ACCEPTED AS FULFILLING IN PART REQUIREMENTS FOR THE DEGREE OF DOCTOR OF PHILOSOPHY.

Committee on Graduate Work

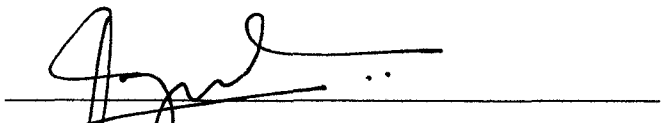

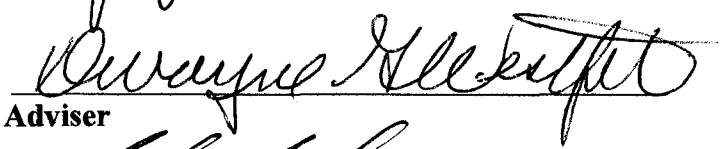

Adviser

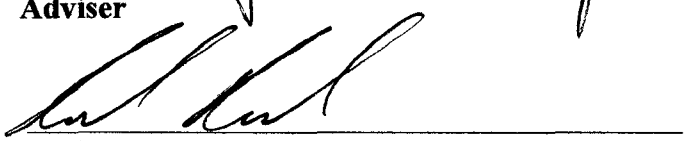

Co-Adviser

Department Head

ABSTRACT OF DISSERTATION

SPATIAL STATISTICAL ANALYSIS OF SOIL PROPERTIES AND CROP YIELDS FOR PRECISION AGRICULTURE APPLICATIONS

Soil properties, as well as many natural resource properties, vary continuously in space. Geostatistical techniques attempt to quantify and predict the variation of these spatial properties. Geostatistics and the theory of "regionalized variables" utilizes the fact that properties in space tend to display spatial structure and spatial dependence. Once the underlying spatial dependence is quantified, geostatistical techniques are used to interpolate or estimate a continuous 'surface' of the property of interest. Recent advances in global positioning systems and geographic information systems for agriculture have resulted in the rapid development of research initiatives in the area of spatial statistics applied to agricultural systems with the ultimate goal of implementing precision farming technologies.

The objective of this study was to examine several spatial sampling and spatial interpolation techniques related to precision farming technologies. This dissertation is composed of five chapters. The common theme throughout this study is the necessity of capturing the spatial dependence of the soil parameter of interest. Capturing spatial dependence is the key to properly interpolating soil properties and ultimately to improving precision farming technologies. Chapter 1 is a general introduction to spatial interpolation techniques for natural resources data.

The objective of chapter 2 was to evaluate an alternative procedure for principal component kriging designed to benefit from the utilization of a spatial correlation matrix. Principle component kriging has been purported to take advantage of the orthogonality of principal components. The assumed benefit of principal component kriging is that computational effort is reduced by kriging *n* principal components as opposed to cokriging *n* variables. My hypothesis was that principal components constructed with a spatial correlation matrix are more effective than 'linear' principal components for kriging purposes because kriging is an inherently spatial interpolation technique. The spatial correlation matrix was constructed with a modified Moran's *I* statistic. The goodness-of-fit statistics ranged from 0.771 to 0.965 and correlations from back-transformation ranged from 0.790 to 0.986. Based on the goodness-of-fit statistic and back-transformation results, both techniques were equally effective for principal component kriging.

The objective of chapter 3 was to examine an alternative spatial analysis tool called the cumulative correlogram that is useful for understanding the underlying spatial patterns of soil properties. My hypothesis was that cumulative correlograms would be more useful than standard correlograms or variograms because cumulative correlograms can elucidate the maximum scale-of-pattern of a soil parameter. In most soil sampling situations, the scales-of-pattern associated with soil parameters occur at separation distances much smaller than the separation distances observed with a typical grid sampling approach. Kriging models for grid-sampled soil parameters performed poorly based on goodness-of-fit statistics. Evaluation of point autocorrelation coefficients and cumulative correlograms indicated that two factors contribute to the poor performance of

the kriging models: anomalous characteristics present in the grid-sampled data sets, and, large separation distances among grid samples.

The objective of chapter 4 was to develop an alternative sampling approach designed to capture small scale variability of soil parameters. My hypothesis was that utilizing a cluster sampling approach as well as auxiliary data layers would be a more effective sampling approach because small scale variation would be present data sets. The design utilizes auxiliary data layers and an alternative cluster-sampling approach to data collection. The new, alternative sampling design is compared to a traditional grid-sampling design. The cluster-sampling design improved all parameter estimates; the grid-sampling design improved one parameter. Average improvement for the cluster-sampling was 34% (minimum = 1%, and maximum =72%). Bias estimates from the cluster-sampling design were small and estimates of root mean squared error suggest the cluster-sampling design is a better predictor of small-scale variation when compared to the grid-sampling design.

Recent research has focused on delineating field-specific soil-productivity management zones to be used as prescription, fertilizer application maps for variable rate application technologies. The objective of chapter 5 was to analyze four techniques for delineating soil-productivity management zones. Each of the methods uses a unique set of soils, yield, and or remotely sensed data. My hypothesis was that management zone techniques that utilize soils data at the outset of the delineation procedure would be more effective than techniques that fail to utilize soils data. Analysis of variance for the majority of yields among management zones indicated yields among management zones were different. A non-parametric analysis of crop yields also provided evidence to

conclude that management zone delineation techniques resulted in yield patterns that were different from random yield patterns. Overall, delineation techniques that combined secondary soils information and soil-sample analysis results were the most effective techniques.

William J. Gangloff
Department of Soil and Crop Sciences
Colorado State University
Fort Collins, CO 80523
Spring 2004

DEDICATION

For Dad, Mom, Jeanne, and Chris

ACKNOWLEDGEMENTS

I could not have completed this work without the dedicated assistance of my advisors. Drs. Dwayne Westfall and Robin Reich were always there for me and I will always be grateful for their guidance. I would also like to thank Drs. Raj Khosla and Gary Peterson for their assistance in completing my work. I was very lucky to have such an outstanding graduate committee. Finally, I would like to thank my family. They always told me I could do whatever I wanted. They always supported my decisions even if they did not completely understand them. I could not have completed this without them.

TABLE OF CONTENTS

LIST OF TABLES

LIST OF FIGURES

1 Introduction to Spatial Interpolation Techniques for Natural Resources

1.1 Introduction

Soil properties, as well as many other natural resource properties, vary continuously in space. Geostatistical techniques attempt to quantify, predict, and explain the variation of these spatial properties. This introductory chapter presents a basic summary of some of the primary, underlying assumptions essential for the proper application of geostatistics. Many of the techniques described in this chapter are referenced throughout this dissertation.

Geostatistics and the theory of "regionalized variables" utilizes the fact that properties in space tend to display spatial structure and spatial dependence. Once the underlying spatial dependence is quantified, geostatistical techniques are used to interpolate or estimate a continuous 'surface' of the property of interest. A regionalized variable is a variable that is distributed in space (Journel and Huijbregts, 1978). Examples of regionalized variables include: soil properties, crop yield, topographic elevation, and precipitation. The value of a regionalized variable at any place on the earth's surface is a function of its spatial position (Webster and Oliver, 1990).

Classical statistical procedures assume data are independent and display no spatial dependence. This assumption is not always true with natural systems. Natural systems usually display systematic or periodic variations in time or space (i.e. spatial dependency). This is particularly true with soil systems where continuous landscapes develop due to parent material, climate, and biological factors. The result is a system

where samples separated by small distances are more similar than samples separated by large distances. There are two major components of geostatistics:

1. The first component is the modeling of spatial correlation with variograms.
2. The second component of geostatistics is focused on estimating variable values at unsampled locations with techniques such as kriging or cokriging.

1.2 Variogram

The foundation of geostatistics is based on Matheron's (1963) theory of regionalized variables. Geostatistics was originally developed to estimate ore-reserves but has been used in disciplines such as engineering, mathematics, natural resources, and soil science. The basic premise of the regionalized variable theory is that a given variable is distributed in space, and the variable values are a function of position in space. The variogram is one of the core tools used in geostatistics. Variograms express the variation and spatial continuity among data points as a function of the distance separating them. The variogram measures the average dissimilarity among data points separated by some distance h and can be estimated from sample data (Goovaerts, 1997):

$$\gamma(h) = \frac{1}{2N(h)} \sum_{i=1}^{N(h)} [Z(x) - Z(x+h)]^2 \qquad [1.1]$$

where $Z(x)$ is the sample value of variable Z at position x, $Z(x+h)$ is the sample value of variable Z at position $x+h$, and $N(h)$ is the number of pairs of observations separated by distance h. The plot of $\gamma(h)$ versus h is called the variogram.

The variogram, $\gamma(h)$, is equal to zero when $h = 0$. However, when h is very small $\gamma(h)$ often displays a discontinuous increase in value. This is called the nugget effect, C_0.

The nugget effect represents factors such as sampling error and short range variability that can not be captured with standard sampling procedures. As h increases, $\gamma(h)$ (i.e. variance) increases due to decreasing dependence among points (Lascano and Hatfield, 1992). Typically, $\gamma(h)$ will approach a value at some distance, a, after which it will remain approximately constant. Once a is reached, $\gamma(h)$ is the variance of the data set and is called the sill, C_a. The value $h = a$ is called the range and represents the maximum distance for correlation among samples. Samples collected at distances greater than the range are spatially independent (Vieira et al., 1981; Nielsen and Alemi, 1989).

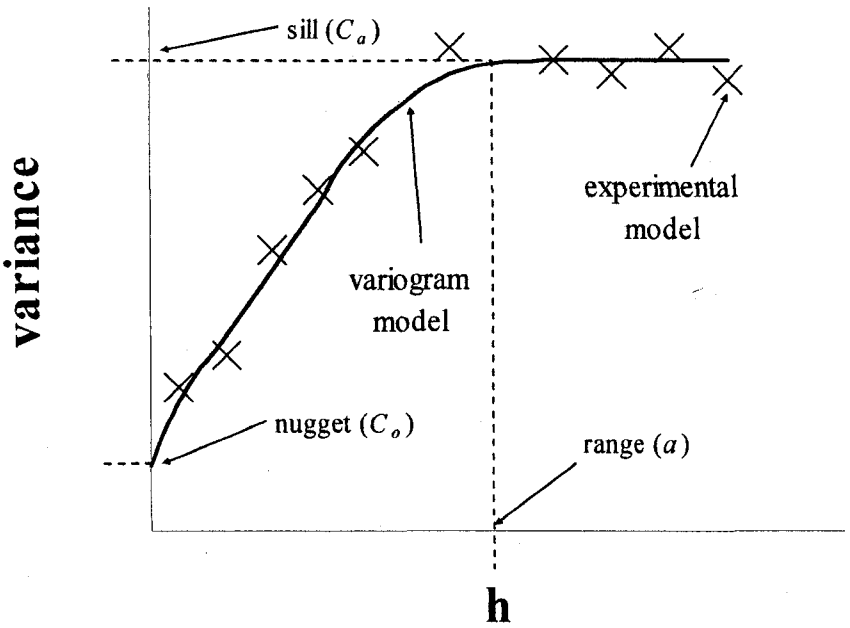

Figure 1.1 Example of a sample variogram. The solid line represents a model fitted to the sample data.

The accuracy of the variogram calculation is proportional to the number of data points available. Hohn (1998) and Olea (1994) give three rules to ensure proper variogram estimation:

1. For each computed value of the variogram the number of pairs should be greater than 30.
2. The region of interest on the fitted variogram model is the positively sloped section of the graph (i.e. from h=0 to h=a). This region should be represented by three to four values. This region indicates the degree of spatial dependence of samples separated by small sample distances. In contrast, samples separated by large distances typically make-up the region of graph where the model reaches an asymptote (i.e. h>a) indicating spatial independence.
3. The maximum lag should be limited to one-half of the extreme distance in the sampling area. Lag is defined as the separation distance among soil samples to be considered in the calculation of the variogram value.

The discussion of variograms to this point has focused on correlation independent of orientation or direction (i.e. isotropic or omnidirectional variograms). However, it is possible for correlation to vary with direction (i.e. anisotropy). In cases of anisotropy, directional variograms can be computed. Details of this procedure can be found in Isaaks and Srivastava (1989) and Reich (2000). There are two types of anisotropy: geometric and zonal anisotropy. Geometric anisotropy occurs when the sills of the variograms are the same in all directions, but the ranges are different. Zonal anisotropy occurs when the ranges of the variograms are the same in all directions, but the sills are different.

Cross-variograms can also be computed when using multivariate data. The cross-variogram measures how pairs of variables vary jointly over separation distance h. The cross-variogram can be estimated as:

$$\gamma_{zw}(h) = \frac{1}{2N(h)} \sum_{i,j=1}^{N(h)} \left[Z(x_i) - Z(x_i + h) \right] \cdot \left[w(x_j) + w(x_j + h) \right] \right] \qquad [1.2]$$

where $\gamma_{zw}(h)$ is the cross-variogram value for the dependent variable z and the secondary variable w separated by distance h; $w(x_j)$ is the sample value of the variable w at location x_j; and, $w(x_j + h)$ is the sample value of the variable w at location $x_j + h$. When dealing with several variables, each variable (the variable of interest, and the auxiliary variables) is characterized by its own variogram, and each pair of the variables is characterized by its cross-variogram.

The regionalized variable theory assumes stationarity of the data. This means that the expected value at a given location is equal to an overall mean, that does not depend on spatial location, plus a random spatially correlated variation, which is quantified by the variogram. It can be shown that for the rule of stationarity to apply:

$$\lim_{h \to \infty} \frac{\gamma(h)}{|h|^2} = 0 \qquad [1.3]$$

This result suggests that if $\gamma(h)$ increases more rapidly than h^2, the variable is nonstationary, and a trend exists (Armstrong, 1998).

Several mathematical models can be fit to variograms and cross-variograms to obtain the weights used in kriging and cokriging models. The following notation will be used to describe three of the more common variogram models (Isaaks and Srivastava, 1989): h is the lag distance, a is the range, C_0 is the nugget effect, $C_0 + C_1$ is the sill, and $\gamma(h)$ is the variogram value at lag h.

Gaussian model:

$$\gamma(h) = C_0 + C_1 \cdot \left[1 - \exp\left(-\frac{3h^2}{a^2}\right)\right] \qquad [1.4]$$

The Gaussian model is commonly used to model continuous data. The model reaches its sill asymptotically and the practical range is defined as the distance where the variogram model is 95% of the sill (Hunner, 2000).

Spherical model:

$$\gamma(h) = C_0 + C_1 \cdot \begin{cases} 1.5 \cdot \frac{h}{a} - 0.5 \cdot \left(\frac{h}{a}\right)^3 & \text{if } h \le a \\ C_0 + C_1 & \text{otherwise} \end{cases} \qquad [1.5]$$

The spherical model is the most commonly used variogram model (Hunner, 2000).

Exponential model:

$$\gamma(h) = C_0 + C_1 \cdot \left[1 - \exp\left(-\frac{3h}{a}\right)\right] \qquad [1.6]$$

The exponential model reaches its sill asymptotically. The practical range is defined as the distance where the variogram value is 95% of the sill.

Power model:

$$\gamma(h) = C_0 + C_1 \cdot h^{\alpha} \qquad [1.7]$$

with $0 < \alpha < 2$. The linear model with $\alpha = 1$ is a special case of the power model. The power model does not reach a sill, but increases proportionally to h.

Variogram models can be divided into two groups: bounded and unbounded models. Bounded models (or transitional models) have a sill. The spherical, exponential, and Gaussian variogram models are examples of bounded models. Unbounded models (or non-transition models) do not have a sill. The linear model is an unbounded model.

Regionalized variables that meet the requirement of stationarity will have bounded variogram models. Unbounded variograms models result from variables that are non-stationary (Armstrong, 1998).

1.3 Ordinary Kriging

Kriging was developed by the South African mining engineer Danie G. Krige and the French mathemetician Georges Matheron. However, most credit for the development of kriging is given to Matheron. Matheron developed the theory of regionalized variables which laid the foundation of geostatistics and led to the spatial estimation technique known as kriging (Hunner, 2000). Kriging is a spatial statistical (or geostatistical) estimation technique that is used to estimate, or interpolate values of a variable at unsampled locations in space. Originally, kriging was primarily used in the mining industry but it has since been used by various disciplines including soil science and agronomy (Burgess and Webster, 1980a,b; Goovaerts and Journel, 1995).

Ordinary Kriging (OK) is a simple application of the regionalized variable theory for estimating values at unsampled locations. Kriging techniques are often called best linear unbiased estimators (BLUE). Kriging is a linear interpolation method where the prediction Z^*_{OK} at any location x_0 is assumed to be a linear combination of the known values Z already measured at other locations x_i. This relationship can be expressed mathematically as (Nielsen and Alemi, 1989; Gotway et al., 1996):

$$Z^*_{OK}(x_0) = \sum_{i=1}^{n} \lambda_i \cdot Z(x_i) \qquad [1.8]$$

The weights, λ_i, are estimated from the variogram (Eq. 1.1) and selected in such a way that the expected value and variance of $[Z^*_{OK}(x_0) - Z(x_0)]$ are zero and minimum,

respectively (Nielsen and Alemi, 1989). To ensure that kriged estimates are unbiased, the sum of the weights (λ_i) must be equal to one:

$$\sum_{i=1}^{n} \lambda_i = 1 \qquad [1.9]$$

The OK variance is estimated as (Isaaks and Srivastava, 1989):

$$\sigma_{OK}^2 = C(x_0, x_0) - \sum_{i=1}^{n} \lambda_i \cdot C(x_i, x_0) + \mu \qquad [1.10]$$

where $C(x_0,x_0)$ is the covariance of the point to estimate at location x_0 with itself; $C(x_i,x_0)$ is the covariance of the sample point at location x_i and the point to be estimated at location x_0; λ_i is weight for sample point i at location x_i; n is the number of sample points; and μ is a Lagrange parameter used to convert the original constrained minimization problem into an unconstrained problem.

The regionalized variable theory assumes stationarity of the data, meaning the variogram is a function that depends only on separation distance between pairs of observations (Gotway and Hergert, 1997). However, in many natural settings, this assumption is violated and underlying trends exist in the data. Several techniques can be used to remove trends from spatial data. One method involves subtracting an analytical function, such as a polynomial, from the sample data (Olea, 1994). Another common technique to remove underlying trends is universal kriging, or kriging with a trend. This technique takes account of local trends in the data associated with estimation (Goovaerts, 1997; Journel and Rossi, 1989). Modified residual kriging (MRK) is a third technique used to remove underlying trends from a spatial set. The first step in MRK is modeling the spatial data with a simple regression model of the form:

$$Var = f(x, y, z_1, ..., z_p) \quad [1.11]$$

where *Var* is the variable of interest, x and y represent locations in space, and $z_1, ..., z_p$ represent additional useful variables for modeling *Var*. The first step in MRK describes large-scale variability, or large-scale trends in the data. The second step in MRK is analyzing and modeling the residuals from the regression model. Modeling the residuals is only necessary if the residuals display significant spatial autocorrelation. The residuals are typically modeled with variogram models but other techniques such as binary regression tree analysis can also be used. If the residuals from the regression model do not display significant spatial autocorrelation then residual modeling is not necessary. The second step in MRK describes small-scale variability, or small-scale trends in the data.

1.4 Cokriging

Cokriging (CK) utilizes multivariate information to determine estimates at unsampled locations (Hunner, 2000). The premise of CK is that estimation can be improved by incorporating additional information from correlated secondary variables. The CK technique is most useful when the variable of interest is expensive or difficult to sample compared to an easily sampled secondary variable. Cokriging is an unbiased estimation technique that minimizes the variance of estimation errors by using information from the spatial cross-correlation between the variable of interest and a set of secondary variables. Similar to OK, CK assumes stationarity of primary and secondary variables. The CK estimate, $Z^*_{CK}(x_0)$, at a location is expressed as:

$$Z^*_{CK}(x_0) = \sum_{i=1}^{n} \lambda_i^Z \cdot Z(x_i) + \sum_{j=1}^{m} \lambda_j^W \cdot W(x_j) \qquad [1.12]$$

Where λ_i^Z and λ_j^W are weights for the primary and secondary variables, respectively, and $Z(x_i)$ and $W(x_j)$ are sample values for the primary and secondary variables, respectively. Variogram models for the primary and each secondary variable, as well as cross-variograms for each combination of these variables are used to determine the estimation weights, (Hunner, 2000). Cokriging estimates are unbiased and the model is subject to the following linear constraints:

$$\sum_{i=1}^{n} \lambda_i^Z = 1 \quad \text{and} \quad \sum_{j=1}^{m} \lambda_i^W = 0 \qquad [1.13]$$

where λ_i^Z are the weights for the n data values of the primary variable Z, and λ_i^W are the weights for the m data values of the secondary variable W (Isaaks and Srivastava, 1989). The CK variance is estimated as:

$$\sigma^2_{CK}(x_0) = C^Z(x_0^Z, x_0^Z) + \mu_1 - \sum_{i=1}^{n} \lambda_i^Z \cdot C^Z(x_i^Z, x_0^Z) - \sum_{j=1}^{m} \lambda_j^W \cdot C^{WZ}(x_j^W, x_0^Z) \qquad [1.14]$$

where $C^Z(x_0^Z, x_0^Z)$ is the covariance of primary variable Z at unsampled location x_0 with itself; $C^Z(x_i^Z, x_0^Z)$ is the covariance of primary variable Z at location x_i and primary variable Z at unsampled location x_0; $C^{WZ}(x_j^W, x_0^Z)$ is the cross-covariance of secondary variable W at locations x_j and primary variable Z at unsampled locations x_0; λ_i^Z is the weight for primary variable Z at location x_i; λ_j^W is the weight for secondary variable W at location x_j; and, μ_1 is a Lagrange parameter used to convert the original constrained minimization problem into an unconstrained problem.

1.5 Summary and Conclusions

This introduction provides the basis for many of the spatial statistical techniques used to interpolate natural resource properties. Although most spatial statistical software packages have packaged these techniques, a basic understanding of the techniques and their underlying assumptions is necessary to properly apply them. It is particularly important to identify the underlying spatial dependence of samples. Spatial dependence is at the core of most of the geostatistical techniques used to interpolate or estimate a continuous 'surface' of the property of interest.

1.6 References

Armstrong, M. 1998. Basic linear geostatistics. Springer, New York.

Burgess, T.M., and R. Webster. 1980a. Optimal interpolation and isarithmic mapping of soil properties I: the semivariogram and punctual kriging. J. Soil Sci. 31: 315-331.

Burgess, T.M., and R. Webster. 1980b. Optimal interpolation and isarithmic mapping of soil properties II: block kriging. J. Soil Sci. 31: 333-341.

Goovaerts, P. 1997. Geostatistics for natural resources evaluation. Oxford University Press, New York.

Goovaerts, P., and A.G. Journel. 1995. Integrating soil map information in modeling the spatial variation in continuous soil properties. Eur. J. Soil Sci. 46: 397-414.

Gotway, C.A., and G.W. Hergert. 1997. Incorporating spatial trends and anisotropy in geostatistical mapping of soil properties. Soil Sci. Soc. Am. J. 61:298-309.

Gotway, C.A., R.B. Ferguson, G.W. Hergert, and T.A. Peterson. 1996. Comparison of kriging and inverse distance methods for mapping soil parameters. Soil Sci. Soc. Am. J. 60: 1237-1247.

Hohn, M.E. 1998. Geostatistics and Petroleum Geology. Kluwer Academic Publishers, Dordrecht, The Netherlands.

Hunner, G. 2000. Modeling forest stand structure using geostatistics, geographic systems, and remote sensing. Ph.D. diss. Colorado State Univ, Fort Collins, CO.

Isaaks, E.H., and R.M. Srivastava. 1989. An introduction to applied geostatistics. Oxford University Press, New York.

Journel, A.G., and C.J. Huijbregts. 1978. Mining geostatistics. Academic Press, London.

Journel, A.G., and M.E. Rossi. 1989. When do we need a trend model in kriging? Math. Geol. 21: 715-740.

Lascano, R.J., and J.L. Hatfield. 1992. Spatial variability of evaporation along two transects of a bare soil. Soil Sci. Soc. Am. J. 56:341-346.

Matheron, G. 1963. Principles of geostatistics. Econ. Geol. 53: 1246-1266.

Nielsen, D.R., and M.H. Alemi. 1989. Statistical opportunities for analyzing spatial and temporal heterogeneity of field soils. Plant Soil. 115: 285-296.

Olea, R.A. 1994. Fundamentals of semivariogram estimation, modeling and usage. *In* Yarus, J.M., and R.L. Chambers (ed.) Stochastic modeling and geostatistics: principles, methods, and case studies. American Association of Petroleum Geologists, Tulsa, OK.

Reich, R.M. 2000. Introduction to spatial statistical modeling of natural resources. University Text. Colorado State University. Fort Collins, CO.

Vieira, S.R., D.R. Nielsen, and J.W. Biggar. 1981. Spatial variability of field-measured infiltration. Soil Sci. Soc. Am. J. 45: 1040-1048.

Webster, R., and M.A. Oliver. 1990. Statistical methods in soil and land resource survey. Oxford University Press, New York.

2 Utilization of a Spatial Correlation Matrix in Principal Component Kriging

2.0 Abstract

Interpolation techniques for spatial statistics applied to agricultural systems include ordinary kriging, cokriging, and modified residual kriging. Another technique applied to multivariate data sets is principal component kriging. Principle component kriging has been purported to take advantage of the orthogonality of principal components. The assumed benefit of principal component kriging is that computational effort is reduced by kriging *n* principal components as opposed to cokriging *n* variables. The core of this assumption is that principal components maintain orthogonality at separation distances greater than 0. Previous researchers have concluded that this assumption often does not apply to spatial data-sets. Principal components are typically constructed with a linear correlation matrix. I tested the hypothesis that principal components constructed with a spatial correlation matrix are more effective than 'linear' principal components. The spatial correlation matrix was constructed with a modified Moran's *I* statistic. Soil from a 4.65 hectare agricultural field was sampled to a depth of 0.2 m on a non-aligned systematic grid and analyzed for 5 variables using standard, analytical procedures: Clay (%), phosphorus (P), pH, ammonium (NH_4-N), and Iron (Fe). Orthogonality of standard (PC) and spatial principal components (PS) was analyzed with cross-correlograms. The PC and PS were kriged and the effectiveness of the interpolation was tested with the goodness-of-fit statistic and with a back-transformation procedure. Neither the linear nor

the spatial approach resulted in orthogonal principal components. The goodness-of-fit statistics ranged from 0.771 to 0.965 and correlations from back-transformation ranged from 0.790 to 0.986. Based on the goodness-of-fit statistic and back-transformation results, both techniques were equally effective for principal component kriging.

2.1 Introduction

Recent advances in global positioning systems (GPS) and geographic information systems (GIS) for agriculture have resulted in the rapid development of research initiatives in the area of spatial statistics applied to agricultural systems. This area of research often involves large multivariate data sets. Typical analyses involve interpolation techniques such as ordinary kriging (OK), cokriging (CK), or modified residual kriging (MRK) to estimate the value of a variable at unsampled locations. Another technique that has been applied to multivariate data sets is principal component kriging (PCK). Principle component kriging is a technique that is purported to take advantage of the orthogonality of principal components. The assumed benefit of principal component kriging is that computational effort can be reduced by kriging n principal components as opposed to cokriging n variables (Davis and Greenes, 1983).

Principal component analysis (PCA) is used to develop linear combinations of the original variables in a data set. Principal component analysis was first described by Pearson (1901). The objective of principal component analysis is to take p variables X_1, $X_2,...,X_p$ and find combinations of these to produce indices Z_1, $Z_2,...,Z_p$ that are uncorrelated (i.e. the indices are orthogonal) (Manly, 1998). This is useful because the resulting indices, or principal components, are measuring different 'dimensions' of the data (Manly, 1998). Another way to think of this is that the resulting indices contain

unique information and lack redundancy. Theoretically, PCA results in as many principal components as variables used in the analysis. However, only the first few principal components (i.e. indices) that explain most of the variance in the data are used beyond PCA (Ortega, 1997).

Principle component analysis is achieved by generating a correlation matrix (**C**) of the original p variables. By definition, the elements of the main diagonal of C will be 1.

$$\mathbf{C} = \begin{matrix} 1_{11} & c_{12}\cdots & c_{1p} \\ c_{21} & 1_{22}\cdots & c_{2p} \\ c_{p1} & c_{p2}\cdots & 1_{pp} \end{matrix} \qquad [2.1]$$

The eigenvector matrix (A) of C is then calculated and used to generate principal components by multiplying the original data matrix (D) by A:

$$\mathbf{D} = \begin{matrix} d_{11} & d_{12}\cdots & d_{1p} \\ d_{21} & d_{22}\cdots & d_{2p} \\ d_{31} & d_{32}\cdots & d_{3p} \\ d_{n1} & d_{n2}\cdots & d_{np} \end{matrix} \times \mathbf{A} = \begin{matrix} a_{11} & a_{12} & a_{1p} \\ a_{21} & a_{22} & a_{2p} \\ a_{p1} & a_{p2} & a_{pp} \end{matrix} = \mathbf{PC} = \begin{matrix} pc_{11} & pc_{12}\cdots & pc_{1p} \\ pc_{21} & pc_{22}\cdots & pc_{2p} \\ pc_{31} & pc_{32}\cdots & pc_{3p} \\ pc_{n1} & pc_{n2}\cdots & pc_{np} \end{matrix} \qquad [2.2]$$

The resulting PC matrix of values can be thought of as standardized linear combinations (i.e. principal components) of the original p variables. By definition the principal components are linearly orthogonal and the variance is maximized within each principal component vector (Goovaerts, 1997). The variances of the principal components are the eigenvalues (λ) of the matrix C:

$$\lambda = \begin{matrix} \lambda_{11} & 0 & 0 \\ 0 & \lambda_{22} & 0 \\ 0 & 0 & \lambda_{pp} \end{matrix} \qquad [2.3]$$

where $\lambda_{11} = \mathrm{Var}(PC_1)$, and $\mathrm{Var}(PC_1) > \mathrm{Var}(PC_2),\ldots,>\mathrm{Var}(PC_p)$.

An attractive feature of PCA is the ability to reduce the dimensionality of large data sets and remove the effects of correlated data. It is often the case that a data set with a large number of variables, p, can be mathematically summarized with the first few principal components. Another important feature of principal components is their ability to be 'back-transformed' to generate the original data set. Back-transformation is achieved by multiplying the **PC** matrix by the inverse of **A**. This is simply the reverse of the procedure to generate **PC** in Eq. 2.2.

$$\mathbf{PC} \times \mathbf{A}^{-1} = \mathbf{D} \qquad [2.4]$$

Principle component kriging is a technique that takes advantage of the orthogonality of principal components. The assumed benefit of principal component kriging is that computational effort can be reduced by kriging n principal components as opposed to cokriging n spatially correlated variables (Davis and Greenes, 1983). The core of this assumption is that principal components maintain orthogonality at separation distances greater than 0. However, principal components are constructed with a linear correlation matrix. By definition, the linear correlation matrix only estimates correlation at separation distances equal to zero (Goovaerts, 1993). Goovaerts (1993) concluded that this assumption often does not apply to spatial data sets. Spatial principal components remain orthogonal only if the correlation structure is the same for all spatial scales. This condition is rarely met with natural or biological data sets.

The spatial correlation matrix is constructed with a modified Moran's I statistic. The Moran's I statistic is analogous to a weighted correlation coefficient between possible pairs of n observations (z_i and z_j, $i \neq j$) (Czapleswski et al., 1994) and is defined as:

$$I = \left(\frac{\sum_{i=1}^{n} \sum_{j=1}^{n} w_{ij} z_i z_j}{W Var(z)} \right) \qquad [2.5]$$

where w_{ij} is a weight that quantifies the hypothesized spatial association or proximity between observations (z_i and z_j) at sites i and j, and $w_{ii}=0$; W is the sum of all n^2 values of w_{ij}; $Var(z)$ is the variance of the n observations; and observations are transformed to center on zero (i.e. sum of all z_i's equals zero). Moran's I is a dimensionless statistic that usually ranges from –1 to 1. Larger absolute values of Moran's I indicate a strong autocorrelation (i.e. positive or negative), while a value of zero indicates complete spatial independence among samples. The modified Moran's I statistic, herein referred to as the BiMoran's I statistic, is used to estimate spatial cross-correlation between two variables, y_i and z_i, observed at n locations:

$$I_{YZ} = \left(\frac{\sum_{i=1}^{n} \sum_{j=1}^{n} w_{ij} y_i z_j}{W \sqrt{Var(y) \cdot Var(z)}} \right) \qquad [2.6]$$

where w_{ij} is a scalar that quantifies the degree of spatial association between locations i and j; y_i is the observed value of the variable y transformed to have a mean of zero (i=1,2,…,n); z_i is the observed value of the variable z transformed to have a mean of zero (i=1,2,…,n); W is the sum of all n^2 values of w_{ij}; $Var(y)$ is the sample variance of y_i; and $Var(x)$ is the sample variance of z_i

The denominator of Eq. 2.6 makes I_{YZ} a dimensionless statistic that can be interpreted as a Pearson product moment correlation between variables y and z. One would expect I_{YZ} to range over the interval of –1 to 1, however, it can exceed these limits

for an irregular pattern of weights, or if extreme values are heavily weighted (Cliff and Ord, 1981).

Given a set of $n!$ equally likely random permutations of sample data, the expected value and variance of the cross-correlation statistic, I_{YZ} under the null hypothesis of no spatial correlation between two response variables, y_i and z_i, is given by:

$$E[I_{YZ}] = \frac{-Cov(yz)}{(n-1)\sqrt{Var(y)Var(z)}} = \frac{\rho_{YZ}}{n-1} \qquad [2.7]$$

$$Var(I_{YZ}) = \left(\begin{array}{l} \left(\frac{Cov(yz)n}{Var(y)Var(z)}\right)\left[2(W^2 - S_2 + S_1) + (\frac{S_1 - S_2}{2})(n-3) + \frac{S_1}{2}(n-2)(n-3)\right] \\ + \left(\frac{-m_{Y^2Z^2}}{Var(y)Var(z)}\right)\left[6(W^2 - S_2 + S_1) + (4S_1 - 2S_2)(n-3) + S_1(n-2)(n-3)\right] \\ + n\left[(W^2 - S_2 + S_1) + (\frac{S_1 - S_2}{2})(n-3) + \frac{S_1}{2}(n-2)(n-3)\right] \\ \hline (n-1)(n-2)(n-3)W^2 \end{array} \right) - \left(\frac{-\rho_{YZ}}{n-1}\right)^2 \qquad [2.8]$$

where

$$m_{Y\,Z^2} = \frac{\sum_{i=1}^{n} y_i^2 z_i^2}{n} \qquad [2.9]$$

$$S_1 = \sum_{i=1}^{n}\sum_{j=1}^{n} w_{ij}^2 \qquad [2.10]$$

$$S_2 = \sum_{i=1}^{n}\sum_{j=1}^{n}\sum_{i'=1}^{n} w_{ij} w_{ji'} \qquad [2.11]$$

and ρ_{yz} is the linear correlation between y_i and z_i.

Detailed derivations of these statistics are given in Czaplewski and Reich (1993). The authors indicate that for moderate sample sizes (n>40) it is sufficient to take $T = (I_{YZ} - E[I_{YZ}])/Var(I_{YZ})^{0.5}$ as a standard normal variate, where I_{YZ} is the observed cross-correlation statistic defined in Eq. 2.7. The null hypothesis of no spatial cross-correlation between two response variables is rejected when $|T| > z_{\alpha/2}$. A value of I_{YZ} significantly different from $E[I_{YZ}]$ would indicate a positive or negative spatial cross-correlation depending on the sign of the estimated linear correlation coefficient $\hat{\rho}_{YZ}$. I hypothesize that utilizing a spatial correlation matrix will improve principal component kriging when compared with principal component kriging which is based on a linear correlation matrix.

2.2 Materials and Methods

In 1998, soil from a 4.65 hectare (152 x 204 m), rectangular, agricultural field was sampled on a non-aligned systematic grid. The size of each grid cell was 0.023 ha (i.e. 15 x 15 m). Soils in the field included Valentine sand (sandy, mixed nonacid, mesic Typic Ustipsamment), a Bijou loamy sand (coarse loamy, mixed, mesic Mollic Haplargid), and a Truckton loamy sand (coarse loamy, mixed, mesic Udic Argiustoll). Geographical UTM coordinates were determined at each sample location with a differential GPS unit. Soil samples were collected from the 0 to 0.2 m surface zone at 198 locations and analyzed for 5 variables using standard, analytical procedures: Clay (%), phosphorus (P), pH, ammonium (NH_4-N), and Iron (Fe) (Miller et al., 1998).

Correlograms were constructed with the data from the soil samples. A total of 15 separation distances (i.e. bins) were used to construct the correlograms and the maximum separation distance used in the construction of correlograms was 150 m. The correlogram statistic is defined as:

$$\rho(I) = \left(\frac{\sum_{i=1}^{N(h)} \sum_{j=1}^{N(h)} w_{ij} z_i z_j}{WVar(z)} \right) \qquad [2.12]$$

where w_{ij} is a weight that quantifies the hypothesized spatial association or proximity between observations (z_i and z_j) at sites i and j (w_{ii}=0), W is the sum of all $N(h)^2$ values of w_{ij}, $Var(z)$ is the variance of the $N(h)^2$ observations, and observations are transformed to center on zero (i.e. sum of all z_i's equals zero). This equation puts a restriction on the calculation of $\rho(I)$ by the term $N(h)$. This restriction limits pairs of points used in the calculation of $\rho(I)$ to those pairs of points separated by distances within the interval $[a,b)$. The interval $[a,b)$ represents one of the 15 bins used to construct the correlogram and the lag distance $h \equiv b\text{-}a$. For example, bin number 1 covers those pairs of points separated by a distance of 0 to 10 m, and bin number 15 covers those pairs points separated by a distance of 140 to 150 m. In both bins, the lag distance h = 10 m. Final correlograms were constructed by plotting $\rho(I)$ versus separation distance.

Standard principal component analysis was performed on the data set to estimate principal component scores for each variable observation (PRINCOMP; S-PLUS©[1], Statistical Sciences, 1999). The analysis resulted in five principal components (PC_1,...,PC_5) each with 198 PC scores. The individual scores are analogous to a variable

[1] Mention of a trade name, proprietary product, or specific equipment does not constitute a guarantee, warranty, or endorsement by Colorado State University.

value at location x, y and the individual principal components are analogous to a variable name.

Spatial principal component analysis was performed by generating a spatial correlation matrix with the BiMoran's I (Eq. 2.6). Unlike a linear correlation matrix, the elements of the main diagonal of the spatial correlation matrix can differ from 1. Eigenvectors were then generated from the spatial correlation matrix with the EIGEN command in S-PLUS© (Statistical Sciences, 1999). The spatial principal component scores were then calculated by multiplying the original data set matrix by the eigenvector matrix. The analysis resulted in five spatial principal components (PS_1,...,PS_2) each with 198 PS scores.

Since one of the perceived benefits of PCA is orthogonality of the PC scores (i.e. absence of correlation among principal components), spatial cross-correlograms were constructed for all pairs of PC and PS scores. Spatial cross-correlograms summarize the spatial correlation between variables, or in this case principal components, at specific separation distances. Spatial cross-correlograms differ from standard cross-correlograms because they are constructed with the BiMoran's I. Standard cross-correlograms are constructed with the linear correlation statistic, ρ_{yz}, and do not account for spatial autocorrelation in the data.

Data were analyzed using the BiMoran's I to test the null hypothesis that the distribution of the data were spatially independent. The null hypothesis of no spatial cross-correlation was rejected when the p-value associated with the test statistic T, was less than 0.05. Spatial cross-correlation was estimated at 10 m intervals to a maximum 150 m (i.e. 15 lag intervals).

Standard and spatial principal component scores were used to generate empirical variograms. As explained in Chapter 1, variogram functions describe how spatial continuity or spatial interdependence among soil samples changes as a function of separation distance and direction. Gaussian, exponential, and spherical variogram models were fit to the empirical variograms using the Spatial Library developed by Reich and Davis (1998) in S-PLUS©. The optimum model was selected as the model that minimized the Akaike's Information Criteria (AIC) and optimum models were used to krig the principal component data using ordinary kriging (OK) (Akaike, 1977).

Kriged surfaces were cross-validated to determine the effectiveness of the models. Cross-validation involves deleting one observation from the data set and predicting the deleted observation using the remaining observations in the data set (PREDKRG; S-PLUS©, Reich and Davis, 1998). This process is repeated for all observations in the data set. Residuals are computed as the observed minus predicted values. The effectiveness of the model is determined with the goodness-of-prediction statistic (G) (Agterberg, 1984; Guisan and Zimmermann, 2000; Schloeder et al., 2001). The G-statistic is a measure of how effective a prediction might be relative to that which could have been derived by the sample mean and is defined as (Agterberg, 1984):

$$G = 1 - \left(\frac{\sum_{i=1}^{n} \left[Z_i - \hat{Z}_i \right]^2}{\sum_{i=1}^{n} \left[Zi - \overline{Z} \right]^2} \right) \qquad [2.13]$$

where Z_i is the observed value of the i^{th} observation, $\hat{Z}_i$ is the predicted value of the i^{th} observation, and $\overline{Z}$ is the sample mean. A G-statistic equal to 1 indicates perfect prediction, a positive value indicates that the model is more reliable than if one had used

the sample mean, a negative value indicates the model is less reliable than if one had used the sample mean, and a value of zero indicates that the model is equivalent to using the sample mean to estimate *Z*.

Finally, PC and PS values were back-transformed to generate original values for the variables clay, P, pH, NH_4-N, and Fe at each sampled location. Back-transformed values were compared with original variable values via correlation analysis.

2.3 Results and Discussion

Selected soil properties of the soil samples collected from the experimental sites are presented in Table 2.1. The context of this study was focused on the comparison of two techniques for kriging principal components and the discussion of raw soil parameters is limited to the following numerical summary. Soil pH ranged from 7.4-7.9, and clay percentage ranged from 6-20%. Soil P ranged from 7-32 mg kg^{-1}, and NH_4-N ranged from 3-6 mg kg^{-1}. Iron levels ranged from 9-12 mg kg^{-1}. These values were typical for fields in the region and there were no abnormally high or low values.

Correlograms for the initial 5 soil parameters are displayed in Figures 2.1 to 2.5. Based on the overall Moran's *I* statistic, all parameters had significant positive spatial autocorrelation. However, inspection of Moran's *I* values at individual lag distances, *h*, indicates that some parameters had much stronger spatial correlation than others. For example, the spatial autocorrelation of Fe is not significant at many of the lag distances (*h*) and suggests distribution of Fe concentrations are only weakly correlated. In contrast, the spatial autocorrelation of clay is very significant at almost all lag distances (*h*) indicating clay patterns are spatially correlated. The spatial autocorrelation patterns for NH_4-N, P, and pH were more significant than Fe and less significant than clay.

Correlation matrices for standard (PC) and spatial (PS) principal component construction are displayed in Table 2.2. All correlation values for the PC on the main diagonal are 1. This is expected since the correlation between the same soil parameter at separation distance h=0 will always be 1. Positive correlations exist between clay and P, clay and Fe, and clay and NH_4-N. These relationships are reasonable since Fe, and NH_4-N exist as cations and clays have higher cation exchange capacities than coarser, sandier soils. Although the soil was not analyzed for calcium-phosphate minerals, it is reasonable to assume these precipitates accumulate in higher-clay areas of the field and lead to a strong positive correlation. Positive correlations also existed for P and NH_4-N, and, Fe and P. These relationships are also reasonable since all three parameters are positively related to clay concentrations. Negative correlations exist between pH and P, pH and clay, and pH and Fe. Again, these relationships are reasonable given P precipitates more readily as pH increases, clay soils are typically more acidic than coarser soils, and Fe is typically more soluble at lower pH.

In contrast to the correlation matrix, values on the main diagonal for spatial correlation matrix are not 1. The spatial correlation matrix values on the main diagonal can range from -1 to 1. This is due to the fact that a soil parameters spatial correlation with itself can vary as the separation distance increases (i.e. h>0). Correlation values on the main diagonal for PS ranged from 0.07 (Fe) to 0.9 (clay). This suggests clay samples remained well correlated (i.e. displayed a strong spatial pattern) over the 4.65 ha field while Fe samples were variable (i.e. displayed a weak spatial pattern). Correlation values on the off-diagonal display the same sign pattern as the linear correlation matrix.

However, the overall spatial correlations (negative and positive) are weaker than the linear correlation matrix.

Eigenvectors for construction of PC and PS are displayed in Table 2.3. Final construction of principal components (PC and PS) was achieved by multiplying the 5x198 matrix of raw data values by the appropriate 5x5 eigenvector matrix. This operation resulted in a 5x198 matrix of PC or PS scores.

Cross-correlograms for the resulting PC and PS are displayed in Figures 2.6 to 2.15 and 2.16 to 2.25 respectively. One of the perceived benefits of PCA is orthogonality of the principal component scores (i.e. absence of correlation among principal components). Spatial cross-correlograms summarize the spatial correlation between variables, or in this case principal components, at specific separation distances. Utilization of a simple correlation matrix to construct PC resulted in cross-correlograms that were spatially dependent for all 5 PC. Similarly, utilization of a spatial correlation matrix resulted in cross-correlograms that were spatially dependent for all 5 PS. Neither the correlation matrix nor the spatial correlation matrix succeeded in removing spatial correlation from the newly constructed principal components when $h>0$. Another way to interpret Figures 2.6 to 2.15 is to say that spatial orthogonality of the PC and PS was not achieved since they displayed significant spatial correlation when $h>0$.

In this study, Gaussian variogram models minimized the AIC for the principal components and results are summarized in Table 2.4. The range value for the modeled PC and PS varied from approximately 40 to 300 m. The range value indicates the separation distance among samples where spatial independence is reached. Nugget

values for the PC and PS ranged from 0.0-0.3 and suggest the amount of sampling error was relatively small.

All ten principal components (5 PC, and 5 PS) were interpolated using ordinary kriging. The kriged data were cross-validated to determine the effectiveness of the models. The effectiveness of the model was evaluated with the goodness-of-prediction statistic (*G*) (Agterberg, 1984; Guisan and Zimmermann, 2000; Schloeder et al., 2001) and is summarized in Table 2.5. Overall, both techniques of principal component kriging performed similarly based on *G*-statistics. In all cases, the PS *G*-statistics were larger than PC. Although a larger *G*-statistic indicates better predictive performance, it may not be objective to conclude the PS outperformed the PC since the differences were small.

Correlation results from back-transformation of PC and PS are summarized in Table 2.6. Correlation between original parameter values and back-transformed values was positive, large, and ranged from 0.79 to 0.986 for PC and from 0.818 to 0.986 for PS. These results indicate both the PC and PS approach to generating principal components performed equally well. The PC and PS were back-transformed to the original parameter values with 79 to 98% accuracy.

2.4 Summary and Conclusions

The soil parameters clay, P, pH, NH_4-N, and Fe all displayed significant positive spatial autocorrelation within the sampled field (Figures 2.1-2.5). Additionally, these parameters also displayed significant spatial and linear correlations among each other (Tables 2.2).

Principal component analysis is often used as an approach to remove correlations in multivariate data. The primary objective of principal component analysis is to reduce the

amount of redundancy in the data by removing correlations. Principal component analysis is occasionally used with spatial data sets in an attempt to reduce the computational effort of cokriging n spatially correlated variables to kriging n principal components (Davis and Greenes, 1983). While principal component analysis is highly effective with non-spatial data, it can be suspect with spatial data sets. This is primarily due to a lack of orthogonality in the data if $h>0$.

I used a spatial correlation matrix in an attempt to improve principal component kriging techniques. The spatial correlation matrix was constructed with the BiMoran's I statistic and the linear correlation matrix was constructed with $\rho_{yz}(I)$ statistic. Eigenvectors were generated from the correlation matrices using standard computer software and used to create principal components (PC and PS) (Table 2.3). Cross-correlograms for the resulting PC and PS indicate the principal components were not orthogonal regardless of the technique used to generate principal components (Figures 2.6-2.25). The same results have been found by previous researchers and may lead to questionability about the principal component kriging technique (Goovaerts, 1993; Goovaerts, 1997).

Despite a lack of orthogonality, the PC and PS were kriged in order to compare the effectiveness of the two principal component kriging approaches. The two approaches were evaluated with the G-statistic and via back-transformation (Tables 2.5 and 2.6). Both approaches seemed to perform equally well although the G-statistics for the PS approach were slightly higher than the PC approach. Although a larger G-statistic indicates better predictive performance, it may not be objective to conclude the PS outperformed the PC since the G-statistic differences were small.

The sign pattern of the spatial correlation matrix was the same as the linear correlation matrix, but the actual values within the matrices were quite different (Table 2.2). Although the spatial correlation matrix only slightly improved the principla component kriging technique, it is important to note that I was able to generate another (spatial correlation) matrix that, at a minimum, performed equally well, when compared with the traditional approach to principal component kriging. There is no evidence of this 'spatial correlation matrix' approach to principal component kriging in the literature and so at the minimum, this research has shown that alternative matrices can be used for principal component kriging.

Back-transformation of both PC and PS resulted in very good estimates of the original soil parameters (Table 2.6). This is another indication that the PS approach to principal component kriging is a valid technique. Overall, the lack of orthogonality in the PC and PS did not hinder the ability to effectively interpolate the principal components. Similar results were found by Davis and Greenes (1983). However, in their study of principal component kriging the authors were not directly examining the orthogonality of the principal components. Overall, the PS and PC approaches to principal component kriging performed equally well based on *G*-statistics and back-transformation results. Although it is beyond the scope of this research project, it may be of interest to examine the effectiveness of cokriging compared to principal component kriging with PS.

2.5 References

Agterberg, F.P. 1984. Trend surface analysis. *In* G.L. Gaile and C.J. Willmott (ed.) Spatial statistics and models. Reidel, Dordrecht, The Netherlands.

Akaike, H. 1977. On entropy maximization principle. *In* P.R. Krishnaiah (ed.) Applications of Statistics. North-Holland, Amsterdam, The Netherlands.

Cliff, A.D., and J.K. Ord. 1981. Spatial processes: models and applications. Pion, London.

Czaplewski, R.L., and R.M. Reich. 1993. Expected value and variance of Moran's bivariate spatial autocorrelation statistic under permutations. Res. Pap. Rm-309. U.S. Dept. of Ag., Rocky Mountain Forest and Range Experiment Station, Fort Collins, CO.

Davis, B.M., and K.A. Greenes. 1983. Estimating using spatially distributed multivariate data: an example with coal quality. Math. Geol. 15:287-300.

Goovaerts, P. 1993. Spatial orthogonality of the principal components computed from coregionalized variables. Math. Geol. 25: 281-302.

Goovaerts, P. 1997. Geostatistics for natural resources evaluation. Oxford University Press, New York.

Guisan, A., and N.E. Zimmermann. 2000. Predictive habitat distribution models in ecology. Eco. Model. 135:147-186.

Manly, B.J. 1998. Multivariate statistical methods: a primer. Chapman and Hall/CRC, New York.

Miller, R.O., J. Kotuby-Amacher, and J.B. Rodriguez. 1998. Western states laboratory proficiency testing program, soil and plant analytical methods. Version 4.10.

Ortega, R.A. 1997. Spatial variability of soil properties and dryland crop yields over "typical" landforms of eastern Colorado. Ph.D. diss. Colorado State Univ, Fort Collins, CO.

Pearson, K. 1901. On lines and planes of closest fit to a system of points in space. Philos. Mag. 2:557-572.

Reich, R.M., and R.A. Davis. 1998. On-line spatial library for the S-PLUS© statistical software package. Colo. State. Univ., Fort Collins, CO.

Schloeder, C.A., N.E. Zimmerman, and M.J. Jacobs. 2001. Comparison of methods for interpolating soil properties using limited data. Soil Sci. Soc. Am. J. 65: 470-479.

Statistical Sciences. 1999. S-PLUS© 2000. Statistical software package for personal computers. StatSci Division, MathSoft, Inc., Seattle, WA.

Table 2.1 Selected soil properties of samples collected from experimental site.

	pH	Clay	P	NH_4-N	Fe
		--- % ---	---------- mg kg^{-1} ----------		
Average	7.7	9.5	16.9	5.6	12.8
Minimum	7.4	5.9	7.4	3.4	8.9
Maximum	7.9	20.1	31.7	7.7	20.5
Median	7.7	7.9	15.8	5.7	11.9

Table 2.2 A) Correlation matrix and B) spatial correlation matrix for construction of standard (PC) and spatial (PS) principal components.

(A)

	clay	P	pH	NH_4-N	Fe
clay	1	0.803	-0.626	0.388	0.899
P		1	-0.820	0.723	0.978
pH			1	-0.263	-0.836
NH_4-N				1	0.599
Fe					1

(B)

clay	P	pH	NH_4-N	Fe
0.846	0.454	-0.340	0.218	0.203
	0.510	-0.286	0.268	0.187
		0.442	-0.116	-0.066
			0.526	0.063
				0.068

Table 2.3 A) Correlation eigenvectors and B) spatial correlation eigenvectors for construction of standard (PC) and spatial (PS) principal components.

(A)

0.442	0.221	-0.757	0.368	-0.220
0.506	-0.099	0.144	0.234	0.812
-0.423	-0.465	-0.621	-0.257	0.391
0.335	-0.848	0.119	0.131	-0.370
0.508	0.078	-0.081	-0.853	-0.047

(B)

0.668	-0.379	-0.516	-0.362	0.107
0.513	0.109	0.124	0.762	0.359
-0.382	0.229	-0.834	0.289	0.153
0.330	0.889	-0.028	-0.306	-0.083
0.187	-0.044	-0.149	0.333	-0.911

Table 2.4 Summary statistics from variogram models for kriged principal components constructed with a linear correlation matrix (PC) and a spatial correlation matrix (PS).

Matrix	Component	Sill	Range	Nugget
PC	1	48.6	129.3	0.0
PC	2	0.8	47.9	0.1
PC	3	8.3	142.0	0.0
PC	4	0.2	66.7	0.0
PC	5	13.7	88.4	0.0
PS	1	48.6	135.1	0.0
PS	2	1.6	85.5	0.3
PS	3	4.4	142.2	0.0
PS	4	16.8	85.7	0.0
PS	5	0.3	291.6	0.0

Table 2.5 The *G*-statistics for principal components constructed with a linear correlation matrix (PC) and a spatial correlation matrix (PS).

Component	PC	PS
1	0.956	0.965
2	0.836	0.857
3	0.942	0.948
4	0.771	0.873
5	0.880	0.947

Table 2.6 Correlation between back-transformed principal components and original soil parameter values. Principal components were constructed with a linear correlation matrix (PC) and a spatial correlaltion matrix (PS).

	PC	PS
Clay	0.986	0.986
P	0.958	0.958
pH	0.790	0.818
NH_4-N	0.935	0.933
Fe	0.975	0.974

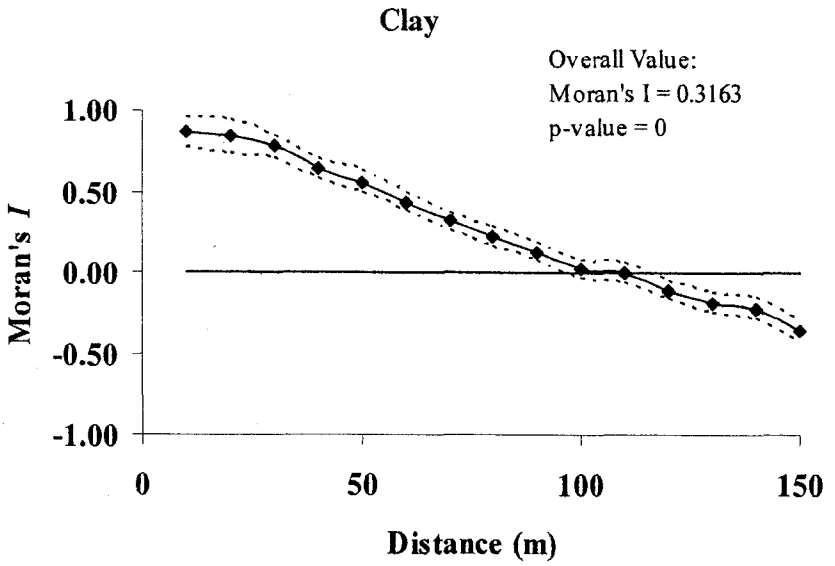

Figure 2.1 Correlogram for clay. Dashed line indicates one standard deviation. Solid horizontal line is expected Moran's *I* under the null hypothesis of complete spatial randomness.

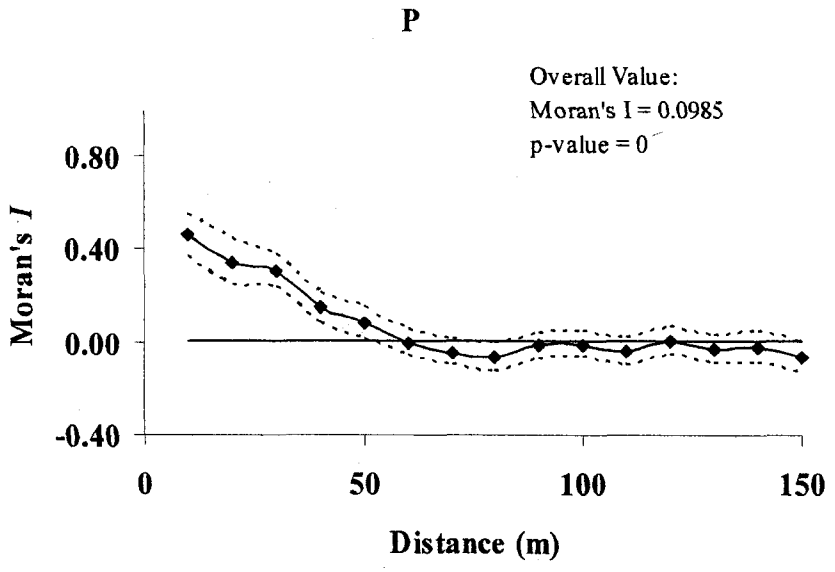

Figure 2.2 Correlogram for P. Dashed line indicates one standard deviation. Solid horizontal line is expected Moran's *I* under the null hypothesis of complete spatial randomness.

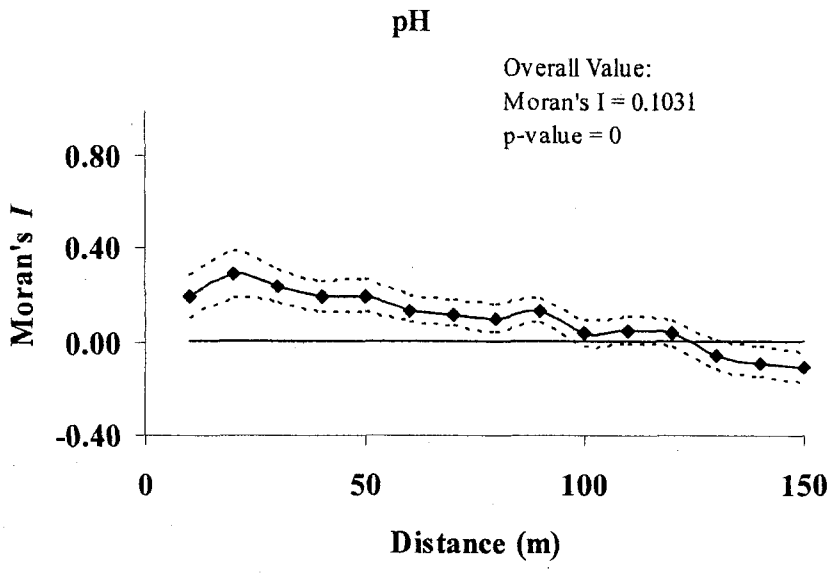

Figure 2.3 Correlogram for pH. Dashed line indicates one standard deviation. Solid horizontal line is expected Moran's *I* under the null hypothesis of complete spatial randomness.

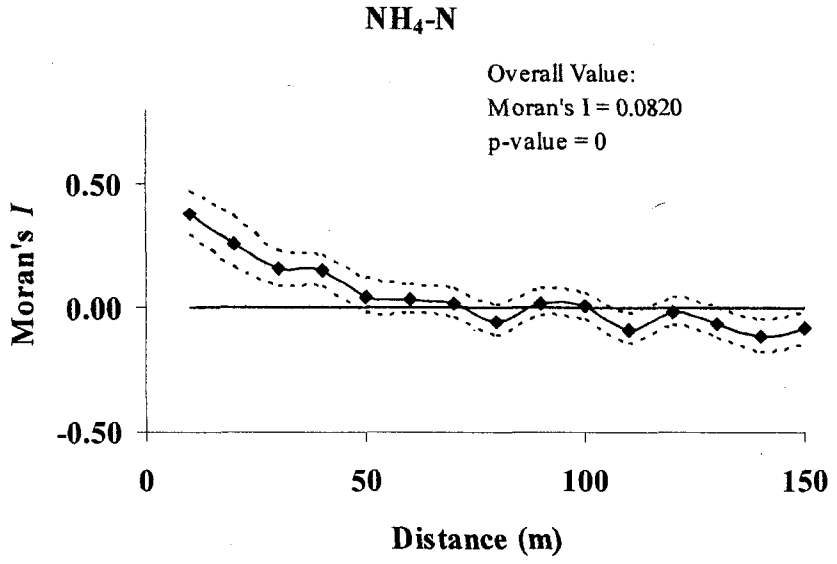

Figure 2.4 Correlogram for NH_4-N. Dashed line indicates one standard deviation. Solid horizontal line is expected Moran's *I* under the null hypothesis of complete spatial randomness.

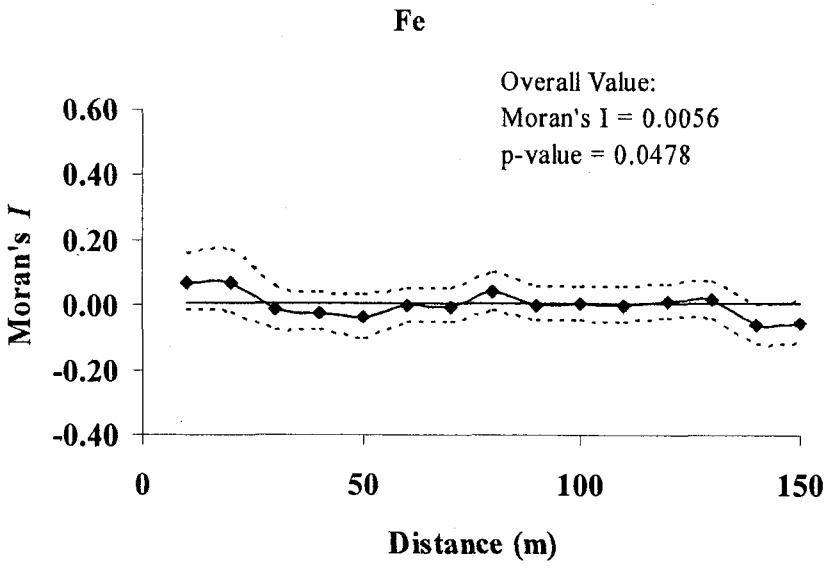

Figure 2.5 Correlogram for Fe. Dashed line indicates one standard deviation. Solid horizontal line is expected Moran's *I* under the null hypothesis of complete spatial randomness.

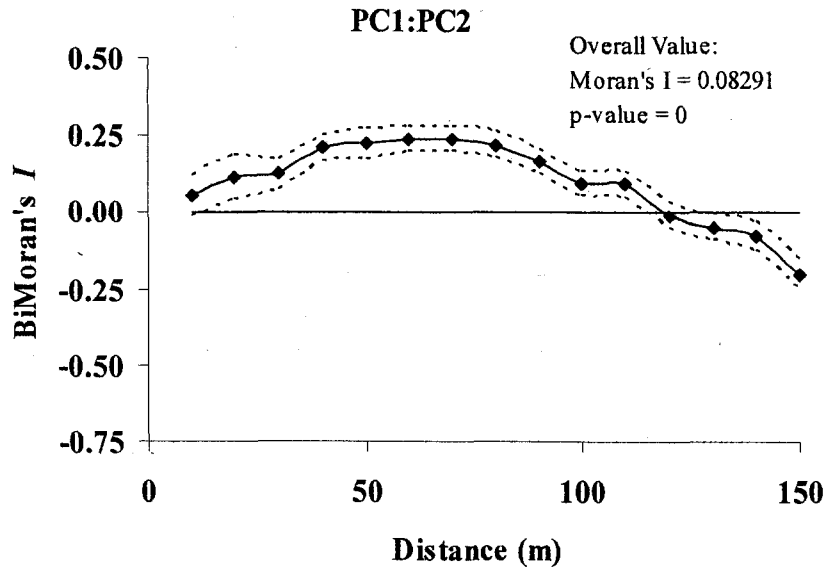

Figure 2.6 Cross-correlogram for PC1:PC2. Dashed line indicates one standard deviation. Solid horizontal line is expected BiMoran's *I* under the null hypothesis of complete spatial randomness.

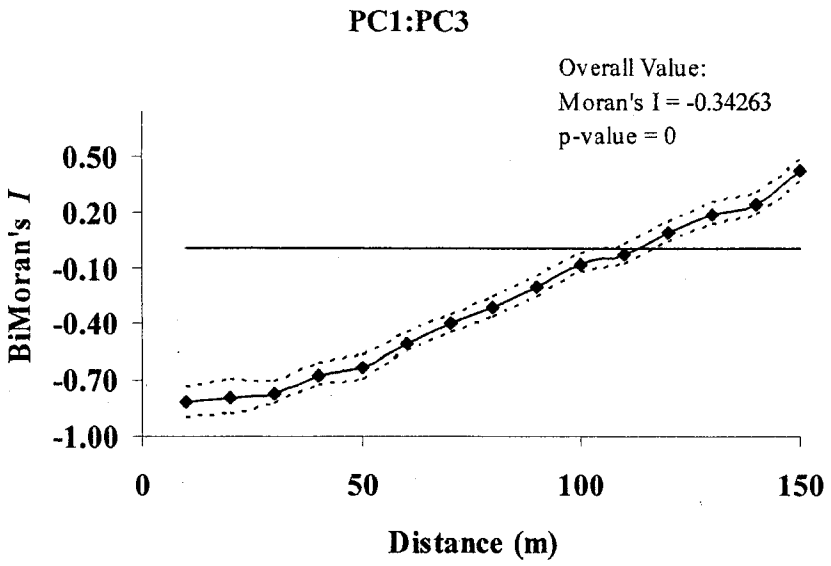

Figure 2.7 Cross-correlogram for PC1:PC3. Dashed line indicates one standard deviation. Solid horizontal line is expected BiMoran's *I* under the null hypothesis of complete spatial randomness.

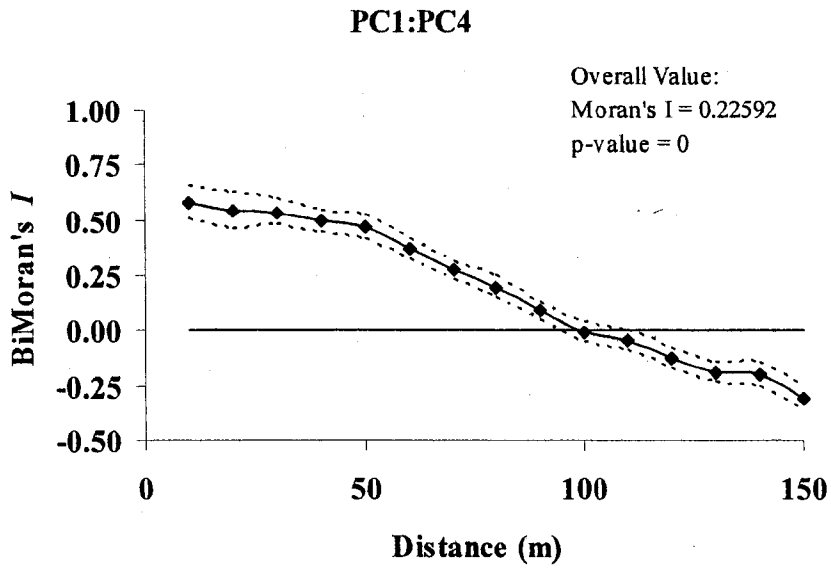

Figure 2.8 Cross-correlogram for PC1:PC4. Dashed line indicates one standard deviation. Solid horizontal line is expected BiMoran's *I* under the null hypothesis of complete spatial randomness.

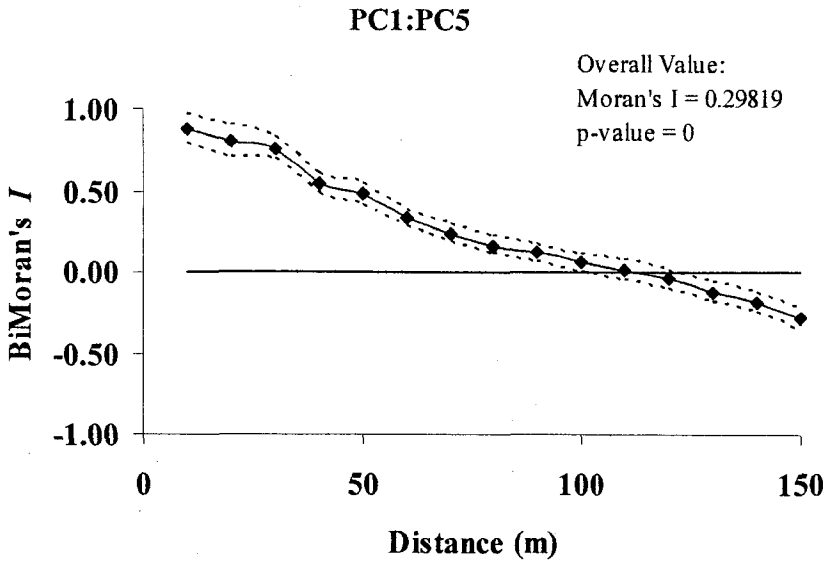

Figure 2.9 Cross-correlogram for PC1:PC5. Dashed line indicates one standard deviation. Solid horizontal line is expected BiMoran's *I* under the null hypothesis of complete spatial randomness.

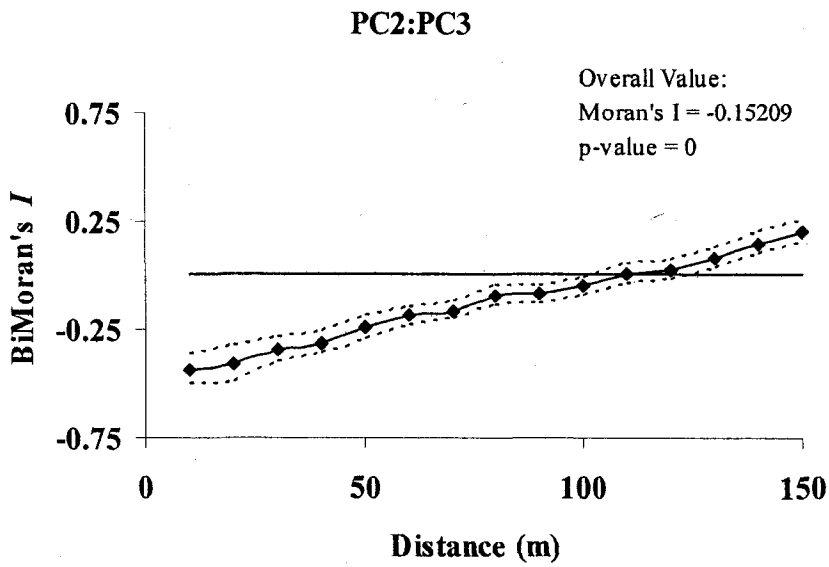

Figure 2.10 Cross-correlogram for PC2:PC3. Dashed line indicates one standard deviation. Solid horizontal line is expected BiMoran's *I* under the null hypothesis of complete spatial randomness.

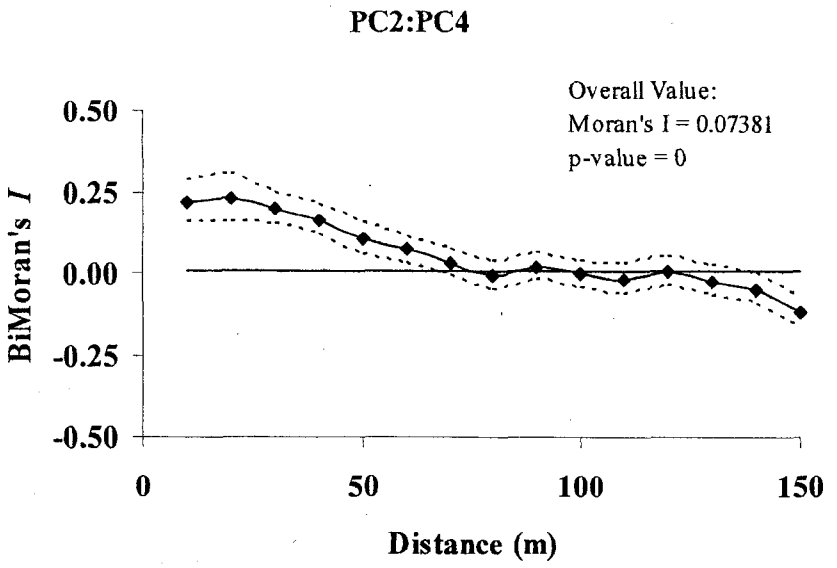

Figure 2.11 Cross-correlogram for PC2:PC4. Dashed line indicates one standard deviation. Solid horizontal line is expected BiMoran's *I* under the null hypothesis of complete spatial randomness.

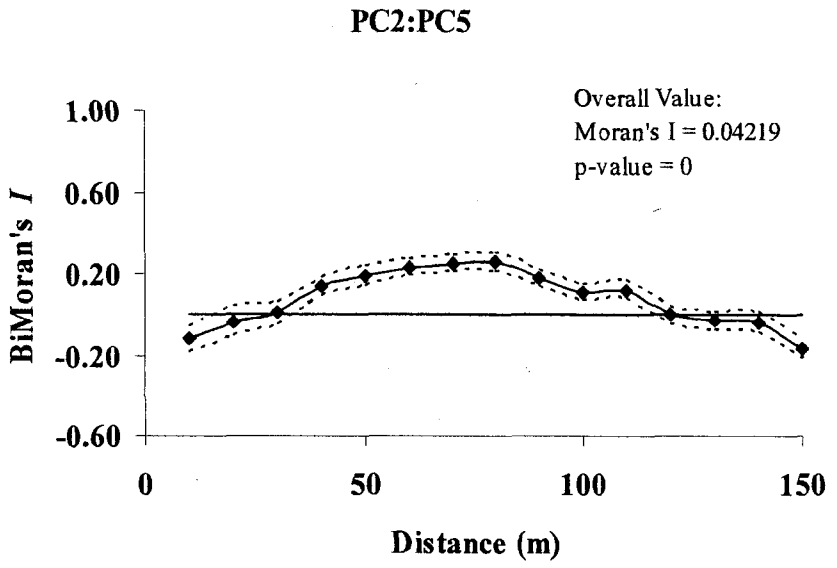

Figure 2.12 Cross-correlogram for PC2:PC5. Dashed line indicates one standard deviation. Solid horizontal line is expected BiMoran's *I* under the null hypothesis of complete spatial randomness.

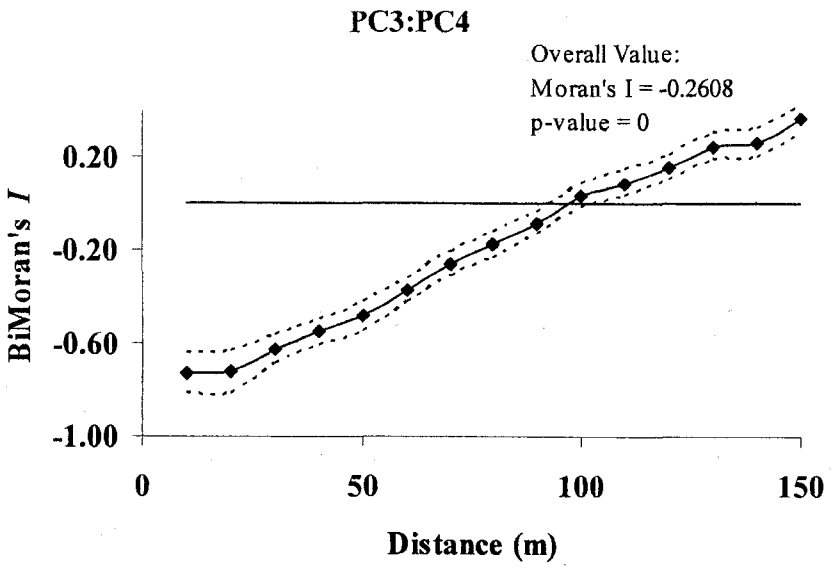

Figure 2.13 Cross-correlogram for PC3:PC4. Dashed line indicates one standard deviation. Solid horizontal line is expected BiMoran's *I* under the null hypothesis of complete spatial randomness.

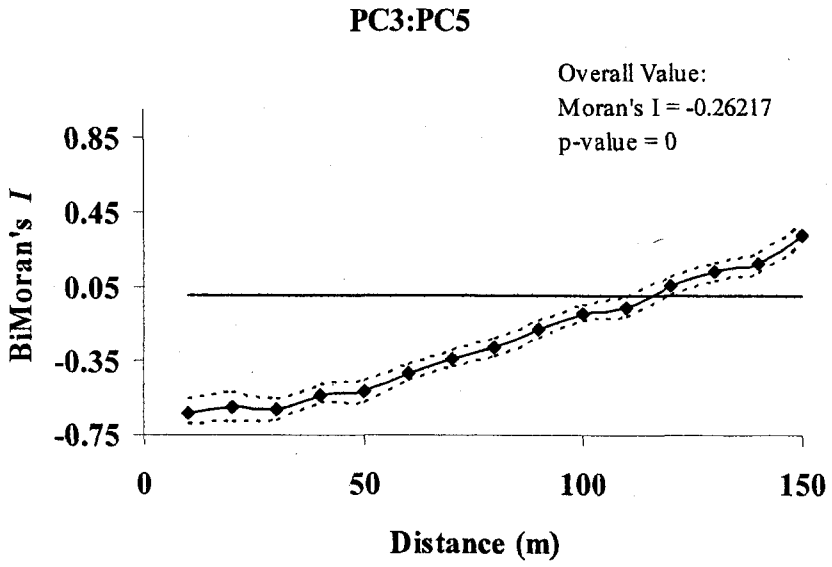

Figure 2.14 Cross-correlogram for PC3:PC5. Dashed line indicates one standard deviation. Solid horizontal line is expected BiMoran's *I* under the null hypothesis of complete spatial randomness.

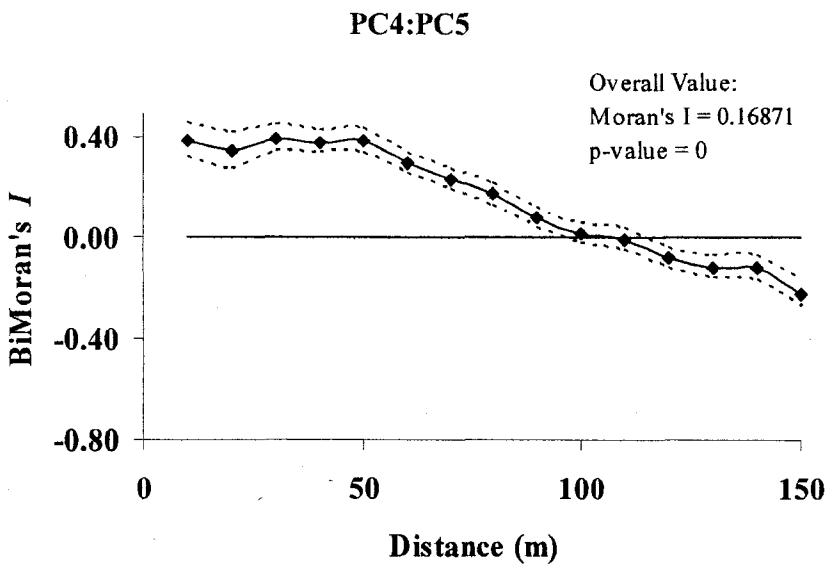

Figure 2.15 Cross-correlogram for PC4:PC5. Dashed line indicates one standard deviation. Solid horizontal line is expected BiMoran's *I* under the null hypothesis of complete spatial randomness.

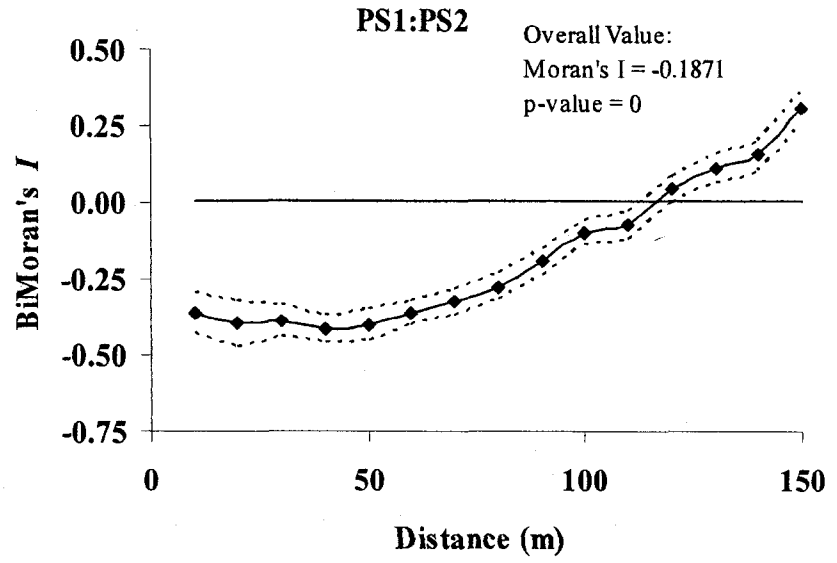

Figure 2.16 Cross-correlogram for PS1:PS2. Dashed line indicates one standard deviation. Solid horizontal line is expected BiMoran's *I* under the null hypothesis of complete spatial randomness.

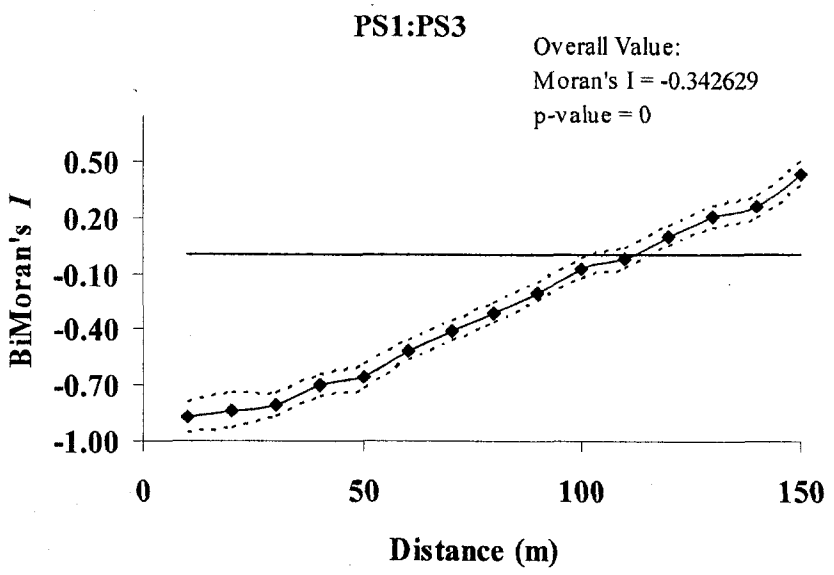

Figure 2.17 Cross-correlogram for PS1:PS3. Dashed line indicates one standard deviation. Solid horizontal line is expected BiMoran's *I* under the null hypothesis of complete spatial randomness.

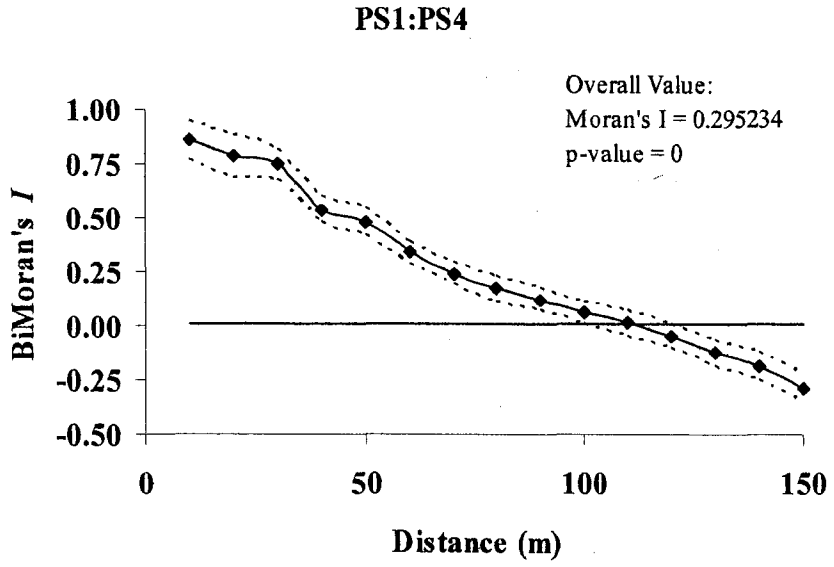

Figure 2.18 Cross-correlogram for PS1:PS4. Dashed line indicates one standard deviation. Solid horizontal line is expected BiMoran's *I* under the null hypothesis of complete spatial randomness.

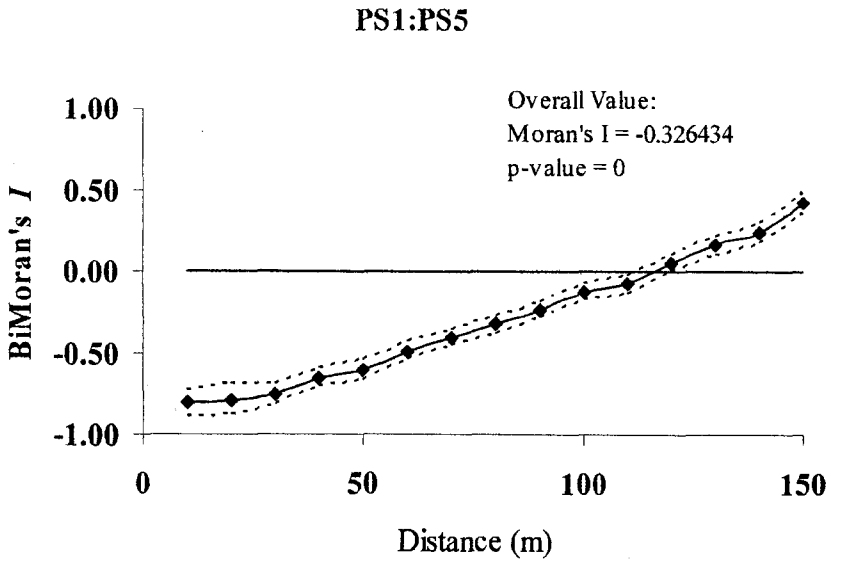

Figure 2.19 Cross-correlogram for PS1:PS5. Dashed line indicates one standard deviation. Solid horizontal line is expected BiMoran's *I* under the null hypothesis of complete spatial randomness.

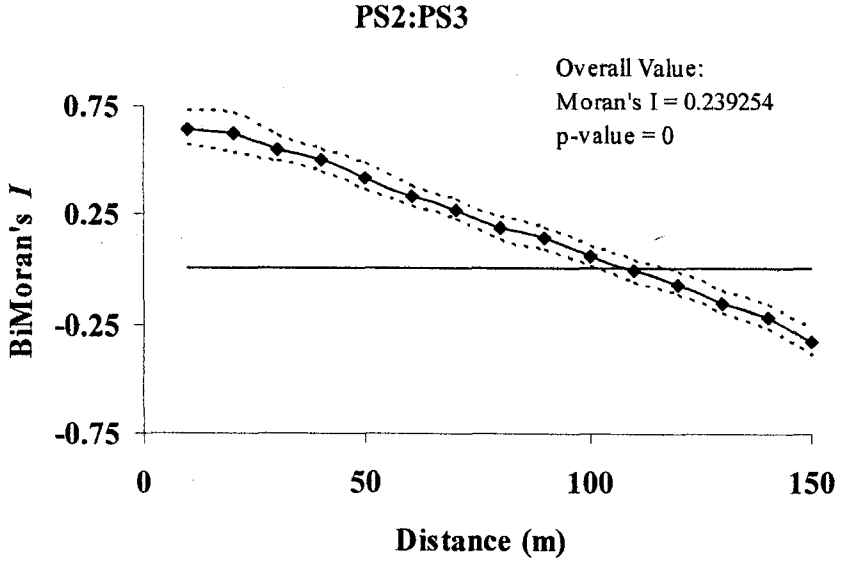

Figure 2.20 Cross-correlogram for PS2:PS3. Dashed line indicates one standard deviation. Solid horizontal line is expected BiMoran's *I* under the null hypothesis of complete spatial randomness.

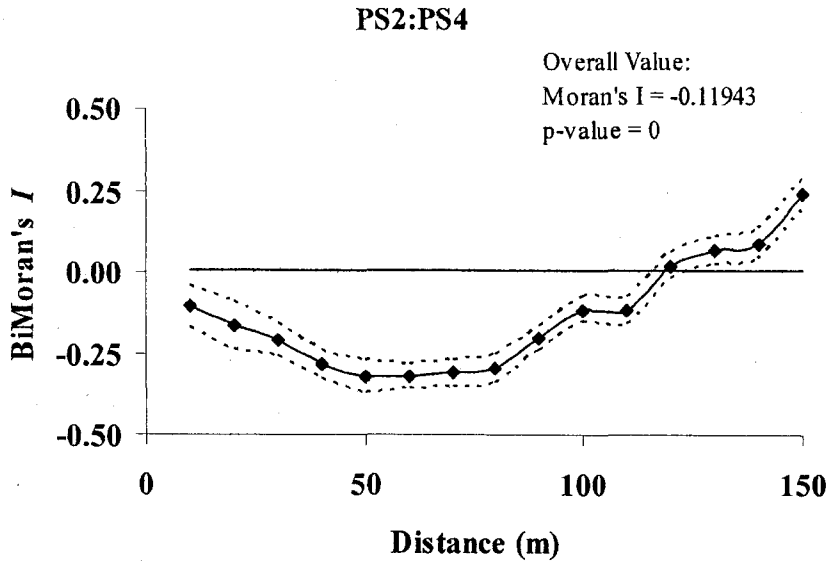

Figure 2.21 Cross-correlogram for PS2:PS4. Dashed line indicates one standard deviation. Solid horizontal line is expected BiMoran's *I* under the null hypothesis of complete spatial randomness.

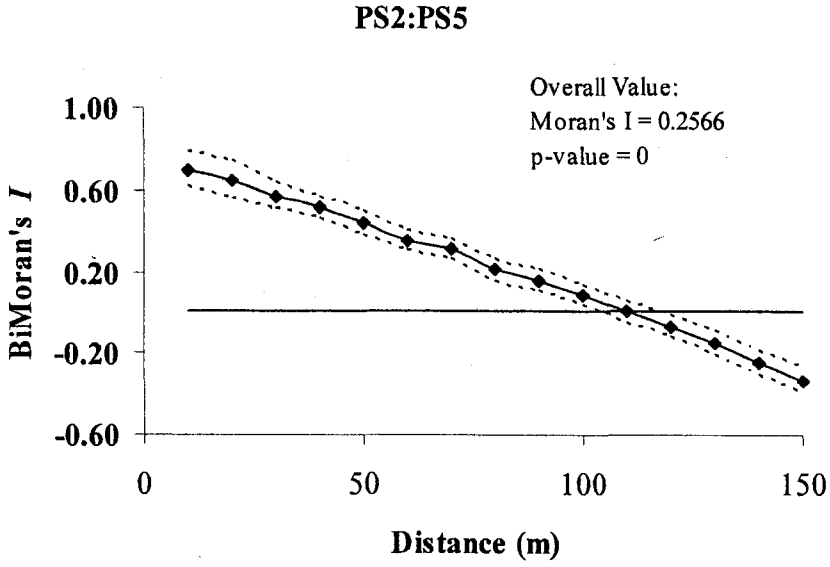

Figure 2.22 Cross-correlogram for PS2:PS5. Dashed line indicates one standard deviation. Solid horizontal line is expected BiMoran's *I* under the null hypothesis of complete spatial randomness.

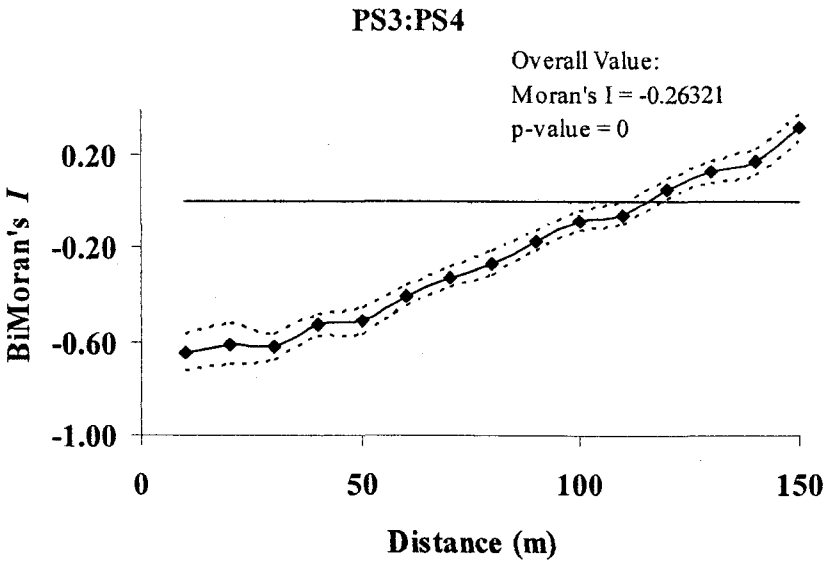

Figure 2.23 Cross-correlogram for PS3:PS4. Dashed line indicates one standard deviation. Solid horizontal line is expected BiMoran's *I* under the null hypothesis of complete spatial randomness.

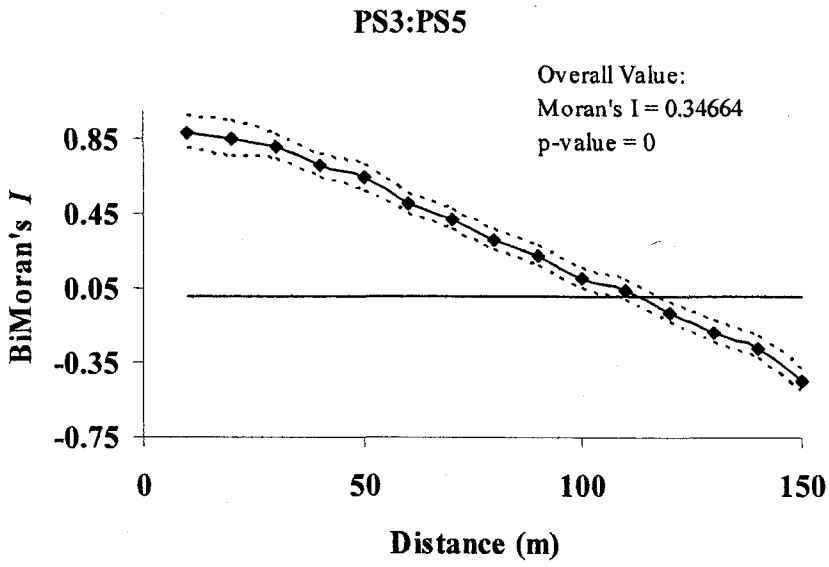

Figure 2.24 Cross-correlogram for PS3:PS5. Dashed line indicates one standard deviation. Solid horizontal line is expected BiMoran's *I* under the null hypothesis of complete spatial randomness.

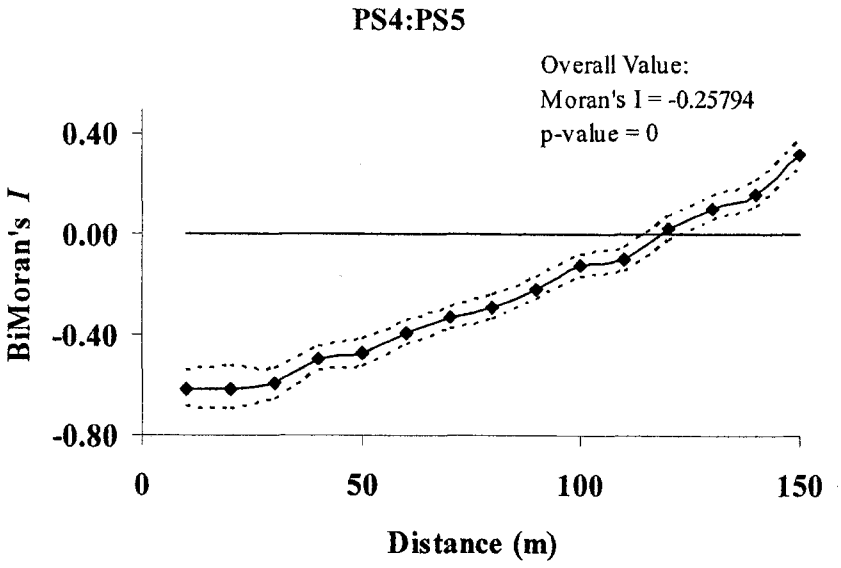

Figure 2.25 Cross-correlogram for PS4:PS5. Dashed line indicates one standard deviation. Solid horizontal line is expected BiMoran's *I* under the null hypothesis of complete spatial randomness.

3 Spatial Analysis of Soil Properties with Cumulative Correlograms

3.0 Abstract

Variable rate application maps for agricultural inputs are often based on a grid sampling approach. The main problems associated with this approach are primarily due to the large separation distances between sample locations. In most cases, the scales-of-pattern associated with soil variables occur at separation distances much smaller than the separation distances observed with a typical grid sampling approach. The objective of this study was to illustrate and quantify problems associated with a grid sampling approach. Two fields were sampled for P, K, organic matter, pH, NO_3-N, NH_4-N, and Zn. Fields were sampled on a 76 x 76 m (0.58 ha) coarse grid (CG), and a portion of each field was sampled on a 15 x 15 m (0.023 ha) fine grid (FG). The CG data were tested for spatial autocorrelation using Moran's *I* statistic. The point autocorrelation coefficient was also determined for each variable at each sample location. Variogram models were used to krig the various soil parameters. Effectiveness of the models was tested with cross-validation and the goodness-of-prediction statistic (*G*). The FG data were analyzed with correlograms and cumulative correlograms. Correlograms and cumulative correlograms were constructed with the Moran's *I* statistic. Kriging models for the CG data performed poorly based on the *G*-statistics. At least two factors are contributing to this poor performance. First, point autocorrelation coefficients suggest some sample locations exhibit anomalous characteristics. Second, based on evaluation of cumulative correlograms, separation distance among samples is too large. When

standard and cumulative correlograms are compared only cumulative correlograms are effective for elucidating scales-of-pattern in soils. Alternative sampling designs that capture scales-of-pattern may include double sampling and/or regression approaches that utilize auxiliary data such as soil color or topography.

3.1 Introduction

Proper soil sampling designs are primary when attempting to build reliable soil-nutrient maps for precision farming (PF) applications. The primary goal for a proper soil sampling design is to 'capture spatial dependency' among soil samples. Classical statistics is founded on the premise that samples from a population are independent of one another. Conversely, spatial statistics focuses on the dependence among samples from a population. Effective and accurate spatial models are predicated on spatially dependent samples. In the realm of soil science or agronomy, spatial dependence can only be captured if samples are collected from regions of influence (i.e. small separation distances). If samples are not collected within a region of influence, data may be spatially independent and this can preclude the proper application of spatial models. With respect to agronomic applications, lack of spatial dependency may generate models and soil-property maps that may not accurately represent the field variability.

Variable rate application maps for agricultural inputs are often based on a grid sampling approach. Production fields are divided into 1 ha grid cells and sample locations are randomly located within each cell. The limitations of this approach have been addressed in past research (Gotway et. al, 1996; Hammond, 1993; Franzen and Peck, 1995; Mueller et al., 2001). The main problems associated with this approach are primarily due to the large separation distances between sample locations. The result is a

lack of appropriate sample numbers to develop sound spatial predictive models for the soil properties of interest. This is because in most cases the scales-of-pattern associated with soil variables occur at separation distances much smaller than the separation distances observed with a typical grid sampling approach (i.e. ~1 ha). Mueller et al., (2001) concluded that a commercial sampling approach with 100 x 100 m (1 ha) grids was inadequate for developing sound soil nutrient maps. Franzen and Peck (1995) found that a distance of 65 m (0.42 ha) among samples was acceptable to generate reasonable soil-property maps. Similarly, Hammond (1993) found that a 60 m (0.36 ha) grid was adequate for developing nutrient level maps.

The objective of this study was to illustrate and quantify the major problems associated with a grid sampling approach to precision farming applications. I will also introduce a tool, the cumulative correlogram, which can be used to elucidate scales-of-pattern in soil parameters. It is my goal to emphasize the importance of capturing small-scale variability (i.e. small scales-of-pattern) for any type of interpolation modeling in general, and illustrate the usefulness of the cumulative correlogram for elucidating scales-of-pattern in particular.

3.2 Materials and Methods

The study was conducted on two agricultural fields in 1997 and 1998. Both fields were center pivot irrigated fields located in northeastern Colorado. Field 1 was 71 ha and Field 2 was 52 ha. Field 1 was sampled in 1997 and 1998, while Field 2 was sampled only in 1997 (i.e. three site years of data from two fields). Soils in both fields included Valentine sand (sandy, mixed nonacid, mesic Typic Ustipsamment), a Bijou loamy sand (coarse loamy, mixed, mesic Mollic Haplargid), and a Truckton loamy sand (coarse

loamy, mixed, mesic Udic Argiustoll). The fields were in continuous corn (*Zea mays* C.) throughout the study. Each field has been managed and operated by the same farmers since 1977.

3.2.1 Soil Sampling

Each field was sampled using a coarse grid (CG) technique and the size of each grid cell was 76 x 76 m (i.e. 0.58 ha) (Fleming, et. al, 2000). Sample locations were randomly located within each cell and recorded with a differential global positioning system (DGPS). Soil samples were collected from the 0 to 0.2 m surface zone and analyzed for phosphorus (P), potassium (K), organic matter (OM), pH, nitrate-N (NO_3-N), ammonium-N (NH_4-N), and zinc (Zn) using standard soil testing procedures (Miller et al., 1998).

A 4.65 ha portion (i.e. 152 x 304 m) of each field was also sampled using a fine grid (FG) cell size of 0.023 ha (i.e. 15 x 15 m). Sample locations were randomly located within each cell, recorded with a DGPS, and soil samples were collected and analyzed as described above.

3.2.1 Coarse Grid Analysis

Sample data must exhibit spatial dependence (i.e. spatial autocorrelation) in order to generate accurate spatial models. We used the Moran's *I* statistic (*I*) to test for spatial autocorrelation in the soil parameters from the CG data sets (Moran, 1948). The Moran's *I* statistic is analogous to a weighted correlation coefficient between possible pairs of *n* observations (z_i and z_j, $i \neq j$) (Czapleswski et al., 1994) and is defined as:

$$I = \left(\frac{\sum_{i=1}^{n} \sum_{j=1}^{n} w_{ij} z_i z_j}{WVar(z)} \right) \qquad [3.1]$$

where w_{ij} is a weight that quantifies the hypothesized spatial association or proximity between observations (z_i and z_j) at sites i and j, and w_{ii}=0; W is the sum of all n^2 values of w_{ij}; $Var(z)$ is the variance of the n observations; and observations are transformed to center on zero (i.e. sum of all z_i's equals zero). Moran's I is a dimensionless statistic that usually ranges from –1 to 1. Larger absolute values of Moran's I indicate a strong autocorrelation (i.e. positive or negative) while a value of zero indicates complete spatial independence among samples. Weight matrices were calculated using inverse distance that linearly decreases weight with distance between pairs of observations.

The point autocorrelation coefficient (I_i) was also determined for each soil variable at each sample location. This statistic can be used to identify outliers, extreme data or local anomalies (Reich et al., 1994). The point autocorrelation coefficient is calculated by decomposing the Moran's I statistic to obtain the relative contribution of each sample point to the overall Moran's I statistic. The point autocorrelation statistic is defined as:

$$I_i = \left(\frac{\sum_{j=1}^{n} w_{ij} z_j}{WVar(z)} \right) \qquad [3.2]$$

Summing across all samples will yield the standard Moran's I defined in Eq. 3.1. The location of each sample point is then plotted along with its corresponding point autocorrelation coefficient. Areas with large (positive or negative) point autocorrelation

statistics surrounded by areas with small statistics indicate a local anomaly, or a possible outlier.

Data collected from the CG was used to generate empirical variograms. Variogram functions describe how spatial continuity or spatial interdependence among soil samples changes as a function of separation distance and direction. The variogram function, $\gamma(h)$, is given by:

$$\gamma(h) = \frac{1}{2N(h)} \sum_{(ij)|h_{ij}=h} (z_i - z_j)^2 \qquad [3.3]$$

In general, as distance (h) between pairs of points increases, the corresponding variance ($\gamma[h]$) will increase. At some distance, $\gamma(h)$ will reach a plateau. The distance at which $\gamma(h)$ reaches this plateau is called the range and is generally viewed as the separation distance at which sample parameters are independent. When $h = 0$, $\gamma(h) = 0$, however because of sampling error and short scale variability $\gamma(h)$ may not be zero at small distances. The vertical increase from 0 at the origin to the small value of $\gamma(h)$ at extremely small separation distances is called the nugget effect. If the jump from 0 is too large, the empirical variogram is called a "nugget effect variogram". In effect, a nugget effect variogram indicates that samples collected from all separation distances are spatially independent. Gaussian, exponential, and spherical variogram models were fit to the empirical variograms using the Spatial Library developed by Reich and Davis (1998) in S-PLUS©[1]. The optimum model was selected as the model that minimized the Akaike's Information Criteria (AIC) and models were used to krig the soils data (Akaike, 1977). Kriging is a spatial statistical (or geostatistical) estimation technique that is used to

[1] Mention of a trade name, proprietary product, or specific equipment does not constitute a guarantee, warranty, or endorsement by Colorado State University.

estimate, or interpolate values of a variable at unsampled locations in space. Originally, kriging was primarily used in the mining industry but it has since been used by various disciplines including soil science and agronomy (Burgess and Webster, 1980a,b; Goovaerts and Journel, 1995). Resulting kriged surfaces were cross-validated to determine the effectiveness of the models. Cross-validation involves deleting one observation from the data set and predicting the deleted observation using the remaining observations in the data set. This process is repeated for all observations. Residuals are computed as the observed minus predicted values. The effectiveness of the model is determined with the goodness-of-prediction statistic (*G*) (Agterberg, 1984; Guisan and Zimmermann, 2000; Schloeder et al., 2001). The *G*-statistic is a measure of how effective a prediction might be relative to that which could have been derived by the sample mean and is defined as (Agterberg, 1984):

$$G = 1 - \left(\frac{\sum_{i=1}^{n} \left[Z_i - \hat{Z}_i \right]^2}{\sum_{i=1}^{n} \left[Z_i - \overline{Z} \right]^2} \right) \qquad [3.4]$$

where Z_i is the observed value of the i^{th} observation, $\hat{Z}_i$ is the predicted value of the i^{th} observation, and $\overline{Z}$ is the sample mean. A *G*-statistic equal to 1 indicates perfect prediction, a positive value indicates that the model is more reliable than if one had used the sample mean, a negative value indicates the model is less reliable than if one had used the sample mean, and a value of zero indicates that the model is equal to that of the sample mean to estimate *Z*.

3.2.2 Fine Grid Analysis

The Moran's *I* statistic was used to test for spatial autocorrelation in the soil parameters from the FG data sets. Empirical variograms models were also generated and Gaussian, exponential, and spherical variogram models were fit to the empirical variograms. The optimum model was selected as the model that minimized the AIC. The models were cross-validated to determine their effectiveness with the *G*-statistic.

Correlograms were constructed with the FG data and a total of 18 separation distances (i.e. bins) were used in their construction. The maximum separation distance used in the construction of correlograms was 162 m. The correlogram statistic is defined as:

$$\rho(I) = \left(\frac{\sum_{i=1}^{N(h)} \sum_{j=1}^{N(h)} w_{ij} z_i z_j}{WVar(z)} \right) \qquad [3.5]$$

This equation is similar to Eq. 3.1 and the remaining variables were defined there. The main difference between Eq 3.1 and 3.5 is the restriction placed on the calculation of $\rho(I)$ by the term $N(h)$. This restriction limits pairs of points used in the calculation of $\rho(I)$ to those pairs of points separated by distances within the interval $[a,b)$. The interval $[a,b)$ represents one of the 18 bins used to construct the correlogram and the lag distance $h \equiv b-a$. For example, bin number 1 covers those pairs of points separated by a distance of 0 to 9 m, and bin number 18 covers those pairs points separated by a distance of 153 to 162 m. In both bins, the lag distance $h = 9$ m. Final correlograms were constructed by plotting $\rho(I)$ versus separation distance.

Cumulative correlograms were also constructed with data from the FG. The cumulative correlogram provides an objective measure of the spatial scale-of-pattern

under investigation. A total of 18 bins were used to construct cumulative correlograms and the maximum lag distance was 162 m. The equation for calculating cumulative correlogram is identical to Eq. 3.5. The only difference for calculating the cumulative correlogram is the restriction placed on the equation by the term $N(h)$. In the calculation of the cumulative correlogram, the restriction limits pairs of points used in the calculation of $\rho(I)$ to those pairs of points separated by distances within the interval $[0,b)$. The interval $[0,b)$ represents one of the 18 bins used to construct the correlogram and the lag distance $h \equiv b\text{-}0$. For example, bin number 1 covers those pairs of points separated by a distance of 0 to 9 m, and bin number 18 covers those pairs points separated by a distance of 0 to 162 m. The lag distance h increases by 9 m with each successive iteration in the calculation of the cumulative correlogram. This technique is similar to Greig-Smith's (1952) method of pattern analysis based on the use of contiguous quadrats for measuring aggregation. The lags (h) used to construct the cumulative correlogram can be thought of as the radii associated with an area surrounding each sample point. If one graphs the change in the $\rho(I)$ versus h, one should be able to identify which distance category yields the strongest evidence of a spatial autocorrelation. When I reaches a maximum, the associated h_{max} reveals the mean area of the pattern under investigation. If I decreases when $h>h_{max}$ this indicates the pattern is regularly distributed in space (Greig-Smith, 1952; Reich et al., 1994). If the pattern is randomly distributed, the cumulative correlogram should remain constant with increasing distance. Final cumulative correlograms were constructed by plotting Moran's I versus h.

3.3 Results and Discussion

3.3.1 Field Sites

Sampling locations for the CG and FG are displayed in Figure 3.1. Results from chemical analysis of soil samples (i.e. CG and FG) are summarized in Table 3.1. Average and median values for measured variables in the CG and the FG appeared similar. Nitrogen values were the most variable between grids and among fields.

Since sample locations within each 76 x 76 m CG cell were randomly located, it is beneficial to categorize the range of sample separation distances. A summary of separation distances is also useful when using spatial analysis tools such as variograms, correlograms, and cumulative correlograms because it allows a more meaningful interpretation of the data set with respect to spatial dependence and spatial independence. A parametric and non-parametric summary of separation distance for CG data is presented in Table 3.2. The median value divides the data set, arranged from lowest to highest, into two parts of equal size; the first quartile separates the lower quarter from the upper three-quarters, and the third quartile separates the upper quarter from the lower three-quarters. Median separation distance among soil sample locations for the three fields ranged from 70 to 75 m and corresponded well with the grid size of the CG (i.e. 76 x 76 m). Minimum separation distances ranged from 19 to 32 m and maximum separation distances ranged from 78 to 86 m.

3.3.2 Coarse Grid Analysis

The Moran's *I* statistic is analogous to a weighted correlation coefficient between possible pairs of observations (i.e. soil samples) and was used to test the CG data sets for spatial autocorrelation. Spatial autocorrelation of soil parameters from the CG is

summarized in Table 3.3. All parameters were spatially correlated on all fields in the CG, except P on Field 2. Because spatially autocorrelated data are required to develop useful spatial models the results summarized in Table 3.3 suggests the data sets can be spatially modeled.

Variogram functions describe how spatial continuity or spatial interdependence among soil samples changes as a function of separation distance and direction. In general, as distance between pairs of points increases, the corresponding variogram will increase. At some distance, the variogram will reach a plateau. The distance at which the variogram reaches this plateau is called the range. In this study, Gaussian variogram models minimized the AIC for the soil parameters used and results are summarized in Table 3.4. The range value for most models was less than 75 m (i.e. similar to median separation distances). Visual inspection of variogram models also suggested most models had rapidly increasing variances as the lag distance (h) increased from 0 (Figures 3.2-3.8).

As an example, this trend can be seen in variogram models for OM in (Figure 3.4). Range values for OM varied from 15 to 50 m on the three fields. The range value on the variogram indicates the separation distance where soil samples are spatially independent. In the context of sampling designs, these results suggest spatial dependency at small scales is not being captured since median sample separation distances are greater than 70 m and this value is much larger than the range values. These data suggest that predictive interpolation models using the CG data would not accurately reflect the spatial variability of the tested parameters. This is an important consideration when trying to develop predictive interpolation models. Variogram models for NH_4-N, pH, and K

behaved similarly to OM and the range values were generally smaller than the observed median separation distances (Table 3.4). This suggests these parameters are reaching spatial independence at distances that are smaller than median sample separation distances. Essentially, based on the variograms, the soil samples from the CG are spatially independent and this make application of spatial models difficult. Range values for the parameters Zn, NO_3-N and P were generally larger than the previously mentioned parameters. This suggests these parameters are reaching spatial independence at distances that are larger than median sample separation distances. Another way to interpret the Zn, NO_3-N and P variograms is to say they can be more effectively interpolated using spatial models since the range to spatial independence is larger than the median sample separation distances.

The *G*-statistics from the cross-validation procedure are summarized in Table 3.5. The *G*-statistic values ranged from –0.03 to 0.50. The negative *G*-statistic was observed with P, on Field 2, 1997 and suggests that it would have been better to use the sample mean for estimating the P soil level, as opposed using kriging to spatially interpolate the data. Based on the variogram model for P on Field 2, 1997, the range to independence was 94 m. This value is greater than 70 m median separation distance for Field 2 and suggests samples were collected within the range of spatial autocorrelation; however, the model still performed poorly. This is most likely due to an overall lack of samples at small lags where spatial autocorrelation is the strongest. This conclusion is supported by an examination of the P variogram which displayed relatively few data values in the interval from lag=0 to lag=range-value (Figure 3.2). As explained in section 1.2, this region of the variogram should be represented by three to four values and indicates the

degree of spatial dependence of samples separated by small sample distances. The same trend is apparent with the remaining soil parameters and there are few data values at lag distances less than 50 m. The remaining variables also had relatively low *G*-statistics further suggesting the spatial dependencies associated with the variables are not being captured or described with the CG sampling approach.

These results seem counter-intuitive given the results of spatial autocorrelation analysis (Table 3.3). Most spatial autocorrelation statistics (*I*) were significant suggesting samples are spatially dependent and can be spatially modeled. However, the Moran's *I* statistic is determined using all data points in the sample set. Consequently in some cases, the significant autocorrelation may be due to a large-scale trend in the data but not due to small-scale or local trends that are needed for spatial interpolation. A partial explanation for the poor results may be gleaned by examining point autocorrelation statistics (I_i). Point autocorrelation statistics can be used to identify outliers, extreme data or local anomalies. The point autocorrelation coefficient is calculated by decomposing the overall Moran's *I* statistic for a measured soil parameter to obtain the relative contribution of each sample point to the overall Moran's *I* statistic. The point autocorrelation statistic can range from -1 to 1.

A graphical summary of the point autocorrelation statistics of four of the soil parameters with the poorest model results are presented in Figures 3.9, 3.12, 3.14, and 3.15. Distribution of I_i across Field 2, for P appeared relatively small and randomly distributed. Results from Moran's *I* analysis confirm this (i.e. *p*-value = 0.35) (Figure 3.9). However, distributions of I_i across Field 1 for P do not appear random and it appears that the west edge of the field is contributing largely to the overall *I* statistic as

indicated by the large, positive point autocorrelation statistics (Figure 3.9). Larger values of I_i are desirable when trying to develop spatial models, but areas with large (positive or negative) I_i surrounded by areas with small I_i indicate a local anomaly, or a possible outlier. Overall Moran's I values for soil pH were significant on all three fields, however, point autocorrelation statistics suggest anomalous areas in the northeast and southwest edges of Field 1 in 1997 and 1998 as indicated by large positive values of the point autocorrelation statistics (Figure 3.12). Similarly, Field 2 displays unusually large point autocorrelation statistics in the north, central region. Overall Moran's I values for NH_4-N and Zn were significant on all three fields. However, both parameters displayed anomalously large, positive point autocorrelation statistics primarily on the edges of the fields (Figures 3.14-3.15). The kriging model results for the remaining three soil parameters (i.e. K, OM, and NO_3-N) were better, however, an examination of their point autocorrelation statistics indicates anomalous regions of the field similar to P, pH, NH_4-N and Zn (Figures 3.10, 3.11, and 3.13). Although I_i values alone cannot explain the poor performance of the kriging models, they provide insight into potential spatial anomalies. A combination of spatial anomalies and less than optimal sampling designs probably contributed to the poor performance of the kriging models.

3.3.3 Fine Grid Analysis

Spatial autocorrelation of soil parameters from the FG is summarized in Table 3.7. All parameters displayed positive spatial autocorrelation on all fields. Similar to the CG, these results indicate the data sets can be spatially modeled.

Gaussian variogram models minimized the AIC for the soil parameters and results are summarized in Table 3.8. The range value for most models was less than 75 m.

Unlike the CG variograms, the FG variograms displayed data values in the interval from lag=0 to lag=range-value (Figures 3.16-3.21). As explained in section 1.2, this region of the variogram should be represented by three to four values and indicates the degree of spatial dependence of samples separated by small sample distances. Soil pH was the only soil parameter that did not display values in this region. This indicates that soil pH samples are spatially independent at very small separation distances. Overall, variograms from the FG sampling design indicate that spatial dependency at small scales is being captured (i.e. with the exception of soil pH).

The *G*-statistics from the cross-validation procedure are summarized in Table 3.9. The *G*-statistic values ranged from -0.04 to 0.80. The negative *G*-statistic was observed with pH, on Field 1, 1998 and suggests that it would have been better to use the sample mean for estimating the soil pH as opposed to using a kriging model. The *G*-statistics for pH on Field 1, 1997, and Field 2, 1998 were were -0.002, and 0.07 respectively. These values, combined with inspection of the variogram models, indicate that the pH parameter was difficult to interpolate using kriging models. Overall, the *G*-statistics from the FG sampling design were larger that the *G*-statistics from the CG sampling design. The few soil parameters that did not have larger *G*-statistics were approximately equal between CG and FG designs. These results indicate that the FG interpolation models perform better than the CG interpolation models.

Correlograms were constructed using the FG data and are displayed in Figures 3.23 to 3.29. Correlogram results can sometimes be difficult to summarize. Ideally, the parameter of interest will have a strong positive correlation at short separation distances and weaker correlation (i.e. positive or negative) at larger separation distances. Organic

matter and pH have this type of correlation pattern which indicates samples collected with short separation distances display similar OM and pH values (Figures 3.25 and 3.26). Potassium and Zn correlograms also display reasonable correlation structure with a strong positive relationship at small separation distances and a slightly negative relationship at large separation distances (Figures 3.24 and 3.29). These results are logical and expected with most soil properties. However, in some situations correlograms do not display a succinct pattern and may fail to shed light on the underlying spatial pattern. An example of such a situation is displayed in Figure 3.27a and b. In this case, soil NO_3-N has an erratic correlation structure (Figure 3.27a), or an initially negative correlation structure (Figure 3.27b). Both examples make summarization of the underlying NO_3-N spatial pattern difficult. Correlograms for P and NH_4-N are similarly erratic and fluctuate between positive and negative correlation (Figures 3.23 and 3.28). In particular, P and NH_4-N have initially negative correlations at very small separation distances on Field 2 (Figures 3.23b and 3.28b). This is counter-intuitive and opposed to FG variogram models that indicate both parameters are spatially correlated at short distances.

An alternative analysis tool to the correlogram is the cumulative correlogram. Cumulative correlograms for the soil parameters tested are shown in Figures 3.30 to 3.36. All of the soil parameters displayed an initially strong, positive spatial correlation at short separation distances. In addition, spatial correlation steadily decreased to approximately zero or slightly negative values as separation distances among soil samples increased. These results are much more succinct than standard correlograms and more clearly describe the underlying spatial correlation structure of the soil parameters.

One of the most important features of the cumulative correlograms is the maximum I value (I_{max}) (Table 3.6). The I_{max} value for almost all variables on all fields occurs at a lag distance of 20-30 m (i.e. h_{max}). This indicates that the maximum spatial autocorrelation among samples occurs at separation distances in this range. Ideally, I_{max} will be recorded at a maximum, as shown in Figure 3.30b, indicating maximum spatial dependency has been captured. In some cases, the maximum may not be recorded indicating the maximum scale-of-pattern is at separation distances smaller than experimentally measured (Figure 3.31a). Another important feature of the cumulative correlogram is the rapid decrease in I as h increases beyond h_{max} (Table 3.6). If I steadily decreases when $h>h_{max}$ this indicates the pattern of interest is regularly distributed in space (Greig-Smith, 1952; Reich et al., 1994). It also indicates the strength of spatial autocorrelation steadily decreases beyond h_{max}. The decrease in spatial autocorrelation beyond h_{max} is summarized in Table 3.6 for lag distances of h = 50, 70, and 100 m. The mean percent reduction in spatial autocorrelation for h = 70 m (i.e. median separation distance for the three fields) was 58% (median = 64%). When h = 100 m (i.e. the standard, commercial grid design), the mean percent reduction in spatial autocorrelation is 73% (median = 76%). In practical terms, these results suggest standard sampling procedures used to develop variable rate application maps are not sufficient for capturing spatial dependency necessary to properly model soil parameters.

3.4 Summary and Conclusions

Soil samples collected from the CG had significant spatial autocorrelation for all variables, except P, based on the Moran's I statistic. This suggests these data are good candidates for spatial modeling techniques such as kriging. However, based on G-

statistics, the kriging models did not perform well. At least two factors are contributing to this poor performance. First, based on evaluation of the partial Moran's *I* statistic (I_i) it appears some sample locations may exhibit anomalous characteristics that influence the overall value of the Moran's *I* statistic. If this is true, these anomalous samples may lead to the conclusion of significant spatial autocorrelation when in fact the data set is spatially independent at the sampled scale. The Moran's *I* statistic is a composite statistic that evaluates the spatial dependence of a variable at several scales (large scales to small scales). In some cases, techniques such as kriging may not be applicable for a data set despite a significant Moran's *I*.

A second factor contributing to poor model performance is that the separation distance among samples from the CG data is too large to accurately capture small-scale variability. Variogram models for the FG soil parameters had more data values in the interval from lag=0 to lag=range-value when compared with the CG data. This indicates that the FG data had more spatially dependent samples in this critical region of the variogram. The ultimate result was larger *G*-statistics for kriged, FG soil parameters compared to the CG soil parameters.

Based on results from FG analysis with cumulative correlograms, the maximum scale of spatial dependency for the soil parameters is 20 to 30 m. However, the CG data set had a median separation distances in the range of 70 to 75 m. On average, the degree of spatial autocorrelation for all variables was reduced 58% at lags of 70 m when compared with I_{max} values. This reduction increases to 73% at lags of 100 m. Range distance on the variogram, relative to minimum median separation distance for samples, is another indicator of a data sets spatial dependence or independence. In this study,

ranges for the CG data sets were 0 to 210 m and the majority had range values less than 100 m. Since the median minimum separation distances on the CG were approximately 72 m, most people would call variograms for these variables "nugget effect" variograms that lack the necessary spatial dependency for modeling. In practical terms, these results suggest proper spatial modeling of the parameters of interest is precluded due to a lack of necessary spatial dependency among samples.

Standard correlograms were not effective for elucidating scales of autocorrelation (i.e. scales-of-pattern). In some cases the correlation statistic, $\rho(I)$, fluctuated from negative to positive values without any discernible pattern and was not a useful tool for this analysis. However, cumulative correlograms were effective for elucidating the scales-of-pattern in the field and were easily interpreted. The most salient feature of the cumulative correlogram is the value h_{max}. This value indicates the lag at which autocorrelation is the strongest (i.e. the maximum scale-of-pattern). The cumulative correlogram can also elucidate how rapidly autocorrelation decreases beyond h_{max} and where the degree of autocorrelation is constant or random (i.e. the asymptote). Unlike the correlogram and the variogram which describe correlation or variation within specific 'bins' (e.g. 0-10 m, 10-20 m), the cumulative correlogram summarizes spatial autocorrelation within increasingly larger areas of association (e.g. <10 m, <20 m, <30 m). This method of pattern analysis, based closely on the use of contiguous quadrats, lends itself well to the analysis of soil patterns. Most soils develop over catenary sequences and properly identifying changes in soil patterns is essential to developing accurate variable rate application maps. Cumulative correlograms can also be generated to account for distance and direction (i.e. anisotropic cumulative correlograms).

It is not feasible to sample on 15 x 15 m grids to collect data for spatial interpolation. However, when data exist or when time and money allow, the cumulative correlogram is a valuable tool for elucidating soil patterns. It will also be desirable to investigate alternative sampling designs for developing variable rate application maps. It is likely that in most situations sampling soils on 100 x 100 m grids will result in spatially independent data sets. Although these data sets can certainly be 'modeled' with most spatial software, the results will be questionable and will not identify the variability that occurs in fields. We are investigating sampling designs that incorporate a stratified and/or cluster sampling design combined with utilization of readily obtainable auxiliary data sets such as bare soil imagery or elevation models. This approach to sampling is explored more thoroughly in Chapter 4 of this dissertation. Another possibility may include a double sampling approach to acquire larger data sets for interpolation (Scheaffer et al., 1996). Ultimately, the development of sound variable rate application maps will be predicated on sound sampling designs focused on capturing spatial dependency among samples.

3.5 References

Agterberg, F.P. 1984. Trend surface analysis. *In* G.L. Gaile and C.J. Willmott (ed.) Spatial statistics and models. Reidel, Dordrecht, The Netherlands.

Akaike, H. 1977. On entropy maximization principle. *In* P.R. Krishnaiah (ed.) Applications of Statistics. North-Holland, Amsterdam, The Netherlands.

Burgess, T.M., and R. Webster. 1980a. Optimal interpolation and isarithmic mapping of soil properties I: the semivariogram and punctual kriging. J. Soil Sci. 31: 315-331.

Burgess, T.M., and R. Webster. 1980b. Optimal interpolation and isarithmic mapping of soil properties II: block kriging. J. Soil Sci. 31: 333-341.

Czaplewski, R.L., R.M. Reich, and W.A. Bechtold. 1994. Spatial autocorrelation in growth of undisturbed natural pine stands across Georgia. Forest Sci. 40: 314-328.

Fleming, K.L., D.G. Westfall, D.M. Wiens, and M.C. Brodahl. 2000. Evaluating farmer defined management zone maps for variable rate fertilizer application. Precis. Agric. 2: 201-205.

Franzen, D.W., and T.R. Peck. 1995. Sampling for site-specific application. p. 535-551. *In* P.C. Robert et al., (ed.) Site-Specific Management for Agricultural Systems. Proc. Int. Conf., 2nd. March 27-30, 1994. Minneapolis, MN. ASA, CSSA, and SSSA, Madison, WI.

Goovaerts, P., and A.G. Journel. 1995. Integrating soil map information in modeling the spatial variation in continuous soil properties. Eur. J. Soil Sci. 46: 397-414.

Gotway, C.A., R.B. Ferguson, and G.W. Hergert. 1996. The effects of mapping scale on variable rate fertilizer recommendations for corn. p. 321-330. *In* P.C. Robert et al., (ed.) Site-Specific Management for Agricultural Systems. Proc. Int. Conf., 3rd. June 23-26, 1996. Minneapolis, MN. ASA, CSSA, and SSSA, Madison, WI.

Greig-Smith, P. 1952. The use of random and contiguous quadrats in the study of the structure of plant communities. Ann. Bot. 16: 293-316.

Guisan, A., and N.E. Zimmermann. 2000. Predictive habitat distribution models in ecology. Eco. Model. 135:147-186.

Hammond, M.W. 1993. Cost analysis of variable fertility management of phosphorus and potassium for potato production in central Washington. p. 213-228. *In* P.C. Robert et al., (ed.) Soil Specific Crop Management. Proc. Workshop, 1st. April 14-16, 1992. Minneapolis, MN. ASA, CSSA, and SSSA, Madison, WI.

Miller, R.O., J. Kotuby-Amacher, and J.B. Rodriguez. 1998. Western states laboratory proficiency testing program, soil and plant analytical methods. Version 4.10.

Moran, P.A.P. 1948. The interpretation of statistical maps. J. Roy. Stat. Soc. 10: 243-251.

Mueller, T.G., F.J. Pierce, O. Schabenberger, and D.D. Warncke. 2001. Map quality for site-specific fertility management. Soil Sci. Soc. Amer. J. 65:1547-1558.

Reich, R.M., and R.A. Davis. 1998. On-line spatial library for the S-PLUS© statistical software package. Colo. State. Univ., Fort Collins.

Reich, R.M., R.L. Czaplewski, and W.A. Bechtold. 1994. Spatial cross-correlation of undisturbed, natural shortleaf pine stands in northern Georgia. Environ. Ecol. Stat. 1:201-217.

Scheaffer, R.L., W. Mendenhall, and R.L. Ott. 1996. Elementary survey sampling. 5th ed. Duxbury Press, New York.

Schloeder, C.A., N.E. Zimmerman, and M.J. Jacobs. 2001. Comparison of methods for interpolating soil properties using limited data. Soil Sci. Soc. Am. J. 65: 470-479.

Table 3.1 Summary statistics for soil parameters used in analysis. Summary data presented for both coarse (CG) and fine grid (FG). Values are averages; values in parentheses are standard deviations.

Field	Year	Grid	P	K	NO_3-N	NH_4-N	Zn	OM	pH
			----------mg kg^{-1}----------					%	
1	1997	CG	20 (18)	175 (47)	8 (5)	7 (2)	4.3 (1.0)	1.0 (0.2)	7.5 (0.2)
2	1997	CG	13 (5)	190 (40)	12 (5)	3 (1)	2.5 (0.5)	1.0 (0.1)	7.6 (0.1)
1	1998	CG	14 (7)	167 (55)	20 (9)	4 (1)	4.0 (1.0)	1.0 (0.2)	7.6 (0.3)
1	1997	FG	15 (6)	162 (41)	16 (5)	2 (1)	3.8 (1.0)	1.0 (0.3)	7.8 (0.2)
2	1997	FG	12 (4)	183 (30)	11 (4)	4 (1)	2.5 (0.5)	1.1 (0.1)	7.6 (0.2)
1	1998	FG	17 (8)	159 (57)	7 (5)	6 (1)	3.8 (1.0)	1.0 (0.3)	7.7 (0.2)

Table 3.2 Summary statistics for minimum separation distances on coarse grid.

Field	Year	Minimum	First Quartile	Median	Mean	Third Quartile	Maximum
		----------	----------	m	----------	----------	
1	1997	31.1	59.9	75.4	68.4	77	81.9
2	1997	19.6	58	70.5	66	75.5	86.8
1	1998	32.5	60.7	74.1	68.4	76.2	78.7

Table 3.3 Spatial autocorrelation statistics for soil parameters on coarse grid.

Field	Year	Parameter	Moran's *I*	p-value
1	1997	P	0.084	<0.001
1	1997	K	0.119	<0.001
1	1997	OM	0.130	<0.001
1	1997	pH	0.033	<0.001
1	1997	NO_3	0.098	<0.001
1	1997	NH_4	0.114	<0.001
1	1997	Zn	0.071	<0.001
2	1997	P	0.000	0.353
2	1997	K	0.058	<0.001
2	1997	OM	0.087	<0.001
2	1997	pH	0.185	0.012
2	1997	NO_3	0.069	<0.001
2	1997	NH_4	0.038	<0.001
2	1997	Zn	0.047	<0.001
1	1998	P	0.030	<0.001
1	1998	K	0.062	<0.001
1	1998	OM	0.124	<0.001
1	1998	pH	0.052	<0.001
1	1998	NO_3	0.073	<0.001
1	1998	NH_4	0.129	<0.001
1	1998	Zn	0.044	<0.001

Table 3.4 Summary of variogram model parameters for coarse grid samples. Gaussian model used for all variables.

Field	Year	Variable	Nugget	Sill	Range
					---m---
1	1997	P	0	23	94
1	1997	K	26	1336	101
1	1997	OM	0	0	15
1	1997	pH	0	0	102
1	1997	NO_3-N	1	16	116
1	1997	NH_4-N	0	1	21
1	1997	Zn	0	0	77
2	1997	P	36	205	210
2	1997	K	0	1445	10
2	1997	OM	0	0	50
2	1997	pH	0	0	60
2	1997	NO_3-N	0	14	116
2	1997	NH_4-N	0	2	79
2	1997	Zn	0	1	92
1	1998	P	0	42	0
1	1998	K	0	2149	17
1	1998	OM	0	0	15
1	1998	pH	0	0	15
1	1998	NO_3-N	0	61	17
1	1998	NH_4-N	0	2	15
1	1998	Zn	0	1	47

Table 3.5 *G*-statistics for kriged coarse grid data using a Gaussian variogram model.

Field	Year	P	K	OM	pH	NO_3-N	NH_4-N	Zn
1	1997	0.360	0.355	0.396	0.011	0.301	0.263	0.188
2	1997	-0.027	0.255	0.382	0.023	0.220	0.116	0.120
1	1998	0.033	0.166	0.498	0.044	0.167	0.339	0.056

Table 3.6 Summary statistics for cumulative correlograms for all variables. I_{max} is maximum I statistic observed; values in parentheses indicate lag (h) where value was observed. I_{50}, I_{70}, and I_{100} are Moran's I values observed at lags of 50, 70, and 100 m respectively; values in parentheses indicate the percent decrease in spatial autocorrelation compared to I_{max} values.

Field	Year	I-value	P	K	OM	pH	NO_3-N	NH_4-N	Zn
1	1997	I_{max}	0.468 (18 m)	0.649 (18 m)	0.841 (18 m)	0.258 (18 m)	0.325 (18 m)	0.274 (18 m)	0.452 (18 m)
1	1997	I_{50}	0.292 (38%)	0.519 (20%)	0.682 (19%)	0.196 (24%)	0.172 (47%)	0.146 (47%)	0.197 (56%)
1	1997	I_{70}	0.197 (58%)	0.432 (33%)	0.561 (33%)	0.165 (36%)	0.130 (60%)	0.116 (58%)	0.130 (71%)
1	1997	I_{100}	0.110 (76%)	0.326 (50%)	0.414 (51%)	0.122 (53%)	0.060 (82%)	0.073 (73%)	0.085 (81%)
2	1997	I_{max}	0.268 (27 m)	0.517 (18 m)	0.610 (18 m)	0.211 (18 m)	0.236 (18 m)	0.499 (18 m)	0.514 (27 m)
2	1997	I_{50}	0.131 (51%)	0.287 (44%)	0.281 (54%)	0.058 (72%)	0.115 (52%)	0.181 (64%)	0.268 (48%)
2	1997	I_{70}	0.067 (75%)	0.187 (64%)	0.157 (74%)	0.020 (91%)	0.085 (64%)	0.052 (90%)	0.174 (66%)
2	1997	I_{100}	0.008 (97%)	0.075 (85%)	0.059 (90%)	-0.001 (100%	0.056 (76%)	-0.016 (100%)	0.078 (85%)
1	1998	I_{max}	0.459 (18 m)	0.829 (18 m)	0.814 (18 m)	0.253 (36 m)	0.545 (18 m)	0.422 (18 m)	0.382 (18 m)
1	1998	I_{50}	0.261 (43%)	0.683 (18%)	0.659 (19%)	0.223 (12%)	0.379 (30%)	0.187 (56%)	0.206 (46%)
1	1998	I_{70}	0.166 (64%)	0.567 (32%)	0.546 (33%)	0.193 (24%)	0.295 (46%)	0.129 (69%)	0.133 (75%)
1	1998	I_{100}	0.087 (81%)	0.426 (49%)	0.417 (49%)	0.164 (35%)	0.237 (57%)	0.078 (81%)	0.094 (75%)

Table 3.7 Spatial autocorrelation statistics for soil parameters on fine grid.

Field	Year	Parameter	Moran's *I*	p-value
1	1997	P	0.098	<0.001
1	1997	K	0.291	<0.001
1	1997	OM	0.287	<0.001
1	1997	pH	0.104	<0.001
1	1997	NO_3	0.167	<0.001
1	1997	NH_4	0.078	<0.001
1	1997	Zn	0.081	<0.001
2	1997	P	0.042	<0.001
2	1997	K	0.105	<0.001
2	1997	OM	0.102	<0.001
2	1997	pH	0.028	<0.001
2	1997	NO_3	0.059	<0.001
2	1997	NH_4	0.061	<0.001
2	1997	Zn	0.100	<0.001
1	1998	P	0.043	<0.001
1	1998	K	0.108	<0.001
1	1998	OM	0.100	<0.001
1	1998	pH	0.025	<0.001
1	1998	NO_3	0.060	<0.001
1	1998	NH_4	0.062	<0.001
1	1998	Zn	0.094	<0.001

Table 3.8 Summary of variogram model parameters for fine grid samples. Gaussian model used for all variables.

Field	Year	Variable	Nugget	Sill	Range
					---m---
1	1997	P	13	70	40
1	1997	K	313	2477	65
1	1997	OM	0	0	63
1	1997	pH	0	0	3
1	1997	NO_3-N	2	18	27
1	1997	NH_4-N	0	2	16
1	1997	Zn	0	1	15
2	1997	P	0	20	13
2	1997	K	215	958	62
2	1997	OM	0	0	100
2	1997	pH	0	0	0
2	1997	NO_3-N	0	13	13
2	1997	NH_4-N	0	2	42
2	1997	Zn	0	0	53
1	1998	P	0	20	13
1	1998	K	208	960	62
1	1998	OM	0	0	60
1	1998	pH	0	0	0
1	1998	NO_3-N	0	13	13
1	1998	NH_4-N	0	2	44
1	1998	Zn	0	0	58

Table 3.9 *G*-statistics for kriged fine grid data using a Gaussian variogram model.

Field	Year	P	K	OM	pH	NO_3-N	NH_4-N	Zn
1	1997	0.30698	0.80446	0.75279	-0.002	0.427	0.334	0.243
2	1997	0.148	0.520	0.634	0.070	0.155	0.405	0.544
1	1998	0.170	0.564	0.606	-0.036	0.145	0.410	0.450

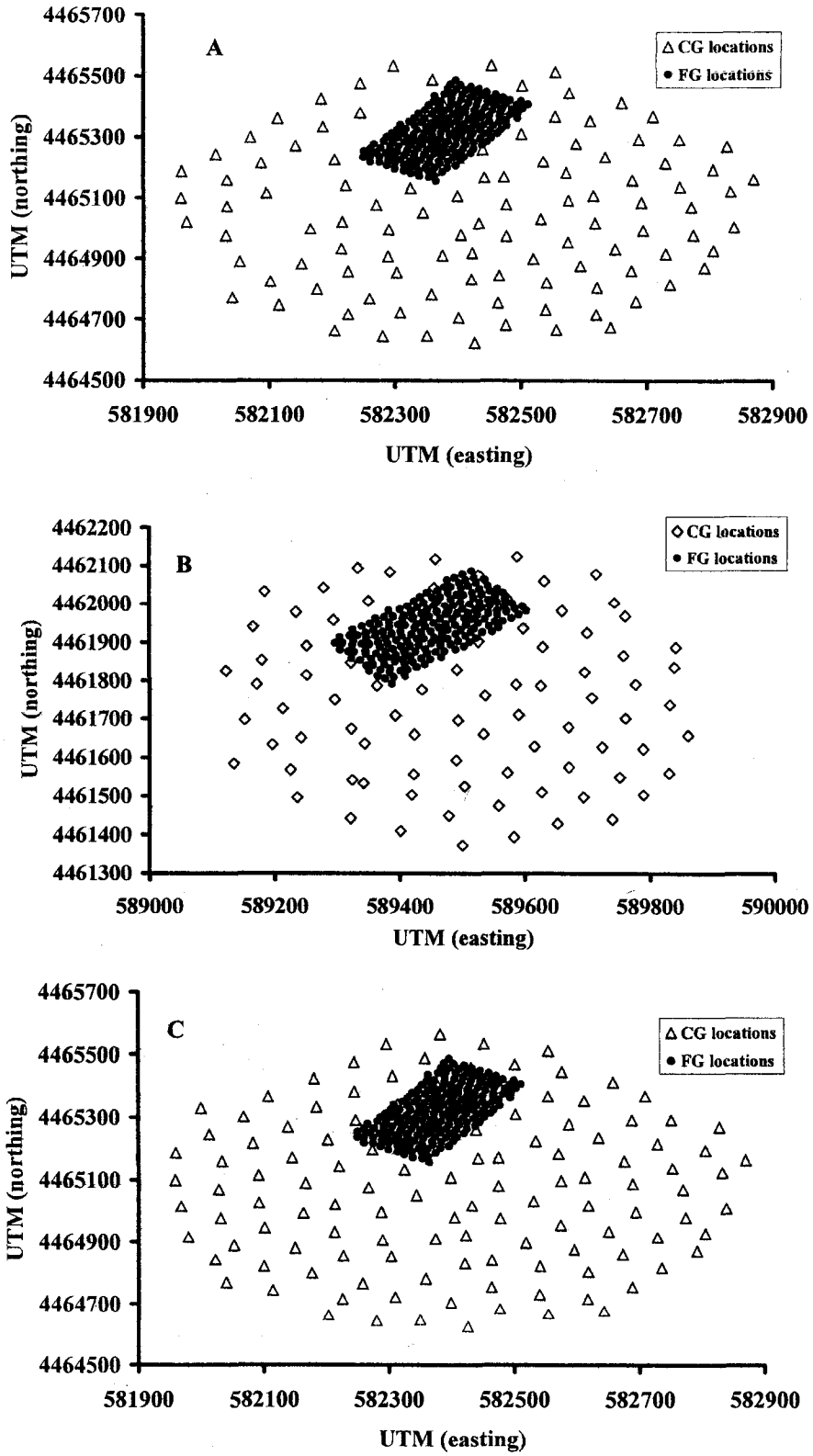

Figure 3.1 Coarse grid and fine grid sampling locations for A) Field 1, 1997, B) Field 2, 1997, and C) Field 1, 1998.

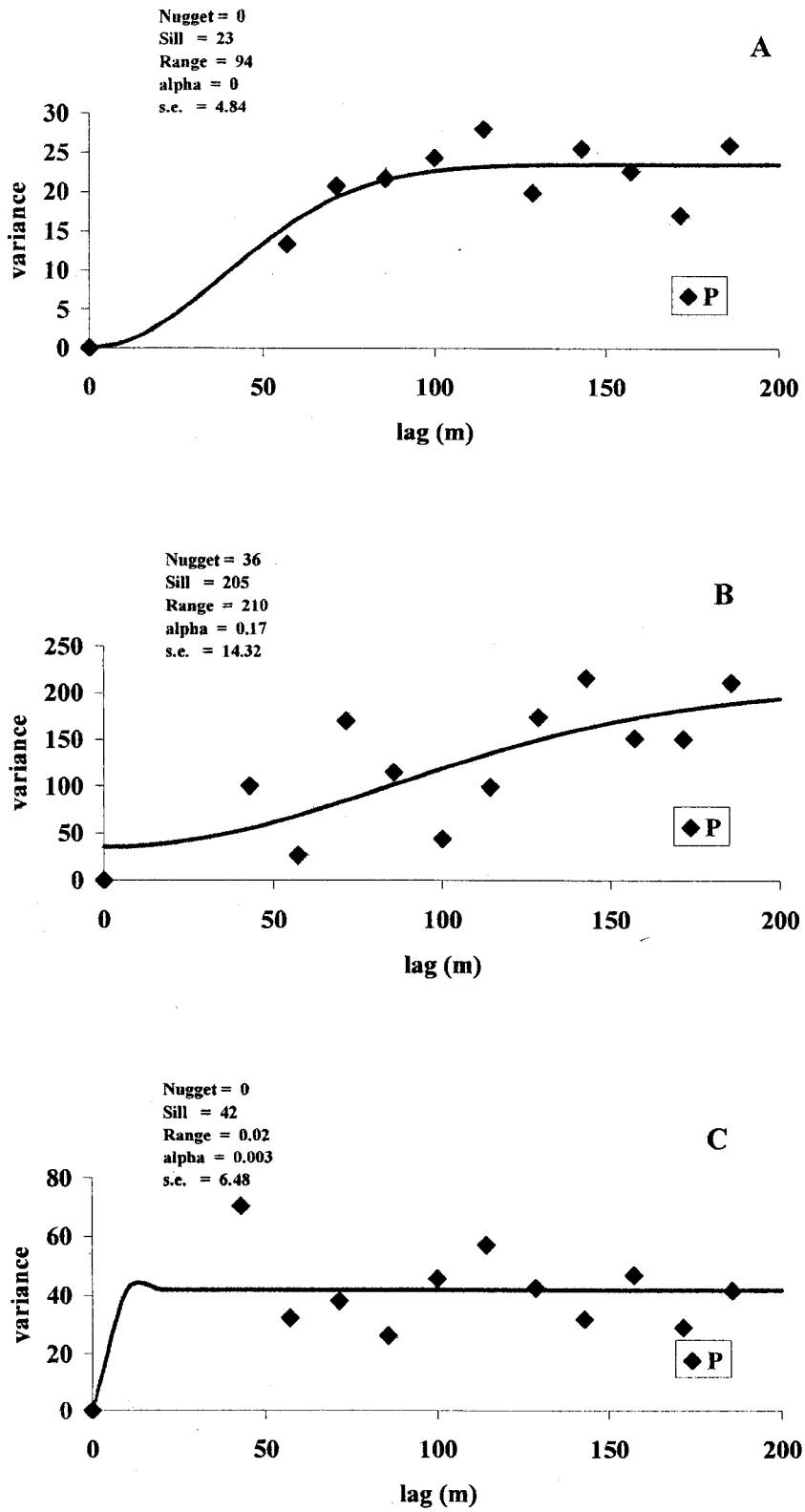

Figure 3.2 Variogram models for P based on coarse grid samples; Gaussian model; A) Field 1, 1997, B) Field 2, 1997, and C) Field 1, 1998.

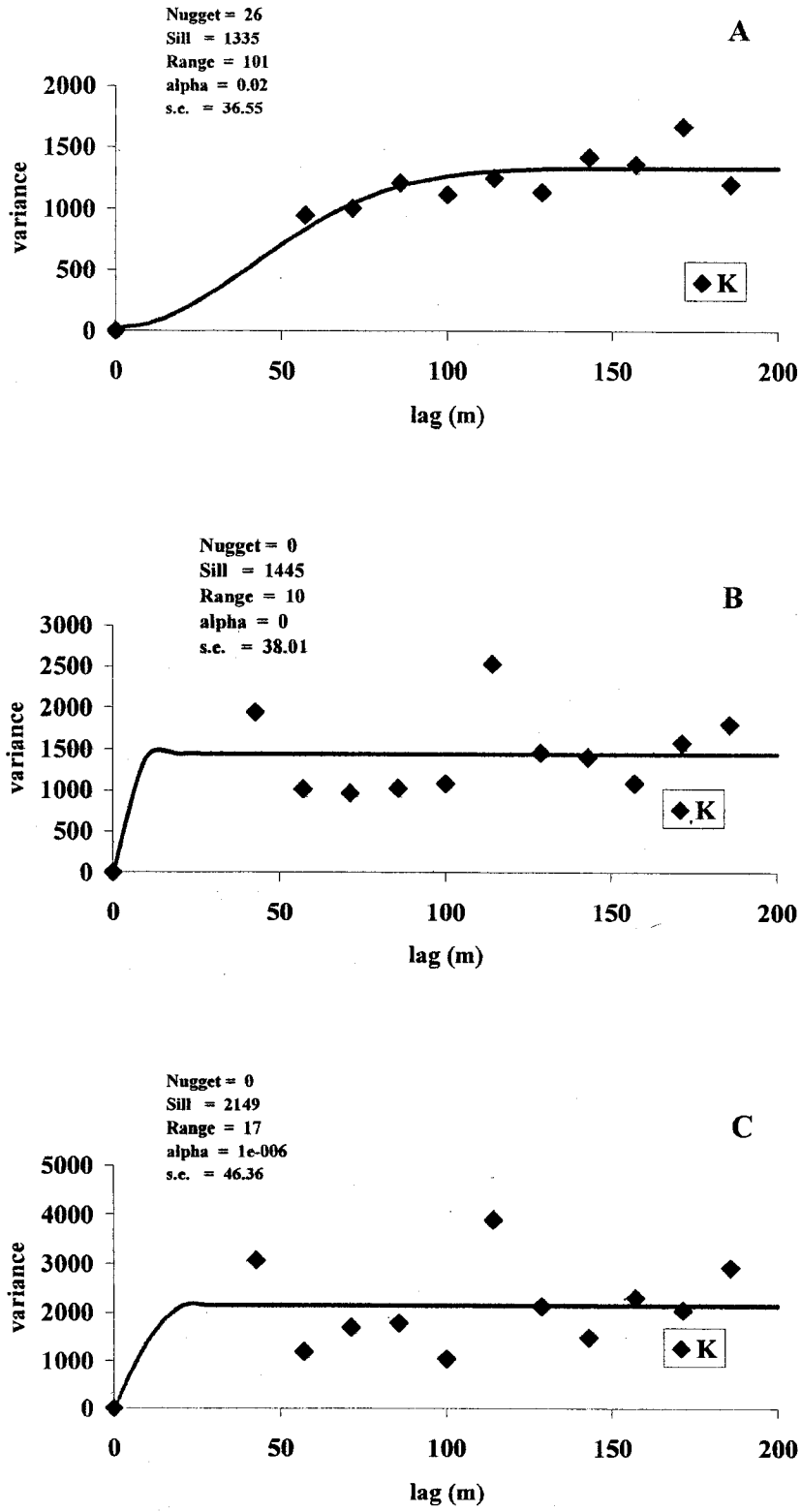

Figure 3.3 Variogram models for K based on coarse grid samples; Gaussian model; A) Field 1, 1997, B) Field 2, 1997, and C) Field 1, 1998.

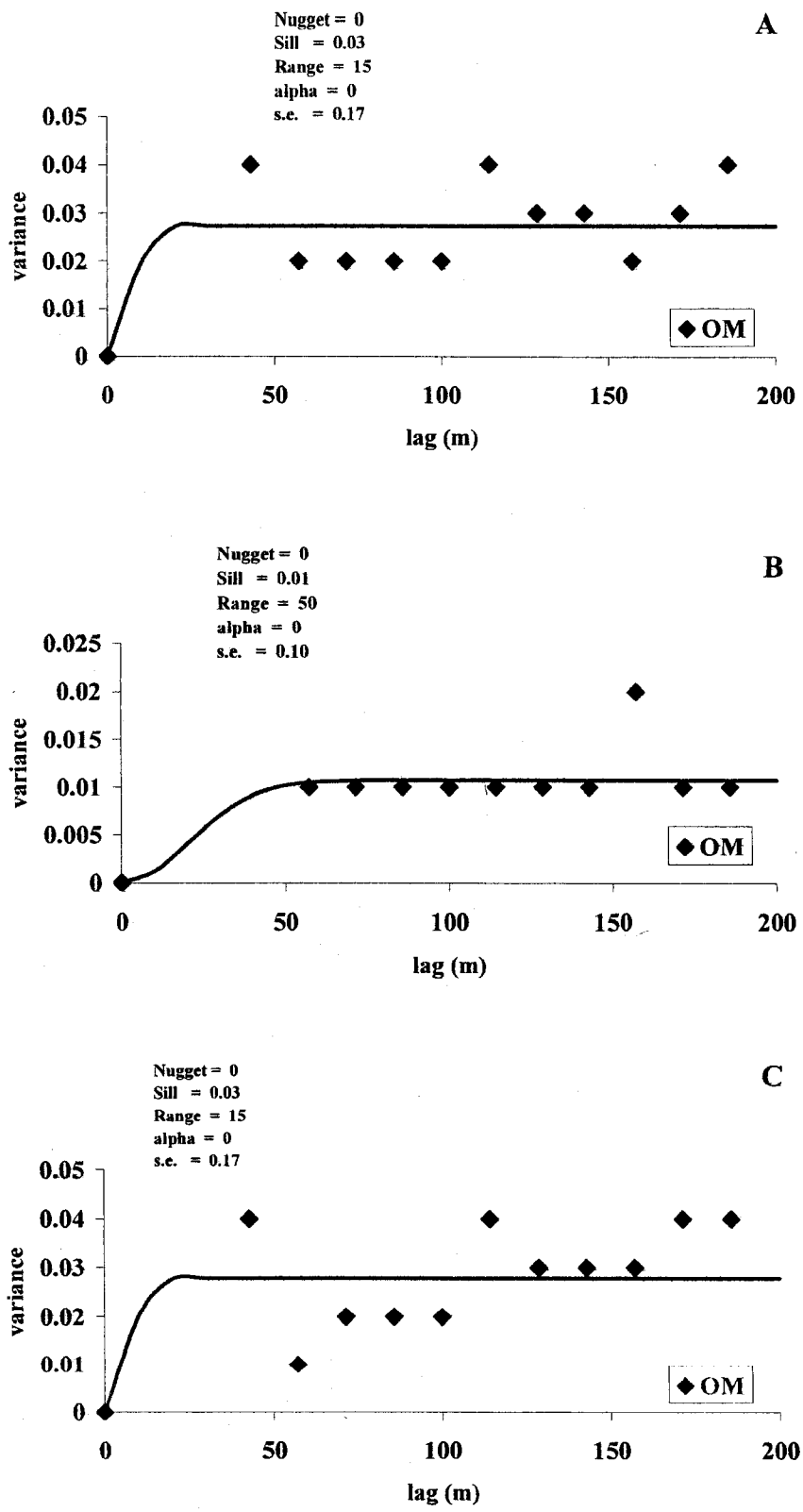

Figure 3.4 Variogram models for OM based on coarse grid samples; Gaussian model; A) Field 1, 1997, B) Field 2, 1997, and C) Field 1, 1998.

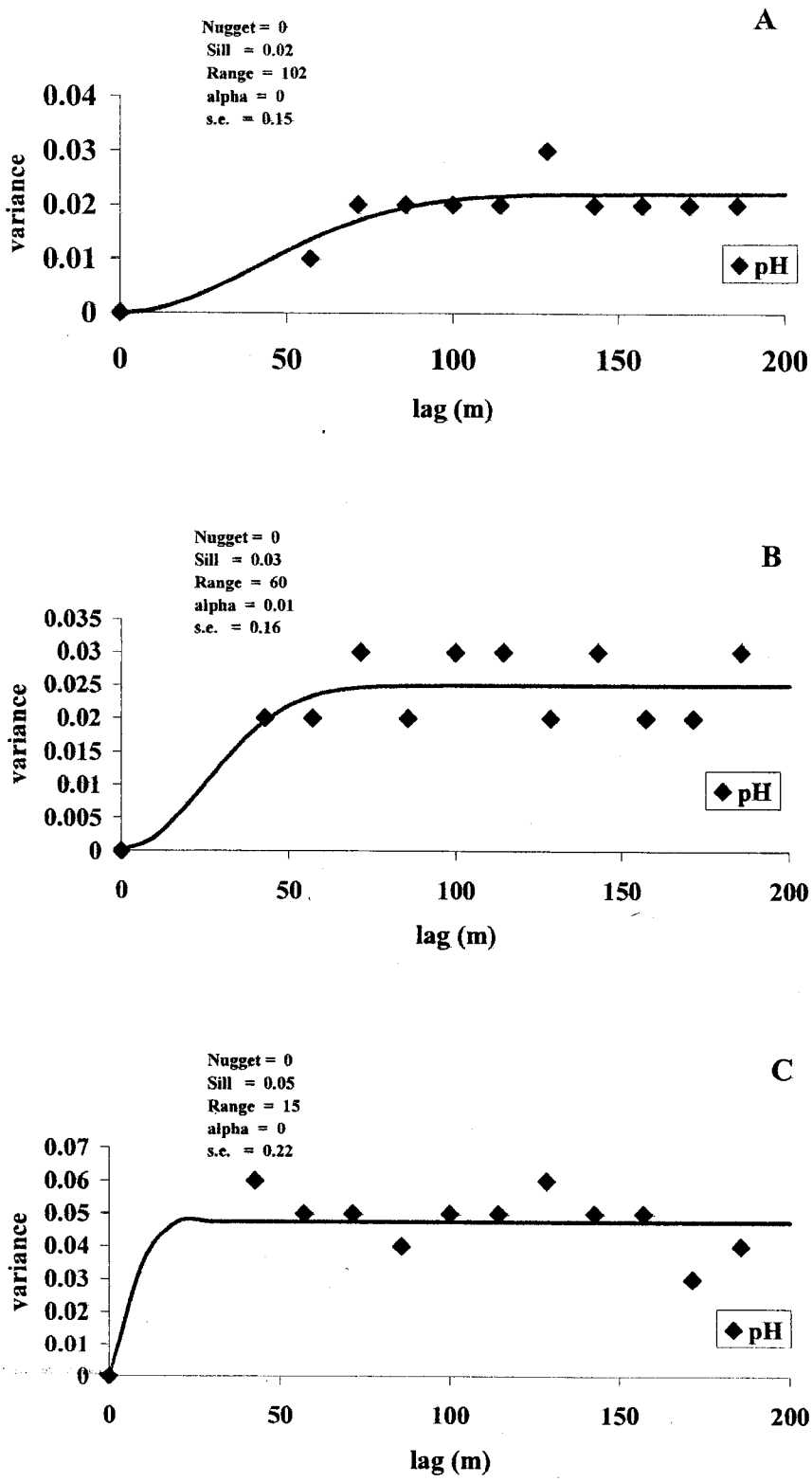

Figure 3.5 Variogram models for pH based on coarse grid samples; Gaussian model; A) Field 1, 1997, B) Field 2, 1997, and C) Field 1, 1998.

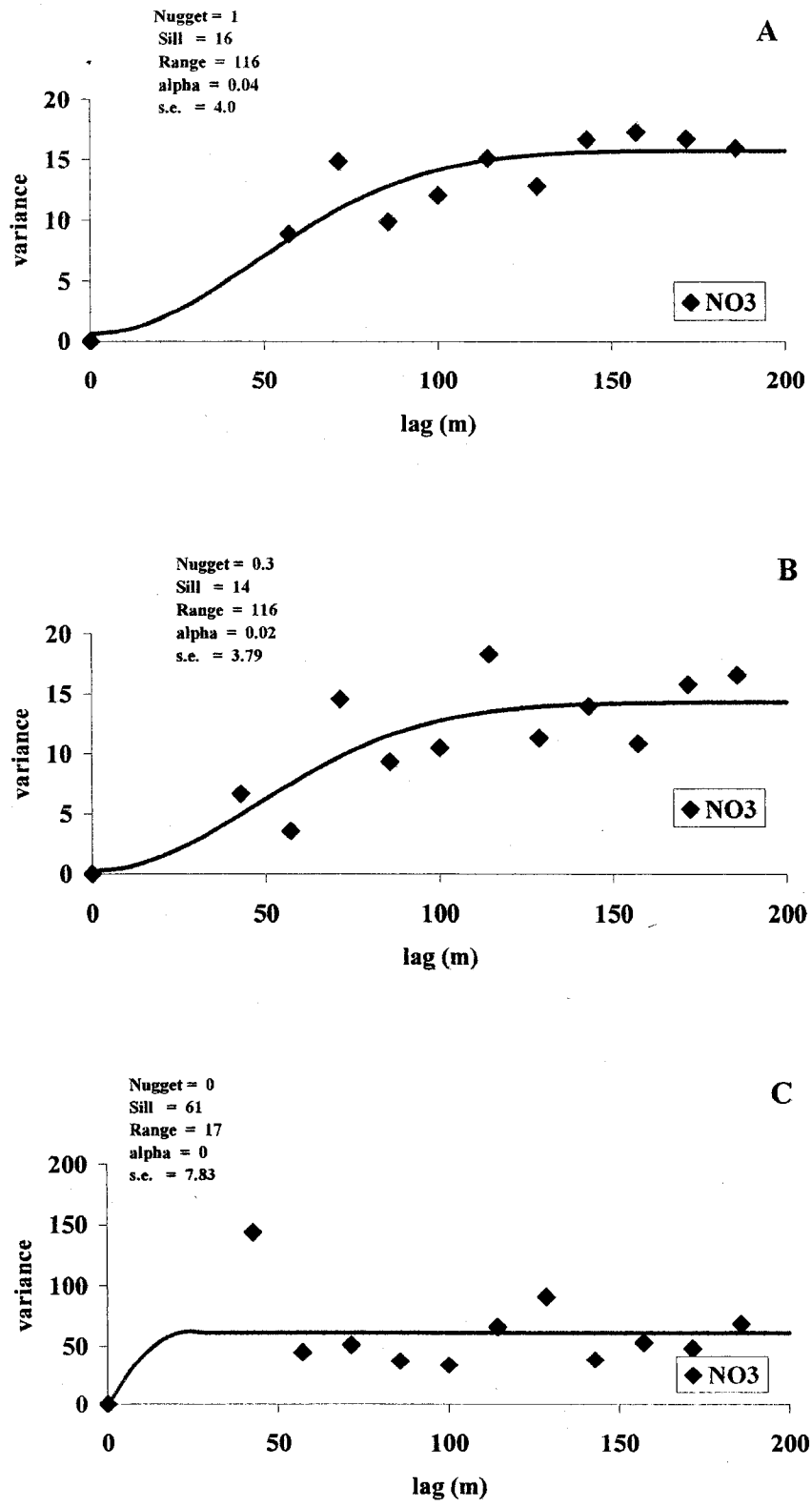

Figure 3.6 Variogram models for NO_3-N based on coarse grid samples; Gaussian model; A) Field 1, 1997, B) Field 2, 1997, and C) Field 1, 1998.

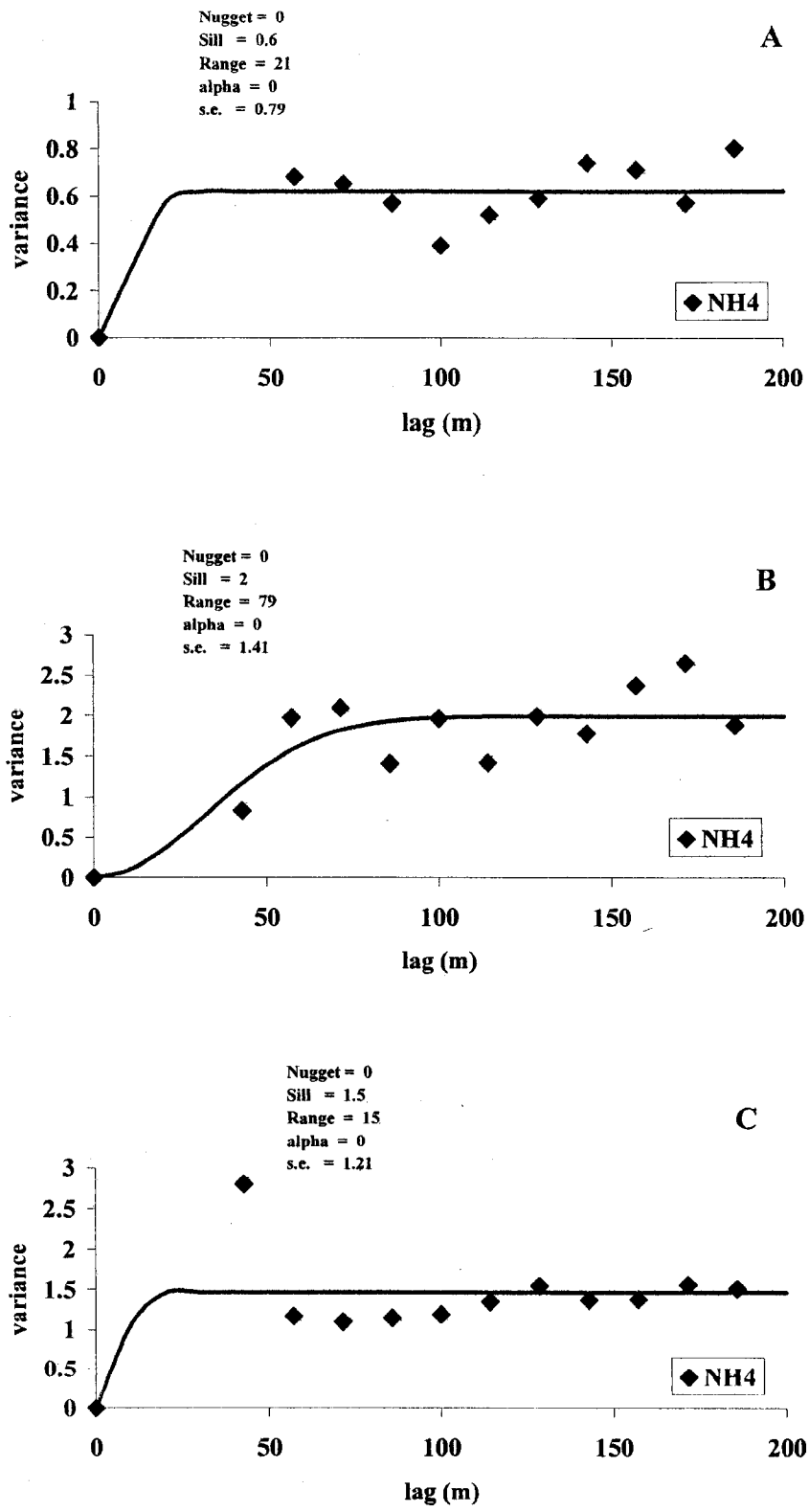

Figure 3.7 Variogram models for NH_4-N based on coarse grid samples; Gaussian model; A) Field 1, 1997, B) Field 2, 1997, and C) Field 1, 1998.

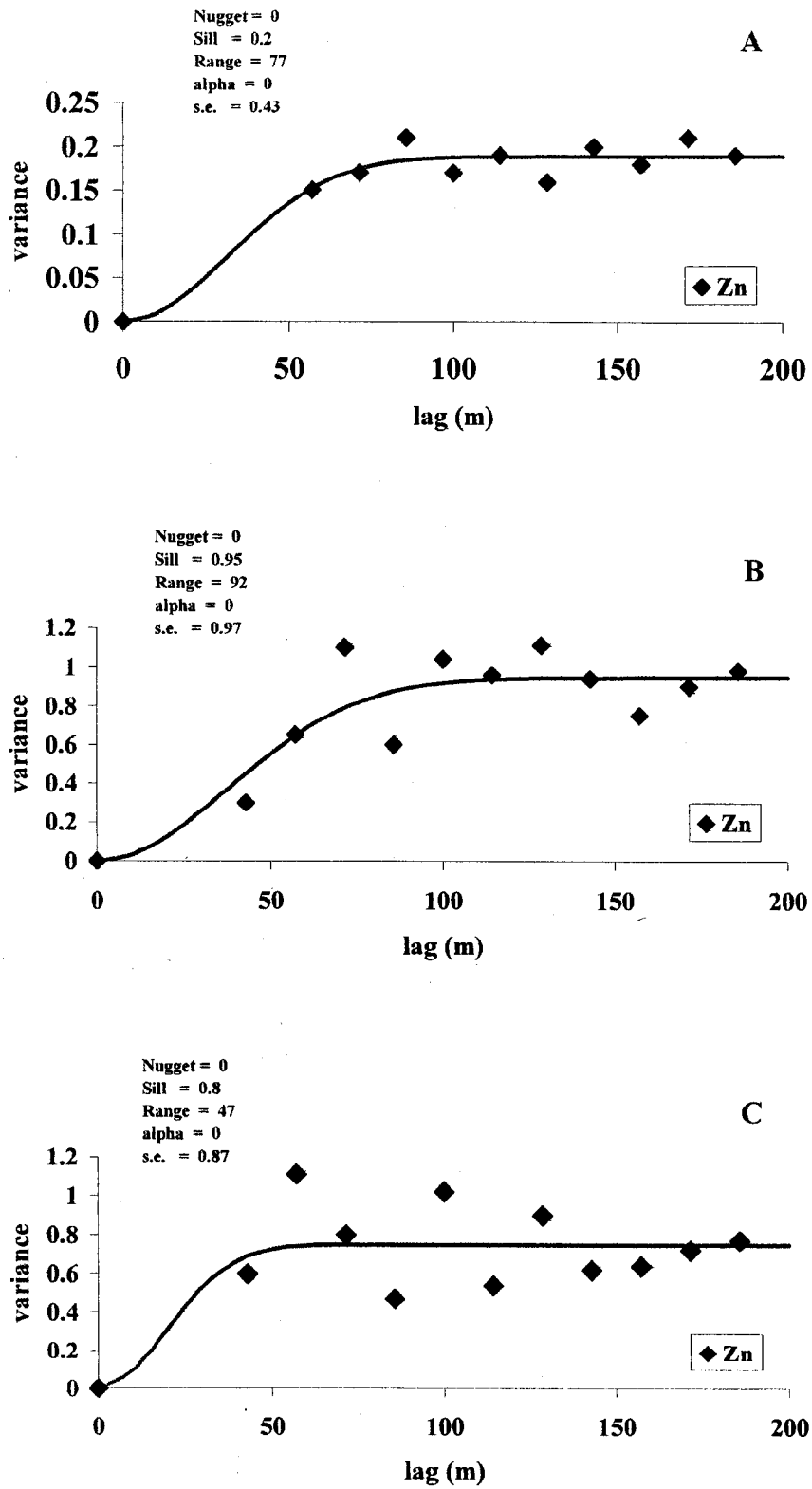

Figure 3.8 Variogram models for Zn based on coarse grid samples; Gaussian model; A) Field 1, 1997, B) Field 2, 1997, and C) Field 1, 1998.

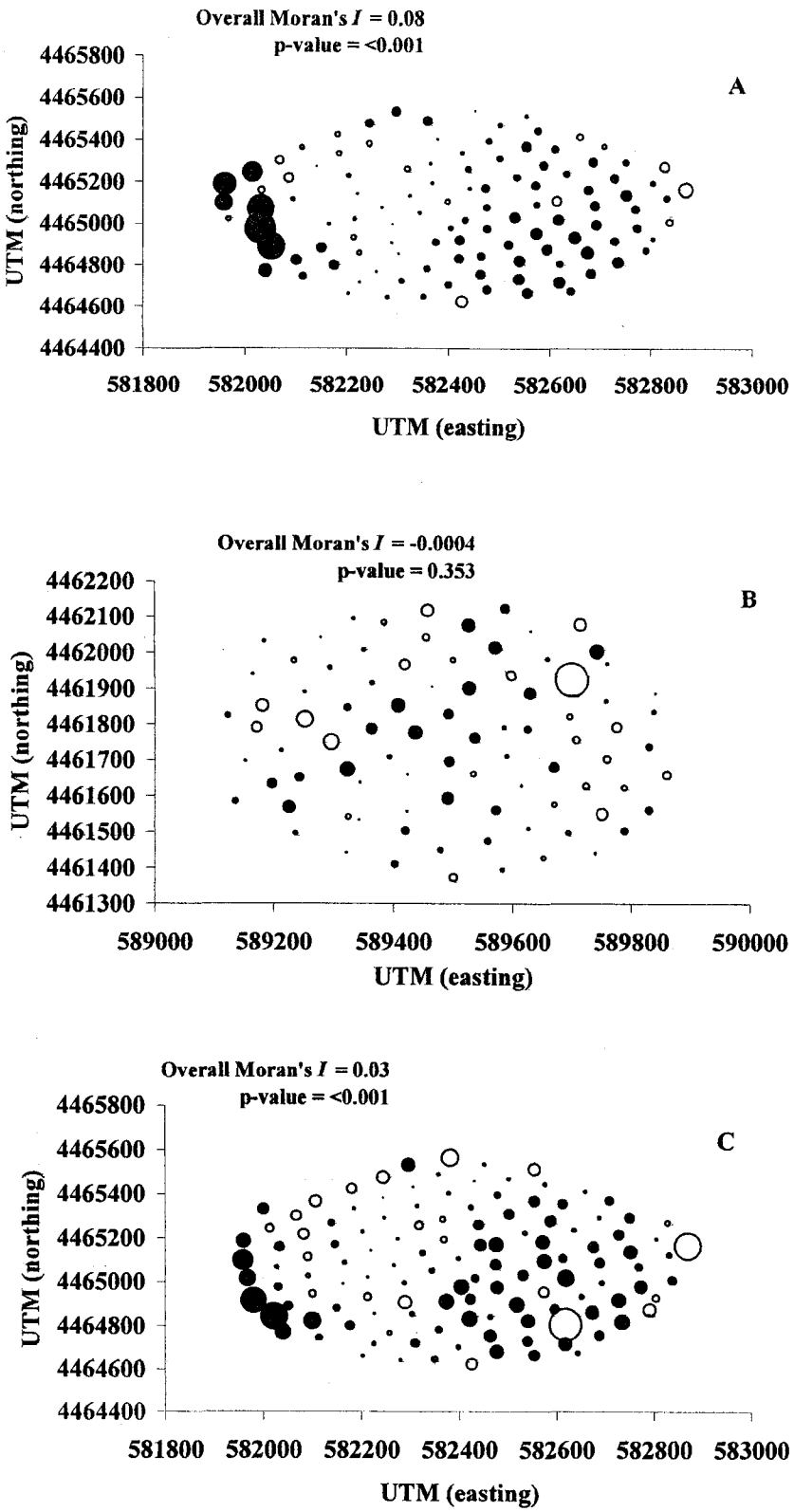

Figure 3.9 Spatial distribution of point autocorrelation statistic (I_i) for P. Magnitude of partial value is indicated by area of circle. Negative values are open circles. A) Field 1, 1997, B) Field 2, 1997, and C) Field 1,1998.

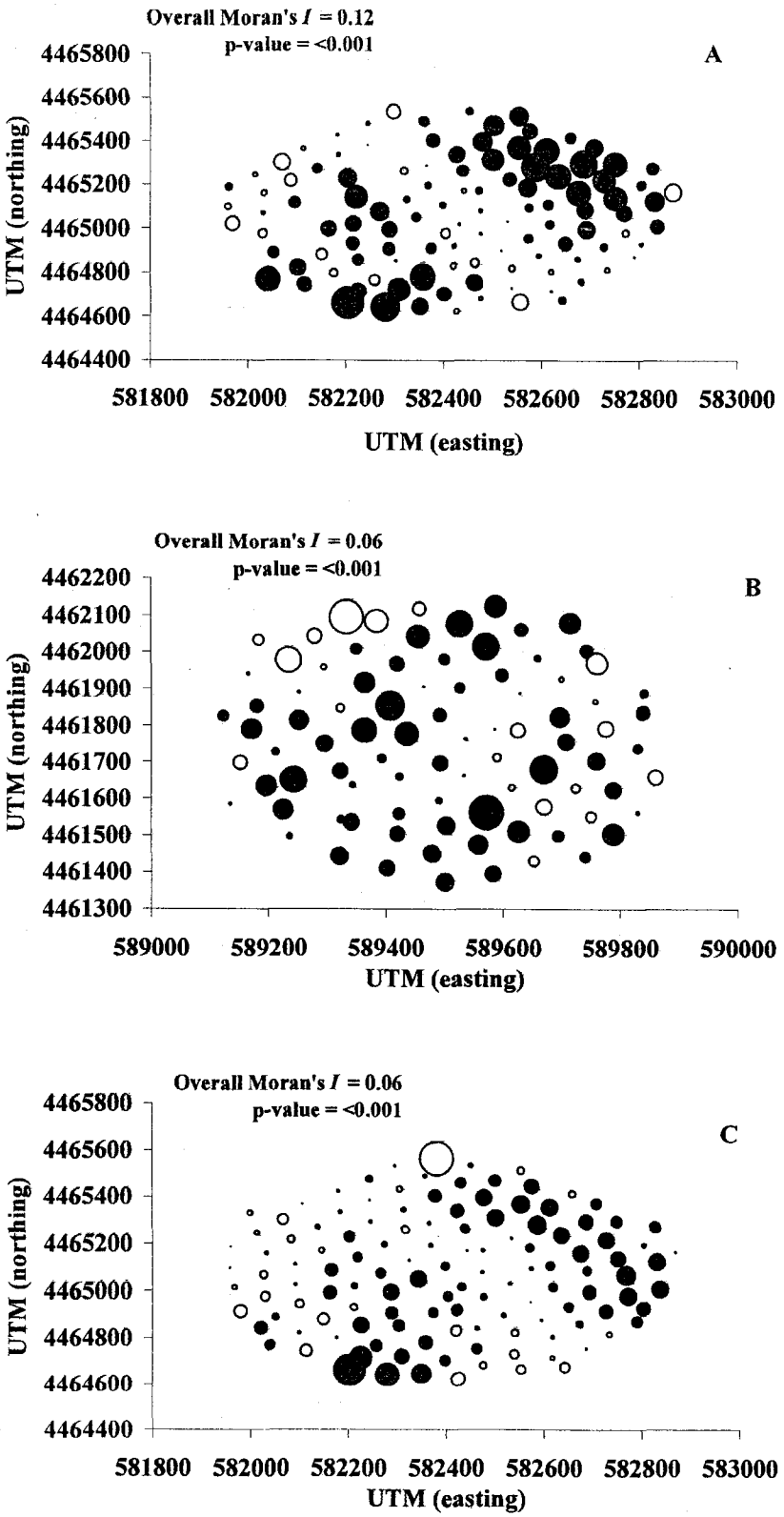

Figure 3.10 Spatial distribution of point autocorrelation statistic (I_i) for K. Magnitude of partial value is indicated by area of circle. Negative values are open circles. A) Field 1, 1997, B) Field 2, 1997, and C) Field 1,1998.

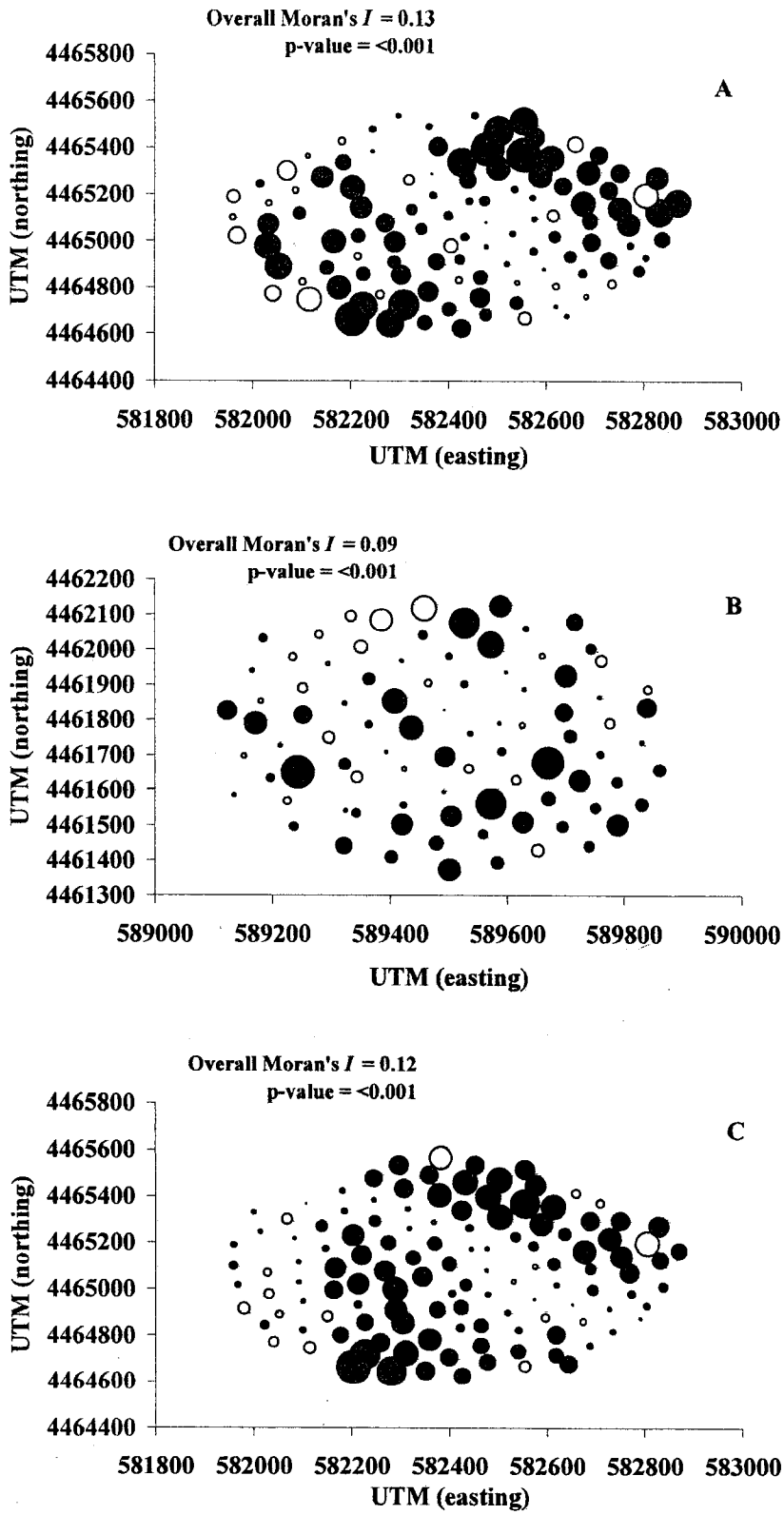

Figure 3.11 Spatial distribution of point autocorrelation statistic (I_i) for OM. Magnitude of partial value is indicated by area of circle. Negative values are open circles. A) Field 1, 1997, B) Field 2, 1997, and C) Field 1,1998.

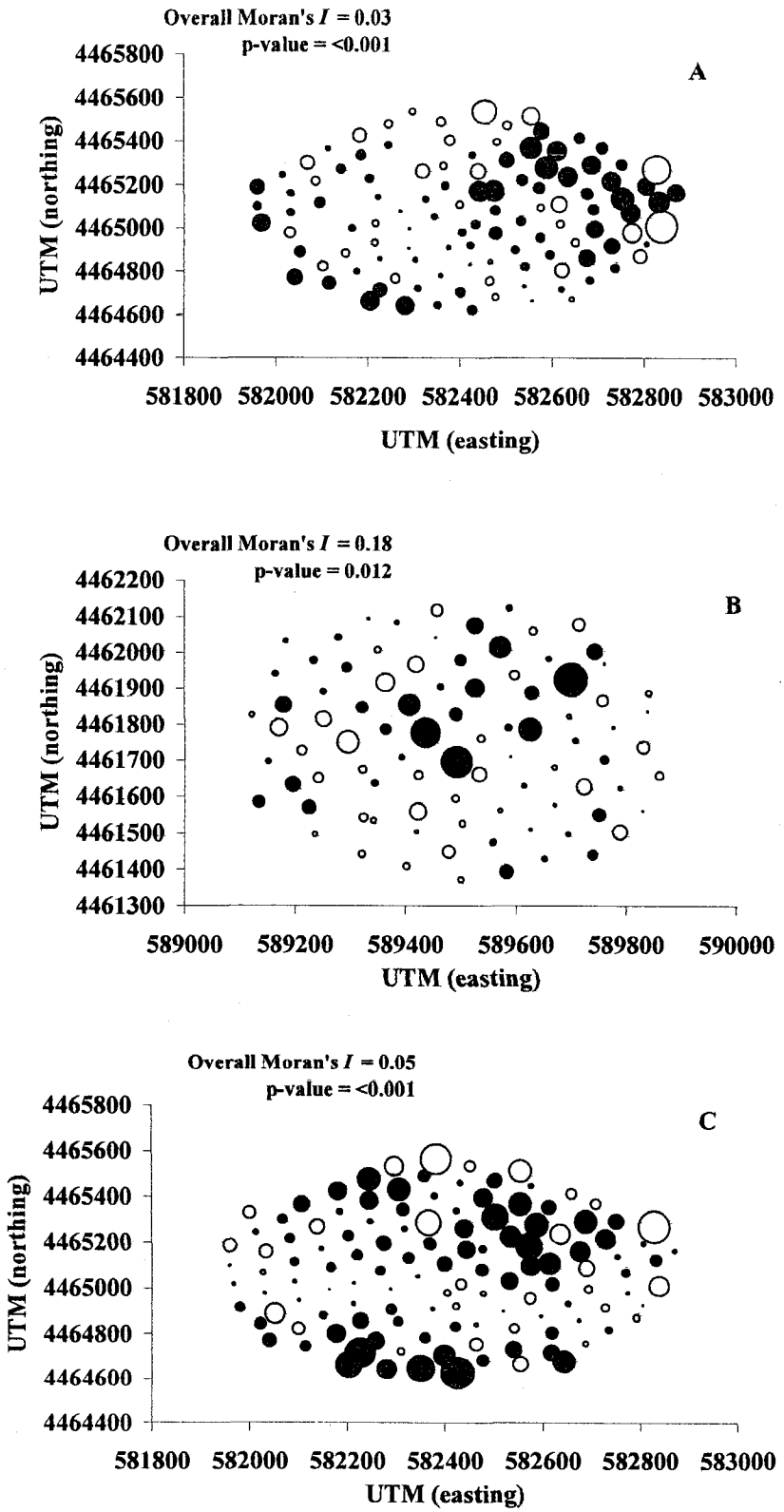

Figure 3.12 Spatial distribution of point autocorrelation statistic (I_i) for pH. Magnitude of partial value is indicated by area of circle. Negative values are open circles. A) Field 1, 1997, B) Field 2, 1997, and C) Field 1,1998.

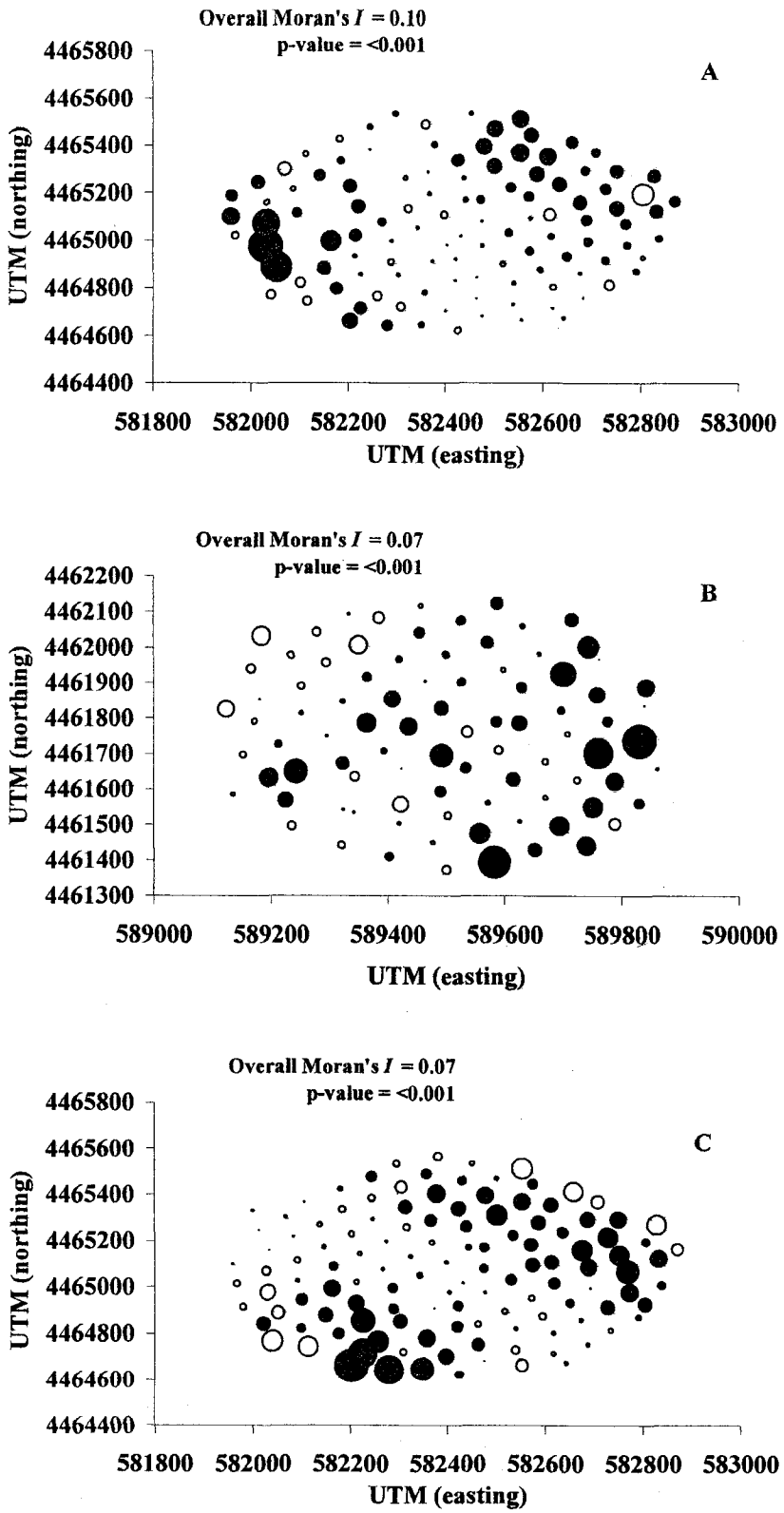

Figure 3.13 Spatial distribution of point autocorrelation statistic (I_i) for NO_3-N. Magnitude of partial value is indicated by area of circle. Negative values are open circles. A) Field 1, 1997, B) Field 2, 1997, and C) Field 1,1998.

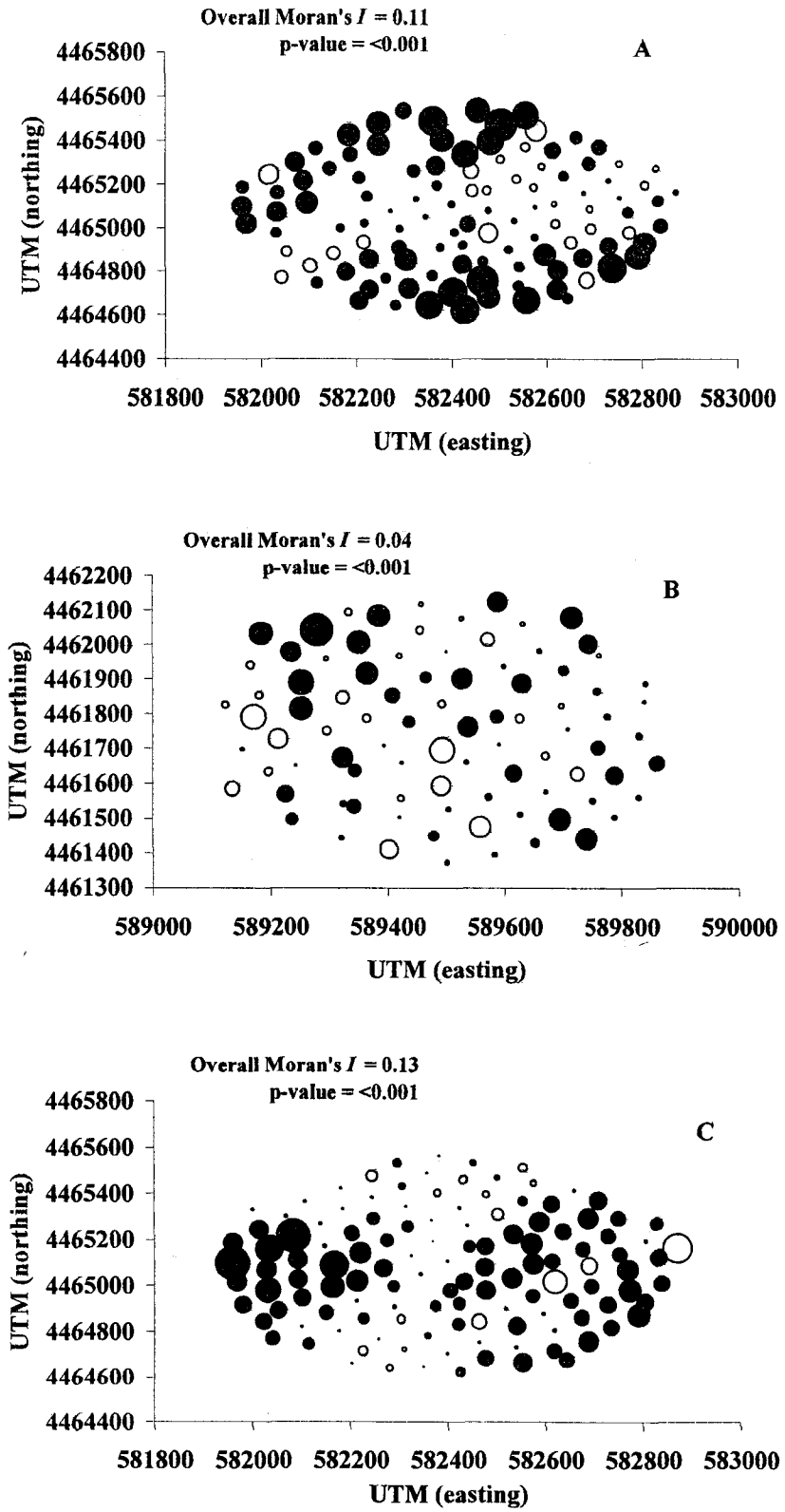

Figure 3.14 Spatial distribution of point autocorrelation statistic (I_i) for NH_4-N. Magnitude of partial value is indicated by area of circle. Negative values are open circles. A) Field 1, 1997, B) Field 2, 1997, and C) Field 1,1998.

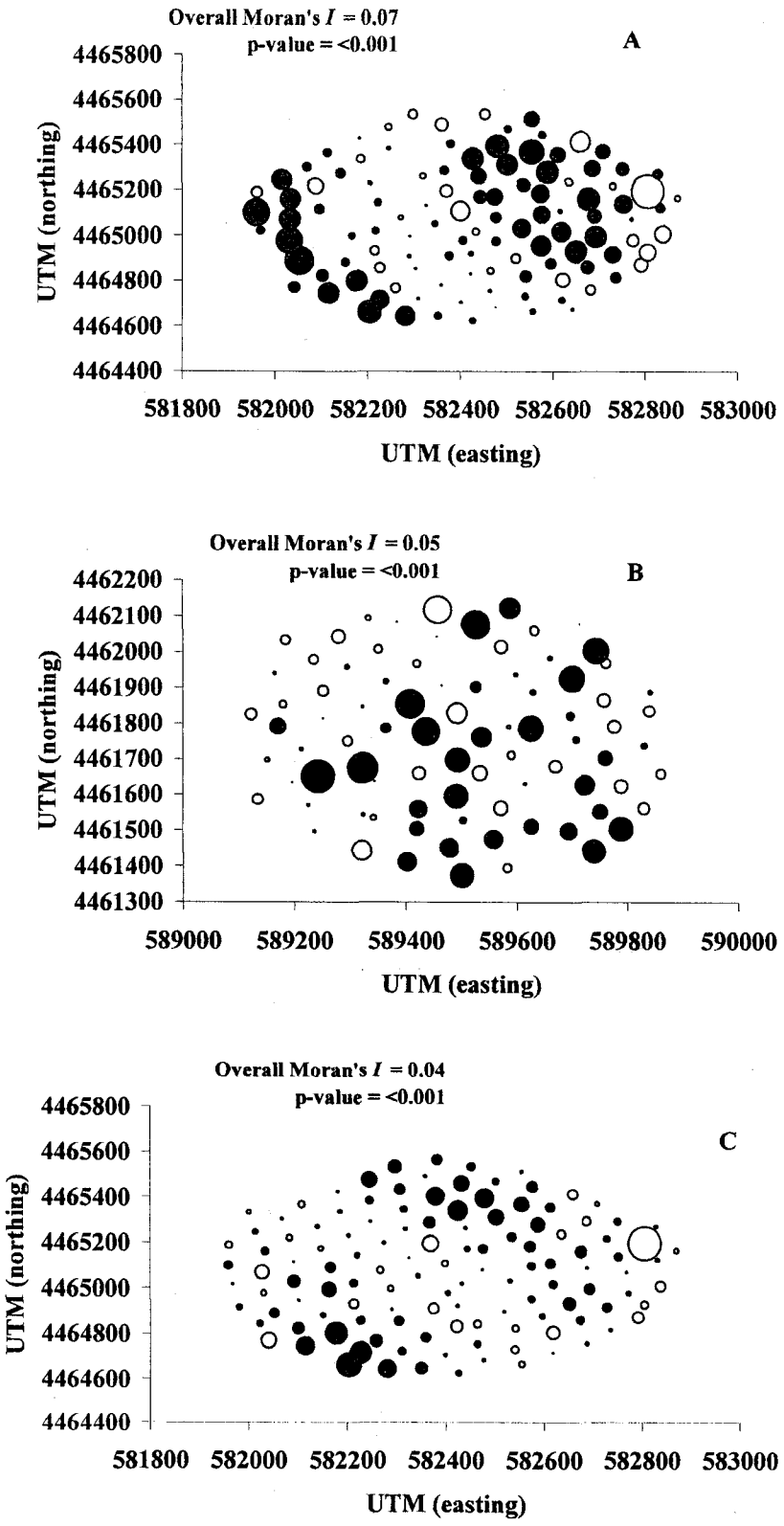

Figure 3.15 Spatial distribution of point autocorrelation statistic (I_i) for Zn. Magnitude of partial value is indicated by area of circle. Negative values are open circles. A) Field 1, 1997, B) Field 2, 1997, and C) Field 1,1998.

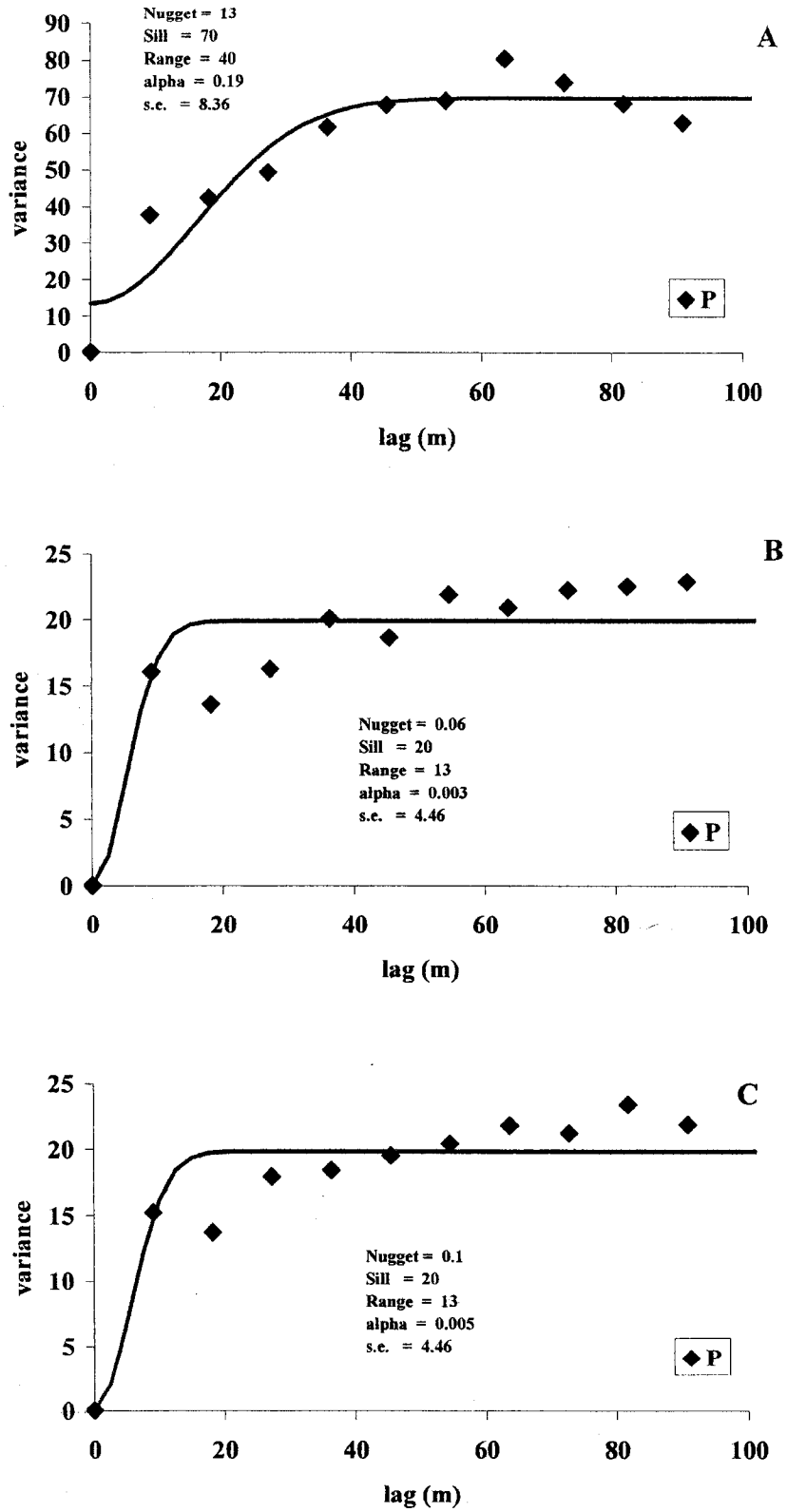

Figure 3.16 Variogram models for P based on fine grid samples; Gaussian model; A) Field 1, 1997, B) Field 2, 1997, and C) Field 1, 1998.

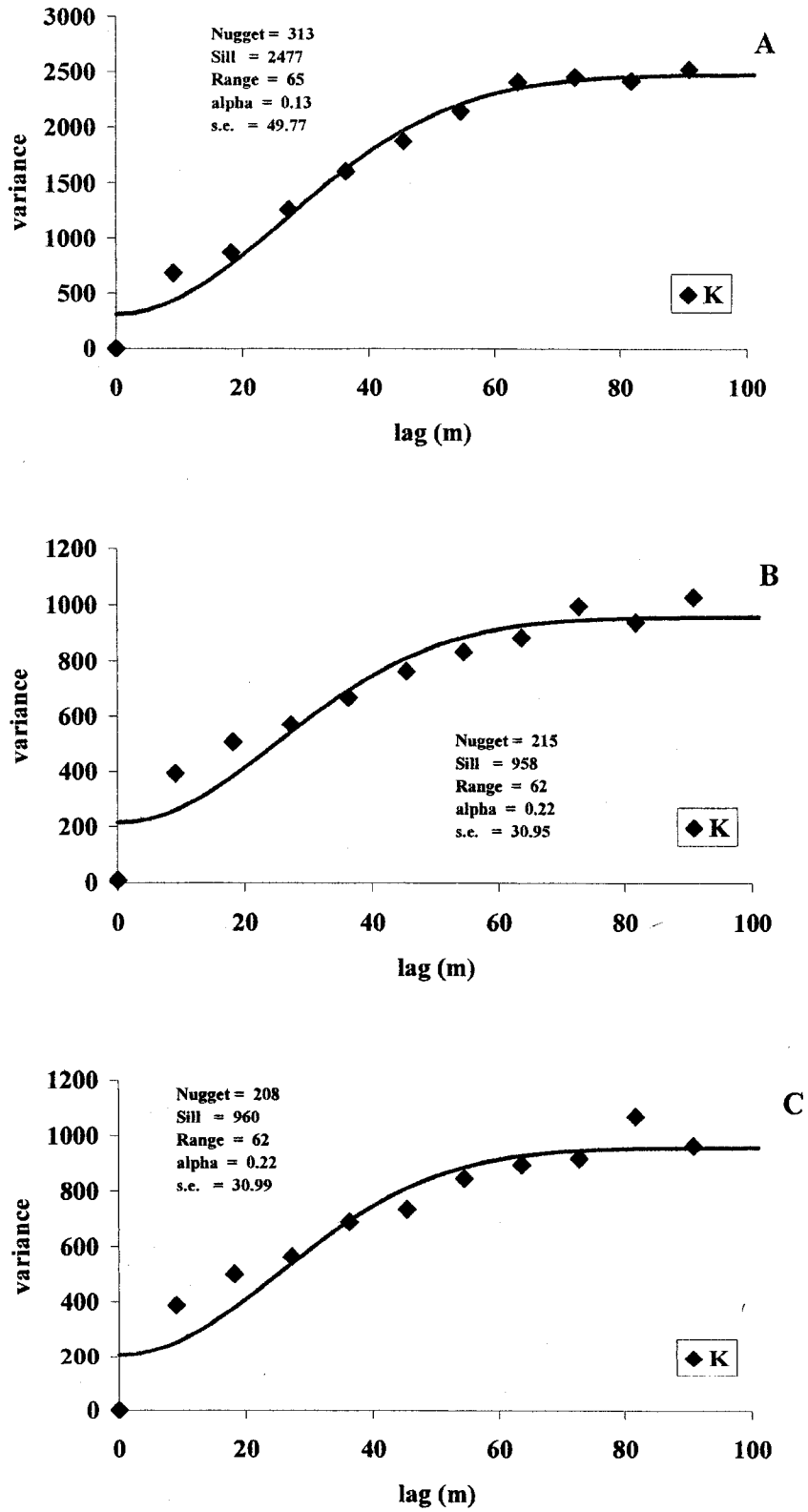

Figure 3.17 Variogram models for K based on fine grid samples; Gaussian model; A) Field 1, 1997, B) Field 2, 1997, and C) Field 1, 1998.

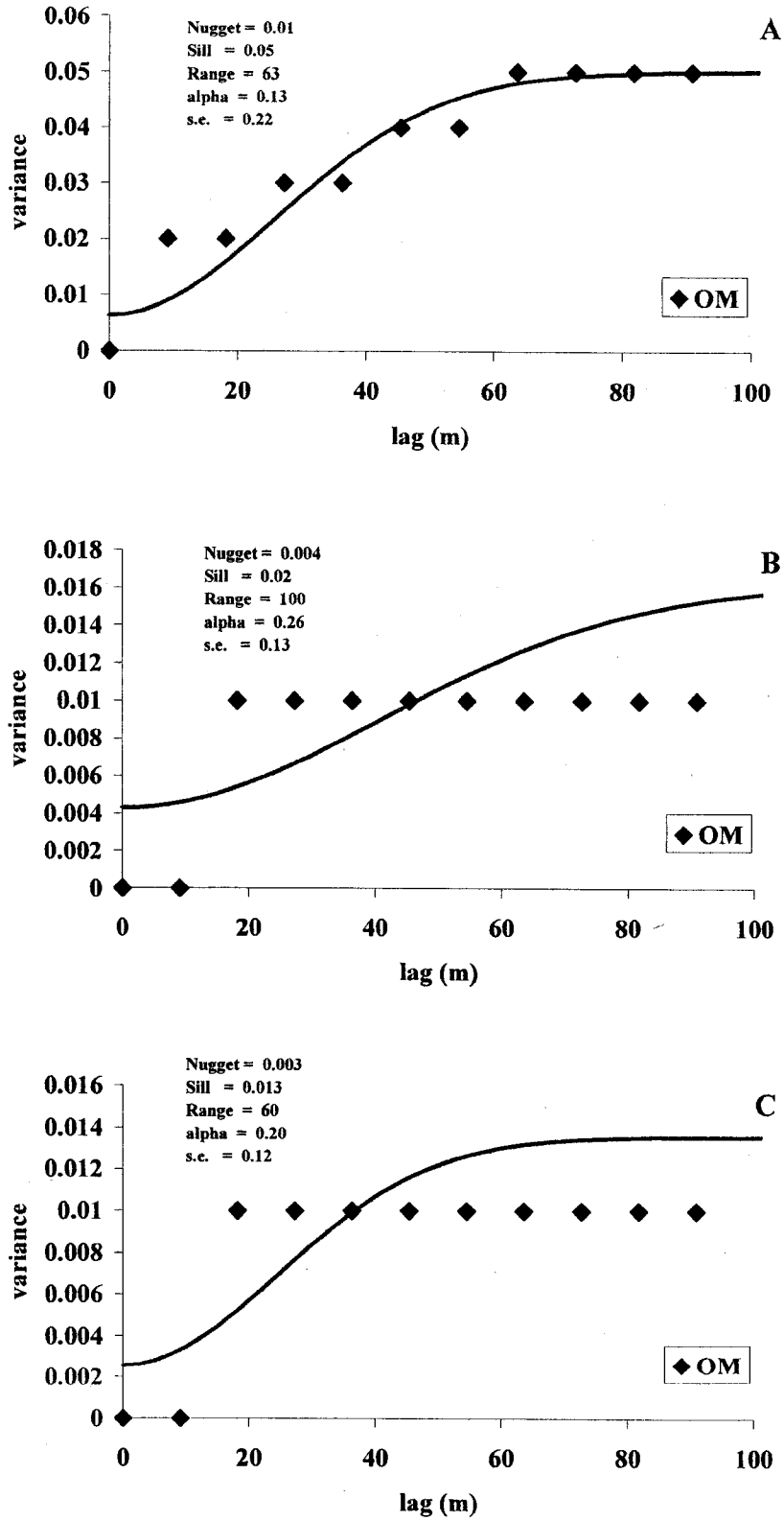

Figure 3.18 Variogram models for OM based on fine grid samples; Gaussian model; A) Field 1, 1997, B) Field 2, 1997, and C) Field 1, 1998.

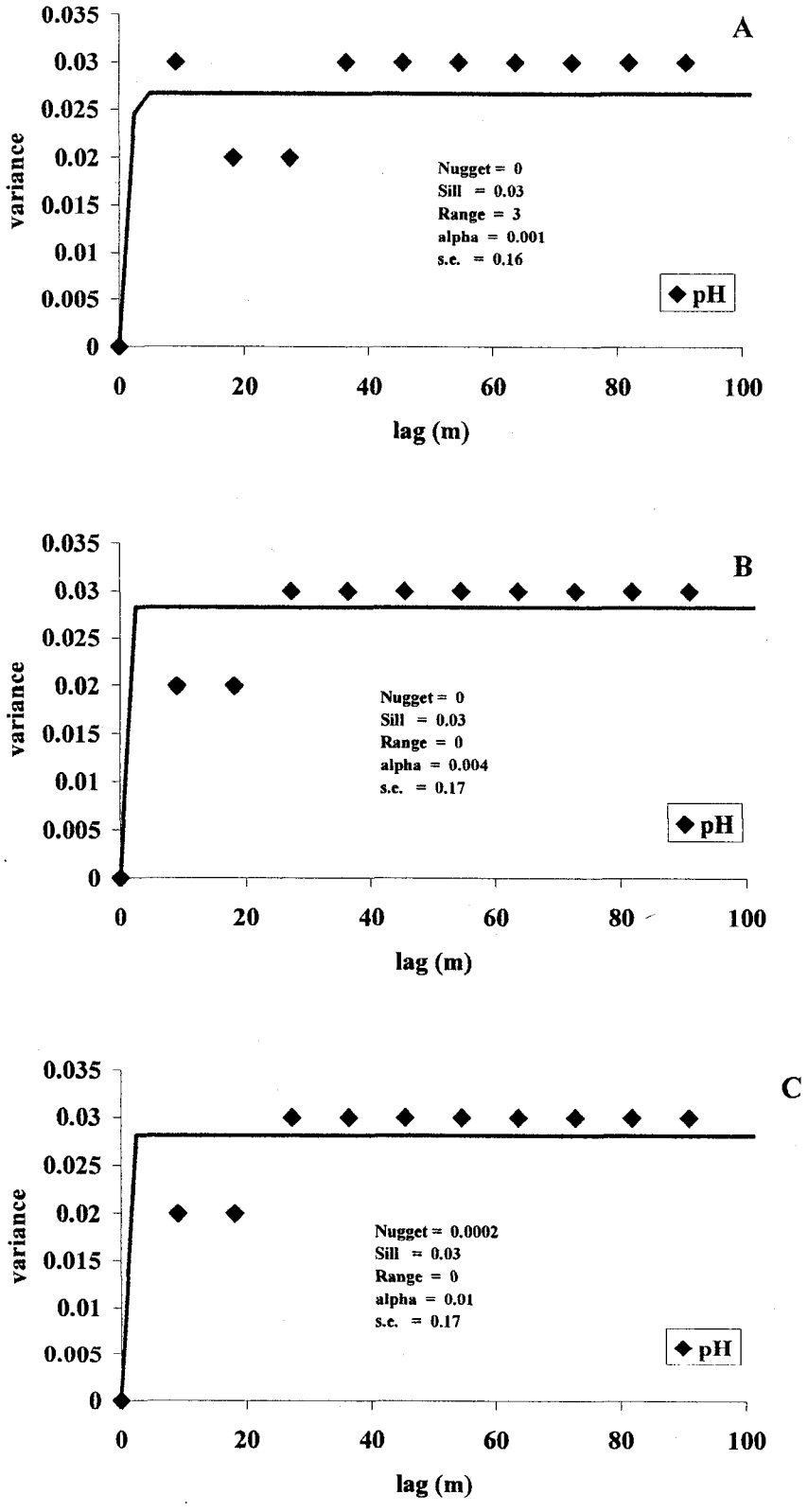

Figure 3.19 Variogram models for pH based on fine grid samples; Gaussian model; A) Field 1, 1997, B) Field 2, 1997, and C) Field 1, 1998.

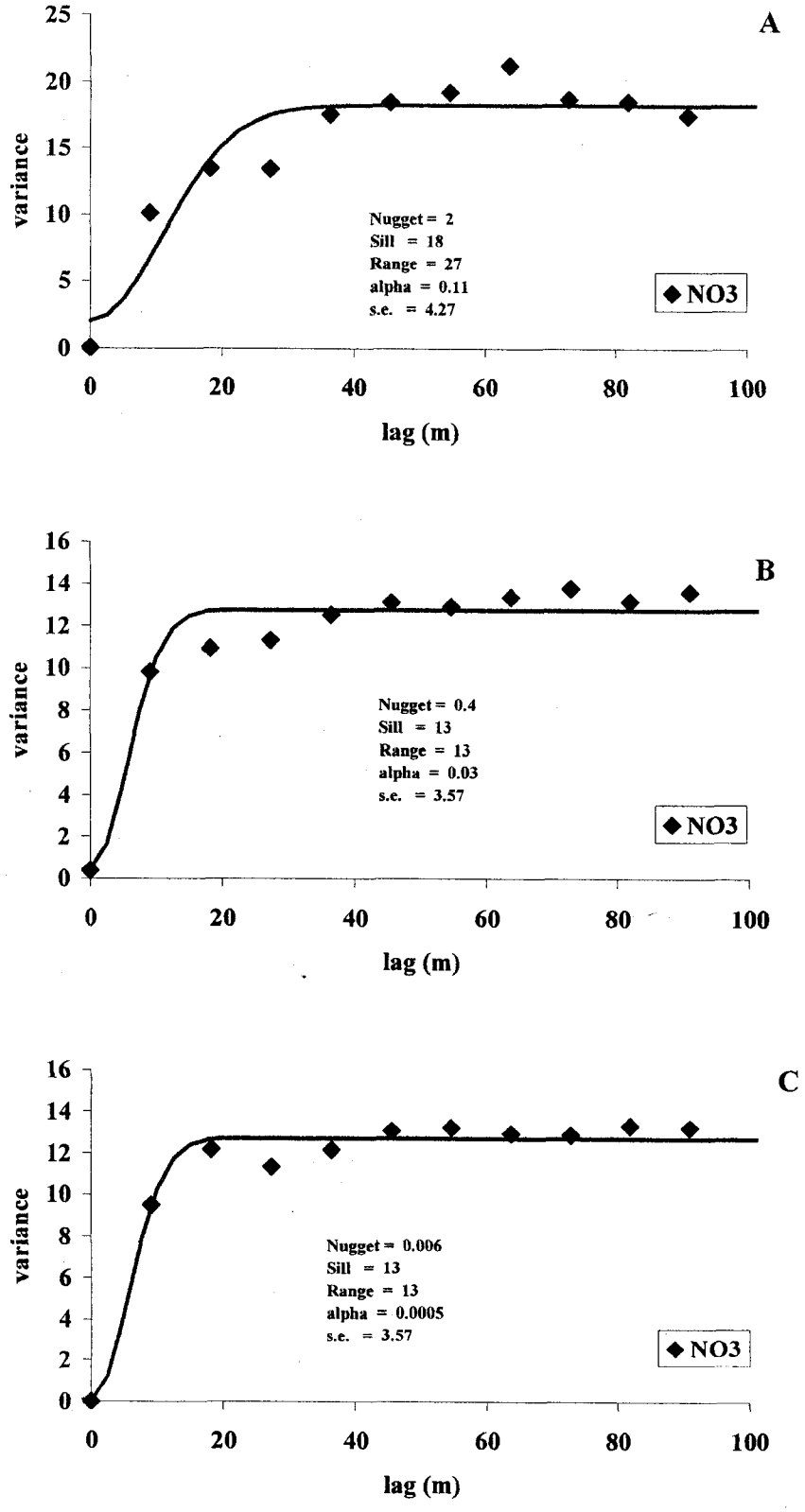

Figure 3.20 Variogram models for NO_3-N based on fine grid samples; Gaussian model; A) Field 1, 1997, B) Field 2, 1997, and C) Field 1, 1998.

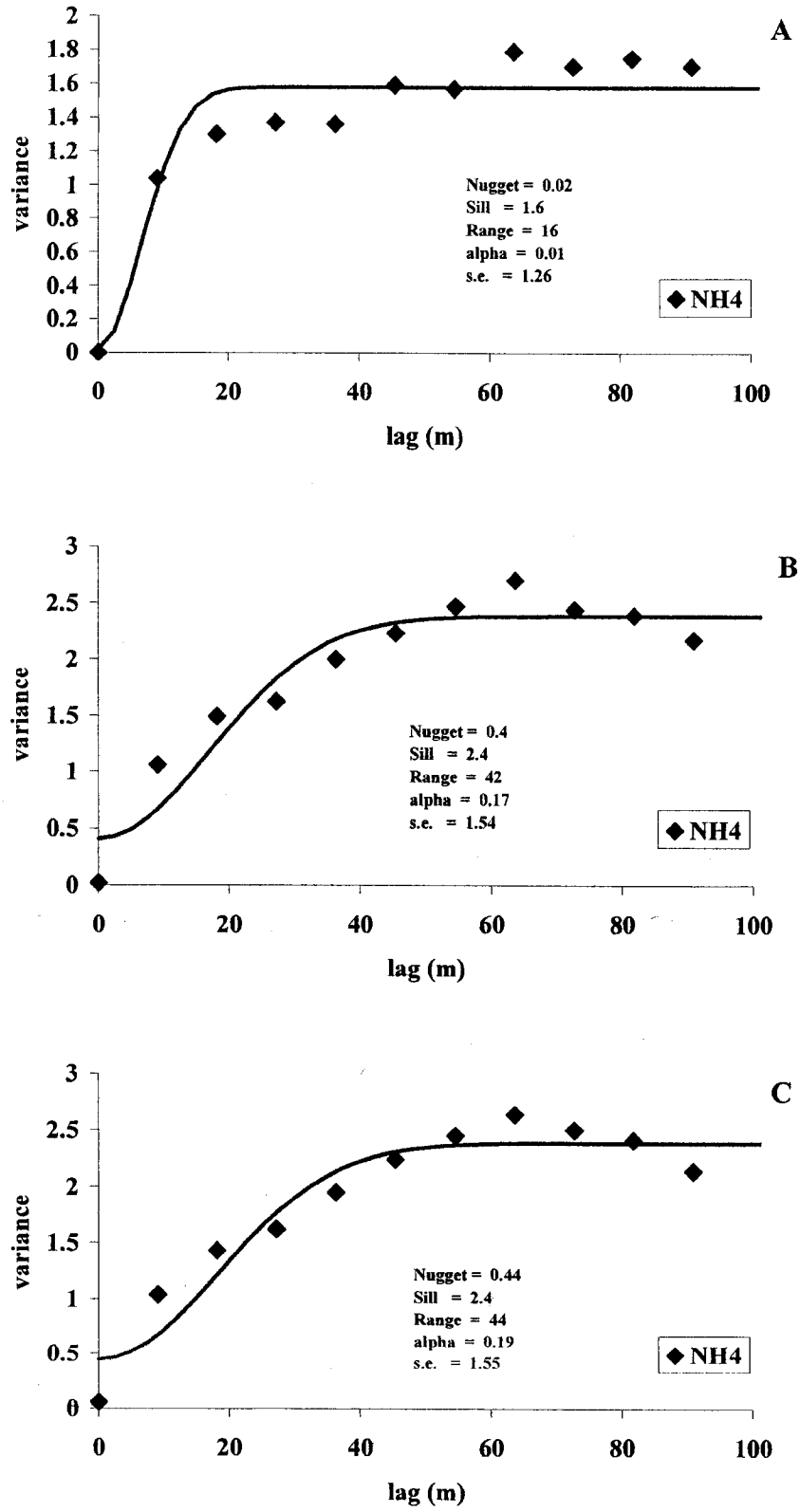

Figure 3.21 Variogram models for NH_4-N based on fine grid samples; Gaussian model; A) Field 1, 1997, B) Field 2, 1997, and C) Field 1, 1998.

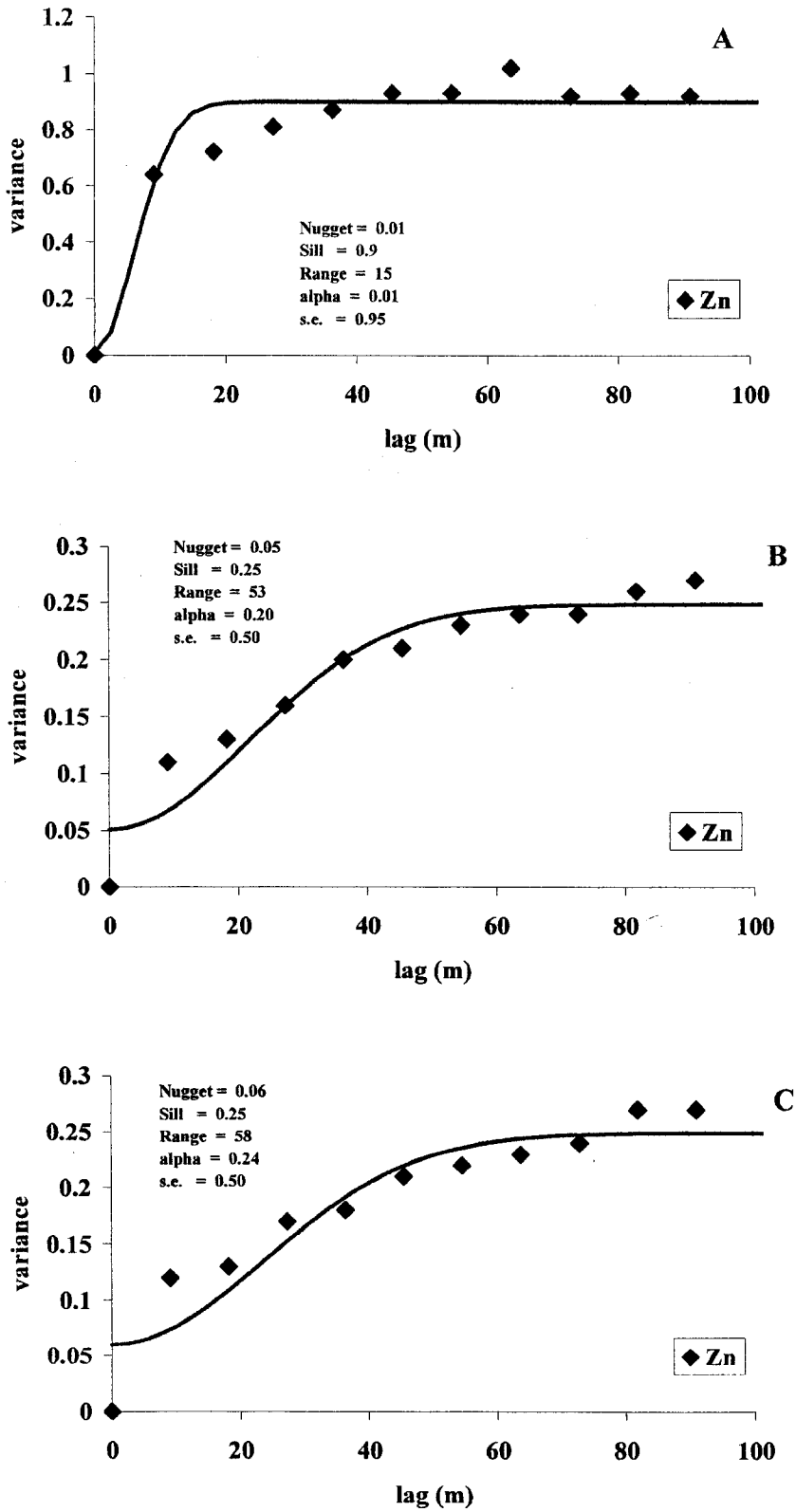

Figure 3.22 Variogram models for Zn based on fine grid samples; Gaussian model; A) Field 1, 1997, B) Field 2, 1997, and C) Field 1, 1998.

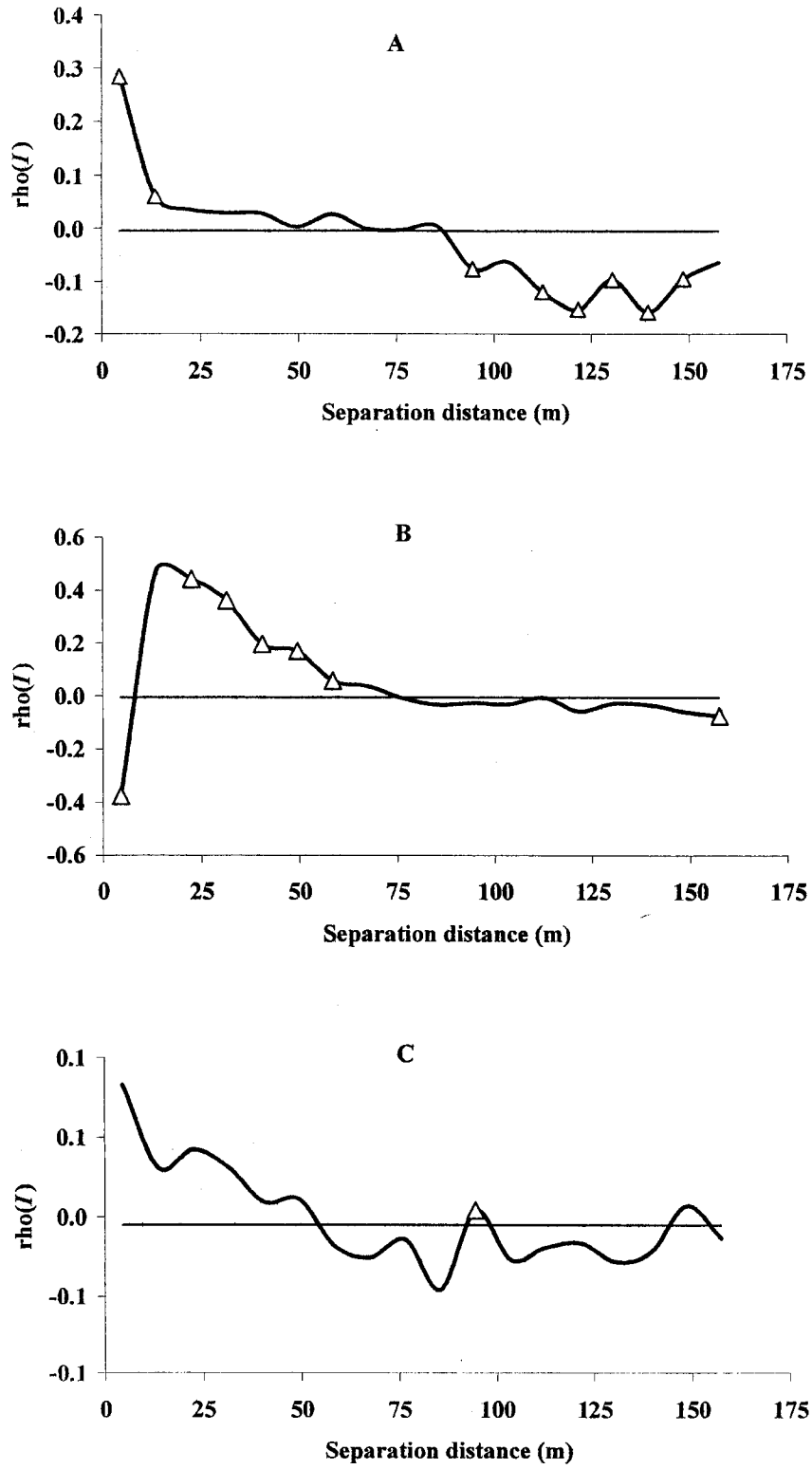

Figure 3.23 Standard correlograms for P. A) Field 1, 1997, B) Field 2, 1997, and C) Field 1, 1998. Triangles indicate bins with significant spatial autocorrelation (i.e. p-value <0.05). Solid horizontal line is expected rho(*I*) under the null hypothesis of complete spatial randomness.

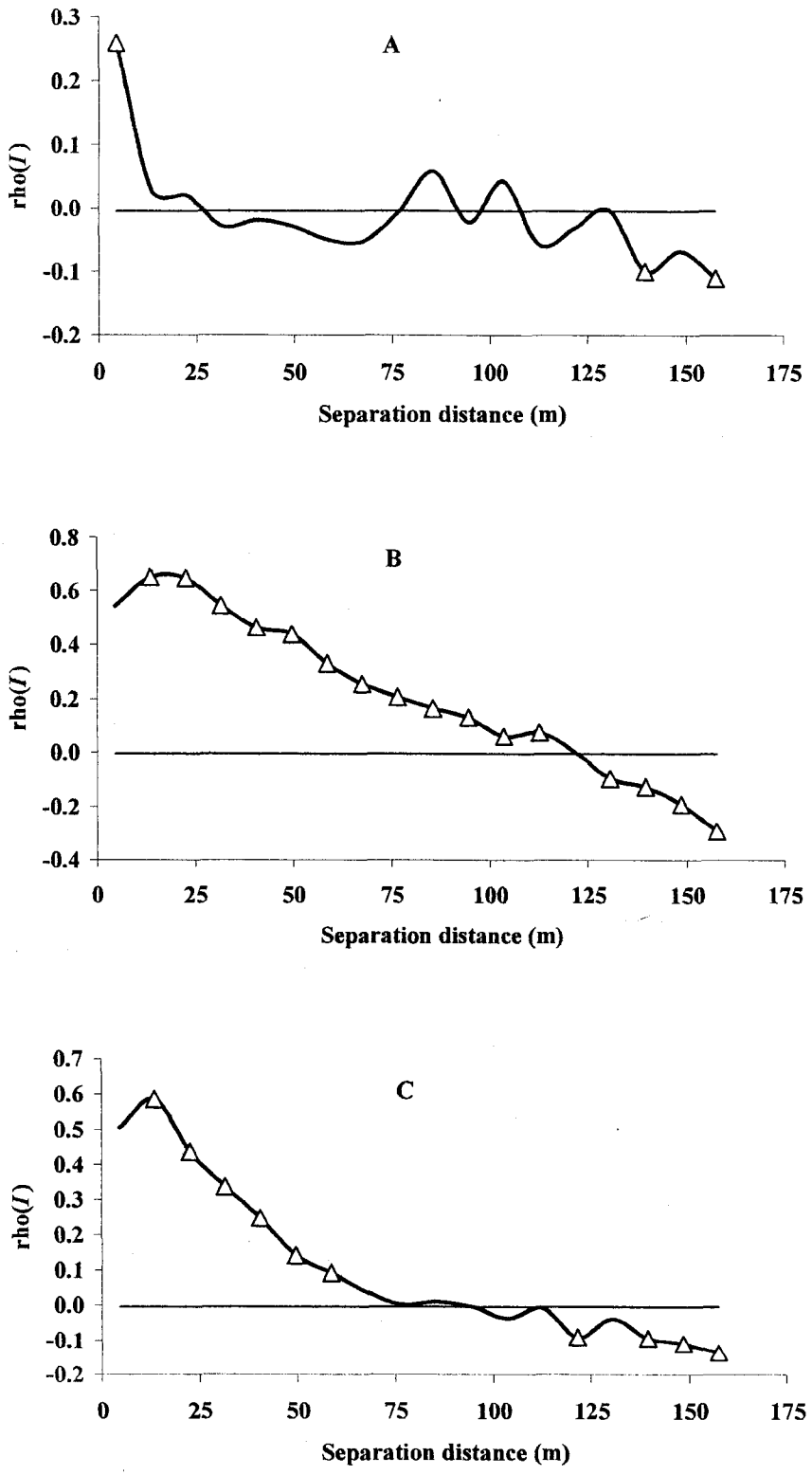

Figure 3.24 Standard correlograms for K. A) Field 1, 1997, B) Field 2, 1997, and C) Field 1, 1998. Triangles indicate bins with significant spatial autocorrelation (i.e. p-value <0.05). Solid horizontal line is expected rho(*I*) under the null hypothesis of complete spatial randomness.

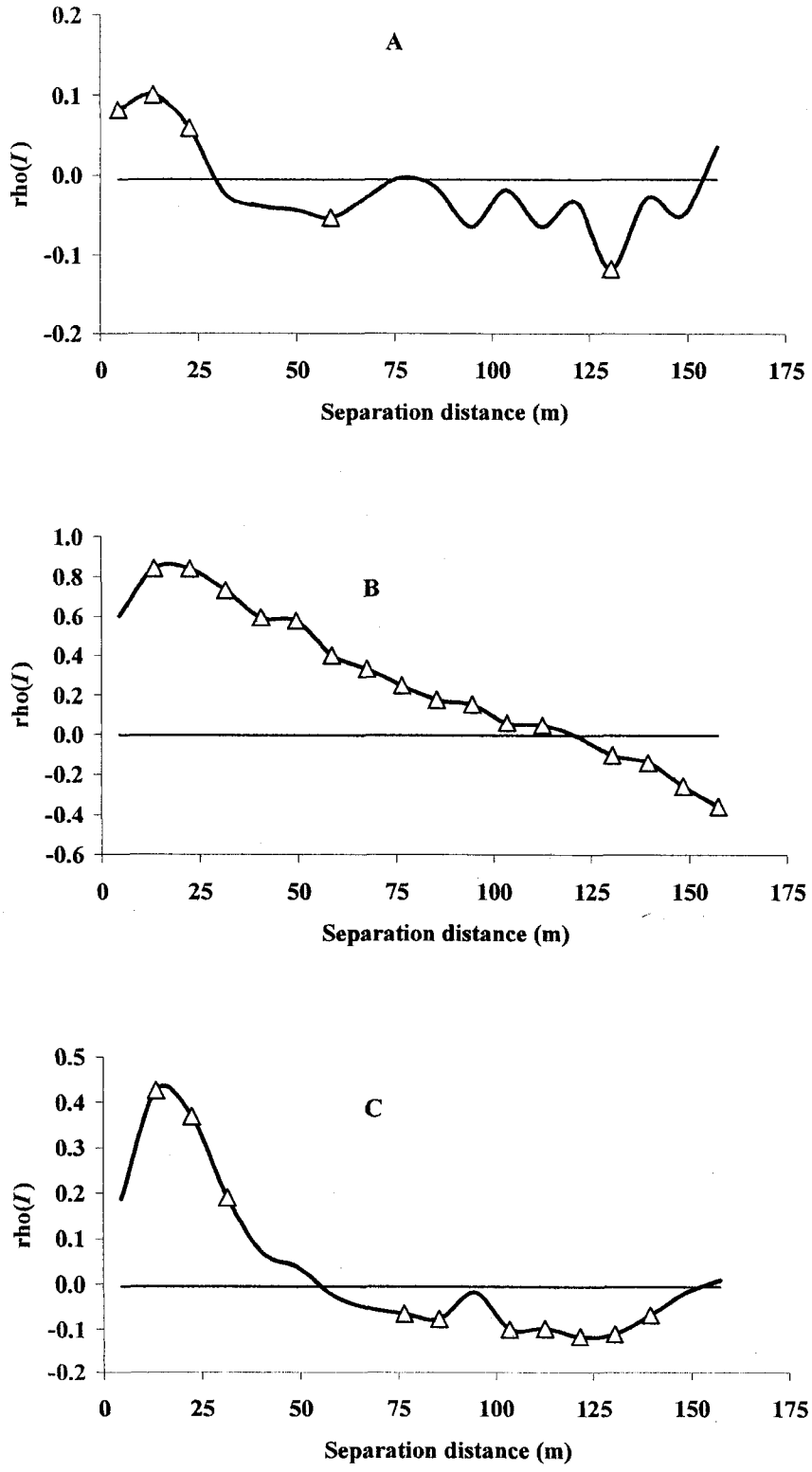

Figure 3.25 Standard correlograms for OM. A) Field 1, 1997, B) Field 2, 1997, and C) Field 1, 1998. Triangles indicate bins with significant spatial autocorrelation (i.e. p-value <0.05). Solid horizontal line is expected rho(*I*) under the null hypothesis of complete spatial randomness.

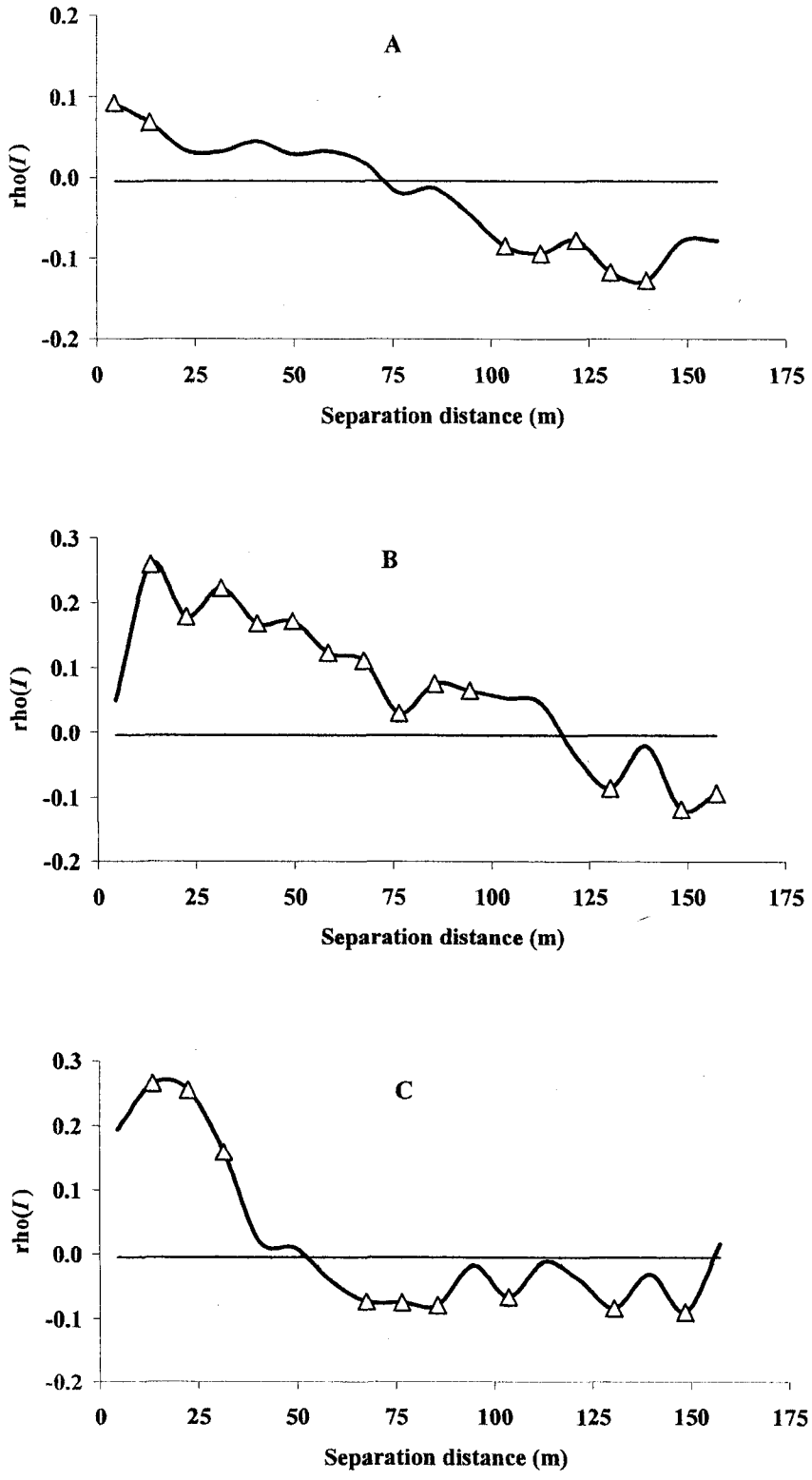

Figure 3.26 Standard correlograms for pH. A) Field 1, 1997, B) Field 2, 1997, and C) Field 1, 1998. Triangles indicate bins with significant spatial autocorrelation (i.e. p-value <0.05). Solid horizontal line is expected rho(*I*) under the null hypothesis of complete spatial randomness.

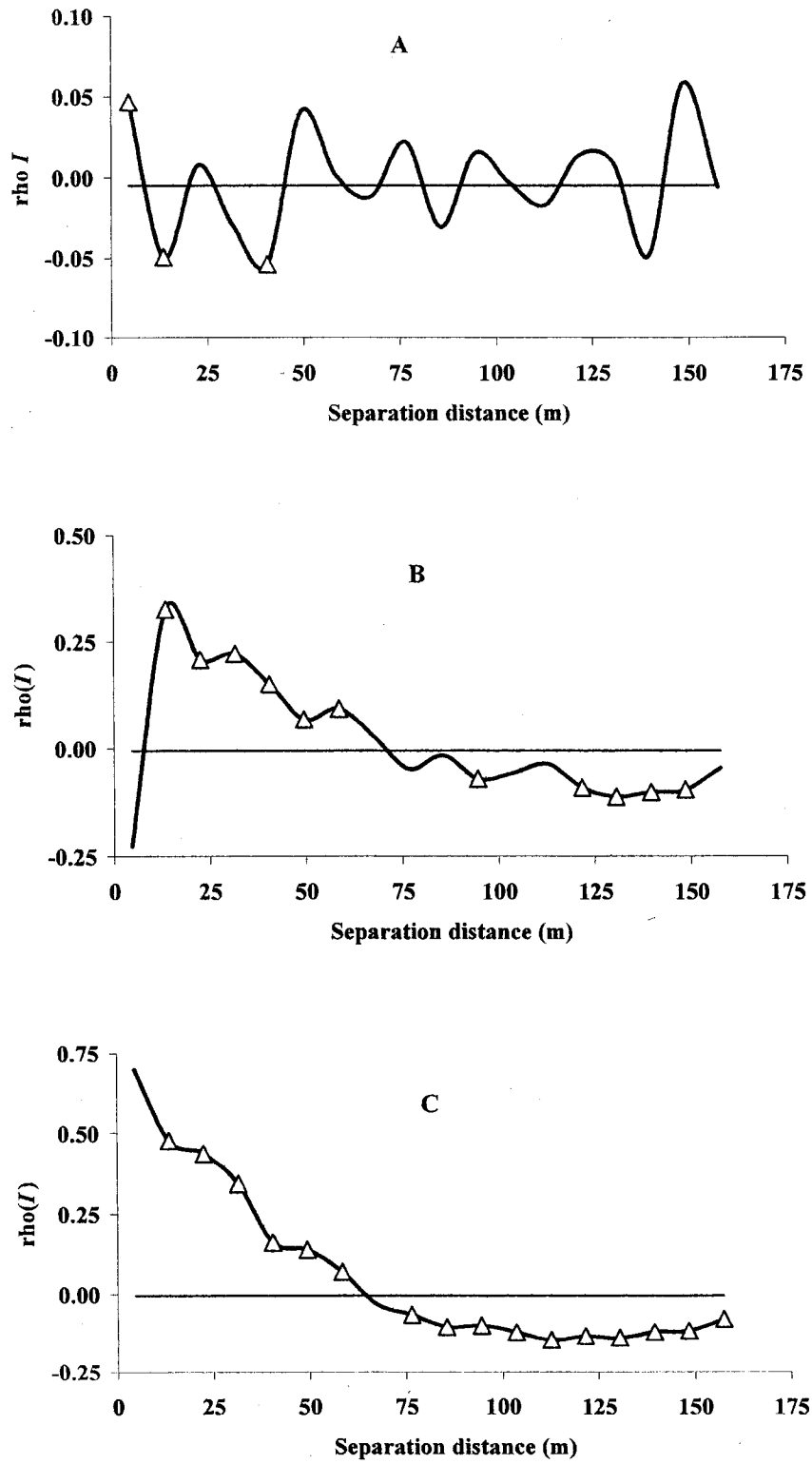

Figure 3.27 Standard correlograms for NO_3-N. A) Field 1, 1997, B) Field 2, 1997, and C) Field 1, 1998. Triangles indicate bins with significant spatial autocorrelation (i.e. p-value <0.05). Solid horizontal line is expected rho(*I*) under the null hypothesis of complete spatial randomness.

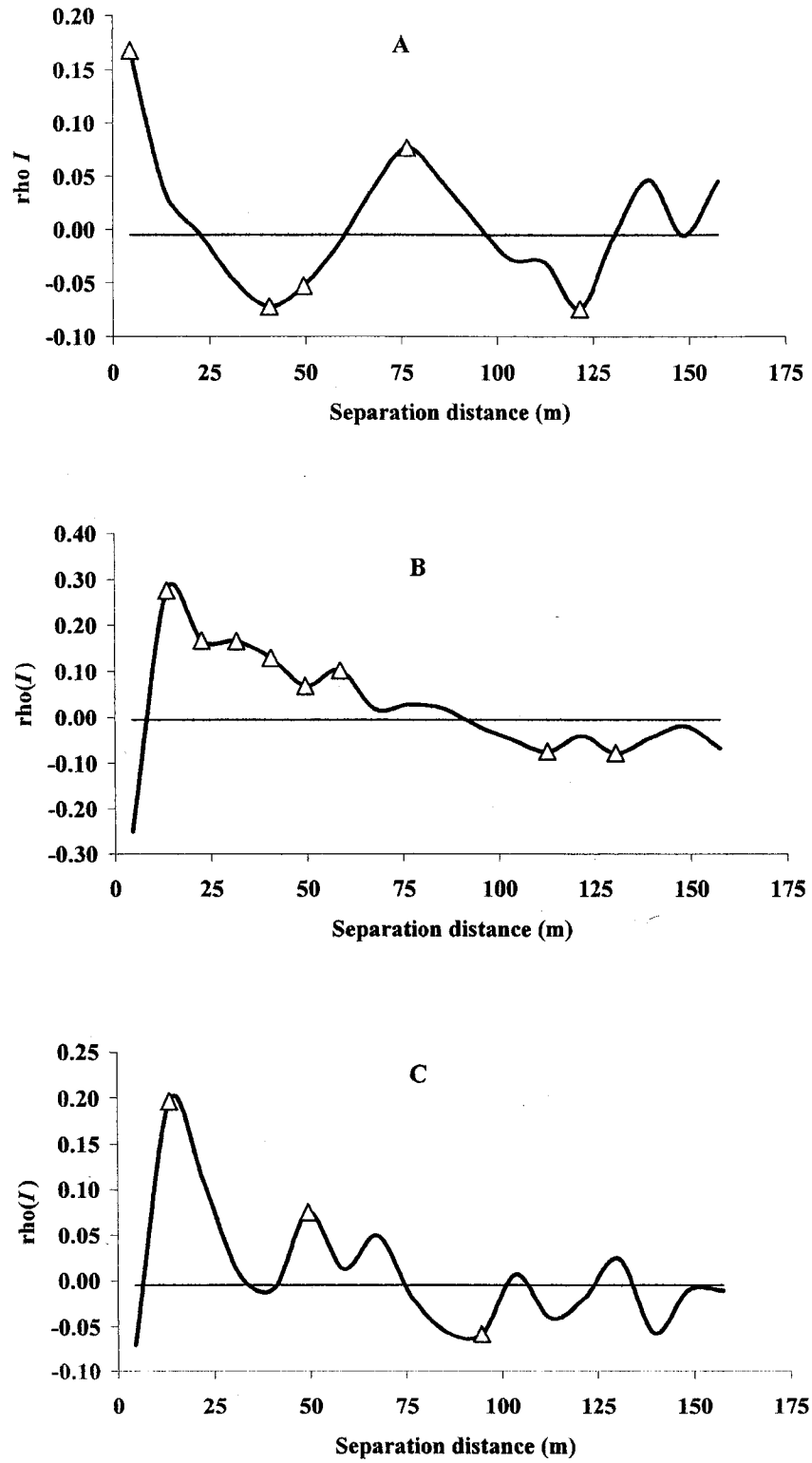

Figure 3.28 Standard correlograms for NH_4-N. A) Field 1, 1997, B) Field 2, 1997, and C) Field 1, 1998. Triangles indicate bins with significant spatial autocorrelation (i.e. p-value <0.05). Solid horizontal line is expected rho(*I*) under the null hypothesis of complete spatial randomness.

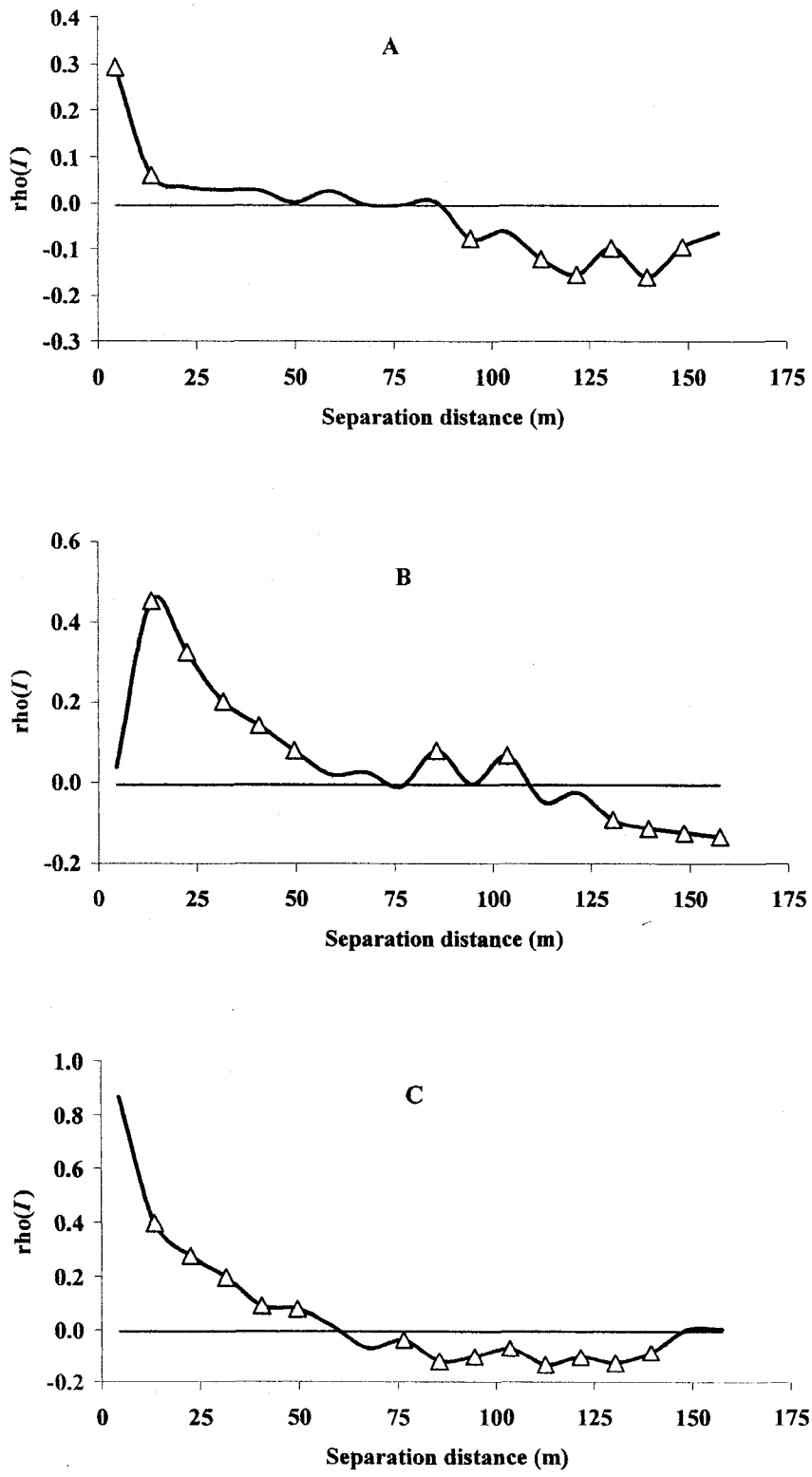

Figure 3.29 Standard correlograms for Zn. A) Field 1, 1997, B) Field 2, 1997, and C) Field 1, 1998. Triangles indicate bins with significant spatial autocorrelation (i.e. p-value <0.05). Solid horizontal line is expected rho(*I*) under the null hypothesis of complete spatial randomness.

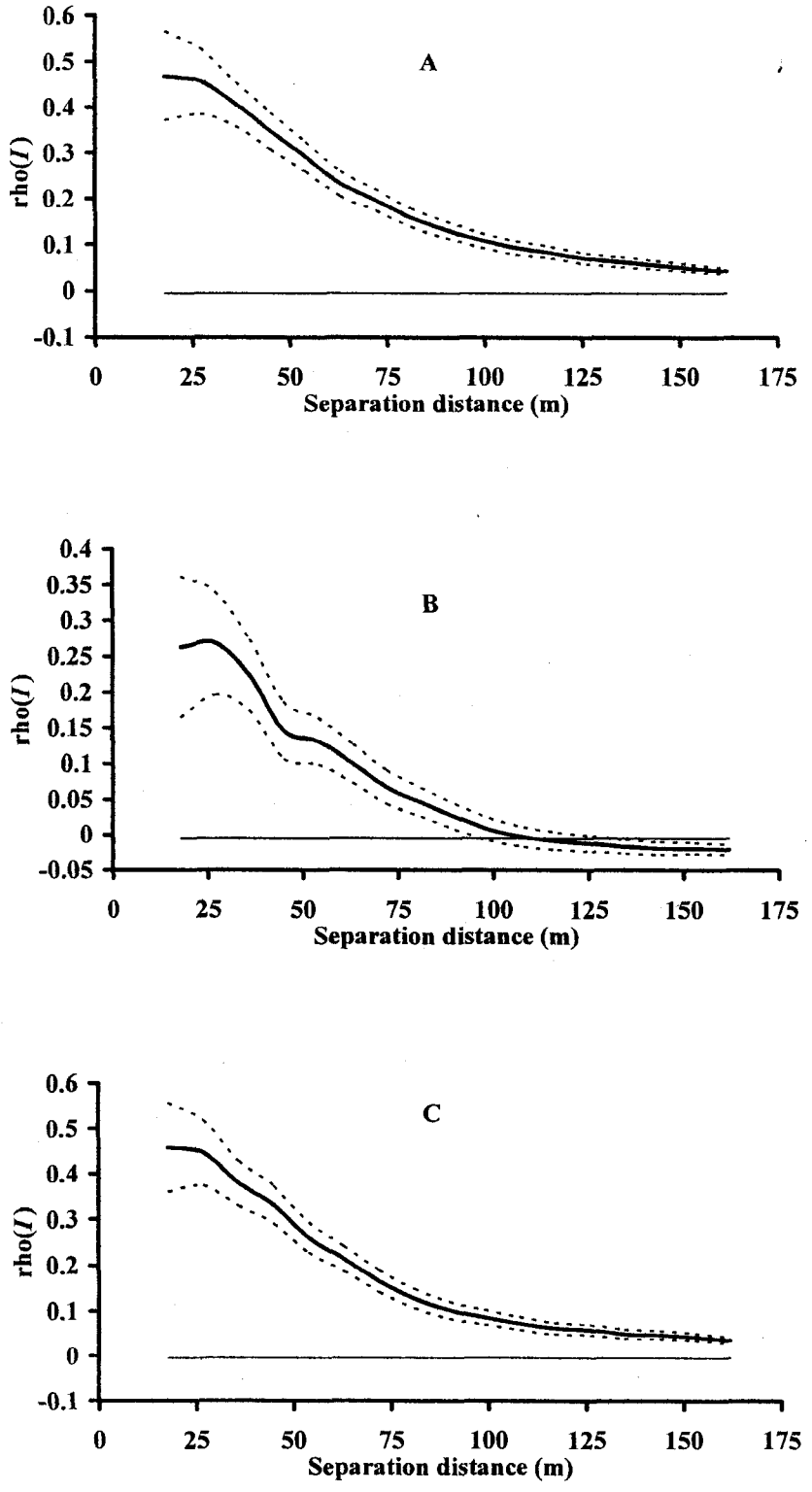

Figure 3.30 Cumulative correlogram for P. Dashed line indicates 95% confidence interval. Solid horizontal line is the expected rho(*I*) under the null hypothesis of complete spatial randomness. A) Field 1, 1997, B) Field 2, 1997, and C) Field 1, 1998.

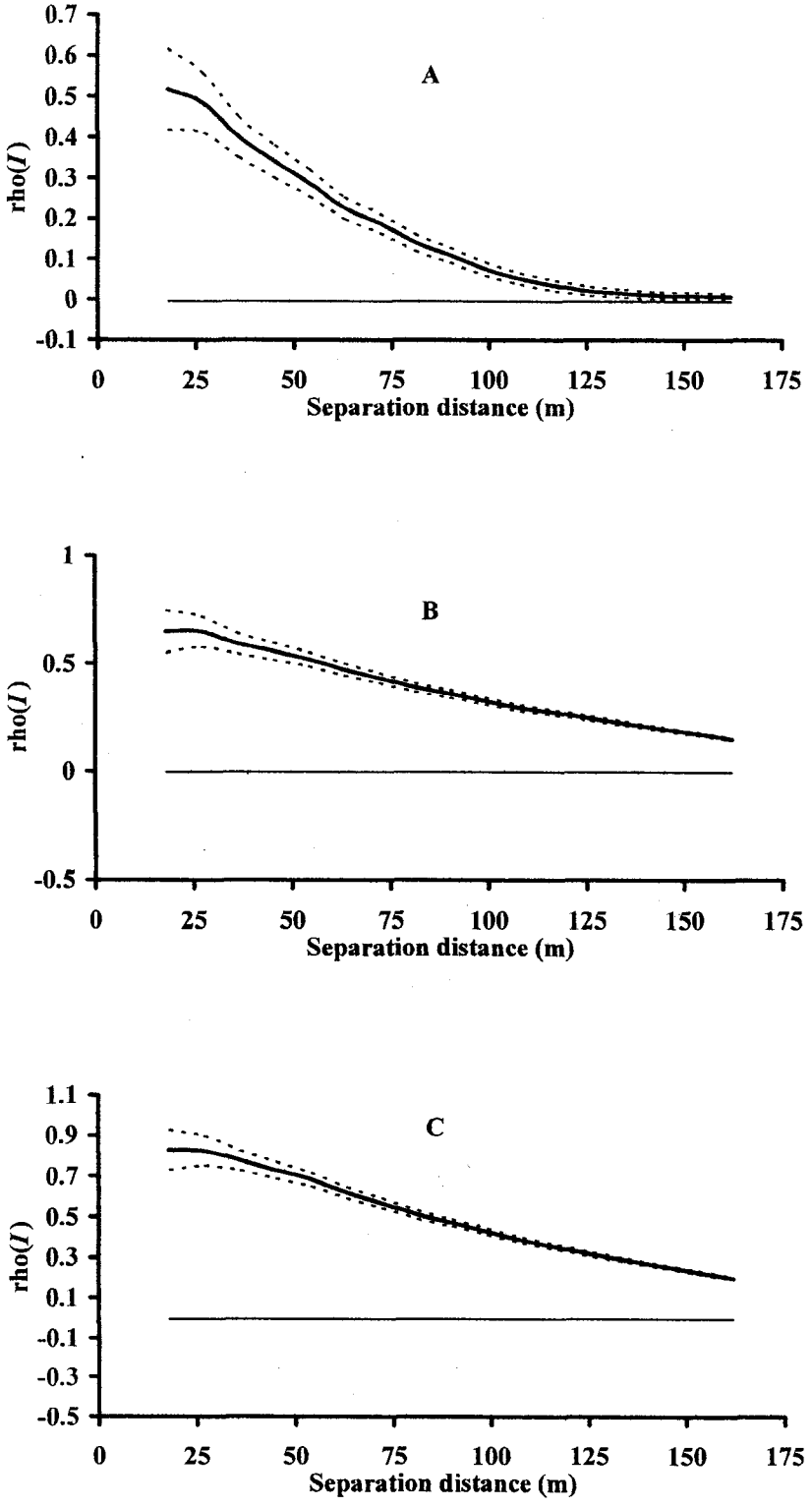

Figure 3.31 Cumulative correlogram for K. Dashed line indicates 95% confidence interval. Solid horizontal line is the expected rho(*I*) under the null hypothesis of complete spatial randomness. A) Field 1, 1997, B) Field 2, 1997, and C) Field 1, 1998.

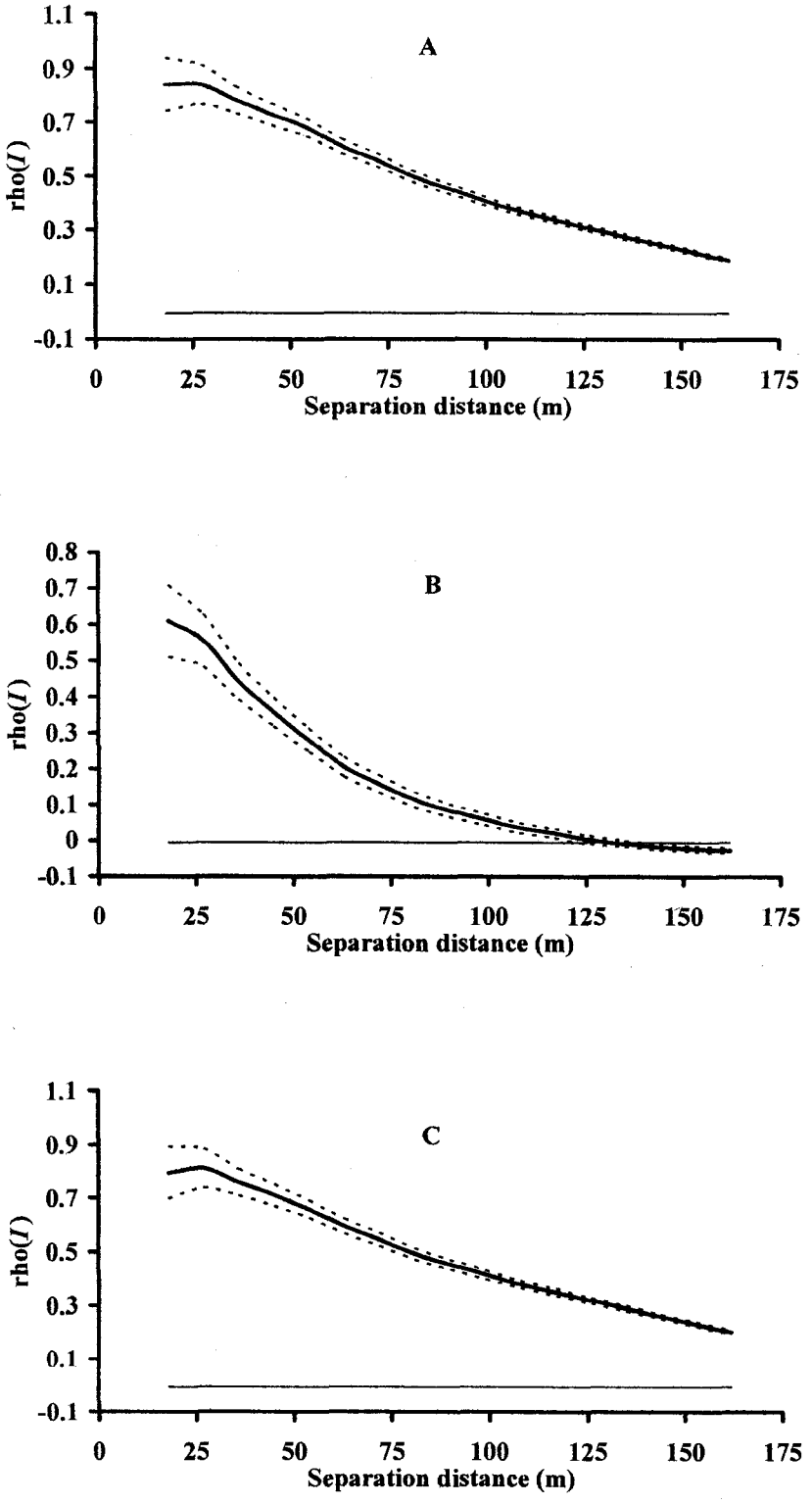

Figure 3.32 Cumulative correlogram for OM. Dashed line indicates 95% confidence interval. Solid horizontal line is the expected rho(*I*) under the null hypothesis of complete spatial randomness. A) Field 1, 1997, B) Field 2, 1997, and C) Field 1, 1998.

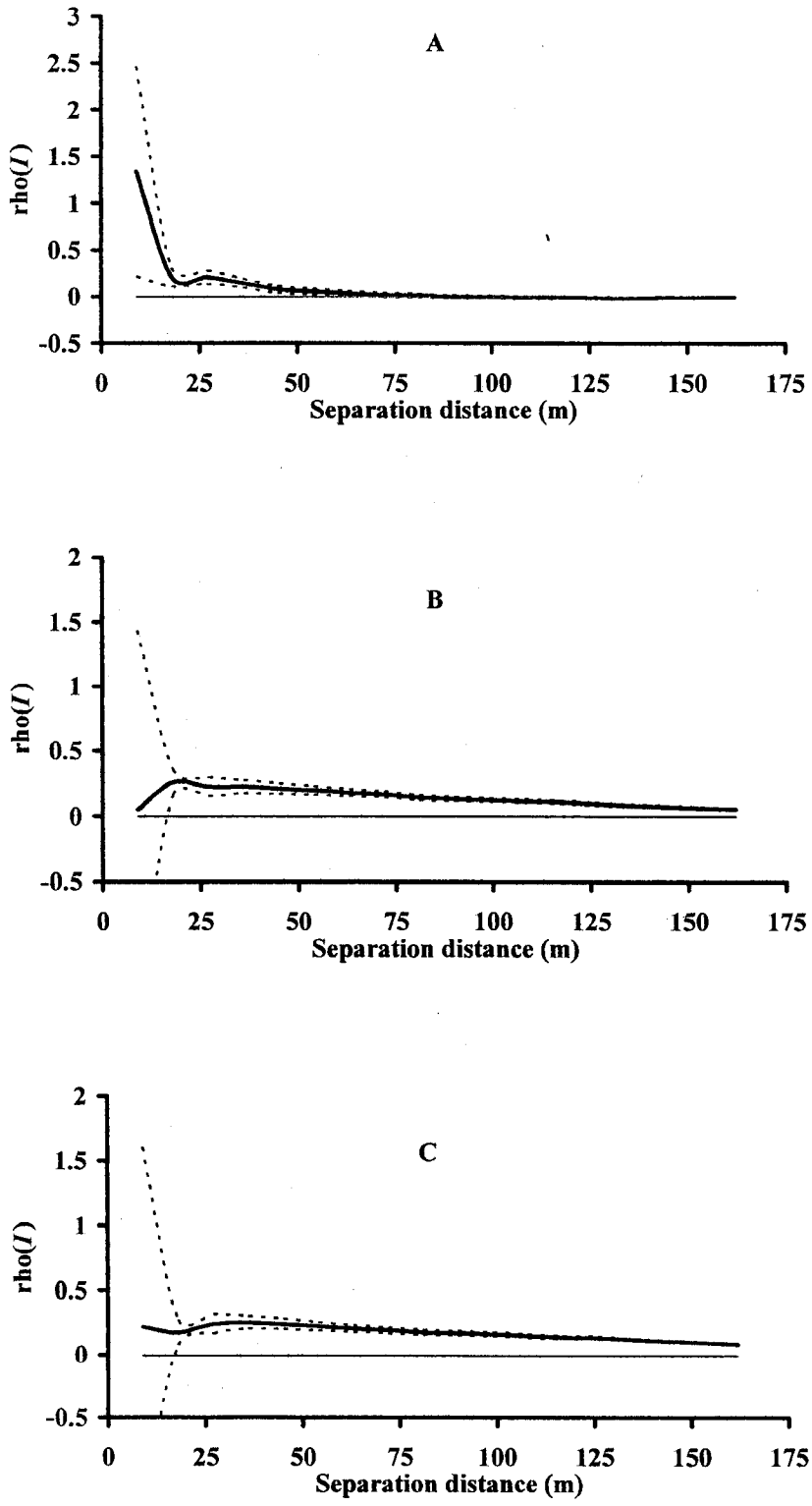

Figure 3.33 Cumulative correlogram for pH. Dashed line indicates 95% confidence interval. Solid horizontal line is the expected rho(*I*) under the null hypothesis of complete spatial randomness. A) Field 1, 1997, B) Field 2, 1997, and C) Field 1, 1998.

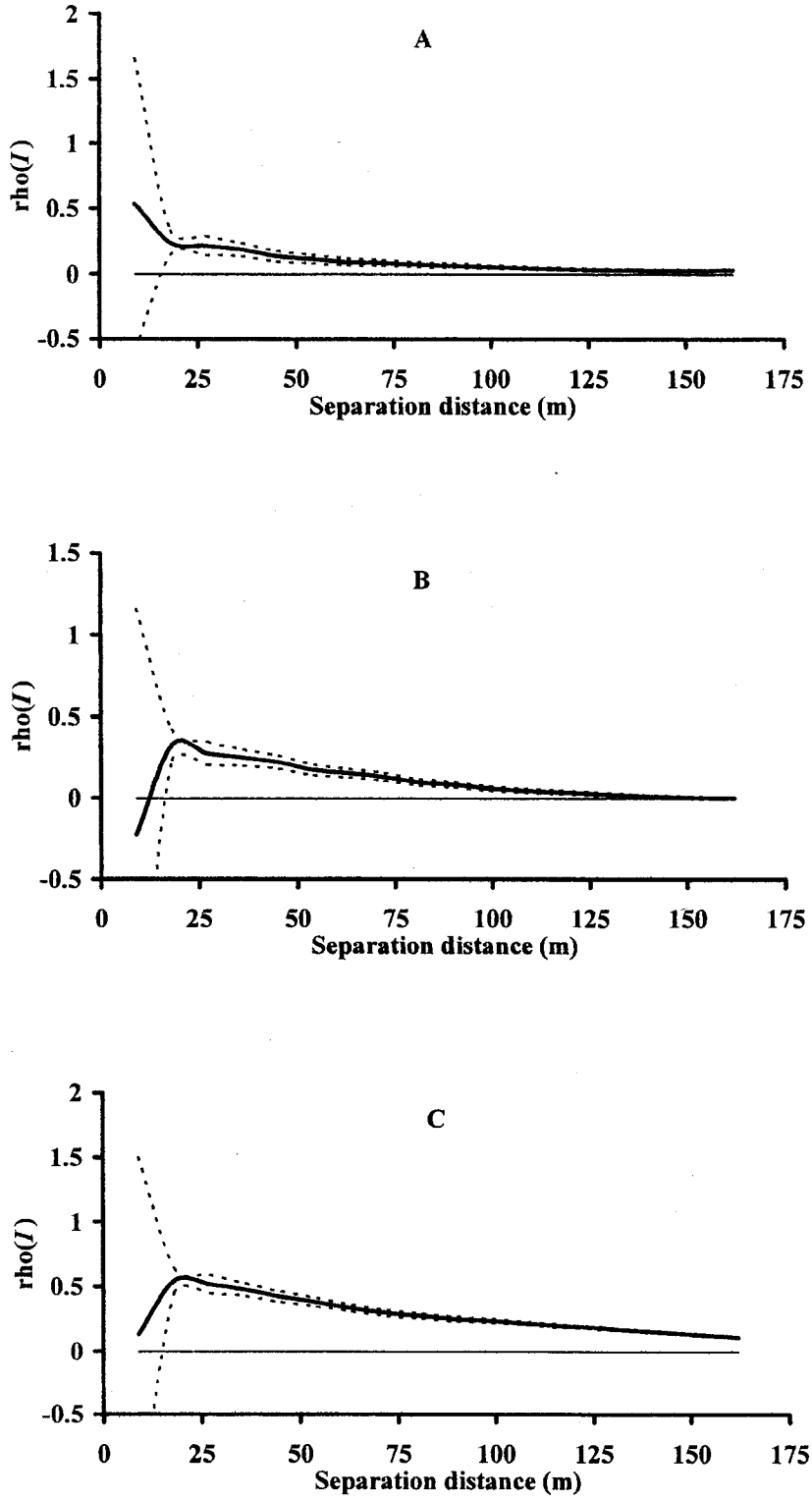

Figure 3.34 Cumulative correlogram for NO_3-N. Dashed line indicates 95% confidence interval. Solid horizontal line is the expected rho(*I*) under the null hypothesis of complete spatial randomness. A) Field 1, 1997, B) Field 2, 1997, and C) Field 1, 1998.

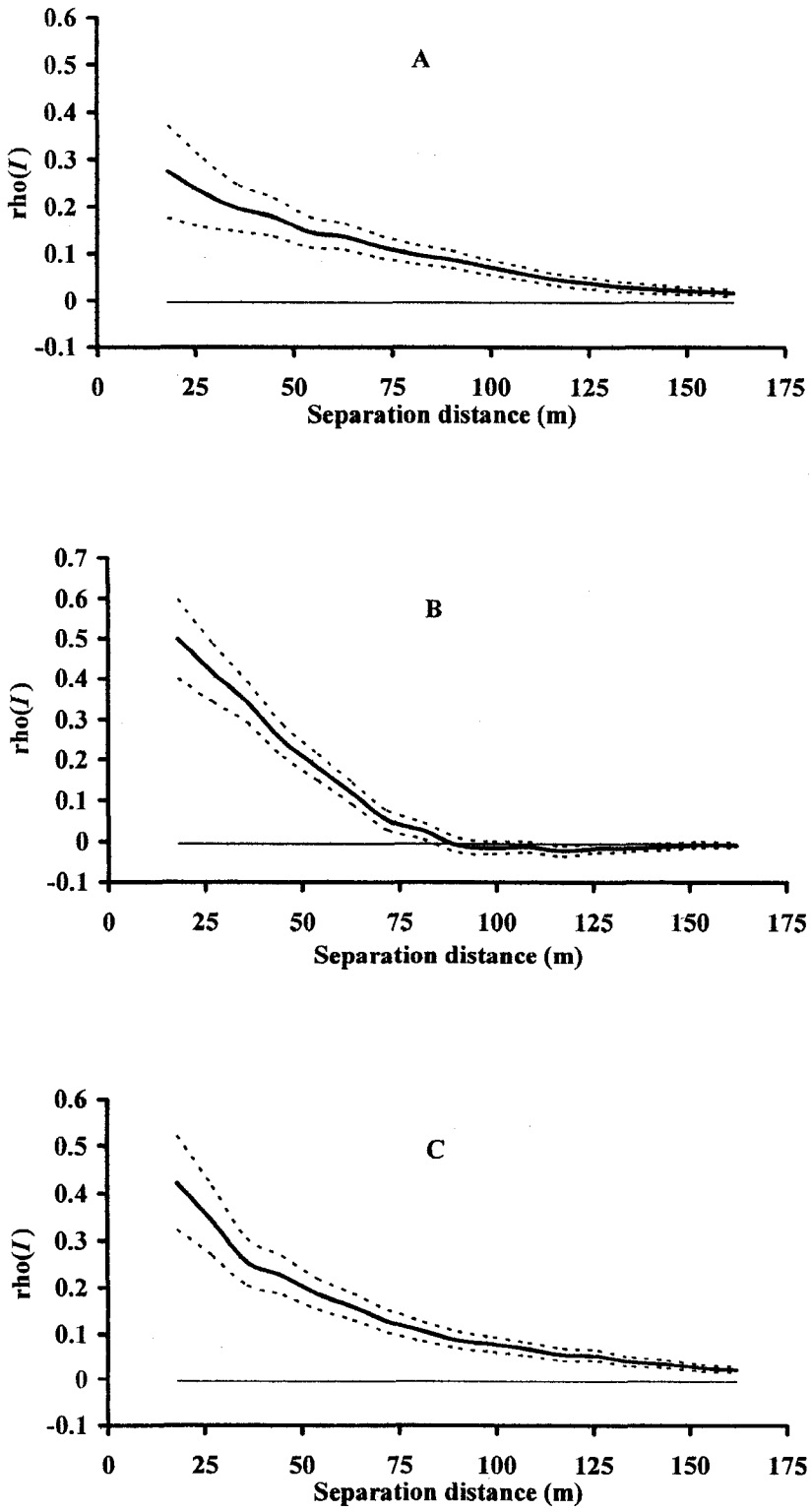

Figure 3.35 Cumulative correlogram for NH_4-N. Dashed line indicates 95% confidence interval. Solid horizontal line is the expected rho(*I*) under the null hypothesis of complete spatial randomness. A) Field 1, 1997, B) Field 2, 1997, and C) Field 1, 1998.

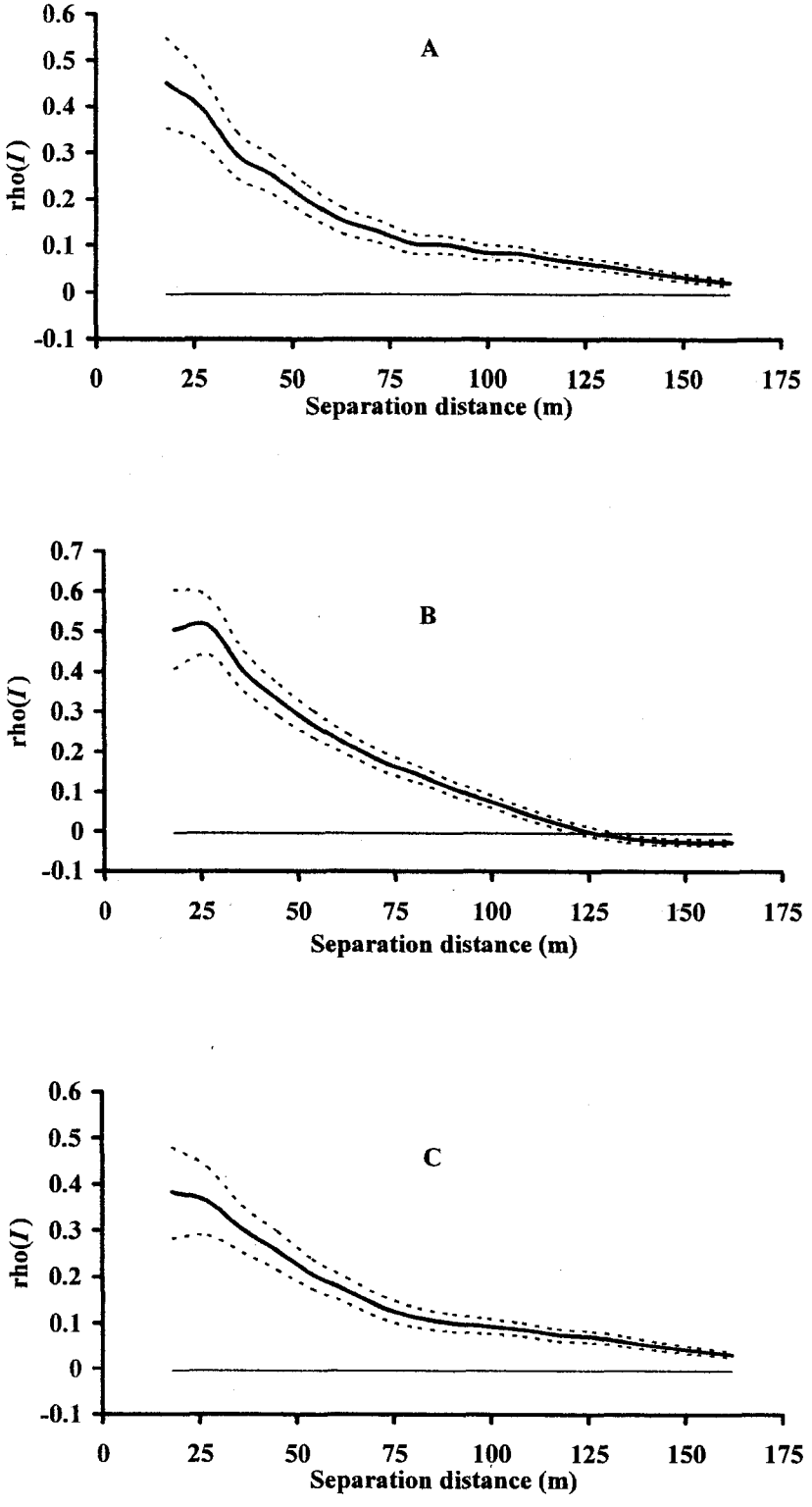

Figure 3.36 Cumulative correlogram for Zn. Dashed line indicates 95% confidence interval. Solid horizontal line is the expected rho(*I*) under the null hypothesis of complete spatial randomness. A) Field 1, 1997, B) Field 2, 1997, and C) Field 1, 1998.

4 Alternative Sampling Design for Interpolating Soil Properties

4.0 Abstract

Implementation of variable-rate application of agricultural inputs depends on an accurate interpolation of the spatial variability of soil properties. Research has suggested that the primary limitation of the commonly used grid-sampling technique is lack of spatial dependency among soil samples. The objective of this study was to develop and analyze a sampling design that utilizes auxiliary data layers and an alternative cluster-sampling approach to data collection. Three fields were sampled using a standard 76 x 76 m grid design. Directed soil sampling was developed for the same fields based on information contained in red, green, and blue image bands. Soil samples were then collected with a cluster-sampling approach designed to capture small-scale variability in the soil parameters organic matter, nitrate-N, ammonium-N, zinc, and electrical conductivity. Models developed from each procedure were evaluated with model-fit statistics: root mean squared error, goodness-of-fit *G*-statistic, prediction bias, mean error, median error, mean absolute error, skewness, kurtosis, Anderson-Darling test of normality, and standard mean squared error. The cluster-sampling design improved all parameter estimates; the grid-sampling design improved one parameter. Average improvement for the cluster-sampling was 34% (minimum = 1%, and maximum =72%). Bias estimates from the cluster-sampling design were small and estimates of root mean squared error suggest the cluster-sampling design is a better predictor of small-scale variation when compared to the grid-sampling design. Sixty-percent of the model

residuals from the interpolated grid-sample soil parameters were considered normally distributed compared to 73% of the model residuals from the cluster-sampling procedure. Overall the cluster-sampling procedure outperformed the grid-sampling procedure.

4.1 Introduction

Classic statistical procedures assume measurements of a variable of interest are independent of one another regardless of their location in a field. This is usually not the case with soil systems because of the spatially continuous nature of landscapes, soil formation processes and climatic zones. It is reasonable to expect that soil measurements taken in close proximity to each other will be similar. Generally, samples taken closer together in the field are more alike than samples taken at greater distances (i.e. spatially dependent) (Nielson and Alemi, 1989). Effective implementation of variable rate application (VRT) of agricultural inputs depends on an accurate characterization of the spatial variability (i.e. spatial dependence) of soil properties (Sawyer, 1994). Grid soil sampling is typically used to develop interpolated, soil-property prescription maps for VRT (Mueller et al., 2001). The primary considerations when performing grid sampling are 1) keeping the number of samples to a minimum for economic optimization and 2) collecting enough samples to provide adequate map quality.

In the USA, grid soil sampling at a density of 1 per ha or larger has conventionally been used to develop VRT maps (Fleming et al., 2000). Past research has suggested that several technical limitations arise from grid sampling. Mueller et al., (2001) concluded that a commercial grid size of 100 x 100 m was inadequate to provide acceptable prediction accuracy. These researchers also concluded that utilizing average fertility values for the soil properties of interest was as effective as grid sampling.

Schloeder et al., (2001) similarly demonstrated spatial interpolation of sparse soil sample data was inappropriate. The primary reason for poor interpolation results was attributed to the spatially independent nature of the data. Whelan et al., (1996) concluded that fields with limited soil samples could only be interpolated with simple geostatistical techniques such as inverse distance weighting; more complex techniques such as kriging were inappropriate. Hammond (1993) concluded that a 60 x 60 m sampling grid was adequate for developing VRT maps for some soil properties. Similarly, Franzen and Peck (1995) found that a grid size of 65 x 65 m was adequate for parameter interpolation when compared with 25 and 98 m grids. More recent research has reported that grids of 20 to 30 m are required for site specific application of agricultural inputs (McBratney and Pringle, 1999).

Failing to capture spatial variability can make interpolation of soil properties difficult. However, the cost associated with collection and analysis of soil samples at a density that accurately captures spatial dependence (e.g. 20 to 60 m) is generally prohibitive, especially for most agronomic crops. In order to fully realize the potential benefits of VRT, economically viable sampling techniques designed to capture, describe, and model variability of soil properties at the field level need to be developed.

In general, the interpolation resolution of soil properties based on grid sampling is limited to the size of the grid used. However, it is possible to improve the spatial resolution of an interpolation model by utilizing remotely-sensed information, such as multi-spectral imagery, that has an inherently higher resolution. Both Metzger (1997) and Joy et al. (2001) were able to improve spatial resolution of interpolation models by combining coarse-resolution spatial data sets with fine-resolution spatial data sets

collected from the same experimental field site. Digitized aerial photographs of bare-soil agricultural fields often have resolutions in the sub-meter to five-meter range and can serve as valuable secondary data layers for interpolation of many soil properties. For example, bare soil surface spectral properties are largely influenced by soil organic carbon and moisture (Schreier et al., 1988).

I hypothesize that a more effective sampling approach can be developed by utilizing auxiliary data layers and by sampling soils with a cluster approach. This new approach uses the detectable, natural variation in soil color as observed with a high altitude, bare soil photograph to initially stratify a field into homogenous zones. The unique strata are then utilized in a directed soil sampling procedure and samples are collected in a cluster design to improve the detection of small-scale variation. The large separation distance among individual clusters as well as the preliminary stratification of the field is designed to capture large-scale variation in soil properties. The final analysis will compare soil properties modeled with a typical grid procedure to the results from the stratification process.

4.2 Materials and Methods

Two center-pivot irrigated fields (Fields 1 and 2) and one furrow irrigated field (Field 3) were studied during the 2002 growing season. All three fields have been managed under corn (*Zea mays* C.) for several years. Field 1 is 58 ha and has soils classified as Albinas loam (fine loamy, mixed, mesic Pachic Argiustolls), Ascalon fine sandy loam (fine loamy, mixed, mesic Aridic Argiustolls), and Haxtun sandy loam (fine loamy, mixed, mesic Pachic Argiustolls). These soil classes represent loamy soils that are well drained with moderate to high available water capacity and moderate to high

infiltration rates. Field 2 is 57 ha and has soils that are classified as Vona sandy loam (coarse loamy, mixed, mesic, Mollic Haplargids), Haverson clay loam (fine loamy, mixed, calcareous, mesic Typic Ustifluvents), and Nunn loam (fine, montmorillonitic, mesic, Typic Argiustolls). These varied from sandy loam to clay loam with moderate to high water holding capacity and from low to high water infiltration rates. Field 3 was used in 2001 and is 18 ha and has soils that are classified as Valentine sand (sandy, mixed nonacid, mesic Typic Ustipsamment), a Bijou loamy sand (coarse loamy, mixed, mesic Mollic Haplargid), and a Truckton loamy sand (coarse loamy, mixed, mesic Udic Argiustoll). These varied from sandy to loamy sand with moderate to excellent water holding capacity and moderate to high water infiltration rates.

4.2.1 Grid Sampling

Three fields were soil sampled in the spring of 2002 using a standard non-aligned grid sampling technique and the size of each grid cell was 76 x 76 m (i.e. 0.58 ha). Sample locations were randomly located within each cell and recorded with a differential global positioning system (DGPS). Soil samples were collected from the 0 to 0.2 m surface zone and analyzed for organic matter (OM), nitrate-N (NO_3-N), ammonium-N (NH_4-N), zinc (Zn), and electrical conductivity (EC) using standard soil testing procedures (Miller et al., 1998).

4.2.2 Stratified Cluster Sampling

In addition to grid sampling, the same three fields were sampled in the spring of 2002 using a stratified cluster sampling technique. Prior to soil sampling, a high-altitude, bare soil image of each field was acquired (~1500 m). Ground, control points were installed prior to image acquisition and the images were georectified with ERDAS

Imagine©[1] software (Leica Geosystems®, 2003). Soil reflectance for each bare soil image was quantified into three distinct bands: Blue (0.48-0.50 μm), green (0.55-0.60 μm), and red (0.62-0.68 μm) with ERDAS Imagine software (Leica Geosystems®, 2003). The three resulting surfaces for each field (i.e. red, green, and blue), were then analyzed with a nonhierarchical *k*-means clustering algorithm for spatial data sets (MSCA; S-PLUS©, Reich and Davis, 1998). Nonhierarchical clustering procedures allocate the *n* 'individuals' from a sample into one of *k* groups, where $n>k$. The clustering procedure considers *p* variables $X_1, X_2,\ldots, X_p$ measured on each individual in the sample. The objective of nonhierarchical clustering procedures is to minimize the variance within groups while maximizing the variance among groups. The variance is estimated with the Euclidean distance function:

$$d_{ij} = \sqrt{\left\{\sum_{k=1}^{p}\left(x_{ik} - x_{jk}\right)^2\right\}} \qquad [4.1]$$

where x_{ik} is the value of variable X_k for individual *i* and x_{jk} is the value of the same variable for individual *j* (Manly, 1998). This equation is easily extendable for multivariate data sets.

For each field, red, green, and blue (herein referred to as *R*, *G*, and *B* respectively) image bands were treated as variables and pixels were treated as individuals in the sample based on the associated *R*, *G*, and *B* image band values (i.e. 0-255). The average pixel size for each field was approximately 1 m. The spatial clustering algorithm (i.e. MSCA) generated a new surface that categorized regions with similar reflectance properties as a

[1] Mention of a trade name, proprietary product, or specific equipment does not constitute a guarantee, warranty, or endorsement by Colorado State University.

unique stratum. The number of strata delineated over each field was determined through a subjective iteration procedure:

1. Ten strata were initially delineated over each field.
2. If the image appeared too pixelated and lacked visually obvious and distinctly contiguous regions the spatial clustering algorithm was run again and the number of output strata reduced by one.
3. This procedure was repeated until visually obvious, and distinctly contiguous regions were apparent.

Seven strata were delineated over Field 1, and six strata were delineated over Fields 2 and 3. Within each stratum at each field, 3 to 4 sampling locations were subjectively selected by recording UTM coordinates with ERDAS Imagine© software (Leica Geosystems®, 2003).

After stratification, soil samples were collected from each field. At each sampling location, 3 soil samples were collected (i.e. a cluster). Samples within a cluster were separated by approximately 5 m, and recorded with a DGPS (Figure 4.1). Samples were collected from the 0 to 0.2 m surface zone and analyzed for organic matter (OM), nitrate-N (NO_3-N), ammonium-N (NH_4-N), zinc (Zn), and electrical conductivity (EC) using standard soil testing procedures (Miller et al., 1998). The large separation distance among sampling locations as well as the preliminary stratification of the field is designed to capture large-scale variation in soil properties. The small separation distance among soil samples within a cluster is designed to capture small-scale variation in soil properties. A flow chart summarizing the cluster sampling procedure is presented in Figure 4.1.

4.2.3 Surface-Model Construction

Trend surface-models were fit to the data from the grid sampling and cluster sampling designs. Trend surface-models contain elements of simple first-order multiple regression models:

$$Y = \beta_0 + \beta_1 a_1 + \beta_2 a_2 + \varepsilon \qquad [4.2]$$

with respect to independent variables ($a_1,\ldots,a_p$), and elements of complete second-order (i.e. quadratic) multiple regression models:

$$Y = \beta_0 + \beta_1 x + \beta_2 y + \beta_3 x^2 + \beta_4 y^2 + \beta_5 xy + \varepsilon \qquad [4.3]$$

with respect to x and y geographic coordinates (ε is an error term). A simple, complete second-order trend surface-model with two independent variables (a_1 and a_2) can be represented as:

$$Y = \beta_0 + \beta_1 x + \beta_2 y + \beta_3 x^2 + \beta_4 y^2 + \beta_5 xy + \beta_6 a_1 + \beta_7 a_2 + \varepsilon \qquad [4.4]$$

In this study, only the cluster sampling technique had independent variables other than x and y coordinates. Independent variables for the cluster sampling technique included R, G, B as well as geographic coordinates. The optimum predictive trend surface-model for each variable and each sampling technique was based on an all-combinations regression program (COMBSCR; S-PLUS©, Reich and Davis, 1998). The all-combinations procedure examines all possible trend surface-models using all combinations of the independent variables. The optimum model is selected as the model that minimizes the Akaike's Information Criteria (Akaike, 1977).

The residuals from grid sampling, trend surface-models were evaluated with the Moran's I statistic for spatial dependency (Eq. 3.1). If the Moran's I for the residuals was significant (i.e. p-value ≤ 0.05) they were used to generate empirical variograms (Eq.

3.3). Gaussian, exponential, and spherical variogram models were fit to the empirical variograms using the Spatial Library developed by Reich and Davis (1998) in S-PLUS©. The optimum kriging model was selected as the model that minimized the Akaike's Information Criteria and models were used to krig the residuals data using ordinary kriging. If the residuals from the trend surface-models were not spatially dependent, the trend surface-model was considered the optimum surface-model and additional residual modeling was not necessary.

The root mean squared error (*RMSE*) was calculated from the grid sampling, trend surface-model residuals. The $RMSE^2$ is a measure of the sum of the squared residuals and the optimum model will minimize the *RMSE*. The *RMSE* is defined as:

$$RMSE = \sqrt{\frac{1}{n}\sum_{i=1}^{n}\left[Z_i - \hat{Z}_i\right]^2} \qquad [4.5]$$

where Z_i is the observed value of the i^{th} observation, and $\hat{Z}_i$ is the predicted value of the i^{th} observation, and n is the number of observations in the sample (Schloeder et al., 2001);.

Residuals from cluster sampling, trend surface-models were evaluated with the Moran's *I* statistic for spatial dependency. If the residuals from the cluster sampling, trend surface-models were not spatially dependent, they were not kriged. However, residuals modeled with a binary regression tree procedure regardless of spatial dependency (TREE; S-PLUS©, Statistical Sciences, 1999). The regression tree procedure is a non-parametric approach to regression that compares all possible splits among the

[2] *RMSE* is also used as a decision tool during the ordinary kriging procedure; the ordinary kriging procedure requires selection of the number of nearest neighbors to use during the interpolation procedure; the number of nearest neighbors that minimizes the *RMSE* is selected as the optimum method having the most accurate local or small-scale estimates.

independent variables using a binary partitioning algorithm that maximizes the dissimilarities among groups (Hansen et al., 1996; De'Ath and Fabricus, 2000). The algorithm recursively splits the data in each subset until the subset is homogenous or the subset contains too few observations to be split further. The main objective of regression tree analysis is to produce accurate classifiers, as well as provide information about the predictive structure of the data (Breiman et al., 1984). Unlike kriging, regression tree analysis does not rely on spatial location and *x, y* coordinates are not used as independent variables. In this analysis, the independent variables used in regression tree analysis included *R*, *G*, *B*, and the predicted values of the variable of interest from the trend surface-modeling procedure. The *RMSE* was also calculated from residuals.

Final soil parameter estimates ($\hat{Z}_{x,y}$) for the two sampling procedures were calculated as the sum of the predicted trend surface values ($\hat{Z}^{TS}_{x,y}$) and the predicted ordinary kriging or regression tree analysis residual values ($\hat{Z}^{Res}_{x,y}$) at interpolated location *x,y*:

$$\hat{Z}_{x,y} = \hat{Z}^{TS}_{x,y} + \hat{Z}^{Res}_{x,y} \qquad [4.6]$$

This is an application of modified residual kriging described in section 1.3. Although the addition of trend surface and regression tree estimates is not modified residual kriging per se, the technique is valid and has been successfully applied to interpolation problems in natural systems (Michaelsen et al., 1994; Balk and Elder, 2000).

If the residuals from the grid sampling, trend surface-models were not spatially dependent the trend surface-model was considered the optimum surface-model and final soil parameters were simply estimated as:

$$\hat{Z}_{x,y} = \hat{Z}^{TS}_{x,y} \qquad [4.7]$$

where $\hat{Z}_{x,y}$ and $\hat{Z}^{TS}_{x,y}$ are defined in Eq. 4.6.

Grids representing the trend surface-models for the different soil parameters were generated in ARC/INFO® (CON; Grid Module, ARC/INFO®, ESRI, 1995). Similarly, grids representing the RT models of the residuals were generated in ARC/INFO®. Ordinary kriging of spatially dependent parameter residuals was performed in S-PLUS© (KRIG; S-PLUS©, Reich and Davis, 1998). Resulting output from the KRIG function was exported into an ASCII text format that could be translated by the ARC/INFO® GIS software (IMPORT; S-PLUS©, Reich and Davis, 1998). Final soil parameter surfaces were generated by adding the values of trend surface-models to the appropriate values of the regression tree and/or kriging models using ARC/INFO®.

4.2.4 Surface-Model Evaluation

The goodness-of-prediction statistic (*G*-statistic) was calculated for each soil parameter interpolated with kriging or regression tree techniques. If soil parameters were only interpolated with simple trend surface-models, the regression coefficient (R^2) is presented as the *G*-statistic. The *G*-statistic is a measure of how effective a prediction might be relative to that which could have been derived by the sample mean. Calculation of the regression coefficient (R^2) is similar to the *G*-statistic. The *G*-statistic is defined as:

$$G = 1 - \left(\frac{\sum_{i=1}^{n} \left[Z_i - \hat{Z}_i \right]^2}{\sum_{i=1}^{n} \left[Z_i - \bar{Z} \right]^2} \right) \qquad [4.8]$$

where Z_i is the observed value of the i^{th} observation, $\hat{Z}_i$ is the predicted value of the i^{th} observation, $\overline{Z}$ is the sample mean, and n is the number of observations in the sample (Agterberg, 1984; Guisan and Zimmermann, 2000; Schloeder et al., 2001). A *G*-statistic equal to 1 indicates perfect prediction, a positive value indicates that the model is more reliable than if one had used the sample mean, a negative value indicates the model is less reliable than if one had used the sample mean, and a value of zero indicates that one should use the sample mean to estimate *Z*. Estimated improvement was also calculated as the difference between final modified residual kriging models and initial trend surface-models expressed as a percentage.

Residuals ($e_{x,y}$) from surface-models constructed in section 4.2.3 were estimated as:

$$e_{x,y} = Z_{x,y} - \hat{Z}_{x,y} \qquad [4.9]$$

where $Z_{x,y}$ is the observed value of soil parameter *Z* at location *x,y*, and $\hat{Z}_{x,y}$ is the final soil parameter estimate from modified residual kriging at location *x,y*. Residuals from the modified residual kriging models for the two sampling procedures were then used to compute prediction bias, mean error, mean absolute error, and *RMSE*.

Prediction bias was calculated for each model as a percentage of the true value:

$$B = \frac{100\sum_{i=}^{n}\left(Z_i - \hat{Z}_i\right)}{\sum_{i=1}^{n} Z_i} \qquad [4.10]$$

where $Z_i, \hat{Z}_i$, and n were defined in Eq. 4.8 (Joy et al., 2001). Ideally, prediction bias will be zero. Negative bias values indicate a tendency for the model to overestimate predictions; positive bias indicates underestimation.

The mean error is a measure of the average error of the residuals and ideally should be 0. The mean error is defined as

$$ME = \frac{1}{n}\sum_{i=1}^{n}\left[Z_i - \hat{Z}_i\right] \qquad [4.11]$$

where where $Z_i, \hat{Z}_i$, and n were defined in Eq. 4.8 (Webster and Oliver, 2001).

The mean absolute error is an indication of the accuracy of global or large-scale estimates and is defined as:

$$MAE = \frac{1}{n}\sum_{i=1}^{n}\left[\left|Z_i - \hat{Z}_i\right|\right] \qquad [4.12]$$

where $Z_i, \hat{Z}_i$, and n were defined in Eq. 4.8 (Schloeder et al., 2001).

4.2.5 Surface-Model Cross-validation

A 10-fold cross-validation procedure was also used to analyze the residuals from the final, predictive models of the interpolated soil parameters (KFLD; S-PLUS©, Reich and Davis, 1998). In this procedure, 10% of the data points from the residual data set are removed and the appropriate trend surface or modified residual kriging model is fit to the remaining 90% of the residuals data. The newly fit model is also used to predict the residual values for the 10% removed. The 10% removed effectively provides an independent data set to test the effectiveness of the model. The procedure is run 10 times to remove all data points, and predicted values from the procedure are compared to the actual values from the appropriate residual data set. The predicted residuals from the

cross-validation procedure were then used to compute the mean error, *RMSE*, mean absolute error, and median error. Estimates of the skewness and kurtosis of the residual distributions were also calculated. Skewness is a measure of asymmetry and a skewness value more than or less than zero indicates skewness in the data. Skewness is also referred to as the standardized 3rd central moment of a distribution and is estimated as:

$$SK = \frac{1}{n-1}\sum_{i=1}^{n}\left(\frac{Z_i - \overline{Z}}{s}\right)^3 \qquad [4.13]$$

where $Z_i, \overline{Z}_i$, and n were defined in Eq. 4.8, and s is the sample standard deviation.

Kurtosis is a measure of how different a distribution is from the standard normal distribution. A positive kurtosis (i.e. leptokurtotic) typically indicates a distribution more peaked than the normal. A negative kurtosis (i.e. platykurtic) typically indicates a distribution flatter than the normal. The kurtosis for a normal distribution is three although most standard calculations adjust this value to zero. Kurtosis is also referred to as the 4th central moment of a distribution and is estimated as:

$$Kr = \frac{1}{n}\sum_{i=1}^{n}\left(\frac{Z_i - \overline{Z}}{s}\right)^4 - 3 \qquad [4.14]$$

where $Z_i, \overline{Z}_i$, and n were defined in Eq. 4.8, and s is the sample standard deviation.

Residuals from the cross-validation procedure were tested for normality with the Anderson-Darling goodness-of-fit test. The Anderson-Darling goodness-of-fit test is a cumulative distribution function test of normality and is estimated as:

$$AD = \sum_{i=1}^{n}\frac{1-2i}{n}\left\{\ln\left(F_0\left[Z_i\right]\right) + \ln\left(1 - F_0\left[Z_{n+1-i}\right]\right)\right\} - n \qquad [4.15]$$

where F_0 is the assumed normal distribution with sample estimated parameters $\bar{x}$ and s; Z_i is the i^{th} sorted, standardized, sample value; n is the sample size, and ln is the natural logarithm, base e (Romeu, 2003). The null hypothesis is that the true distribution is F_0 and is rejected if the calculated Anderson-Darling value is greater than some critical value (i.e. for $\alpha = 0.05$):

$$AD > \frac{0.752}{1 + \frac{0.75}{n} + \frac{2.25}{n^2}} \qquad [4.16]$$

To assess the estimation uncertainty in the models the estimation error variance, $\hat{\sigma}_i^{2(-k(i))}$, was calculated for each observation in the k^{th} part of the data (Isaaks and Srivastava, 1989):

$$\hat{\sigma}_i^{2(-k(i))} = MSE^* \left[\left(X_i^{-k(i)} \right) \left(X^{*\prime} X^* \right) \left(X_i^{-k(i)} \right) + 1 \right] + MSE^{(er)} + 2Cov(\hat{Y}, \hat{\eta}) \qquad [4.17]$$

where MSE^* is the regression mean squared error for the trend surface-model fitted using *K-1* parts of the data, X^* is a matrix of independent variables associated with the *K-1* parts of the data, $X_i^{-k(i)}$ is a vector of independent variables associated with the i^{th} observation in the k^{th} part of the data, $MSE^{(er)}$ is the mean squared error of the kriging model or the regression tree model used to describe the error in the multiple linear regression model, and $Cov(\hat{Y}, \hat{\eta})$ is the covariance between the estimated values, $(\hat{Y})$, from the trend surface-model and the predicted residuals, $(\hat{\eta})$, from the kriging model or regression tree model for the *K-1* parts of the data. If soil parameters were only interpolated with simple trend surface-models the equation to calculate the estimation error variance reduces to:

$$\hat{\sigma}_i^{2(-k(i))} = MSE^* \left[\left(X_i^{-k(i)} \right) \left(X^{*\prime} X^* \right) \left(X_i^{-k(i)} \right) + 1 \right] \qquad [4.18]$$

The consistency between the estimation error variance and the observed estimation error:

$$e_i^{-k(i)} = \left(Z_i - Z_i^{-k(i)}\right) \quad [4.19]$$

was calculated using the standard mean squared error (*SMSE*) (Hevesi et al., 1992):

$$SMSE = \frac{1}{n}\sum_{i=1}^{n}\frac{\left(e_i^{-k(i)}\right)^2}{\hat{\sigma}_i^{2(-k(i))}} \quad [4.20]$$

Estimation error variances were assumed to be consistent with true errors if the *SMSE* fell within the interval $(1\pm2[2/n]^{0.5})$ (Hevesi et al., 1992). The estimation error variances were also used to construct 95% confidence intervals around individual estimates. Coverage rates were calculated as the proportion of individual confidence intervals that contained the true value.

4.3 Results and Discussion

Sampling locations for the two sampling approaches are displayed in Figures 4.2 to 4.4. Results from chemical analysis of soil samples (i.e. grid samples and cluster samples) are summarized in Table 4.1. Average and standard deviation values for measured variables obtained from the two sampling approaches appeared similar with the exception of Zn on Field 2. The average Zn value from the cluster sampling technique was 1.7 mg kg^{-1} compared to 0.6 for the grid sampling technique, however, both techniques had similar standard deviations. The highest Zn values were observed on Field 3 and overall Zn values ranged from 0.6 to 2.3 mg kg^{-1}. Overall OM values were consistent across all fields and ranged from 1.3 to 1.6%. Nitrate-N values were variable and ranged from 7.3 to 21 mg kg^{-1}; highest NO_3-N values were found on Field 3. Ammonium-N values were consistent and ranged from 2.8 to 6.3 mg kg^{-1}. Similarly, EC values were consistent across all fields and ranged from 0.3 to 0.5 mmhos cm^{-1}.

4.3.1 Grid Sampling Trend Surface-Models

From a modeling standpoint trend surface-models are the first step in developing interpolation models to predict soil parameter values across a field. The trend surface-models describe large-scale spatial trends in the soil parameters. Small-scale trends in the data are modeled with the residual values from trend surface-models. However, residuals can only be modeled via kriging if they display spatial correlation. Residuals can also be modeled via regression tree analysis regardless of spatial correlation, but, auxiliary data must be available to utilize the regression tree option. The ability to model residuals is desirable because the final result is a more comprehensive model that includes small-scale and large-scale trends and a better overall fit of the data as indicated by fit statistics.

Optimum trend surface-models based on the grid sampling approach are summarized in Table 4.2. Regression coefficients ranged from 0.11 to 0.72 and all models had significant p-values. Field 1, trend surface-models had the highest R^2 values for EC and NH_4-N when compared with the remaining three parameters; 0.31 and 0.39 respectively. Field 2, trend surface-models had the highest R^2 values for OM and EC (0.72 and 0.58 respectively) and Field 3, trend surface-models had higher R^2 values for OM and Zn (0.65 and 0.60 respectively). Since the trend surface-models predict parameter values in two dimensions, it would be logical to expect them to contain both X and Y location-parameters as important independent variables for prediction purposes. Each trend surface-model contained at least one quadratic term (i.e. X^2, Y^2, or XY) based on the all combinations screening procedure and all but one of the grid sampling, trend surface-models contained both X and Y as dependent variables; Field 3, NO_3-N only

contained location-parameter X as X^2 and suggests NO_3-N concentrations follow a simple quadratic gradient in the X direction.

Moran's I values for the residuals from trend surface-models ranged from -0.043 to -0.006 (Table 4.3). Residuals from two trend surface-models displayed significant Moran's I values (i.e. NO_3-N Field 2; and NH_4-N Field 2). This outcome allows additional modeling of those parameters to describe or model small-scale trends in the data. Residuals from the remaining trend surface-models were spatially independent and further modeling of those data sets would be inappropriate; essentially, these trend surface-models described all of the large-scale variation in the data and the residuals did not contain any additional small-scale variation for modeling purposes.

The *RMSE* can be used to evaluate the small-scale estimation of the trend surface models and they are summarized in Table 4.3. The *RMSE* for the trend surface-models ranged from 0.05 to 8.84. Nitrate-N and NH_4-N consistently had the highest *RMSE* when compared with OM, Zn, and EC; *RMSE* ranged from 1.0 to 8.8 for the N parameters. Electrical conductivity had smallest *RMSE* values (0.05 to 0.08). The large *RMSE* associated with N parameters suggests some N values in the data set may be large and contribute to overestimation errors (i.e. contain outliers) or N concentrations vary across fields.

4.3.2 Cluster Sampling Trend Surface-Models

Optimum trend surface-models based on the cluster sampling approach are summarized in Table 4.4. Regression coefficients ranged from 0.09 to 0.81 and all models had significant p-values. Field 1, trend surface-models had the highest R^2 values for OM and EC when compared with the remaining three parameters; 0.40 and 0.27

respectively. Field 2, trend surface-models had the highest R^2 values for OM and Zn (0.81 and 0.63 respectively) and Field 3, trend surface-models had higher R^2 values for NO_3-N and EC (0.19 and 0.25 respectively). Since the cluster sampling, trend surface-models can contain *X* and *Y* location-parameters as well as auxiliary variables *R*, *G*, and/or *B* they are not as likely to contain both *X* and *Y* in the final models when compared with the grid sampling approach. Four cluster sampling, trend surface-models contain only *X* or *Y* location-parameters. In all four models, secondary variables were identified as important based on the all combinations screening procedure (Field 1, OM and Zn; Field 3, OM and NH_4-N). One cluster sampling, trend surface-model contained only auxiliary variables (i.e. *R* and *G*; Field 2, NH_4-N) as important independent variables. The additional information provided by the auxiliary variables is most likely the reason that five of the cluster sampling, trend surface-models contain one or less *X* or *Y* location-parameters.

Moran's *I* values for the residuals from trend surface-models ranged from -0.09 to 0.35 (Table 4.5). Residuals from seven trend surface-models displayed significant Moran's *I* values; compared with two for the grid sampling technique. The primary differences between the two sampling approaches for this step of the modeling procedure is the inclusion of auxiliary variables *R*, *G*, and *B* as well as small separation distances among some of the samples with the cluster sampling design. A benefit of having spatially dependent residuals is the opportunity to improve interpolation of the soil parameter(s) by further modeling residuals via MRK procedures.

The *RMSE* for the trend surface-models ranged from 0.05 to 6.10 (Table 4.4). Nitrate-N and NH_4-N consistently had the highest *RMSE* when compared with OM, Zn,

and EC; *RMSE* ranged from 0.7 to 2.6 for the N parameters. Electrical conductivity had smallest *RMSE* values (0.05 to 0.30). The large *RMSE* associated with N parameters suggest N concentrations vary across fields while small *RMSE* associated with EC suggests EC concentrations are consistent and vary little across fields.

Both sampling approaches had trend surface-models with similar parameter estimation properties with respect to R^2 and *RMSE*. This suggests the two approaches have similar large-scale estimation abilities since the trend surface-model essentially explains the large-scale trends in the data. The two approaches differ when considering the spatial dependency of model residuals. Seven cluster sampling, trend-surface-models resulted in spatially dependent residuals, compared with two for the grid sampling approach. Spatial dependency of the residuals suggests small-scale information still remains in the data set, and provides an opportunity to improve predictive performance of the models. The cluster sampling, trend surface-models more often resulted in residuals data sets that contained additional small-scale information; this was only true for two residual data sets from the grid sampling approach.

Both grid sampling and cluster sampling approaches have similar large-scale predictive properties for the soil parameters of interest as indicated by R^2 and *RMSE* statistics. However, the cluster sampling approach was most effective at capturing small-scale trends in the data as indicated by Moran's *I* analysis. This is a desirable property for researchers interested in interpolating soil parameters because it affords an opportunity to improve model predictions beyond large-scale trends.

4.3.3 Grid Sampling Modified Residual Kriging Models

The only soil parameters with spatially dependent residuals after grid sampling, trend surface-model construction were NO_3-N and NH_4-N from Field 2. The remaining soil parameters could not be effectively modeled beyond the trend surface-model stage. This is a common outcome when separation distance among sample locations is too large. It is apparent that at our sampling intensity, the grid sampling technique captured large-scale trends in the data but failed to capture small-scale trends for almost all of the soil parameters of interest. Consequently, only the spatially dependent residuals data sets (i.e. NO_3-N and NH_4-N from Field 2) were modeled using an ordinary kriging procedure. The spherical variogram model minimized the Akaike's Information Criteria for NO_3-N and was selected as optimum; the exponential model was optimum for NH_4-N. Final, predictive modified residual kriging models were calculated by summing the trend surface and ordinary kriging surfaces as explained in Eq. 4.6.

All surface-models generated with the grid sampling, modified residual kriging are displayed in Appendix A and are briefly discussed here. Since all but two of the grid sampling, modified residual kriging models are simple trend surface-models, their visual representations take the form of simple gradient models across the fields. The only grid sampling, modified residual kriging models that incorporated ordinary kriging components were NO_3-N and NH_4-N from Field 2 (Figures A.6 and A.7). The grid sampling, modified residual kriging NO_3-N model displayed increasing N values as one moves-out from the center of the field. Alternatively, the NH_4-N grid sampling, modified residual kriging model displayed decreasing N values as one moves-out from the center of the field.

The *G*-statistics for the final modified residual kriging models are summarized in Table 4.6. Although only two residual data sets were kriged, *G*-statistics for all models (i.e. trend surface and modified residual kriging models) are presented for consistency; $G = R^2$ for trend surface-models. The modified residual kriging models improved estimates of NH_4-N on Field 2 by 16% when compared with trend surface-models alone. The modified residual kriging model did not improve estimates of NO_3-N on Field 2 and actually resulted in poorer estimates than using a trend surface-model alone (i.e. 27% decrease). Although I can not conclude decisively as to the cause of the decrease in model efficiency, the two most probable causes of poor model performance are outliers and/or overfitting of the model. For example, if only a few samples displayed strong spatial dependency, they may have contributed spatial dependence to an otherwise spatially independent data set.

Bias estimates for the modified residual kriging models are summarized in Table 4.7. Bias for trend surface-models alone (i.e. all parameters except for NO_3-N and NH_4-N) is, by definition of the regression estimator, 0 since those models were constructed only with simple trend surface-models. Essentially, unless the residuals from a trend surface-model are further modeled, the bias is by definition, 0. However, bias for the residuals from the modified residual kriging models was -42.7% and -163.0% for NO_3-N and NH_4-N, respectively. The large negative bias values indicate that the models overestimate N values when compared with observed values. The tendency to overestimate is primarily due to the presence of very large outliers in the data set.

Estimates of *RMSE* for the modified residual kriging models were not improved over the grid sampling, trend surface-models (Table 4.7). Although modified residual

kriging improved the large-scale fit of the NH_4-N data by 16% (Table 4.6), *RMSE* values from the modified residual kriging models suggest modeling beyond the trend surface-model was not helpful in predicting N parameters with respect to small-scale variation. The mean error was slightly negative for both, N parameters. Similar to bias estimates, this suggests a tendency of the models to overestimate. Mean absolute errors were 4.0 and 1.4 for NO_3-N and NH_4-N respectively.

With respect to NO_3-N and NH_4-N modified residual kriging models, large-scale fit was improved only for NH_4-N. However, small-scale fits were not improved when compared to the trend surface-models for NO_3-N and NH_4-N as is indicated by the small-scale fit statistic *RMSE*. In addition, both of the modified residual kriging models had a tendency to overestimate as indicated by the bias and mean error statistics.

4.3.4 Cluster Sampling Modified Residual Kriging Models

Seven soil parameters displayed spatially dependent residuals after trend surface-models were developed based on the cluster sampling technique. The spherical variogram model minimized the Akaike's Information Criteria for OM at Fields 1, 2, and 3 and was selected as optimum. The exponential model was optimum for NO_3-N and NH_4-N at Field 1. The Gaussian model was optimum for EC and NH_4-N at Field 3. The increased number of soil parameters displaying spatially dependent residuals after trend surface modeling suggests the cluster sampling technique is more apt to capture small-scale trends in the data when compared with the grid sampling technique. Modeling spatially dependent residuals provides the opportunity to improve the overall interpolation of the data by incorporating both large-scale and small-scale components of the parameter of interest.

Another benefit of the cluster sampling technique is the presence of auxiliary variables for modeling purposes. Soil parameters that did not display spatially dependent residuals after trend surface modeling can be modeled with regression tree analysis. This option is not possible for the grid sampling approach because auxiliary variables are not used with the grid sampling technique. The regression tree is a non-parametric approach to regression.

All surface-models generated with the cluster sampling, modified residual kriging models are displayed in Appendix A and are briefly discussed here. The cluster sampling, modified residual kriging models that have only *X* and *Y* independent variable components in the initial trend surface-models generated visual representations that maintain an underlying 'gradient appearance'. This is to be expected since the trend surface-model describes large-scale variability and large-scale variability generally composes the majority of surface-models. Only modified residual kriging models that had *R*, *G*, or *B* components in the initial trend surface-model generated a 'smooth appearance'. The band information is less likely to maintain an underlying linear component compared to a trend surface-model that is composed only of *X* and *Y* independent variables.

The *G*-statistics for the final cluster sampling, modified residual kriging approach are summarized in Table 4.8. The modified residual kriging procedure improved the trend surface-models in every instance. The average improvement was 34%; minimum = 1%, and maximum =72%. Bias estimates for the cluster sampling, modified residual kriging models were small and are summarized in Table 4.9. On average, bias was negative (i.e. -0.8%) although 8 of the 15 estimates were positive; minimum bias = -

5.8%, and maximum bias = 1.8%. These bias estimates indicate the cluster sampling, modified residual kriging models overestimate soil parameters, on average, by a small percentage.

Estimates of *RMSE* for the cluster sampling, modified residual kriging models were improved over the trend surface-models in all but one instance (Table 4.9). The improved *RMSE* statistics indicate that the modified residual kriging models are better at predicting small-scale variation when compared with trends surface-models alone. The average mean error was slightly negative for the modified residual kriging models (i.e. -0.02) although 10 of the 15 estimates are positive. Similar to the bias estimates, this suggests a tendency of these models to overestimate. Average mean absolute error was 0.6; minimum 0.03, and maximum 3.47.

With respect to cluster sampling, modified residual kriging models, the large-scale fit of the data was improved for all the soil parameters when compared with the cluster sampling, trend surface-models. Additionally, small-scale fits were improved for all of the soil parameters when compared to the cluster sampling, trend surface-models as is indicated by the small-scale fit statistic *RMSE*. In addition, the cluster sampling, modified residual kriging models had relatively small bias and mean error statistics; particularly when compare to the grid sampling approach.

4.3.5 Grid Sampling Cross-validations

Grid sampling 'observed vs. predicted' summary statistics for the 10-fold cross-validation procedure are presented in Table 4.10. As explained and defined in section 4.2.5, 10% of the data points from the residual data set are removed and the appropriate trend surface or modified residual kriging model is fit to the remaining 90% of the

residuals. The newly fit model is also used to predict the residual values for the 10% removed. The 10% removed effectively provides an independent data set to test the effectiveness of the model. The procedure is run 10 times to remove all data points, and predicted values from the procedure are compared to the actual values from the appropriate residual data set. Overall, predicted residual estimates from the cross-validation procedure were similar when compared to original residual values.

Residuals-analysis statistics for the grid sampling, cross-validation procedure are summarized in Table 4.11. The average mean error was 0.04; minimum = -0.11, and maximum = 0.30. Ideally the mean error should be approximately 0 and in this case mean error estimates deviate little from 0. The median error estimates were also small and deviated little from 0. The *RMSE* values from grid sampling, cross-validations were similar to those generated from the modified residual kriging and were not improved beyond the trend surface-model; *RMSE* actually increased compared to the trend surface-models. Most of the grid sampling, cross-validation parameters were positively skewed; 4 were negatively skewed. Cross-validation residuals from Field 2, ordinary kriging model for NO_3-N had the highest skewness and the highest *RMSE* values. The high values were probably the result of the large outliers in the observed data set. Most of the cross-validation residuals had positive kurtosis values. As explained and defined in section 4.2.5, kurtosis is a measure of how different a distribution is from the normal distribution. A negative value (i.e. platykurtic) typically indicates a distribution that is flatter than the standard normal distribution. A positive value (i.e. leptokurtotic) typically indicates a distribution more peaked than the standard normal. The kurtosis for a normal distribution is 3 although most calculations standardize this value to 0. Positive kurtosis

values indicate most of the residual data sets were leptokurtotic. As with large skewness and *RMSE* values, this suggests an observed data set that may have contained outliers.

Results from the Anderson-Darling normality test indicate that residuals from six of the cross-validations are not normal (Table 4.11). Residuals from cross-validation for NO_3-N and Zn from Field 2 were among the non-normal residual data sets. As explained and defined in section 4.2.5, estimation error variances were assumed to be consistent with true errors if the *SMSE* fell within the interval $1\pm2[2/n]^{0.5}$. Cross-validations with *SMSE* that fell within the intervals displayed in Table 4.12 were assumed to be consistent with the observed residuals. Ten of the cross-validations had *SMSE* that fell within the prescribed intervals. All of the predictive models had coverage rates ranging from 0.90 to 0.98 with a mean of 0.94.

The cross-validations for the grid sampling approach indicate the trend surface and modified residual kriging models performed well. Histograms of the residual distributions suggest a relatively normal distribution for the cross-validations (see Appendix B). Although some of the residuals-analysis statistics indicate the predicted residuals deviate from a normal distribution, the cross-validations on-the-whole indicate the predictive models are effective.

4.3.6 Cluster Sampling Cross-validations

Cluster sampling 'observed vs. predicted' summary statistics for the 10-fold cross-validation procedure are presented in Table 4.13. Overall, predicted residuals from the cross-validation procedure were reasonable when compared to observed residual values. Residuals-analysis statistics for the cluster sampling, cross-validation procedure are summarized in Table 4.14. The average mean error was -0.26; minimum = -5.39, and

maximum = 0.12. Ideally the mean error should be approximately 0 and in this case mean error estimates are slightly negative mainly because the mean error for NH_4-N from Field 3, ordinary kriging model was so large. The median error estimates were also small and deviated little from 0. The *RMSE* values were slightly higher than those generated from the modified residual kriging models. Again, prediction of the N parameters was not improved beyond the trend surface-model and *RMSE* actually increased compared to the trend surface-models. In all cases, the parameters with the highest *RMSE* (i.e. poorest performers) were the N parameters. Most of the cross-validation residual estimates were positively skewed; 7 were negatively skewed. Half of the cross-validation residual estimates had positive kurtosis values. Positive kurtosis values indicate most of the residual data sets were leptokurtotic. As with large skewness and *RMSE* values, this suggests an observed data set that may have contained outliers.

Results from the Anderson-Darling normality test indicate that residuals from six of cross-validations are not normal (Table 4.14). Nitrogen and EC parameters composed all of the non-normal residual data sets. Cross-validations with *SMSE* that fell within the intervals displayed in Table 4.12 were assumed to be consistent with the observed residuals. Six of the cross-validations had *SMSE* that fell within the prescribed intervals. All of the models had coverage rates ranging from 0.65 to 1.0 with a mean of 0.93. Nitrogen parameters had the lowest coverage rates.

The cross-validations for the cluster sampling approach indicate the modified residual kriging models performed well. Histograms of the residual distributions suggest a relatively normal distribution for the cross-validations (see Appendix B). Although some of the residuals-analysis statistics indicate the predicted residuals deviate from a

normal distribution, the cross-validations on-the-whole indicate the predictive models are effective.

4.4 Summary and Conclusions

Regression coefficients for grid sampling, trend surface-models ranged from 0.11 to 0.72 and all models had significant *p*-values. Similarly, regression coefficients for cluster sampling, trend surface-models ranged from 0.09 to 0.81 and all models had significant *p*-values. This suggests that trend surface-models developed with a grid sampling or cluster sampling approach will perform similarly. This is expected since trend surface-models generally explain large-scale trends in a data set. However, for interpolation of soil parameters, small-scale variation is of primary interest since this is the component that is more difficult to explain with a mathematical model. Typical grid sampling designs are more likely to capture large-scale variability but they often fail to capture small-scale trends in the data due to large separation distances among samples. This is evident from the lack of spatial dependency in the residuals from all but two of the grid sampling, trend surface-models. In contrast, residuals from seven cluster sampling, trend surface-models displayed significant Moran's *I* values. The primary differences between the grid sampling and cluster samping techniques for this step of the modeling procedure is the inclusion of auxiliary variables *R*, *G*, and *B* as well as small separation distances among some of the samples with the cluster sampling design. The primary result is the benefit of having spatially dependent residuals that are useful for additional modeling via modified residual kriging procedures. Also, by utilizing auxiliary data beyond *x* and *y* coordinates, the cluster sampling approach can produce modified residual estimates by combining cluster sampling, trend surface estimates with

cluster sampling, regression tree estimates of the residuals since regression tree analysis does not require spatially dependent residuals.

As explained in section 4.2.3, if the residuals from a trend surface-model are not spatially dependent, the trend surface-model is considered the optimum surface-model and additional residual modeling is not applicable. Only NO_3-N and NH_4-N from Field 2 were modeled using the grid sampling data, with a modified residual kriging procedure. These were the only two soil parameters from the grid sampling technique that displayed spatially dependent (i.e. spatially correlated) residuals; they were the only two data sets with information available for modeling small-scale trends in the data. The grid sampling, modified residual kriging procedure improved estimates of NH_4-N on Field 2 by 16% but did not improve estimates of NO_3-N on Field 2 and actually resulted in poorer estimates than using a trend surface-model alone (i.e. 27% decrease). It is not possible to exactly explain why NO_3-N estimates were so poor after the modified residual kriging procedure. However, based on the evidence that is available from this study, the two most probable causes of poor model performance are outliers and/or overfitting of the model. Bias for the residuals from the modified residual kriging was -42.7% and -163.0% for NO_3-N and NH_4-N, respectively. The large negative bias values indicate that the models overestimate N values when compared with observed values. Also, estimates of *RMSE* for the grid sampling, modified residual kriging models were not improved over the grid sampling, trend surface-models.

In comparison, the cluster sampling, modified residual kriging procedures improved trend surface-models for all of the soil parameters. The average improvement was 34%; minimum = 1%, and maximum =72%. Bias estimates for the cluster sampling,

modified residual kriging models were small and estimates of *RMSE* were improved over the cluster sampling, trend surface-models in all but one instance (Table 4.9). The improved *RMSE* statistics indicate that the cluster sampling, modified residual kriging models are better at predicting small-scale variation when compared with cluster sampling, trend surface-models as well as the grid sampling, trend surface-models. This important result cannot be over emphasized. The cluster sampling procedure, in combination with auxiliary data sets allows additional modeling of the small-scale variation in the data. This additional, small-scale modeling results in improved overall estimates, and improved small-scale estimates of the soil parameters as indicated by *G*-statistics and small-scale fit statistics. For all but two of the grid sampling, soil parameters the additional modeling of small-scale variation was not possible due to spatially independent residuals.

The 'observed vs. predicted' statistics from the 10-fold cross-validation procedure were reasonable when compared to observed residual values for both the grid and cluster sampling designs. The two parameters with the highest coefficient of variation for predicted residuals from grid sampling were Field 2, NO_3-N and Zn. In both cases, the predicted residuals appeared to be skewed to the right. The parameter with the highest coefficient of variation for predicted residuals from cluster sampling was Field 2, modified residual kriging OM. Again, the predicted residuals appeared to be skewed to the right suggesting the presence of outliers in the original data set. Overall, the results from cross-validation of grid and cluster sampling models indicate both sets of models are acceptable interpolators.

Ideally, the residuals from any predictive model will be normally distributed with mean 0. The Anderson-Darling normality test was used to test the underlying residuals distribution from cluster and grid sampling, cross-validations. Sixty-percent of the model residuals from the grid sampling, cross-validation were considered normally distributed compared to 73% of the model residuals from the cluster sampling, cross-validation. It is important consider the fact that 80% of the model residuals from the grid sampling, cross-validation were constructed from simple trend surface-models. Generally, it is easier to develop simple trend surface-models with ideally distributed residuals since the model only estimates large-scale trends. In contrast, all model residuals from the cluster sampling, cross-validation were estimated from more complex modified residual kriging models that estimate large-scale and small-scale trends. In general, the histograms of the cross-validation residuals suggest the predictive models generated reasonably normal residuals.

This study demonstrated the potential applications of an alternative sampling design for interpolating soil properties. The alternative (i.e. cluster sampling) approach resulted in spatially correlated residuals for seven of the trend surface-models; only two of the grid sampling, residuals data sets were spatially correlated. The inclusion of auxiliary variables in the cluster sampling procedure also allowed the modeling of spatially independent residuals data sets; this was not possible with residual data sets from the grid sampling procedure. Also, the residuals modeling procedure for the cluster sampling approach improved overall estimates of the parameter of interest on the average of 34%; residuals modeling only improved one soil parameter for the grid sampling

approach (i.e. NH_4-N). Overall, interpolation of soil parameters utilizing the cluster sampling approach was greatly improved compared to the grid sampling approach.

The cluster sampling design provides a foundation for future research designed to improve interpolation of agricultural (or any natural resource variable) soil properties. Scale of spatial dependency is the first important consideration when designing a soil sampling program for interpolating soil properties. There has been abundant research to suggest grid sampling designs are not appropriate for interpolating soil properties. The scale of spatial dependency for soil properties is typically much smaller than traditional sampling grids capture. However, it should be feasible to develop alternative sampling designs that can capture spatial dependency and still remain economically realistic. Auxiliary data sets are the second important consideration when designing a soil sampling program for interpolating soil properties. Auxiliary data sets may include additional spectral reflectance surfaces, topography, surface curvature, etc. These data sets are often readily available, relatively inexpensive, and often provide surface resolution that is not attainable with soil sampling alone. Improved sampling and interpolation procedures will be essential for the effective implementation of precision farming in general and variable rate application of agricultural inputs in particular.

4.5 References

Agterberg, F.P. 1984. Trend surface analysis. *In* G.L. Gaile and C.J. Willmott (ed.) Spatial statistics and models. Reidel, Dordrecht, The Netherlands.

Akaike, H. 1977. On entropy maximization principle. *In* P.R. Krishnaiah (ed.) Applications of statistics. North-Holland, Amsterdam, The Netherlands.

Balk, B., and K. Elder. 2000. Combining binary decision tree and geostatistical methods to estimate snow distribution in a mountain watershed. Water Resour. Res. 36: 13-26.

Breiman, L., J.H. Friedman, R.A. Olshen, and C.J. Stone. 1984. Classification and regression trees. Wadsworth Ind. Group, Belmont, CA.

De'Ath, G., and K.E. Fabricius. 2000. Classification and regression trees: a powerful yet simple technique for ecological data analysis. Ecology. 81: 3178-3192.

ESRI. 1995. ARC/INFO® software and on-line help manual. Environmental Research Institute Inc., Redlands, CA.

Fleming, K.L., D.G. Westfall, D.W. Wiens, and M.C. Brodahl. 2000. Evaluating farmer defined management zone maps for variable rate fertilizer application. Precis. Agric. 2:201-215.

Franzen, D.W., and T.R. Peck. 1995. Sampling for site-specific application. p. 535-551. *In* P.C. Robert et al., (ed.) Site-Specific Management for Agricultural Systems. Proc. Int. Conf., 2nd. March 27-30, 1994. Minneapolis, MN. ASA, CSSA, and SSSA, Madison, WI.

Guisan, A., and N.E. Zimmermann. 2000. Predictive habitat distribution models in ecology. Ecol. Model. 135:147-186.

Hammond, M.W. 1993. Cost analysis of variable fertility management of phosphorus and potassium for potato production in central Washington. p. 213-228. *In* P.C. Robert et al., (ed.) Soil Specific Crop Management. Proc. Workshop, 1st. April 14-16, 1992. Minneapolis, MN. ASA, CSSA, and SSSA, Madison, WI.

Hansen, M., R. Dubayah, and R. Defries. 1996. Classification trees: an alternative to traditional land cover classifiers. J. Remote Sens. 17: 1075-1081.

Hevesi, J.A., J.D. Istok, and A.L. Flint. 1992. Precipitation estimation in mountainous terrain using multivariate geostatistics. Part I: structural analysis. J. Appl. Meteorol. 31:661-676.

Isaaks, E.H., and R.M. Srivastava. 1989. An introduction to applied geostatistics. Oxford University Press, New York.

Joy, S.M., R.M. Reich, and R.T. Reynolds. 2001. Modeling small-scale variability in the composition of goshawk habitat on the Kaibab National Forest. *In* Proceedings of the 8th biennial forest service remote sensing applications conference, 10-14 April, 2000, Albuquerque, NM.

Leica Geosystems. 2003. Image analysis for ArcGIS. Image analysis software for personal computers. Leica Geosystems, Atlanta, GA.

Manly, B.J. 1998. Multivariate statistical methods: a primer. Chapman and Hall/CRC, New York.

McBratney, A.B., and M.J. Pringle. 1999. Estimating average and proportional variograms of soil properties and their potential use in precision agriculture. Precis. Agric. 1:219-236.

Metzger, K. 1997. Modeling forest stand structure to a ten meter resolution using Landsat TM data. MS Thesis, Colo. State Univ., Fort Collins.

Michaelsen, J., D.S. Schimel, M.A. Friedl, F.W. Davis, and R.C. Dubayah. 1994. Regression tree analysis of satellite and terrain data to guide vegetation sampling and surveys. J. Veg. Sci. 5: 673-686.

Miller, R.O., J. Kotuby-Amacher, and J.B. Rodriguez. 1998. Western states laboratory proficiency testing program, soil and plant analytical methods. Version 4.10.

Mueller, T.G., F.J. Pierce, O. Schabenberger, and D.D. Warncke. 2001. Map quality for site-specific fertility management. Soil Sci. Soc. Amer. J. 65:1547-1558.

Nielsen, D.R., and M.H. Alemi. 1989. Statistical opportunities for analyzing spatial and temporal heterogeneity of field soils. Plant Soil. 115: 285-296.

Reich, R.M., and R.A. Davis. 1998. On-line spatial library for the S-PLUS statistical software package. Colo. State. Univ., Fort Collins.

Romeu, J.L. 2003. Anderson-Darling: a goodness of fit test for small samples assumptions [Online]. Available http://rac.alionscience.com/pdf/A_DTest.pdf (verified 30 Sep. 2003.)

Sawyer, J.E. 1994. Concepts of variable rate technology with considerations for fertilizer application. J. Prod. Agric. 7:195-201.

Schloerder, C.A., N.E. Zemmerman, and M.J. Jacobs. 2001. Comparison of methods for interpolating soil properties using limited data. Soil Sci. Soc. Am. J. 65:470-479.

Schreier, H., R. Wiart, and S. Smith. 1988. Quantifying organic matter degradation in agricultural fields using PC-based image analysis. J. Soil Water Conserv. 43: 421-424.

Statistical Sciences. 1999. S-PLUS© 2000. Statistical software package for personal computers. StatSci Division, MathSoft, Inc., Seattle, WA.

Whelan, B.M., A.B. McBratney, and R.A. Viscarra-Rossel. 1996. Spatial prediction for precision farming. p. 331-342. *In* P.C. Robert et al., (ed.) Precision Agriculture. Proc. Intl. Conf., 3rd. June 23-26, 1995. Minneapolis, MN. ASA, CSSA, and SSSA, Madison, WI.

Table 4.1 Summary statistics for soil parameters used in analysis. Summary data presented for both grid samples (GS) and cluster samples (SC). Values are averages; values in parentheses are standard deviations.

		OM	NO_3-N	NH_4-N	Zn	EC
		%	---------mg kg^{-1}----------			--mmhos cm^{-1}--
Field 1	GS	1.6 (0.3)	9.6 (2.9)	2.8 (1.3)	1.7 (0.5)	0.3 (0.1)
Field 2	GS	1.4 (0.4)	7.3 (9.5)	5.3 (2.2)	0.6 (0.4)	0.4 (0.1)
Field 3	GS	1.3 (0.2)	20.2 (5.5)	4.7 (1.4)	2.3 (0.4)	0.5 (0.1)
Field 1	SC	1.4 (0.2)	10.0 (2.8)	6.3 (1.5)	1.8 (0.6)	0.3 (0.1)
Field 2	SC	1.3 (0.5)	9.2 (3.1)	5.6 (0.7)	1.7 (0.7)	0.4 (0.1)
Field 3	SC	1.3 (0.2)	20.9 (6.8)	6.3 (1.5)	1.8 (0.6)	0.3 (0.1)

Table 4.2 Optimum trend surface models for interpolation of soil parameters for soil samples collected with a standard grid sampling technique. Models were selected with an all-combinations regression procedure. *X* indicates UTM coordinate in the easting direction and *Y* indicates UTM coordinate in the northing direction. Regression model coefficients and associated *p*-values are displayed.

		R^2	*p*-value
Field 1	$OM = 1.80675 - 0.001458798X + 0.000001608248X^2 - 0.000003247433Y^2 + 0.000002544091XY$	0.171	0.013
Field 1	$NO_3\text{-}N = 12.59058 - 0.00718372X - 0.0231127Y + 0.00005631467XY$	0.186	0.003
Field 1	$Zn = 2.132419 - 0.002803367X - 0.001702644Y + 0.000002346287X^2 + 0.000006691789XY$	0.135	0.043
Field 1	$EC = 0.2681389 + 0.0000001636846X^2 + 0.0000003438844Y^2$	0.315	<0.0001
Field 1	$NH_4\text{-}N = 3.048013 - 0.005294069X + 0.000004933266X^2 + 0.00001730553Y^2$	0.395	<0.0001
Field 2	$OM = 2.36353 - 0.005691985X - 0.005555005Y + 0.000009118999X^2 + 0.000007408733Y^2 + 0.000005055842XY$	0.724	<0.0001
Field 2	$NO_3\text{-}N = 15.5178 - 0.05876478Y + 0.00007583777Y^2$	0.111	0.029
Field 2	$Zn = 1.344318 - 0.005579954Y + 0.000006239009Y^2 + 0.000003156423XY$	0.411	<0.0001
Field 2	$EC = 0.6343667 - 0.0005535443X - 0.001405081Y + 0.000001916743Y^2 + 0.000001158078XY$	0.583	<0.0001
Field 2	$NH_4\text{-}N = 1.038858 + 0.02096963X + 0.01401707Y - 0.00003493504X^2 - 0.00001689598Y^2$	0.389	<0.0001
Field 3	$OM = 1.025422 + 0.003107532X - 0.000003835312X^2 - 0.000003384404XY$	0.654	<0.0001
Field 3	$NO_3\text{-}N = 18.12098 + 0.00004053736X^2$	0.121	0.012
Field 3	$Zn = 1.776865 + 0.002296345X + 0.003215983Y - 0.000008491049Y^2$	0.599	<0.0001
Field 3	$EC = 0.5305473 + 0.0000006697764Y^2 - 0.0000008077559XY$	0.170	0.012
Field 3	$NH_4\text{-}N = 6.140233 - 0.00521841Y - 0.00001838271X^2 + 0.00001589984XY$	0.186	0.021

Table 4.3 Residuals-analysis statistics for trend surface models; soil samples collected with a traditional grid sampling design.

	Soil parameter	Moran's *I*	*p*-value	*RMSE*†
Field 1	OM	-0.014	0.987	0.264
Field 1	NO_3-N	-0.032	0.219	2.573
Field 1	Zn	-0.006	0.565	0.464
Field 1	EC	-0.025	0.446	0.045
Field 1	NH_4-N	-0.034	0.111	0.996
Field 2	OM	-0.009	0.667	0.234
Field 2	NO_3-N	-0.039	0.002	8.837
Field 2	Zn	-0.043	0.093	0.318
Field 2	EC	-0.037	0.175	0.083
Field 2	NH_4-N	0.019	0.029	1.899
Field 3	OM	-0.006	0.447	0.108
Field 3	NO_3-N	-0.013	0.699	5.076
Field 3	Zn	-0.012	0.656	0.264
Field 3	EC	-0.009	0.531	0.079
Field 3	NH_4-N	-0.040	0.231	1.260

† Root mean squared error

Table 4.4 Optimum trend surface models for interpolation of soil parameters for soil samples collected with a cluster sampling technique. Models were selected with an all-combinations regression procedure. *X* indicates UTM coordinate in the easting direction and *Y* indicates UTM coordinate in the northing direction; *R*, *G*, and *B* indicate bare soil imagery bands. Regression model coefficients and associated *p*-values are displayed.

		R^2	*p*-value
Field 1	$OM = 2.95424 - 0.02550551R + 0.009576205B - 0.0000007261709X^2$	0.3976	<0.0001
Field 1	$NO_3\text{-}N = 10.14477 + 0.003088867X - 0.00675499Y$	0.1376	0.003
Field 1	$Zn = 2.351579 - 0.03815211G + 0.04403212B - 0.006029178Y + 0.00001318298Y_2$	0.2145	0.001
Field 1	$EC = 0.2621838 + 0.0001400115X + 0.0000002565288Y^2$	0.2695	<0.0001
Field 1	$NH_4\text{-}N = 9.977526 - 0.02537495G + 0.007925601X - 0.002508981Y - 0.00001101353X^2$	0.2395	0.000
Field 2	$OM = 2.669277 - 0.009133214X - 0.005334531Y + 0.00000874875X^2 + 0.000004475065Y^2 + 0.00001441906XY$	0.8082	<0.0001
Field 2	$NO_3\text{-}N = 16.14526 - 0.05618016X - 0.02166656Y + 0.00007276577X^2 + 0.00001576532Y^2 + 0.00006868927XY$	0.5442	<0.0001
Field 2	$Zn = 2.459875 - 0.03648502R + 0.03249121B - 0.007975518Y + 0.000007743802X^2 + 0.00001203426Y^2$	0.6293	<0.0001
Field 2	$EC = 0.7373443 - 0.002164326X - 0.001225759Y + 0.000003053295X^2 + 0.000001281088Y^2 + 0.000002600252XY$	0.5174	<0.0001
Field 2	$NH_4\text{-}N = 7.37828 - 0.04006555R + 0.02781046G$	0.1619	<0.0111
Field 3	$OM = 1.808585 - 0.003422139B - 0.0006481863X$	0.1309	0.008
Field 3	$NO_3\text{-}N = 52.8612 - 0.2239721R - 0.1527283X + 0.01542674Y + 0.000481229X^2$	0.1863	0.007
Field 3	$Zn = 2.995205 - 0.00000119745Y^2 + 0.000005168847XY$	0.0932	0.034
Field 3	$EC = 0.4386923 + 0.000004465144X^2 + 0.000003383363Y^2 - 0.000007503145XY$	0.2532	0.000
Field 3	$NH_4\text{-}N = 12.76835 - 0.02830726B - 0.0363791X + 0.0001385051X^2$	0.1374	0.018

Table 4.5 Residuals-analysis statistics for trend surface models; soil samples collected with an alternative cluster sampling design.

	Soil parameter	Moran's *I*	*p*-value	*RMSE*†
Field 1	OM	0.226	<0.0001	0.168
Field 1	NO_3-N	0.101	0.017	2.611
Field 1	Zn	0.078	0.055	0.517
Field 1	EC	0.184	<0.0001	0.052
Field 1	NH_4-N	0.025	0.426	1.377
Field 2	OM	0.354	<0.0001	0.306
Field 2	NO_3-N	-0.022	0.968	2.267
Field 2	Zn	0.065	0.248	0.395
Field 2	EC	-0.026	0.920	0.113
Field 2	NH_4-N	-0.087	0.340	0.655
Field 3	OM	0.211	<0.0001	0.163
Field 3	NO_3-N	0.036	0.166	6.100
Field 3	Zn	-0.016	0.957	0.339
Field 3	EC	0.049	0.019	0.297
Field 3	NH_4-N	-0.089	0.034	1.892

† Root mean squared error

Table 4.6 Summary of *G*-statistics from ordinary kriging (OK) of residuals for soil samples collected with a standard grid approach. In some cases, residuals from trend surface models (TS) did not display spatial dependency (i.e. Moran's *I*, Table 4.3) and additional modeling was not applicable (na). The model improvement resulting from residuals modeling is also displayed as a percentage.

	Interpolation technique	Soil parameter	$G^{\dagger}$	Improvement
Field 1	TS	OM	0.171	na
Field 1	TS	NO_3-N	0.186	na
Field 1	TS	Zn	0.135	na
Field 1	TS	EC	0.315	na
Field 1	TS	NH_4-N	0.395	na
Field 2	OK	NO_3-N	-0.164	-27%
Field 2	OK	NH_4-N	0.228	+16%
Field 2	TS	OM	0.724	na
Field 2	TS	Zn	0.411	na
Field 2	TS	EC	0.583	na
Field 3	TS	OM	0.654	na
Field 3	TS	NO_3-N	0.121	na
Field 3	TS	Zn	0.599	na
Field 3	TS	EC	0.170	na
Field 3	TS	NH_4-N	0.186	na

† *G*-statistic is equivalent to R^2 for trend surface models.

Table 4.7 Residuals-analysis statistics for ordinary kriging (OK) or trend surface model (TS) residuals (i.e. residuals from small-scale variation models, Table 4.6); soil samples collected with a standard grid.

	Interpolation technique	Soil parameter	*B* †	*RMSE* ‡	*ME* §	*MAE* ¶
			---%---			
Field 1	TS	OM	0	0.264	0.000	0.193
Field 1	TS	NO_3-N	0	2.573	0.000	2.108
Field 1	TS	Zn	0	0.464	0.000	0.371
Field 1	TS	EC	0	0.045	0.000	0.036
Field 1	TS	NH_4-N	0	0.996	0.000	0.581
Field 2	OK	NO_3-N	-43	10.218	-0.050	4.034
Field 2	OK	NH_4-N	-163	1.961	-0.137	1.426
Field 2	TS	OM	0	0.234	0.000	0.186
Field 2	TS	Zn	0	0.318	0.000	0.216
Field 2	TS	EC	0	0.083	0.000	0.058
Field 3	TS	OM	0	0.108	0.000	0.089
Field 3	TS	NO_3-N	0	5.076	0.000	3.927
Field 3	TS	Zn	0	0.264	0.000	0.223
Field 3	TS	EC	0	0.079	0.000	0.062
Field 3	TS	NH_4-N	0	1.260	0.000	0.823

† Percent bias.

‡ Root mean squared error.

§ Mean error.

¶ Mean absolute error.

Table 4.8 Summary of *G*-statistics for residuals interpolation models (i.e. ordinary kriging [OK], and regression trees [RT]) for soil samples collected with an alternative cluster approach. The model improvement resulting from residuals modeling is also displayed as a percentage.

	Interpolation technique	Soil parameter	$G^{\dagger}$	Improvement
Field 1	OK	OM	0.807	+41%
Field 1	OK	NO_3-N	0.592	+45%
Field 1	OK	EC	0.456	+19%
Field 1	RT	OM	0.683	+29%
Field 1	RT	NO_3-N	0.518	+38%
Field 1	RT	Zn	0.935	+72%
Field 1	RT	EC	0.607	+34%
Field 1	RT	NH_4-N	0.556	+32%
Field 2	OK	OM	0.819	+1%
Field 2	RT	OM	0.926	+12%
Field 2	RT	NO_3-N	0.566	+2%
Field 2	RT	Zn	0.802	+17%
Field 2	RT	EC	0.731	+21%
Field 2	RT	NH_4-N	0.345	+18%
Field 3	OK	OM	0.683	+55%
Field 3	OK	EC	0.619	+37%
Field 3	OK	NH_4-N	0.701	+56%
Field 3	RT	OM	0.699	+57%
Field 3	RT	NO_3-N	0.578	+39%
Field 3	RT	Zn	0.487	+39%
Field 3	RT	EC	0.459	+20%
Field 3	RT	NH_4-N	0.425	+29%

† *G*-statistic

Table 4.9 Residuals-analysis statistics for ordinary kriging (OK) or regression tree (RT) model residuals (i.e. residuals from small-scale variation models, Table 4.8); soil samples collected with a cluster approach.

	Interpolation technique	Soil parameter	*B*†	*RMSE*‡	*ME*§	*MAE*¶
			---%---			
Field 1	OK	OM	-0.853	0.095	-0.012	0.073
Field 1	OK	NO_3-N	-0.200	1.795	-0.020	1.350
Field 1	OK	EC	-2.195	0.098	-0.007	0.064
Field 1	RT	OM	-3.608	0.181	-0.050	0.140
Field 1	RT	NO_3-N	0.855	1.952	0.086	1.574
Field 1	RT	Zn	0.916	0.382	0.016	0.289
Field 1	RT	EC	-2.756	0.038	-0.009	0.030
Field 1	RT	NH_4-N	1.849	0.996	0.117	0.782
Field 2	OK	OM	-1.088	0.210	-0.014	0.143
Field 2	RT	OM	-0.097	0.134	-0.001	0.106
Field 2	RT	NO_3-N	0.098	2.023	0.009	1.560
Field 2	RT	Zn	-0.134	0.289	-0.002	0.237
Field 2	RT	EC	-0.189	0.069	-0.001	0.054
Field 2	RT	NH_4-N	0.000	0.579	0.000	0.408
Field 3	OK	OM	-0.283	0.055	-0.004	0.035
Field 3	OK	EC	-0.062	0.212	0.000	0.070
Field 3	OK	NH_4-N	-5.754	1.056	-0.449	0.715
Field 3	RT	OM	-0.004	0.096	0.000	0.076
Field 3	RT	NO_3-N	0.005	4.378	0.001	3.473
Field 3	RT	Zn	0.001	0.255	0.000	0.187
Field 3	RT	EC	-3.652	0.253	-0.021	0.106
Field 3	RT	NH_4-N	0.012	1.464	0.001	0.972

† Percent bias.
‡ Root mean squared error.
§ Mean error.
¶ Mean absolute error.

Table 4.10 Observed vs. predicted statistics from 10-fold cross-validation procedure; soil samples collected with a standard grid sampling approach.

	Interpolation technique†	Soil parameter	Observed					Predicted				
			Min	*Mean*	*Max*	*SDEV*‡	*CV*§	*Min*	*Mean*	*Max*	*SDEV*	*CV*
Field 1	TS	OM	0.9	1.6	2.5	0.3	0.2	1.2	1.6	2.1	0.2	0.1
Field 1	TS	NO_3-N	5.0	9.6	19.0	2.9	0.3	7.4	9.7	13.3	1.3	0.1
Field 1	TS	Zn	0.4	1.7	2.7	0.5	0.3	1.3	1.7	2.4	0.2	0.1
Field 1	TS	EC	0.2	0.3	0.4	0.1	0.2	0.2	0.3	0.4	0.0	0.1
Field 1	TS	NH_4-N	1.0	2.8	10.8	1.3	0.5	1.8	2.7	4.1	0.7	0.3
Field 2	OK	NO_3-N	2.0	7.3	77.0	9.5	1.3	1.9	7.7	26.0	5.9	0.8
Field 2	OK	NH_4-N	2.0	5.3	10.9	2.2	0.4	0.8	4.8	8.9	1.9	0.4
Field 2	TS	OM	0.7	1.4	2.5	0.4	0.3	0.8	1.4	2.3	0.4	0.3
Field 2	TS	Zn	0.1	0.6	2.2	0.4	0.7	0.1	0.6	1.3	0.3	0.5
Field 2	TS	EC	0.2	0.4	0.8	0.1	0.3	0.3	0.4	0.7	0.1	0.2
Field 3	TS	OM	0.9	1.3	1.8	0.2	0.1	0.9	1.3	1.5	0.2	0.1
Field 3	TS	NO_3-N	9.0	20.2	34.0	5.5	0.3	15.2	20.1	24.1	2.4	0.1
Field 3	TS	Zn	1.5	2.3	3.2	0.4	0.2					
Field 3	TS	EC	0.4	0.5	0.9	0.1	0.2	0.5	0.5	0.6	0.0	0.1
Field 3	TS	NH_4-N	3.2	4.7	9.9	1.4	0.3	3.1	4.6	5.7	0.7	0.2

† Interpolation techniques are trend surface models (TS) and ordinary kriging (OK).

‡ Standard deviation.

§ Coefficient of variation.

Table 4.11 Residuals-analysis statistics for 10-fold cross-validation procedure; soil samples collected with a standard grid sampling approach.

	Interpolation technique	Soil parameter	*ME*†	*MedianE*‡	*RMSE*§	*MAE*¶	*SK*#	*Kr*††	*AD*‡‡	*SMSE*§§	Coverage rate
Field 1	TS	OM	-0.017	0.024	0.330	0.261	0.144	0.168	0.267	1.511	0.914
Field 1	TS	NO3-N	-0.112	-0.600	2.893	2.355	0.484	0.214	0.632	1.119	0.929
Field 1	TS	Zn	-0.065	-0.080	0.548	0.422	-0.306	1.276	1.276	1.171	0.957
Field 1	TS	EC	-0.001	0.000	0.053	0.043	0.196	-0.445	0.196	1.257	0.929
Field 1	TS	NH4-N	0.074	-0.031	1.138	0.653	3.524	19.213	3.826	1.794	0.957
Field 2	OK	NO3-N	0.157	0.120	11.590	4.808	4.187	24.580	6.968	9.688	0.980
Field 2	OK	NH4-N	0.093	-0.050	2.155	1.723	-0.047	-0.519	0.185	1.332	0.900
Field 2	TS	OM	0.013	0.012	0.332	0.258	0.502	1.073	0.449	1.628	0.900
Field 2	TS	Zn	0.001	-0.025	0.387	0.266	0.976	1.888	1.578	1.336	0.900
Field 2	TS	EC	-0.003	-0.014	0.097	0.070	1.274	3.419	1.109	1.362	0.950
Field 3	TS	OM	0.003	0.028	0.073	0.110	-0.743	0.670	0.554	0.654	0.950
Field 3	TS	NO3-N	0.309	-0.390	5.563	4.234	0.561	0.702	0.355	1.157	0.940
Field 3	TS	Zn	0.005	-0.009	0.365	0.305	-0.072	-0.852	0.514	1.531	0.940
Field 3	TS	EC	0.000	-0.010	0.073	0.056	0.818	1.034	0.437	0.654	0.950
Field 3	TS	NH4-N	0.114	0.058	1.436	1.011	1.362	2.576	1.359	1.046	0.940

† Mean error.
‡ Median error.
§ Root mean squared error.
¶ Mean absolute error.
# Skewness.
†† Kurtosis.
‡‡ Anderson-Darling goodness-of-fit test; the null hypothesis is that the true distribution is F_0 and is rejected if AD > critical value (0.74) (i.e. for $\alpha = 0.05$).
§§ Standard mean squared error.

Table 4.12 Standard mean squared error (*SMSE*) intervals used to assess estimation uncertainty of cross-validation results for grid sampling (GS) and cluster sampling (CS) approaches. *SMSE* that fall within intervals are assumed to be consistent with observed data.

	Field 1	**Field 2**	**Field 3**
GS	[0.662,1.338]	[0.635,1.365]	[0.600,1.400]
CS	[0.682,1.316]	[0.600,1.400]	[0.662,1.338]

Table 4.13 Observed vs. predicted statistics from 10-fold cross-validation procedure; soil samples collected with a cluster sampling approach.

	Interpolation technique†	Soil parameter	Observed					Predicted				
			Min	*Mean*	*Max*	*SDEV*‡	*CV*§	*Min*	*Mean*	*Max*	*SDEV*	*CV*
Field 1	OK	OM	0.9	1.4	1.8	0.2	0.2	0.0	1.3	1.8	0.3	0.3
Field 1	OK	NO_3-N	5.0	10.1	18.0	2.8	0.3	0.0	9.9	20.6	4.1	0.4
Field 1	OK	EC	0.2	0.3	0.5	0.1	0.2	0.2	0.3	0.4	0.0	0.1
Field 1	RT	OM	0.9	1.4	1.8	0.2	0.2	0.9	1.4	1.7	0.2	0.1
Field 1	RT	NO_3-N	5.0	10.1	18.0	2.8	0.3	6.3	10.4	15.6	2.1	0.2
Field 1	RT	Zn	0.6	1.8	3.6	0.6	0.3	0.9	1.7	2.6	0.4	0.3
Field 1	RT	EC	0.2	0.3	0.5	0.1	0.2	0.2	0.3	0.4	0.0	0.1
Field 1	RT	NH_4-N	2.7	6.3	11.5	1.5	0.2	4.1	6.3	8.7	1.0	0.2
Field 2	OK	OM	0.7	1.3	2.8	0.5	0.4	0.5	1.3	2.6	0.5	0.4
Field 2	RT	OM	0.7	1.3	2.8	0.5	0.4	0.7	1.3	2.4	0.4	0.3
Field 2	RT	NO_3-N	5.0	9.2	19.0	3.1	0.3	5.2	9.5	14.5	2.6	0.3
Field 2	RT	Zn	0.7	1.7	3.3	0.7	0.4	0.8	1.6	3.1	0.6	0.3
Field 2	RT	EC	0.3	0.4	0.9	0.1	0.3	0.3	0.4	0.8	0.1	0.2
Field 2	RT	NH_4-N	4.1	5.6	7.9	0.7	0.1	4.6	5.5	6.8	0.5	0.1
Field 3	OK	OM	0.9	1.3	1.8	0.2	0.1	1.0	1.3	1.6	0.2	0.1
Field 3	OK	EC	0.4	0.6	3.3	0.3	0.6	0.4	0.5	0.7	0.1	0.2
Field 3	OK	NH_4-N	5.1	7.8	16.3	1.9	0.2	0.0	13.1	78.5	15.7	1.2
Field 3	RT	OM	0.9	1.3	1.8	0.2	0.1	1.0	1.3	1.7	0.2	0.1
Field 3	RT	NO_3-N	9.0	20.9	42.0	6.8	0.3	12.7	21.1	32.4	4.2	0.2
Field 3	RT	Zn	2.2	3.0	4.0	0.4	0.1	2.6	3.0	3.4	0.2	0.1
Field 3	RT	EC	0.4	0.6	3.3	0.3	0.6	0.4	0.6	1.2	0.2	0.3
Field 3	RT	NH_4-N	5.1	7.8	16.3	1.9	0.2	6.9	7.9	11.0	0.8	0.1

† Interpolation techniques are ordinary kriging (OK) and regression tree analysis (RT).

‡ Standard deviation.

§ Coefficient of variation.

Table 4.14 Residuals-analysis statistics for 10-fold cross-validation procedure; soil samples collected with a cluster sampling approach.

	Interpolation technique	Soil parameter	*ME*†	*MedianE*‡	*RMSE*§	*MAE*¶	*SK*#	*Kr*††	*AD*‡‡	*SMSE*§§	Coverage rate
Field 1	OK	OM	0.109	0.066	0.344	0.225	1.650	4.492	2.707	1.491	0.913
Field 1	OK	NO3-N	0.116	0.366	4.938	3.686	-0.181	0.378	0.563	6.709	0.650
Field 1	OK	EC	0.007	-0.002	0.069	0.051	0.227	0.209	0.080	1.717	0.863
Field 1	RT	OM	0.018	0.024	0.177	0.144	0.158	-0.207	0.233	0.460	0.988
Field 1	RT	NO3-N	-0.358	-0.410	3.695	3.065	0.320	-0.705	0.585	0.778	0.988
Field 1	RT	Zn	0.070	0.089	0.627	0.495	0.367	0.130	0.246	0.580	0.975
Field 1	RT	EC	0.000	-0.006	0.054	0.040	0.439	0.172	1.069	0.460	1.000
Field 1	RT	NH4-N	0.055	0.046	1.509	1.144	-0.146	0.667	0.635	0.474	1.000
Field 2	OK	OM	-0.018	-0.051	0.316	0.248	-0.082	-0.082	0.257	1.020	0.940
Field 2	RT	OM	0.003	0.002	0.373	0.293	-0.047	-0.519	0.323	0.849	1.000
Field 2	RT	NO3-N	-0.129	0.071	2.479	1.974	-0.185	-0.126	0.316	0.442	1.000
Field 2	RT	Zn	0.024	-0.055	0.566	0.463	0.408	-0.586	0.457	0.597	0.980
Field 2	RT	EC	0.013	-0.005	0.154	0.115	0.721	0.568	0.689	0.972	0.940
Field 2	RT	NH4-N	0.096	0.066	0.933	0.732	0.469	-0.237	0.361	0.730	0.960
Field 3	OK	OM	-0.008	-0.021	0.222	0.171	0.168	-0.109	0.403	1.559	0.886
Field 3	OK	EC	0.038	0.002	0.382	0.130	6.195	42.188	13.387	12.253	0.957
Field 3	OK	NH4-N	-5.385	-0.718	17.317	8.829	-2.703	7.616	7.276	25.409	0.657
Field 3	RT	OM	-0.025	-0.014	0.240	0.199	-0.021	-0.623	0.345	1.043	0.929
Field 3	RT	NO3-N	-0.289	-0.801	7.104	5.384	0.409	0.470	0.569	0.508	0.986
Field 3	RT	Zn	0.015	0.020	0.389	0.305	0.130	0.092	0.163	0.527	0.986
Field 3	RT	EC	-0.003	-0.016	0.421	0.190	4.655	29.567	7.983	11.466	0.957
Field 3	RT	NH4-N	-0.171	-0.450	2.244	1.617	1.260	3.310	1.243	0.574	0.986

† Mean error.

‡ Median error.

§ Root mean squared error.

¶ Mean absolute error.

Skewness.

†† Kurtosis.

‡‡ Anderson-Darling goodness-of-fit test; the null hypothesis is that the true distribution is F_0 and is rejected if AD > critical value (0.74) (i.e. for $\alpha = 0.05$).

§§ Standard mean squared error.

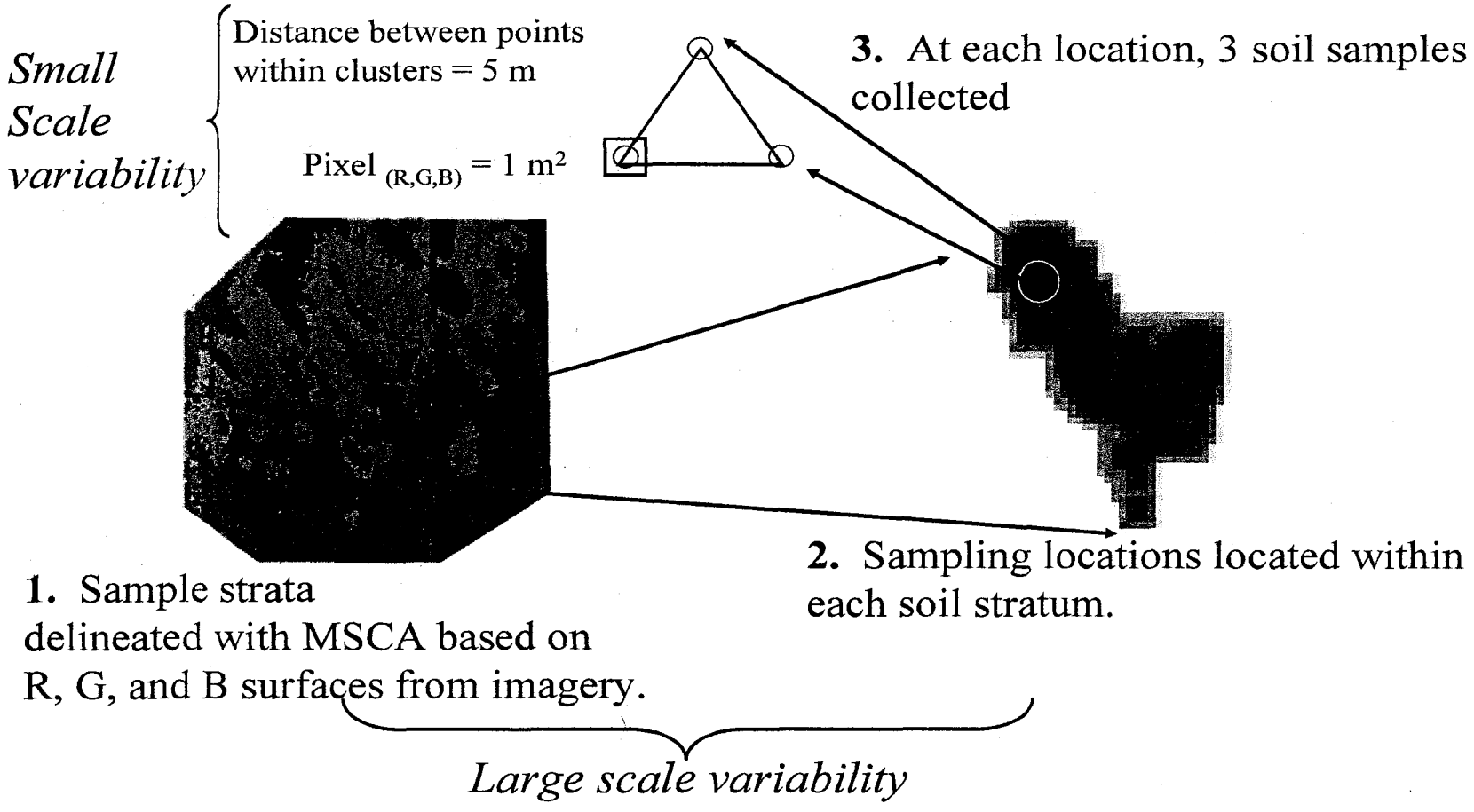

Figure 4.1 Flow chart summarizing the major steps in the cluster sampling approach to soil sampling for interpolation of soil properties. In the first step, sampling strata are delineated across the field based on spectral charateristics of the bare soil imagery. Sampling locations are then subjectively located within the representative strata; 3-4 sampling locations per stratum. Soil samples are then collected at each sampling location. At each sampling location, 3 soil samples are collected; each of the 3 soil samples is a composite of 6-8 soil cores. Samples are separated by approximately 5 m. Ideally, this design will capture large-scale and small-scale variability which will be used during the interpolation procedure.

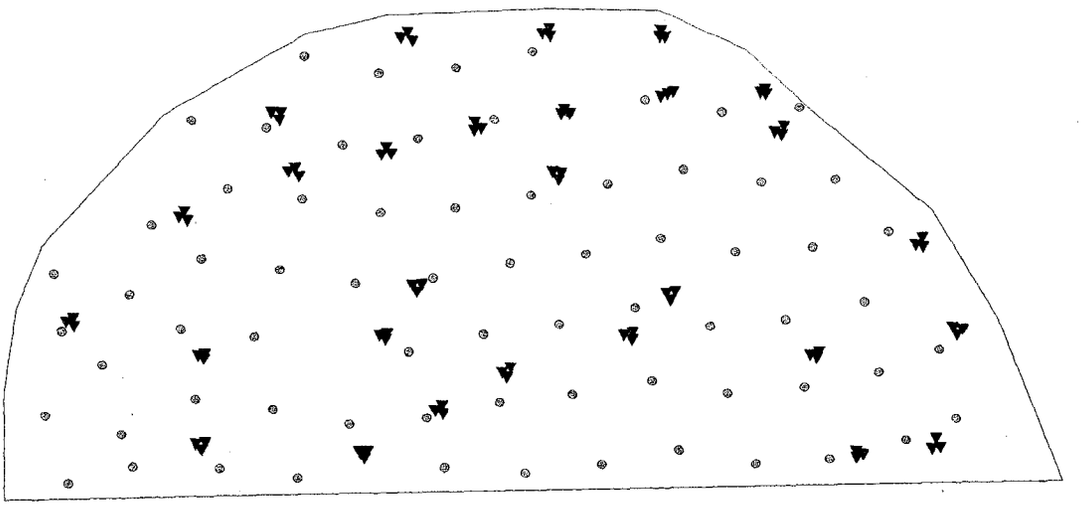

Figure 4.2 Areal location of sampling locations at Field 1. Circles indicate grid sampling locations and triangles indicate cluster sampling locations.

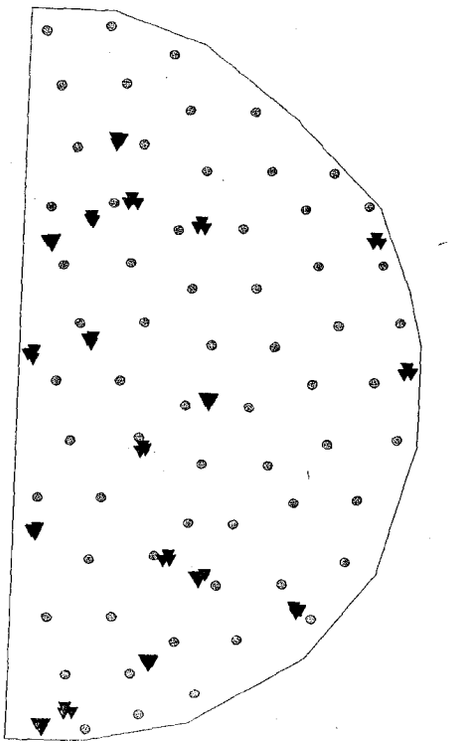

Figure 4.3 Areal location of sampling locations at Field 2. Circles indicate grid sampling locations and triangles indicate cluster sampling locations.

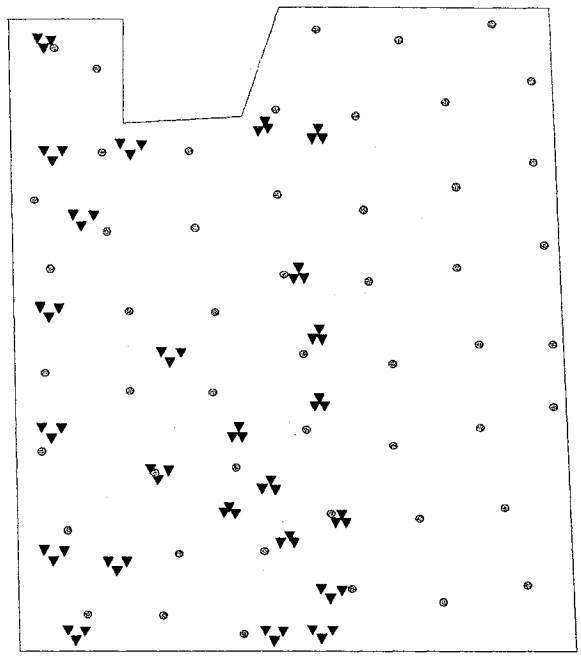

Figure 4.4 Areal location of sampling locations at Field 3. Circles indicate grid sampling locations and triangles indicate cluster sampling locations.

5 Delineation of Soil Productivity Management Zones: Yield Response

5.0 Abstract

Research has suggested that several technical limitations arise from the grid sampling approach to delineating variable rate fertilizer application (VRT) maps. The primary limitation is attributed to the spatially independent nature of data resulting from grid sampling. Recent research has focused on delineating field-specific soil-productivity management zones to be used as VRT maps. The objective of this study was to analyze four techniques for delineating management zones. Each of the methods uses a unique set of soils, yield, and/or remotely sensed data. Three fields were sampled using a standard 76 x 76 m grid design. Directed soil sampling was developed for the same fields based on information contained in auxiliary data layers generated from bare soil imagery. Delineation techniques 1 and 2 (i.e. soil color management zone technique [SCMZ], and apparent electrical conductivity technique [EC_aMZ]) utilize secondary soils information such as bare soil photography, but do not utilize soil-sample analysis results at the outset of the delineation process. Techniques 3 and 4 (i.e. yield based management zone technique [YBMZ], and remotely sensed data and cluster sampling management zone technique [RCMZ]) utilized secondary soils information in conjunction with soil-sample analysis results. Analysis of variance (ANOVA) for the majority of yields among management zones indicated yields between management zones were different. A non-parametric analysis (*S*-statistic) of crop yields also provided evidence to conclude that management zone delineation techniques resulted in yield patterns that were different

from random yield patterns. Goodness-of-fit analysis (χ^2) indicated significant areal association among management zone delineations in 91% of comparisons. The χ^2 results also suggest the YBMZ and RCMZ techniques outperform the SCMZ and EC_aMZ techniques. The Kappa statistic (κ) was also used to evaluate delineation techniques. The κ-statistic did not provide as much evidence of effective management zone delineations when compared with ANOVA, *S*-statistics, and χ^2 goodness-of-fit analyses. However, the κ-statistic did provide evidence indicating the RCMZ technique outperformed the remaining techniques; YBMZ technique was the next most effective delineation technique. Overall, the two delineation techniques that combined secondary soils information and soil-sample analysis results were the most effective techniques.

5.1 Introduction

A 1998 survey of approximately 8,400 farmers indicated 4% of US farms utilize precision farming technologies (Daberkow and McBride, 2000). Twenty-seven percent of surveyed farmers indicated they may implement precision farming technologies in the near future and those producers account for nearly half (i.e. 49%) of farm acres in the US. The remaining 70% of producers indicated they were unaware of precision farming techniques. Overall, producers using precision farming technologies accounted for nearly 62 million acres or 14% of all crop acres in the US; farm size was positively correlated with the probability of utilizing precision farming technologies. The survey also indicated the most widely adopted precision farming techniques were grid-soil sampling and variable rate fertilizer application (VRT); 53 and 51% of adopting farms, respectively.

Soil-sample analysis results from 1 ha grid sampling designs are conventionally used to delineate VRT maps (Fleming et al., 2000). A VRT map is a georeferenced map prescribing fertilizer application rates over a field. The VRT map assigns a nutrient application rate to every manageable section within a field. The size of the 'manageable section' is primarily dependent on the width of the applicator boom. The desired results from VRT include spatially optimizing crop inputs, increasing farm profitability and providing the potential for reduced environmental degradation. Research has suggested that several technical limitations arise from the grid sampling approach to delineating VRT maps. Mueller et al., (2001) concluded that a commercial grid size of 100 x 100 m was inadequate to provide acceptable prediction accuracy due to a lack of spatial dependency among soil samples. These researchers also concluded that utilizing average fertility values of the soil properties of interest was as effective as grid sampling. Schloeder et al., (2001) also demonstrated spatial interpolation of sparse soil sample data was inappropriate. The primary reason for poor interpolation results was attributed to the spatially independent nature of the data. Whelan et al., (1996) concluded that fields with limited soil samples could only be interpolated with simple geostatistical techniques such as inverse distance weighting; more complex techniques such as kriging were inappropriate. Hammond (1992) concluded that a 60 x 60 m sampling grid was adequate for developing VRT maps for some soil properties. Similarly, Franzen and Peck (1994) found that a grid size of 65 x 65 m was adequate for parameter interpolation when compared with 25 and 98 m grids. More recent research has reported that grids of 20 to 30 m are required for VRT (McBratney and Pringle, 1999).

The concurrent conclusions in these studies highlight two important considerations with regard to PF:

1. Failing to capture spatial variability can make it impossible to develop accurate VRT maps.
2. The cost associated with analysis of soil samples collected at a density appropriate for developing useful VRT maps (e.g. 20 to 60 m) is generally prohibitive, especially for most agronomic crops.

Recent precision agriculture research has focused on delineating field-specific soil-productivity management zones to be used as VRT maps. Several studies have indicated that management zones could be used as an alternative to grid-soil sampling to develop VRT maps (Khosla and Alley, 1999; Khosla et al., 2002). Management zones are defined as "subregions of a field that express a homogenous combination of yield limiting factors and for which a single crop input is appropriate to attain maximum efficiency of farm inputs" (Doerge, 1999). Three management zones are typically delineated for agronomic crops: highly productive, moderately productive, and poorly productive. The primary goal of any management zone delineation technique is to develop a VRT map that is effective and reduces the limitations associated with the grid-soil sampling approach to delineating VRT maps.

Delineation of management zones is typically achieved by combining soil sample data with additional, secondary layer information. Secondary information may include such sources as topography, soil survey maps, or high altitude photography. Several management zone techniques have been evaluated for effectiveness in developing VRT maps. For example, Franzen et al. (2002) evaluated the utilization of Order 1 (very

detailed) and Order 2 (detailed) soil survey maps to assist in delineating management zones. They concluded Order 1 maps were effective while Order 2 maps were not effective.

Topography and landscape position have also been useful for delineating management zones. Ortega (1997) used a topography/landscape-position based approach to define management zones in the central Great Plains region. He concluded that corn (*Zea mays* C.) yields were higher in topographically lower management zones and was effectively able to explain 36 to 60% of the total variability in corn yields. A topography-based approach to define management zones was examined in Illinois and Indiana (Kravchencko and Bullock, 2000). These researchers concluded topographical characteristics and selected soil properties (OM, CEC, P, K) accounted for 40% of the grain yield variability. Topography has also been shown to be associated with soil N content (Bruulsema et al., 1996 and Cassel et al., 1996). Similarly, Franzen et al. (2000) effectively used topography to assess soil N and P levels in grain. Another recent study divided fields into management zones based on topography and landscape models and effectively explained 30 to 50% of the variation in yields (Nolan el al., 2000).

Remotely sensed data is another source of secondary layer information. McCann et al. (1996) found that the gray tone pattern in black and white aerial photographs can be a reflection of soil organic matter and moisture characteristics. In another study, Landsat Thematic Mapper images that estimated SOM distribution were found to be highly correlated with the spatial distribution of SOM measured from grid-soil sampling (Bhatti et al, 1991). Chen et al. (2000) concluded the spatial variation in organic C could be determined with remotely sensed bare soil imagery. Fleming et al. (2000) effectively

used topography, farmer experience and soil color, determined with high altitude photography, to develop management zones. Yang et al. (1998) used aerial imagery to classify within field production zones. They concluded that grain yield was significantly different among management zones.

Apparent soil electrical conductivity (EC_a) determined by electromagnetic induction is another source of secondary layer information. The EC_a of a field can be mapped with a conductivity cart that estimates soil electrical conductivity at specified time intervals as it is pulled behind a truck or tractor. The cart must also be linked to a GIS/GPS navigation system for proper map development. Examples of EC_a carts include Geonics EM 38®[1] and Veris® model 3100. The EC_a approach has been utilized to accurately map variations in soil properties such as water content, percent clay, and salinity and to track soluble nutrient levels in soil (Sudduth et al., 1998; Eigenberg et al., 2000). The EC_a has also been used to investigate yield variability caused by soil water differences (Jaynes et al., 1994; Sudduth et al., 1994).

Efficient techniques for developing VRT maps need to be developed to fully realize the benefits of precision farming. Utilization of management zones may be an effective approach to address the shortfalls associated with grid-soil sampling and increase the benefits associated with precision farming. While several techniques have been developed to delineate management zones no single approach has been deemed optimum. In this chapter I will analyze four techniques for delineating management zones based on yield response within zones. Each of the methods uses a unique set of soils, yield, and/or remotely sensed data. The level of technological expertise required to

[1] Mention of a trade name, proprietary product, or specific equipment does not constitute a guarantee, warranty, or endorsement by Colorado State University.

develop the management zones ranges from very simple and commercially available technique (i.e. most producers with limited computer skills could implement) to more complex techniques requiring computer and data management skills.

5.2 Materials and Methods

The study was conducted on three center pivot irrigated fields (Fields 1, 2, and 3) during the 2001 and 2002 growing season. All three fields have been managed under corn for several years. Field 1 was used in 2002 and is 58 ha and has soils classified as Albinas loam (fine loamy, mixed, mesic Pachic Argiustolls), Ascalon fine sandy loam (fine loamy, mixed, mesic Aridic Argiustolls), and Haxtun sandy loam (fine loamy, mixed, mesic Pachic Argiustolls). These soil classes represent loamy soils that are well drained with moderate available water capacity. Field 2 was used in 2002 and is 57 ha and has soils that are classified as Vona sandy loam (coarse loamy, mixed, mesic, Mollic Haplargids), Haverson clay loam (fine loamy, mixed, calcareous, mesic Typic Ustifluvents), and Nunn loam (fine, montmorillonitic, mesic, Typic Argiustolls). Field 3 was used in 2001 and is 71 ha and has soils that are classified as Valentine sand (sandy, mixed nonacid, mesic Typic Ustipsamment), a Bijou loamy sand (coarse loamy, mixed, mesic Mollic Haplargid), and a Truckton loamy sand (coarse loamy, mixed, mesic Udic Argiustoll). These varied sandy to loamy sand soil types range from moderate to high water holding capacity with moderate to high water infiltration rates.

5.2.1 Soil Sampling

Soil from all three fields was sampled in the spring of 2001 or 2002 using a standard grid (GS) sampling technique and the size of each grid cell was 76 x 76 m (i.e. 0.58 ha). Sample locations were randomly located within each cell and recorded with a

differential global positioning system (DGPS). Soil samples were collected from the 0 to 0.2 m surface zone and analyzed for organic matter (OM), nitrate-N (NO_3-N), and ammonium-N (NH_4-N), cation exchange capacity (CEC), and percent sand, silt, and clay using standard soil testing procedures (Miller et al., 1998).

Soil from all three fields was sampled in the spring of 2001 or 2002 using a stratified cluster sampling technique. The stratified cluster sampling technique utilizes a high-altitude, bare soil images to detect natural variation in soil color to initially stratify a field into homogenous zones. The unique strata are then utilized in a directed soil sampling procedure and samples are collected in a cluster design to improve the detection of small-scale variation. Details of this sampling design are explained in section 4.2.2. Soil samples were collected from the 0 to 0.2 m surface zone and analyzed for organic matter (OM), nitrate-N (NO_3-N), and ammonium-N (NH_4-N), electrical conductivity (EC), and zinc (Zn) using standard soil testing procedures (Miller et al., 1998).

5.2.2 Management Zone Delineation

Management zones were delineated to identify areas of high, medium, and low-yield productivity using four techniques. The techniques, explained below, are presented in order from the simplest (technique 1) to the most complex (technique 4). Technique 1, soil color management zone technique (SCMZ), is commercially available and utilizes panchromatic bare-soil imagery, field topography, and farmers past management experiences as the three GIS data layers to delineate management zones. This is the least complex technique. Details of this technique are explained in Fleming et al. (1999) and Khosla et al. (2002). Technique 2, apparent electrical conductivity technique (EC_aMZ), utilizes a Veris® model 3100 EC cart to measure apparent soil conductivity. The

resulting EC_a GIS layer was used to delineate management zones (i.e. higher EC_a indicates higher productivity zones). Details of this technique are explained in Westfall et al. (2003). The GIS data layers used in Technique 3, yield based management zone technique (YBMZ), were: multi-spectral bare-soil imagery, OM, CEC, soil texture (sand, silt, and clay content), and previous years' yield monitor map. Details of this technique are explained in Westfall et al. (2003).

Technique 4, remotely sensed data and cluster sampling management zone technique (RCMZ), combines bare-soil imagery and soil sample results to delineate management zones. The RCMZ is the most complex technique. The objective of the RCMZ is to address the primary shortfall associated with a grid-soil sampling design which is a lack of spatial dependency among soil samples. The RCMZ technique utilizes bare-soil imagery to develop a directed soil sampling procedure that captures more of the small-scale variability associated with soil properties. The directed soil sampling procedure is described in detail in chapter 4. Soil analysis results from the directed sampling procedure were used to interpolate soil properties across each field using modified residual kriging techniques. The five resulting soil-property surfaces (i.e. GIS data layers) for each field (i.e. EC, OM, NH_4-N, NO_3-N, and Zn) were then analyzed with a nonhierarchical *k*-means clustering algorithm for spatial data sets to generate three management regions for each field (MSCA; S-PLUS©, Reich and Davis, 1998). For the YBMZ and RCMZ techniques, the high productivity management zones were assigned as regions with higher OM and NO_3-N levels; low productivity management zones had lower OM and NO_3-N levels.

5.2.3 Experimental Plots

Experimental strip-plots were delineated across the length each field. Each strip-plot was randomly assigned a N fertilization rate. The strip-plots were approximately 18 meters wide (24 rows) corresponding to three applicator widths (8 rows wide) and each ran the length of the entire field. The length of the strip-plots ranged from approximately 600 to 1000 m. In some cases, the strip-plot only crossed one or two of the three management zones. This was an unavoidable consequence of the randomization procedure and individual management zone delineation techniques.

Three N fertilization rates were evaluated in this study: 0 kg-N ha^{-1}, half recommended N rate, and recommended N rate. The recommended N rate was based on the following equation:

$$N_{rate} = 39 + (0.021 \times EY) - (8 \times NO_3N) - (0.0025 \times EY \times OM) - (N_{credits}) \quad [5.1]$$

where N_{rate} is the N rate in kg ha^{-1}, EY is the expected yield in kg ha^{-1}, NO_3-N is the soil-test N level in mg kg^{-1}, OM is the percent soil-test level organic matter, and $N_{credits}$ include all applicable, additional sources (e.g. irrigation water) of N present on the field in kg ha^{-1}. This equation is the SI-unit conversion of the non-SI equation presented by (Mortvedt et al., 1996). Values for NO_3-N, and OM used in Eq. 5.1 were estimated with average values from soil samples collected from each field. The EY was determined based on the farmers' previous field experience and yield information. The EY for all three fields was 11935 kg ha^{-1}. The layout for the experimental plots is displayed for Fields 1, 2, and 3 in Figure 5.1. Recommended N rates were 200, 222, and 191 kg-N ha^{-1} for Fields 1, 2, and 3 respectively.

5.2.4 Field Operations

Each field was planted to corn by managing cooperators in the spring of 2001 and 2002. Nitrogen was applied to strip-plots between V6 and V8 growth stages with an 8-row Kinze® field cultivator designed to deliver liquid nitrogen (i.e. 32% UAN). The cultivator was pulled by a John-Deere 8400 T-tractor® equipped with a Satloc® GPS receiver. Nitrogen application rates were controlled with a Mid-tech® variable rate controller. Fields 1 and 2 were yield mapped with a John Deere 9650 STS® combine harvester equipped with an Ag-Leader® yield monitor system. Field 3 was yield mapped with a John Deere 9650 STS® combine harvester equipped with a Green Star® yield monitor system.

5.2.5 Cleaning Yield Monitor Data

The yield monitor data was examined and cleaned to remove erroneous and otherwise nonsensical data points. The procedure for cleaning the data is presented here as an 8-step process:

1. The columns of raw data in the yield-monitor file were first sorted according to 'pass status'. Pass status indicates the position of the combine header (i.e. 1=down, and 0=up). All entries displaying a pass status of 0 were then deleted from the file.
2. The 'area' of data collection was calculated in m^2 by converting 'swath width' and 'distance' columns from inches to meters and multiplying the two quantities.

3. The 'flow' value (kg) is an uncorrected yield estimate over the area calculated in step 2. The 'flow' values were corrected to a standard moisture content for corn of 15.5% with the following equation:

$$Flow_c = \frac{Flow_{uc} - \left(\left[\frac{\%M}{100}\right] Flow_{uc}\right)}{0.845} \quad [5.2]$$

where $Flow_c$ is the corrected 'flow' value, $Flow_{uc}$ is the uncorrected 'flow' value in the data file, $\%M$ is the estimated moisture content of the harvested grain, and the value 0.845 is equal to 1 minus the standard moisture content (i.e. 0.155).

4. Yield in kg ha^{-1} was calculated as

$$Y = \frac{Flow_c}{A}(10000) \quad [5.3]$$

where $Flow_c$ is the corrected 'flow' value from Eq. 5.2, A is the 'area' calculated in step 2, and 10000 is the area of a hectare of land in m^2.

5. The combine speed was converted from ft sec^{-1} to km h^{-1} by multiplying 'distance' by 3600 (i.e. sec h^{-1}) and dividing that quantity by 3280 (ft km^{-1}).

6. The median speed yield value was identified and data entries in the yield monitor file that were 50% above or 50% below the median value were removed. For example, if the median speed is 3 km h^{-1} delete all data entries > 4.5 and < 1.5 km h^{-1}.

7. Yield values > 25125 and < 630 kg ha^{-1} were deemed nonsensical and deleted.

8. Yield values for each combine pass were sorted according to north/south or east/west geographic coordinates depending on combine harvesting direction. Final yield values were estimated as the average of 5 neighboring yield values. The goal of the final step was to smooth the data and reduce erratic combine yield-estimates across the field.

5.2.6 Yield Response Data Analysis

I utilized a variety of statistical procedures to analyze the yield data from this study. I feel it is more appropriate to make conclusions based on a variety of available 'tools' as opposed to a single test. The merits of combined statistical procedures are typically presented in statistics courses. The primary reasons multiple procedures are recommended include the inherent uncertainty and variability associated with statistical analysis. The procedures used in this study were primarily used to answer two questions: Are we detecting management zones, and, which technique(s) is better.

Processed yield data and management zones were displayed in MapInfo© (MapInfo©, 2002). All yield points falling within 25 m of field borders or management zone borders were removed from the data set to avoid possible transition-zone effects in the data. This procedure was repeated for all management zone techniques on all fields.

A random sample of 30 yield values was extracted from each management zone for each management zone technique and each N treatment. For example, a total of 90 yield values were extracted from the Field 1 data set, SCMZ technique, 0% N rate strip-plot; 30 from high, 30 from medium, and 30 from low management zone. Randomly selected yield values were analyzed with a one-way analysis of variance (ANOVA)

procedure in S-PLUS© (ANOVA; S-PLUS©, Statistical Sciences, 1999). The numerical details of this procedure are summarized in Appendix C.

Significant models were further analyzed to compare individual treatments with the method developed by Tukey (1949). For a group of k treatment means with equal replication, the Tukey's significant difference (also referred to as the Honestly Significant Difference) is estimated as:

$$T_{k,\alpha_E} = q_{\alpha_E,k,\nu}\sqrt{\frac{MSE}{r}} \qquad [5.4]$$

where α_E is the experimentwise error rate, $q_{\alpha,k,\nu}$ is the Studentized range statistic for a range of k treatment means, $\nu=t(r-1)$ and represents degrees of freedom, MSE is equal to $\frac{SSE_f}{t(r-1)}$, and r is the number of replications in each treatment. Tables of q values are readily available in most introductory statistics texts. Simultaneous confidence intervals for pairwise differences are estimated as:

$$\left|\bar{y}_i - \bar{y}_j\right| \pm T_{k,\alpha_E} \qquad [5.5]$$

where $\bar{y}_i$ and $\bar{y}_j$ are means of the i^{th} and j^{th} treatments. Two treatment means are declared unequal when the interval created with Eq. 5.4 does not cover 0.

Random samples of yield values were also analyzed with a non-parametric procedure. The S-statistic is a median-based non-parametric, absolute deviation statistic designed to evaluate the ability of management zones to minimize the variability of yields. The S-statistic is defined as:

$$S_0 = \sum_{i=1}^{t}\sum_{j=1}^{n_i}\left|y_{ij} - y_i^*\right| \qquad [5.6]$$

where t is the number of management zones, n_i is the number of sample yield values in management zone i, y_{ij} is the j^{th} sample yield point in the i^{th} management zone, and y_i^* is the median yield in the i^{th} management zone.

Essentially, the *S*-statistic is used to assist in addressing the research question: Are management zones any better than a random yield pattern in the field? If management zones are capable of differentiating yields into low, medium, and high productivity regions, one would expect the variability of yields within management zones to be at a minimum and we would expect the test statistic, S_0, to be small. In contrast, if yields were randomly assigned to management zones, we would expect the variability of yields within management zones to be large, and thus lead to a large S_0 value. To test this hypothesis, 50,000 Monte Carlo simulations were carried out. In each simulation, sample yield values were randomly assigned to a management zone, and the *S*-statistic calculated. The 50,000 test statistics were then ranked from low to high, along with the observed test statistic, S_0. The probability of observing an *S* smaller than that observed for the data (S_0) is estimated as:

$$p = \frac{r}{R+1} \qquad [5.7]$$

where, r is the rank of S_0, and R is the number of Monte Carlo simulations. A small *p*-value (< 0.05) would lead to the rejection of the null hypothesis and conclude that management zones are differentiating yields. If the *p*-value is large, then the ability of management zones to differentiate yields is no better than a random process.

Treatments displaying significant S_0 statistics were further analyzed using areal association statistics. Areal association statistics are another approach to determine how well delineation techniques worked. All corrected yield values were used for the areal

association analysis (i.e. as opposed to 30 random samples). Before applying areal association statistics, individual yield values were classified as high, medium, or low using three approaches. The classified yield values were then compared with the management zone delineation from where they were collected; ideally, more high yields would be observed in the high management zone. The first approach to classify yield values used an objective, *k*-means clustering algorithm to classify each yield value as high, medium, or low. Details of *k*-means clustering are discussed in section 4.2.2.

The second approach used an objective, non-parametric classification procedure. Yield values were sorted and classified as 'high' if they were greater than the 3rd quartile yield value; 'medium' if they fell within the 1st and 3rd quartiles; and 'low' if they fell below the 1st quartile value. This approach is similar to classifying yield values based on standard deviations (e.g. medium yields would occupy the range ± 1 standard deviation). The non-parametric classification is less sensitive to non-normal data sets and also works well if the data are normally distributed. This flexibility makes the non-parametric classification useful for multiple data sets analysis.

The third classification approach was subjective and based on knowledge of corn yields in the northeast Colorado region. Previous years yield data suggest average irrigated corn yield in the region is ~11300 kg ha^{-1}. Yield values were classified as high (> 11930 kg ha^{-1}), medium (8850-11930 kg ha^{-1}), or low (< 8850 kg ha^{-1}) based on this knowledge. These classifications were also adjusted for individual fields if the mean yield was less than, or greater than 11300 kg ha^{-1}. For example, if the mean corn yield on Field 1 in 2002 was 10675 kg ha^{-1}, all classification categories were shifted down by 625 kg ha^{-1}.

Classified yield values were compared with the associated management zone classification. Results from the comparisons were summarized in a matrix format. The matrix provides a visual summary of management zone classifications and misclassifications in a percentage format. Cells on the diagonal of the matrix correspond to equal classification as determined by yield value and management zone delineation; cells on the off-diagonal are misclassifications. The matrix also provides the opportunity to analyze the effectiveness of management zone delineations with the Chi^2 goodness-of-fit test, X^2, and the Kappa statistic, κ.

The χ^2 goodness-of-fit test provides a measure of agreement between classification techniques (i.e. yield value classification, and management zone delineation). The experimental χ^2-statistic is defined as:

$$X^2 = \sum_{i=1}^{g}\sum_{j=1}^{g}\frac{(O-E)^2}{E} \qquad [5.8]$$

where g is the number of rows or columns in a g x g matrix, O is the number of observations in the ij^{th} cell of the g x g matrix, and E is the number of expected observations in the ij^{th} cell based on chance as determined by normal approximation theory. The expected value, E_{ij}, is calculated as:

$$E_{ij} = \frac{\sum_{j=1}^{g} n_{ij} \sum_{i=1}^{g} n_{ij}}{N} \qquad [5.9]$$

where N is the total number of observations, and n is number of classifications or misclassifications in the ij^{th} cell. The experimental χ^2 is compared to critical χ^2 values with $(g\text{-}1)^2$ degrees of freedom at the desired α level. If the experimental χ^2 is greater than the critical χ^2, the null hypothesis is rejected. Tables of χ^2 critical values are readily

available in most introductory statistics texts. In this study, the p-value generated by computer software was used to test the null hypothesis with α level of 0.05. Significant models were considered to have better than chance classifications. The χ^2-statistic was also used to compare management zone delineation techniques to assess the percentage of correspondence.

The κ-statistic provides another measure of agreement between two 'scorers' that assign each observation into one of g groups. The κ-statistic was originally developed for use in the area of linguistics research but recently has been utilized by remote-sensing and GIS researchers. The term 'scorer' was initially used to define and explain the statistic since it was used to compare linguistic classifications by different evaluators or 'scorers'. With respect to the current study, 'scorers' are the management zone delineations and yield value classifications. The summary of agreement between the two scorers results in a g x g matrix of classifications and misclassifications. Cells on the diagonal of the matrix correspond to equal classification by both scorers and each correct classification is given a weight of 1. Cells on the off-diagonal are misclassifications and are given a weight of 0. The observed proportional agreement between the scorers is calculated as:

$$P(A) = \frac{1}{N}\sum_{i=1}^{g}\sum_{j=1}^{g} w_{ij} n_{ij} \qquad [5.10]$$

where N is the total number of classified observations, g is the number of rows or columns in the g x g matrix, w is the weight assigned to the ij^{th} cell, and n is number of classifications or misclassifications in the ij^{th} cell. The row and column totals of the g x g matrix can be respectively defined as:

$$r_i = \sum_{j=1}^{g} n_{ij} \text{ and } c_j = \sum_{i=1}^{g} n_{ij} \quad [5.11]$$

and the proportional agreement between scorers that is expected just by chance is estimated by:

$$P(E) = \frac{1}{N^2} \sum_{i=1}^{g} \sum_{j=1}^{g} w_{ij} r_c c_j \quad [5.12]$$

The κ-statistic is then calculated as:

$$\kappa = \frac{P(A) - P(E)}{1 - P(E)} \quad [5.13]$$

The κ-statistic has a maximum of 1 when agreement between scorers is perfect and a value of zero when there is no agreement better than chance. The κ-statistic can also be negative if agreement is worse than chance agreement. The primary difference between the κ-statistic and the χ^2 goodness-of-fit statistic is that the κ-statistic considers both classification and misclassification in the calculations.

5.3 Results and Discussion

Average and standard deviation values for primary soil parameters from the three fields appeared similar with the exception of higher NO_3-N and Zn values on Field 3 (Table 5.1). Average NO_3-N values for Field 1 and 2 were 10 and 9.2 mg kg^{-1}, respectively; Field 3 had average NO_3-N of 21 mg kg^{-1}. Average Zn values for Field 1 and 2 were approximately 2 mg kg^{-1} while average Zn values were 3 mg kg^{-1} for Field 3. Overall OM values were consistent across all fields and ranged from 1.3 to 1.4%. Ammonium-N values were consistent and ranged from 5.6 to 7.8 mg kg^{-1}. Similarly, EC values were consistent across all fields and ranged from 0.3 to 0.6 mmhos cm^{-1}.

5.3.1 Management Zone Delineation

Results from management zone delineation techniques are displayed in Figures 5.2 to 5.4. All four techniques delineated the north-west section of Field 1 as a low productivity zone; similarly, high productivity zones were delineated in the south-central and western section of the field. Overall, the medium productivity zones displayed decreased correspondence when the four techniques are compared. The areal correspondence among the delineation techniques was also quantitatively summarized with two-way tables and the χ^2 goodness-of-fit test. The agreement between management zone techniques for Field 1 ranged from 28 to 46% and all comparisons were significant based on the χ^2 goodness-of-fit test (Table 5.2). The YBMZ and EC_aMZ techniques had the highest agreement percentage with each other while YBMZ and RCMZ had the lowest agreement percentage with each other.

The SCMZ, EC_aMZ, and RCMZ techniques all identified high productivity zones in the north and south regions of Field 2; low productivity zones were delineated in the center of the field (Figure 5.2). In contrast, the YBMZ technique identified the center of Field 2 as highly productive. The agreement between management zone techniques for Field 2 ranged from 9 to 49% and all comparisons were significant based on the χ^2 goodness-of-fit test (Table 5.3). The 9% agreement was between the YBMZ and RCMZ techniques. Although the χ^2 goodness-of-fit test indicates this level of correspondence is significant, it is very small. This is most likely due to the large number of observations in the comparison and suggests, as is the case with many statistical procedures, utilizing several analysis techniques is beneficial when trying to make conclusions about large and varied data sets. The EC_aMZ and RCMZ techniques had the highest agreement

percentage with each other while YBMZ and RCMZ had the lowest agreement percentage with each other.

All four management zone techniques identified high productivity zones in the west-central region of Field 3; low productivity zones tended to be adjacent to the high productivity zone (Figure 5.3). In all four techniques, medium productivity zones occupied the edge of the field. The agreement between management zone techniques for Field 3 ranged from 14 to 43% and all comparisons were significant based on the χ^2 goodness-of-fit test (Table 5.4). The EC_aMZ and RCMZ techniques had the highest agreement percentage with each other while YBMZ and SCMZ had the lowest agreement percentage with each other.

Average and standard deviation values for primary soil parameters, partitioned by management zone, are presented for Fields 1 to 3 in Tables 5.5 to 5.7. Overall, there was a general trend for the OM and NO_3-N concentrations to be higher in the high productivity management zones for all four delineation techniques; similarly, lower concentrations were observed in low productivity zones. This initial outcome, based solely on soil sample data, suggests all four delineation techniques are successful at identifying management zones since OM and NO_3-N are commonly identified as important yield affecting parameters. There was no general trend in the remaining measured soil properties between the high, medium or low productivity zones.

5.3.2 Yield Data Summary

Corn yield data (i.e. cleaned and processed data) are presented in Tables 5.8 to 5.10. Data are partitioned by management zone delineation technique, productivity zone, and N treatment. Overall corn yields ranged from approximately 9300 to 15200 kg ha^{-1}

on Field 1. Average yields for Field 1 tend to increase by management zone and N treatment. Seventy-one percent of the yield distributions were leptokurtotic suggesting peaked distributions. Kurtosis is a measure of how different a distribution is from the normal distribution. A negative kurtosis (i.e. platykurtic) typically indicates a distribution flatter than the normal. A positive kurtosis (i.e. leptokurtotic) typically indicates a distribution more peaked than the normal. The adjusted kurtosis for a normal distribution is zero. Eighty-seven percent of the distributions are negatively skewed suggesting some lower yields in these data sets are affecting the skewness statistic. Skewness is a measure of asymmetry and a skewness value more than or less than zero indicates skewness in the data.

Overall corn yields ranged from approximately 8400 to 11800 kg ha^{-1} on Field 2. Average yields for Field 2 do not display a consistent tendency to increase by management zone and N treatment (i.e. compared to Field 1). Ninety-six percent of the yield distributions are platykurtic and 86% of the distributions are negatively skewed. Although almost all of the yield distributions were flatter than the normal (i.e. platykurtic), most of the values were very close to zero indicating relatively normal distributions.

Overall corn yields ranged from 6700 to 13400 kg ha^{-1} on Field 3. Average yields for Field 3 tend to increase by management zone and N treatment. Eighty-six percent of the sample yield distributions were platykurtic and 71% of the distributions are negatively skewed. Similar to Field 2, most of the platykurtic yield distributions were relatively close to zero indicating relatively normal distributions.

The cleaned yield data from all three fields indicate productivity was consistent with approximate average yields for the region (i.e. 11300 kg ha^{-1}). Also, the yields from Fields 1 and 3 appear to increase with higher productivity management zones; this was not the case with Field 2. The kurtosis statistics from Fields 2 and 3 were predominantly negative although they were all very close to zero (i.e. normally distributed). Field 1 had a predominance of positive kurtosis statistics which indicates there is very little variation in yields within management zones when compared with a standard normal distribution. This is logical if we assume each management zone represents homogenous regions in the field that will produce consistent yields. The tendency for yield data to be negatively skewed on all three fields is an indication that some lower yields were present in the samples. This is also logical if we assume the majority of the corn plants are producing at near optimum levels and relatively few plants are under-producing. The inclusion of the minority, under-producing, plants in the sample leads to a tendency for negatively skewed distributions.

5.3.3 Yield Response Data Analysis: ANOVA

5.3.3.1 Field 1

Experimental plots for the SCMZ technique only occupied the low productivity management zone; this prevented an ANOVA of yield data for this technique. The ANOVA for EC_aMZ resulted in significant differences for all three N treatments indicating at least one of the management zone yields was different (Table 5.11). Individual pairwise comparisons, using Tukey's HSD technique, were used to determine which management zone yields were different. Two treatment means are declared unequal when the interval created using Tukey's method does not cover 0; Tukey

intervals are presented in all ANOVA tables. Yields from high and low management zones were not significantly different for the 0 and 100% N treatments; similarly, yields from medium and high management zones were not significantly different for the 50% N treatment. The remaining pairwise comparisons were significantly different.

The ANOVA for YBMZ resulted in significant differences for the 0 and 100% N treatments (Table 5.12). The 0 and 100% N treatments only occupied the low and medium management zones (i.e. only one pairwise comparison was applicable and was significant). The 50% N treatment only occupied the low productivity management zone and prevented ANOVA for that treatment.

The ANOVA for the RCMZ technique resulted in significant difference for the 50% N treatment; 0 and 100% treatments were not significantly different (Table 5.13). The low and medium management zones displayed significant differences based on pairwise comparison while high-low and medium-high pairwise comparisons were not significantly different.

The ANOVA analysis for Field 1 suggests that differences in yield do exist among management zones when the EC_aMZ and YBMZ techniques are used. However, only the 50% N treatment had significant differences for the RCMZ technique. An examination of pairwise comparisons does not indicate a clear trend in yield differences among management zones. A simple research hypothesis would predict that yields from high and low management zones would more often be significantly different. Based on the ANOVA results for Field 1, it is difficult to support this research hypothesis. Another important observation is the general lack of trend in average yields. For example, I would expect to generally see increasing yields with increasing productivity potential.

While yield differences are significant based on the ANOVA results, an obvious trend with respect to delineation technique or N treatment is not apparent.

5.3.3.2 Field 2

The ANOVA for the SCMZ technique resulted in significant difference for all three N treatments (Table 5.14). All three pairwise comparisons were significantly different for the 0% N treatment. The 50% N treatment displayed significant pairwise differences for the low-medium and high-low management zone comparisons; medium-high was not significantly different. The 100% N treatment only occupied medium and high management zones (i.e. only one pairwise comparison was applicable and was significant).

The EC_aMZ technique only occupied low and medium productivity zones (Table 5.15). The ANOVA for all three N treatments was significant indicating management zone yields were different.

The YBMZ ANOVA resulted in significant differences for all three N treatments (Table 5.16). All pairwise comparisons were significantly different with the exception of 50% N, high-low comparison.

The ANOVA for the RCMZ technique resulted in significant differences for all three N treatments (Table 5.17). All pairwise comparisons were significant with the exception of 0% N, low-medium and 100% N, medium high.

The ANOVA analysis for Field 2 suggests that differences in yield do exist among management zones for all four delineation techniques. In addition, almost all pairwise comparisons of yield among management zones were significantly different for Field 2. A subtle trend in average yields was also apparent on Field 2: Higher average

yields tended to be associated with higher productivity management zones, lower yields with low productivity zones. When compared with the results from Field 1, Field 2 seemed to be more responsive to the imposition of management zones and all delineation techniques performed well.

5.3.3.3 Field 3

The ANOVA for the SCMZ technique resulted in significant difference for all three N treatments (Table 5.18). All pairwise comparisons were significantly different with the exception of 0% N, medium-high and 100%, medium-high.

The EC_aMZ ANOVA resulted in significant differences for all three N treatments (Table 5.19). All pairwise comparisons were significantly different with the exception of 50 and 100% N, medium-high.

The ANOVA for the YBMZ technique resulted in significant differences for all three N treatments (Table 5.20). Three pairwise comparisons were determined to be not significant: 0% N, low-medium; 50% N, high-low; and, 100% N, medium-high.

The RCMZ ANOVA resulted in significant differences for all three N treatments (Table 5.21). Three pairwise comparisons were determined to be not significant: 0% N, low-medium; 50% N, medium-high; and, 100% N, medium-high.

The ANOVA analysis for Field 3 suggests that differences in yield do exist among management zones for all four delineation techniques. In addition, similar to Field 2, most of the pairwise comparisons of yield among management zones were significantly different. Results from Field 3 also indicate higher average yields were associated with high productivity management zones; lower yields with low productivity zones. Field 3, similar to Field 2, seemed to be more responsive to the imposition of

management zones and all four delineation techniques performed well. The results from ANOVA alone do not provide evidence to indicate which of the delineation techniques performs better. The analysis does, however, suggest that management zones are being delineated and that Fields 2 and 3 appear more responsive to the applied treatments. Based on the data in this study it is not clear why Fields 2 and 3 'outperform' Field 1.

5.3.4 Yield Response Data Analysis: *S*-statistic

Experimental plots for the SCMZ technique only occupied the low productivity management zone on Field 1; this prevented yield data analysis with the *S*-statistic. The *S*-statistic for the EC_aMZ resulted in significant differences for all three N treatments on Field 1 (Table 5.22). Differences were also significant for the YBMZ technique at the 0 and 100% N treatments; 50% N treatment only occupied the low management zone and prevented *S*-statistic analysis. The RCMZ technique did not display significant yield differences among management zones based on the *S*-statistic at Field 1.

Field 2 had significant *S*-statistics for all techniques with the exception of EC_aMZ 50 and 100% N. All *S*-statistics indicate significant yield differences among management zones for all techniques and treatments at Field 3.

The *S*-statistic is used to assist in addressing the research question: Are management zones any better than a random yield pattern in the field? If management zones are capable of differentiating yields into regions of low, medium, and high productivity, one would expect the variability of yields within management zones to be at a minimum and we would expect the test statistic, S_0, to be small. In contrast, if yields were randomly assigned to management zones, we would expect the variability of yields to be large, and thus lead to a large S_0 value. In most of the analyses with the *S*-statistic

p-values were significantly small indicating the yield patterns under analysis were not random and suggest yield patterns are present. Essentially, this indicates zones are being delineated in most cases. Unlike the ANOVA analysis, the *S*-statistic does not indicate which individual zones are most effective or the magnitude of the differences among zones. It is not clear why four of the analyses were not significant, or more particularly why the RCMZ technique performed so poorly on Field 1. However, it is apparent from the previous ANOVA analysis that Field 1 was less responsive to the imposed treatments.

5.3.5 Yield Response Data Analysis: χ^2 Goodness-of-Fit Test

5.3.5.1 Field 1

Agreement among delineation techniques and the cluster approach to classifying corn yields is summarized in Table 5.23. The cluster approach to classifying yields uses an objective, *k*-means clustering algorithm to classify each yield value as high, medium, or low. Overall percent agreement ranged from 7 to 37%. All comparisons were significant with the exception of the 50 and 100% N treatments for the SCMZ technique based on the χ^2 goodness-of-fit test. The χ^2 goodness-of-fit test is an areal association statistic that provides a measure of agreement between classification techniques (i.e. yield value classification, and management zone delineation). Significant comparisons indicate agreement between management zone classification (high, medium, or low productivity) and yield classification based on the cluster approach (high, medium, or low yield). The EC_aMZ technique had the highest overall percent agreements when compared with the remaining delineation techniques. The SCMZ technique had the lowest percent agreements. The YBMZ and RCMZ delineation techniques had percent

agreements that were lower than the EC_aMZ technique, but higher than the SCMZ technique.

Agreement among delineation techniques and the non-parametric approach to classifying corn yields is summarized in Table 5.24. Briefly, the non-parametric classification procedure classifies a yield value as 'high' if it is greater than the 3rd quartile yield value in the sample; 'medium' if it falls within the 1st and 3rd quartiles; and 'low' if it falls below the 1st quartile value. Overall percent agreement ranged from 18 to 44%. All comparisons were significant with the exception of the SCMZ technique; all SCMZ comparisons were not significant. The YBMZ technique had the highest overall percent agreements when compared with the remaining techniques. The RCMZ technique had the lowest percent agreements although all RCMZ comparisons were significant.

Agreement among delineation techniques and the subjective approach to classifying corn yields is summarized in Table 5.25. Briefly, the subjective approach to classifying yields is based on knowledge of corn yields in the region. Overall percent agreement ranged from 9 to 34%. All comparisons were significant with the exception of the 0 and 50% N treatments for the SCMZ technique. The YBMZ technique had the highest overall percent agreements when compared with the remaining techniques. The SCMZ technique had the lowest percent agreements.

Overall agreement percentages partitioned by yield classification technique and N treatment indicate the non-parametric yield classification approach had the highest agreements. Average overall agreements for the non-parametric approach were 36, 26, and 32% for the 0, 50, and 100% N treatments respectively. Average numbers were 19,

14, and 18% for the cluster approach, and 18, 17, and 27% for the subjective approach (i.e. 0, 50, and 100% N treatments respectively).

The results from the ANOVA and *S*-statistic analyses provided evidence that management zones are being delineated but those analyses did not provide insight into which technique(s) was better. Results from the χ^2 goodness-of-fit test and two-way tables provide the first insight into the differences among the delineation techniques. Overall, on Field 1 the SCMZ technique was the poorest delineation technique and the YBMZ technique was best. Additionally, the non-parametric approach to yield classification had the highest percentage agreements when compared to the cluster and subjective approaches to yield classification.

5.3.5.2 Field 2

Agreement among delineation techniques and the cluster approach to classifying corn yields is summarized in Table 5.26. Overall percent agreement ranged from 24 to 54%. All comparisons were significant with the exception of the 50% N treatment for the EC_aMZ technique. The RCMZ technique had the highest overall percent agreements when compared with the remaining delineation techniques. The YBMZ technique had the lowest percent agreement.

Agreement among delineation techniques and the non-parametric approach to classifying corn yields is summarized in Table 5.27. Overall percent agreement ranged from 18 to 52%. All comparisons were significant with the exception of the 50% N treatment for the EC_aMZ technique. The RCMZ technique had the highest percent agreement when compared with the remaining delineation techniques. The SCMZ technique had the lowest percent agreement.

Agreement among delineation techniques and the subjective approach to classifying corn yields is summarized in Table 5.28. Overall percent agreement ranged from 16 to 52%. All comparisons were significant with the exception of the 50% N treatment for the EC_aMZ technique. The RCMZ technique had the highest percent agreement when compared with the remaining delineation techniques. The EC_aMZ technique had the lowest percent agreements.

Overall agreement percentages partitioned by yield classification technique and N treatment indicate the non-parametric yield classification approach had the highest agreements. Average overall agreements for the non-parametric approach were 39, 31, and 32% for the 0, 50, and 100% N treatments respectively. Average numbers were 39, 30, and 30% for the cluster approach, and 36, 31, and 27% for the subjective approach (i.e. 0, 50, and 100% N treatments respectively).

The χ^2 goodness-of-fit tests on Field 2 indicate the RCMZ technique performed best when compared with the remaining three delineation techniques. Based on the results, it is difficult to conclude which of the remaining three delineation techniques was the poorest; each of the three had poor results in at least one trial. Similar to Field 1, the non-parametric approach to classifying yields was the most successful yield-classification technique on Field 2.

5.3.5.3 Field 3

Agreement among delineation techniques and the cluster approach to classifying corn yields is summarized in Table 5.29. Overall percent agreement ranged from 21 to 54%. All comparisons were significant. The EC_aMZ technique had the highest overall

percent agreements when compared with the remaining delineation techniques. The YBMZ technique had the lowest percent agreement.

Agreement among delineation techniques and the non-parametric approach to classifying corn yields is summarized in Table 5.30. Overall percent agreement ranged from 25 to 43%. All comparisons were significant. The RCMZ technique had the highest percent agreement when compared with the remaining delineation techniques. The SCMZ technique had the lowest percent agreement.

Agreement among delineation techniques and the subjective approach to classifying corn yields is summarized in Table 5.31. Overall percent agreement ranged from 29 to 46%. All comparisons were significant. The EC_aMZ, YBMZ, and RCMZ techniques had equal and the highest percent agreement when compared with the SCMZ technique.

Overall agreement percentages partitioned by yield classification technique and N treatment indicate the cluster yield classification approach had the highest agreements. Average overall agreements for the cluster approach were 39, 39, and 37% for the 0, 50, and 100% N treatments respectively. Average numbers were 35, 36, and 37% for the non-parametric approach, and 37, 36, and 37% for the subjective approach (i.e. 0, 50, and 100% N treatments respectively).

The χ^2 goodness-of-fit tests indicate the RCMZ and EC_aMZ delineation techniques were better when compared with the remaining two techniques. The YBMZ and EC_aMZ techniques were each poor performers in at least one of the trials; although the YBMZ technique performed as well as the RCMZ and EC_aMZ techniques in the third trial. Unlike Fields 1 and 2, the cluster approach to classifying yields was the most

successful yield-classification technique on Field 3. Results from all three fields indicate that the RCMZ technique was the best performing delineation technique in this study; YBMZ and EC_aMZ performed similarly. The SCMZ technique was the poorest delineation technique. Finally, the non-parametric approach to yield classification appears to be the best classification approach in this study. The subjective approach to yield classification was the poorest technique.

5.3.6 Yield Response Data Analysis: κ-statistic

A summary of κ-statistics partitioned by field, percent of recommended N applied, management zone delineation technique, and yield classification technique is presented in Table 5.32. The κ-statistic provides another measure of agreement between two 'scorers' that assign observations into one of g groups. With respect to the current study, 'scorers' are the management zone delineations and yield value classifications. The summary of agreement between the two scorers results in a matrix of classifications and misclassifications. The κ-statistic has a maximum of 1 when agreement between scorers is perfect and a value of zero when there is no agreement better than chance. The κ-statistic can also be negative if agreement is worse than chance agreement. Forty percent of the κ-statistics in Table 5.32 are negative suggesting agreement is worse than chance agreement in those comparisons. Of the remaining 60% of comparisons, 14% have κ-statistics ≥ 0.1. A positive κ-statistic indicates agreement between two scorers (i.e. in this situation management zone delineation, and yield classification are the scorers). The remaining κ-statistics are < 0.1 and would generally be considered ≈ 0; indicating agreement no better than chance between scorers.

Eleven percent of the comparisons based on the SCMZ technique resulted in κ-statistics ≥ 0.1. The EC_aMZ and YBMZ techniques resulted in 11, and 15% of κ-statistics ≥ 0.1, respectively. The RCMZ technique had the highest percentage of κ-statistics ≥ 0.1; 26%. The cluster approach to classifying yield values had the highest percentage of κ-statistics ≥ 0.1 compared to the non-parametric and subjective approaches (i.e. 22, 14, and 11%, respectively). The 0% N treatments had κ-statistics $\geq$ 0.1 in 25% of the comparisons. The 50 and 100% N treatments had κ-statistics ≥ 0.1 in 3 and 19% of the comparisons respectively.

Similar to the χ^2 statistic, the κ-statistic provides another opportunity to address the question: Which delineation technique is better? In this study, the κ-statistic indicates that the RCMZ technique was the best delineation approach; the YBMZ technique was the second most effective. The SCMZ and EC_aMZ techniques were equally poor at delineating management zones. Finally, the cluster approach to classifying yield values was the most effective when compared to the non-parametric and subjective approaches; subjective was the poorest performer.

5.4 Summary and Conclusions

Visually the management zone delineation techniques generated several areas of similar classification (i.e. high, low, or medium productivity zone). This is supported by the significant χ^2 statistics in Tables 5.2 to 5.4. However, there are notable differences between some of the techniques. For example, the YBMZ delineations for Field 2 appear much different than the remaining techniques, particularly with respect to the high productivity zone. Despite the obvious visual differences, the soil properties among the different management zone delineation techniques are similar (Tables 5.5-5.7).

Yields within zones appeared to increase with increasing productivity zone and with increasing N treatment (Tables 5.8-5.10). The yield distributions on Fields 1 and 2 were predominantly normal to slightly platykurtic. The leptokurtotic distribution of yields on Field 3 indicates that there is very little variation in yields within management zones when compared with a standard normal distribution. This is logical if we assume each management zone represents homogenous regions in the field that will produce consistent yields. The tendency for yield data to be negatively skewed is an indication that some lower yields were present in the samples. The majority of the sample yield distributions were also negatively skewed. However, when analyzing data from a natural system, skewness is almost certainly an unavoidable outcome.

All but two of the ANOVA procedures resulted in significant *p*-values (Tables 5.11-5.21). This is objective evidence that mean yields among management zones are not equal. I would expect more of the individual pairwise comparisons of mean yields to be significantly different for the 0% N treatment regardless of management zone technique. This research hypothesis is based on the assumption that without added N the true yield-variability among management zones would not be masked or confounded by N inputs. Examination of the pairwise comparisons using Tukey's HSD supports this hypothesis and a simple trend with respect to N treatments is evident: Twenty-one of twenty-six pairwise comparisons (81%) were significantly different for the 0% N treatment; however, the 50 and 100% N treatments had significantly different pairwise comparisons in twenty of twenty-eight (71%) and eighteen of twenty-four (75%) instances, respectively. Overall, the ANOVA analysis provides evidence that management zones

are being delineated using these four techniques. The analysis does not however provide enough evidence to conclude which of the techniques is better.

The *S*-statistic analysis provides additional evidence to conclude that management zone delineation techniques resulted in yield patterns that were different from random yield patterns (Table 5.22). This conclusion is applicable for all but four of the analyses. In particular, the RCMZ technique on Field 1 had non-significant *p*-values for all three N treatments. I can not say specifically why the RCMZ technique performed poorly, however, it is evident from the ANOVA analysis and *S*-statistic analysis that Field 1 was less responsive to the imposed treatments. Overall, the *S*-statistic analysis provides evidence that management zones are being delineated using these four techniques. Again, however, the analysis does not indicate which technique is better.

The χ^2 goodness-of-fit analysis provides evidence of significant areal association among management zones and yield classifications in 98 of 108 comparisons (Tables 5.23-5.25). If I consider all areal association comparisons as a whole, the average agreement is 25, 26, 29, and 31% for SCMZ, YBMZ, EC_aMZ, and RCMZ techniques respectively. It is also important to note that the only delineation techniques that had non-significant overall areal associations were the SCMZ technique and the EC_aMZ technique (i.e. 20 and 8% non-significant areal associations, respectively). Based on this information I conclude that the RCMZ technique was the better overall delineation technique; the EC_aMZ and YBMZ techniques were equally effective although the YBMZ technique had significant areal associations in all trials. The SCMZ technique was consistently the poorest overall delineation technique compared to the remaining 3 techniques.

The χ^2 goodness-of-fit analysis also provides an opportunity to examine the three different yield classification techniques. The non-parametric and cluster approach to yield classification seem to be the most effective and had the highest overall agreements when compared with the subjective approach. On Field 1, average overall agreements for the non-parametric approach were 36, 26, and 32% for the 0, 50, and 100% N treatments respectively. Average numbers were 19, 14, and 18% for the cluster approach, and 18, 17, and 27% for the subjective approach (i.e. 0, 50, and 100% N treatments respectively). Similarly, on Field 2 average overall agreements for the non-parametric approach were 39, 31, and 32% for the 0, 50, and 100% N treatments respectively. Average numbers were 39, 30, and 30% for the cluster approach, and 36, 31, and 27% for the subjective approach (i.e. 0, 50, and 100% N treatments respectively). The cluster approach to classifying yields was the optimum approach on Field 3. Average overall agreements for the cluster approach were 39, 39, and 37% for the 0, 50, and 100% N treatments respectively. Average numbers were 35, 36, and 37% for the non-parametric approach, and 37, 36, and 37% for the subjective approach (i.e. 0, 50, and 100% N treatments respectively). Based on these results I conclude that the non-parametric approach to classifying yields was the better approach for this study; the cluster approach slightly less effective.

The κ-statistic did not provide as much evidence of effective management zone delineations when compared with ANOVA, *S*-statistics, and χ^2 goodness-of-fit analyses. Forty-percent of the κ-statistics were negative suggesting poor agreement among management zones and yield classifications. However, the κ-statistic did provide additional evidence indicating the RCMZ technique outperformed the remaining

techniques since 26% of the RCMZ trials had a κ-statistic ≥ 0.1; YBMZ technique was the next most effective with $15\% \geq 0.1$. Additionally, the cluster approach to classifying yields was the most effective; the non-parametric approach was the next most effective.

The combination of four management zone delineation techniques, three N treatments, and three yield classification techniques makes a succinct conclusion a difficult task for this study. However, some important conclusions can be drawn from the results. The evidence supports the idea of developing management zone delineation techniques on fields without additional N inputs; or very low N inputs. Pairwise comparisons indicated twenty-one of twenty-six pairwise comparisons (81%) were significantly different for the 0% N treatment; however, the 50 and 100% N treatments had significantly different pairwise comparisons in twenty of twenty-eight (71%) and eighteen of twenty-four (75%) instances, respectively. This type of basic-applied research should be effective for future studies designed to reveal the correct factors that contribute to a management zone. The evidence also supports the need to develop soil productivity management zones with soil sample data from the field of interest. The SCMZ and EC_aMZ techniques do not incorporate soil information into the delineation procedure at the outset. Comparatively, the YBMZ and RCMZ techniques do incorporate soil information for management zone delineation. The YBMZ and RCMZ techniques consistently outperform the other two techniques. My research hypothesis is that the soil information (i.e. from soil samples) is essential to developing effective management zones. Finally, when classifying crop yields as high, medium, or low, the evidence indicates an objective procedure is most effective. The cluster and non-parametric approach to classifying yields consistently outperformed the subjective approach.

5.5 References

Bhatti, A.U., D.J. Mulla, and B.E. Frazier. 1991. Estimation of soil properties and wheat yields on complex eroded hills using geostatistics and thematic mapper images. Remote Sens. Environ. 37:181-191.

Bruulsema, T.W., G.L. Malzer, P.C. Robert, J.G. Davis, and P.J. Copeland. 1996. Spatial relationships of soil nitrogen with corn yield response to applied nitrogen. p. 505-512. *In* P.C. Roberts et al., (ed.) Precision Agriculture. Proc. Int. Conf., 3rd. ASA, CSSA, and SSSA, Madison, WI.

Cassel, D.K., E.J. Kamprath, and F.W. Simmons. 1996. Nitrogen-sulfur relationships in corn as affected by landscape attributes and tillage. Agron. J. 88:133-140.

Chen, F., D.E. Kissel, L.T. West, and W. Adkins. 2000. Field-scale mapping of surface soil organic carbon using remotely sensed imagery. Soil Sci. Soc. Am. J. 64: 746-753.

Daberkow, S.G., and W.D. McBride. 2000. Adoption of precision agriculture technologies by US farmers. *In*: P.C. Roberts et al., (ed) Precision Agriculture. Proc. Int. Conf., 5th. ASA, CSSA, and SSSA, Madison, WI.

Doerge, T. 1999. Defining management zones for precision farming. Crop Insight 8(21): 1-5.

Eigenberg, R.A., J.W. Doran, J.A. Nienaber, and B.L. Woodbury. 2000. Soil conductivity maps for monitoring temporal changes in an agronomic field. *In* Animal Agriculture and Food Processing Wastes. Proc. Int. Sym., 8th. Des Moines, IA.

Fleming, K.L., D.G. Westfall, D.W. Wiens, L.E. Rothe, J.E. Cipra, and D.F. Heermann. 1999. Evaluating farmer developed management zone maps for precision farming. *In*: P.C. Robert et al., (ed.) Proceedings of the 4th international conference on precision agriculture. ASA, CSSA, and SSSA, Madison, WI.

Fleming, K.L., D.G. Westfall, D.W. Wiens, and M.C. Brodahl. 2000. Evaluating farmer defined management zone maps for variable rate fertilizer application. Precis. Agric. 2:201-215.

Franzen, D.W., and T.R. Peck. 1994. Sampling for site specific management. *In*: P.C. Robert et al., (ed.) Proceedings of the 2nd international conference on site-specific management for agricultural systems. ASA, CSSA, and SSSA, Madson, WI.

Franzen, D.W., A.D. Halvorson, and V.L. Hofman. 2000. Management zones for soil N and P levels in the Northern Great Plains. *In*: P.C. Roberts et al. (ed.) Proceedings of the 5th international conference on precision agriculture. ASA, CSSA, and SSSA, Madison, WI.

Franzen D.W., D.H. Hopkins, M.D. Sweeney, M.K. Ulmer, and A.D. Halvorson. 2002. Evaluation of soil survey scale for zone development of site-specific nitrogen management. Agron. J. 94:381-389.

Hammond, M.W. 1992. Cost analysis of variable fertility management of phosphorus and potassium for potato production in central Washington. p. 213-228. *In* P.C. Robert et al., (ed.) Soil specific crop management. ASA, CSSA, and SSSA. Madison, WI.

Jaynes, D.B., T.S. Colvin, and J. Ambuel. 1994. Yield mapping by electromagnetic induction. p. 383-398. *In* P.C. Roberts et al. (ed.) Proceedings of the 2nd international conference on precision agriculture. ASA, CSSA, and SSSA, Madison, WI.

Khosla, R., and M.M. Alley. 1999. Soil-specific nitrogen management on mid-Atlantic coastal plain soils. Better Crops with Plant Food. 83(3): 6-7.

Khosla, R., K. Fleming, J.A. Delgado, T. Shaver, and D.G. Westfall. 2002. Use of site specific management zones to improve nitrogen management for precision agriculture. J. Soil Water Conserv. 57: 513-518.

Kravenko, A.N., and D.G. Bullock. 2000. Correlation of corn and soybean grain yield with topography and soil properties. Agron. J. 92:75-83.

MapInfo©. 2002. MapInfo professional version 7.0. MapInfo Corporation. Troy, NY.

McBratney, A.B., and M.J. Pringle. 1999. Estimating average and proportional variograms of soil properties and their potential use in precision agriculture. Precis. Agric. 1:219-236.

McCann, B.L., D.J. Pennick, C. van Kessel, and F.L. Walley. 1996. The development of management units for site-specific farming. p. 295-302. *In* P.C. Roberts et al. (ed.) Proc. 3rd Int. Conf. Prec. Agric. ASA-CSSA-SSSA. Madison, WI.

Miller, R.O., J. Kotuby-Amacher, and J.B. Rodriguez. 1998. Western states laboratory proficiency testing program, soil and plant analytical methods. Version 4.10.

Mortvedt, J.J., D.G. Westfall, and R.L. Croissant. 1996. Fertilizer suggestions for corn. Colorado State University Cooperative Extension, Service in Action. No. 0.538. Fort Collins, CO.

Mueller, T.G., F.J. Pierce, O. Schabenberger, and D.D. Warncke. 2001. Map quality for site-specific fertility management. Soil Sci. Soc. Amer. J. 65:1547-1558.

Nolan, S.C., T.W. Goddard, and G. Lohstraeter. 2000. Assessing management units on rolling topography. *In* P.C. Roberts et al. (ed.) Proc. 5th Int. Conf. Prec. Agric. ASA, CSSA, and SSSA, Madison, WI.

Ortega, R.A. 1997. Spatial variability of soil properties and dryland crop yields over "typical" landforms of eastern Colorado. PhD Thesis, Colo. State Univ., Fort Collins, CO

Reich, R.M., and R.A. Davis. 1998. On-line spatial library for the S-PLUS statistical software package. Colo. State. Univ., Fort Collins, CO.

Schloerder, C.A., N.E. Zemmerman, and M.J. Jacobs. 2001. Comparison of methods for interpolating soil properties using limited data. Soil Sci. Soc. Am. J. 65:470-479.

Statistical Sciences. 1999. S-PLUS© 2000. Statistical software package for personal computers. StatSci Division, MathSoft, Inc., Seattle, WA.

Sudduth, K.A., N.R. Kitchen, D.F. Hughes, and S.T. Drummond. 1994. Electromagnetic induction sensing as an indicator of productivity on claypan soils. p. 671-681. *In* P.C. Roberts et al. (ed.) Proc. 2nd Int. Conf. Prec. Agric. ASA, CSSA, and SSSA, Madison, WI.

Sudduth, K.A., N.R. Kitche, and S.T. Drummond. 1998. Soil conductivity sensing on claypan soil: comparison of electromagnetic induction and direct methods. p. 979-990. *In* P.C. Roberts et al. (ed.) Proc. 4th Int. Conf. Prec. Agric. ASA, CSSA, and SSSA, Madison, WI.

Westfall, D.G., W.J. Gangloff, R. Khosla, R.M. Reich, A. Hornung, D.F. Heermann, H.J. Farhani, and K. Fleming. 2003. Development of production level management zones for nitrogen fertilization. p. 332. *In* A. Werner and A. Jarfe (ed.) Program book of the joint conference of ECPA-ECPLF. Wageningen Academic Publishers. The Netherlands.

Whelan, B.M., A.B. McBratney, and R.A. Viscarra-Rossel. 1996. Spatial prediction for precision farming. p. 331-342. *In* P.C. Robert et al., (ed.) Proc. 3rd Int. Conf. Prec. Agric. ASA, CSSA, and SSSA, Madison, WI.

Yang, C., G.L. Anderson, J.H. Everitt, and D.E. Escobar. 1998. Mapping plant growth and yield variations from aerial digital videography. p. 577-586. *In* Proc. 1st Intl. Conf. Geospatial Information in Agriculture and Forestry. ERIM International Inc., Ann Arbor, MI.

Table 5.1 Average values of soil test parameters from Fields 1, 2, and 3, and their associated standard deviations in parentheses.

	OM	NO_3-N	NH_4-N	Zn	EC
	%		--------mg kg^{-1}--------		--mmhos cm^{-1}--
Field 1	1.4 (0.2)	10.0 (2.8)	6.3 (1.5)	1.8 (0.6)	0.3 (0.1)
Field 2	1.3 (0.5)	9.2 (3.1)	5.6 (0.7)	1.7 (0.7)	0.4 (0.1)
Field 3	1.3(0.2)	20.9(6.8)	7.8(1.9)	3.0(0.4)	0.6(0.3)

Table 5.2 Agreement between management zone delineation techniques for Field 1, and results of Chi-square goodness-of-fit test. Values are percent.

		Delineation technique								
		EC_aMZ†			SCMZ‡			YBMZ§		
		Management Zone								
Technique	Zone	Hi	Med	Low	Hi	Med	Low	Hi	Med	Low
RCMZ¶	Hi	38	48	32	77	61	34	15	46	5
	Med	36	25	15	1	25	35	70	14	24
	Low	26	27	54	21	13	30	15	40	70
	Overall#	37**			46**			28**		
EC_aMZ	Hi				61	82	42	56	33	38
	Med				24	11	20	32	39	11
	Low				15	6	38	12	29	51
	Overall				40**			47**		
SCMZ	Hi							99	82	15
	Med							1	6	43
	Low							0	12	42
	Overall							42**		

† Apparent electrical conductivity management zone delineation technique.
‡ Soil color management zone delineation technique.
§ Yield based management zone delineation technque.
¶ Remotely sensed data and cluster sampling management zone delineation technique.
# Overall accuracy values with ** indicate p-value <0.05; ns=not significant. Treatments without observed samples are denoted not available (na).

Table 5.3 Agreement between management zone delineation techniques for Field 2, and results of Chi-square goodness-of-fit test. Values are percent.

		Delineation technique								
		EC_aMZ†			SCMZ‡			YBMZ§		
		Management Zone								
Technique	Zone	Hi	Med	Low	Hi	Med	Low	Hi	Med	Low
RCMZ¶	Hi	95	94	21	6	23	0	16	24	21
	Med	5	6	70	71	68	10	4	0	73
	Low	0	0	9	24	9	90	80	76	6
	Overall#	49**			43**			9**		
EC_aMZ	Hi				12	0	0	21	17	1
	Med				65	1	0	2	78	99
	Low				23	99	1	78	6	0
	Overall				14**			32**		
SCMZ	Hi							0	23	19
	Med							0	6	46
	Low							100	71	35
	Overall							16**		

† Apparent electrical conductivity management zone delineation technique.

‡ Soil color management zone delineation technique.

§ Yield based management zone delineation technque.

¶ Remotely sensed data and cluster sampling management zone delineation technique.

Overall accuracy values with ** indicate p-value <0.05; ns=not significant. Treatments without observed samples are denoted not available (na).

Table 5.4 Agreement between management zone delineation techniques for Field 3, and results of Chi-square goodness-of-fit test. Values are percent.

		Delineation technique								
		EC_aMZ†			SCMZ‡			YBMZ§		
		Management Zone								
Technique	Zone	Hi	Med	Low	Hi	Med	Low	Hi	Med	Low
RCMZ¶	Hi	34	48	2	18	45	81	39	42	6
	Med	52	46	55	29	40	12	30	12	1
	Low	14	6	43	53	16	6	31	46	93
	Overall#	43**			26**			41**		
EC_aMZ	Hi				24	59	78	61	15	19
	Med				39	34	0	9	16	3
	Low				37	6	22	30	69	78
	Overall				29**			42**		
SCMZ	Hi							13	30	79
	Med							1	23	21
	Low							86	47	0
	Overall							14**		

† Apparent electrical conductivity management zone delineation technique.

‡ Soil color management zone delineation technique.

§ Yield based management zone delineation technque.

¶ Remotely sensed data and cluster sampling management zone delineation technique.

Overall accuracy values with ** indicate p-value <0.05; ns=not significant. Treatments without observed samples are denoted not available (na).

Table 5.5 Average values of soil test parameters of Field 1 partitioned by management zone delineation technique and productivity zone delineation (i.e. low, medium, and high). Standard deviations are in parentheses.

		OM	NO_3-N	NH_4-N	Zn	EC
		%		--------mg kg^{-1}--------		--mmhos cm^{-1}--
SCMZ†	Low	1.3 (0.2)	9.2 (2.3)	6.3 (1.4)	1.7 (0.6)	0.3 (0.06)
	Med	1.4 (0.2)	11.4 (2.9)	6.4 (1.7)	1.8 (0.6)	0.3 (0.06)
	High	1.5 (0.2)	10.5 (3.1)	6.4 (1.2)	2.0 (0.2)	0.3 (0.06)
EC_aMZ‡	Low	1.4 (0.2)	9.0 (3.1)	6.5 (1.9)	1.5 (0.6)	0.3 (0.06)
	Med	1.3 (0.2)	10.4 (2.6)	6.3 (1.4)	2.0 (0.6)	0.3 (0.06)
	High	1.5 (0.2)	10.8 (2.8)	6.1 (1.1)	1.8 (0.4)	0.3 (0.07)
YBMZ§	Low	1.3 (0.2)	9.1 (2.5)	5.8 (1.4)	1.7 (0.6)	0.4 (0.05)
	Med	1.4 (0.2)	9.5 (2.6)	6.7 (1.4)	1.9 (0.7)	0.3 (0.06)
	High	1.4 (0.2)	11.0 (3.1)	6.4 (1.6)	1.8 (0.5)	0.3 (0.06)
RCMZ¶	Low	1.4 (0.2)	7.6 (1.8)	6.5 (1.4)	1.5 (0.6)	0.3 (0.1)
	Med	1.3 (0.2)	10.3 (2.7)	5.9 (1.4)	1.8 (0.6)	0.4 (0.04)
	High	1.6 (0.2)	11.4 (2.6)	7.0 (1.6)	1.9 (0.4)	0.3 (0.05)

† Soil color management zone delineation technique.

‡ Apparent electrical conductivity management zone delineation technique.

§ Yield based management zone delineation technque.

¶ Remotely sensed data and cluster sampling management zone delineation technique.

Table 5.6 Average values of soil test parameters of Field 2 partitioned by management zone delineation technique and productivity zone delineation (i.e. low, medium, and high). Standard deviations are in parentheses.

		OM	NO_3-N	NH_4-N	Zn	EC
		%		--------mg kg^{-1}--------		--mmhos cm^{-1}--
SCMZ†	Low	1.2 (0.1)	5.5 (3.7)	5.6 (1.0)	1.3 (0.2)	0.4 (0.07)
	Med	1.0 (0.2)	2.3 (0.5)	5.4 (0.5)	1.7 (0.5)	0.4 (0.07)
	High	1.6 (0.7)	4.8 (2.8)	5.7 (0.8)	1.8 (0.8)	0.5 (.2)
EC_aMZ‡	Low	1.1 (0.2)	6.1 (3.8)	5.4 (0.6)	1.5 (0.5)	0.4 (0.1)
	Med	1.8 (0.5)	3.1 (1.7)	6.1 (0.8)	2.2 (0.6)	0.6 (0.2)
	High	2.6 (0.1)	5.7 (2.9)	6.5 (1.0)	2.8 (0.6)	0.7 (0.2)
YBMZ§	Low	1.1 (0.2)	3.0 (0.9)	5.3 (0.7)	1.8 (0.7)	0.4 (0.06)
	Med	1.2 (0.3)	2.5 (0.5)	6.1 (1.0)	2.6 (0.6)	0.6 (0.2)
	High	2.3 (0.6)	4.7 (1.6)	5.5 (0.6)	1.5 (0.5)	0.4 (0.1)
RCMZ¶	Low	1.0 (0.2)	3.1 (1.7)	5.4 (0.5)	1.5 (0.6)	0.4 (0.1)
	Med	1.2 (0.2)	7.3 (3.6)	5.5 (0.8)	1.3 (0.2)	0.4 (0.1)
	High	2.3 (0.4)	5.5 (3.8)	6.2 (0.9)	2.6 (0.5)	0.6 (0.2)

† Soil color management zone delineation technique.

‡ Apparent electrical conductivity management zone delineation technique.

§ Yield based management zone delineation technque.

¶ Remotely sensed data and cluster sampling management zone delineation technique.

Table 5.7 Average values of soil test parameters of Field 3 partitioned by management zone delineation technique and productivity zone delineation (i.e. low, medium, and high). Standard deviations are in parentheses.

		OM	NO_3-N	NH_4-N	Zn	EC
		%	--------mg kg^{-1}--------			--mmhos cm^{-1}--
SCMZ†	Low	1.3 (0.2)	7.4 (1.4)	4.8 (0.8)	4.2 (1.2)	0.3 (0.1)
	Med	1.1 (0.1)	8.8 (2.7)	4.8 (0.4)	3.3 (0.8)	0.2 (0.06)
	High	1.3 (0.2)	10.5 (3.6)	4.0 (0.7)	3.3 (0.6)	0.4 (0.2)
EC_aMZ‡	Low	1.3 (0.2)	8.4 (2.4)	4.5 (1.0)	3.9 (0.6)	0.3 (0.2)
	Med	1.1 (0.2)	11.3 (2.8)	4.6 (0.6)	3.7 (1.4)	0.3 (0.1)
	High	1.5 (0.1)	14.7 (4.0)	4.4 (0.6)	3.4 (0.7)	0.4 (0.08)
YBMZ§	Low	1.0 (0.1)	9.2 (3.6)	4.0 (0.7)	3.7 (0.4)	0.2 (0.1)
	Med	1.0 (0.04)	13.3 (4.3)	3.7 (0.8)	3.2 (0.5)	0.3 (0.2)
	High	1.4 (0.2)	8.4 (2.2)	4.2 (0.4)	3.1 (0.5)	0.4 (0.2)
RCMZ¶	Low	1.1 (0.1)	8.0 (2.1)	4.4 (0.9)	3.4 (0.6)	0.3 (0.1)
	Med	1.4 (0.2)	9.6 (2.7)	4.7 (0.6)	4.6 (1.4)	0.4 (0.2)
	High	1.5 (0.1)	13.1 (3.6)	5.0 (1.1)	3.4 (0.7)	0.4 (0.1)

† Soil color management zone delineation technique.

‡ Apparent electrical conductivity management zone delineation technique.

§ Yield based management zone delineation technque.

¶ Remotely sensed data and cluster sampling management zone delineation technique.

Table 5.8 Average, standard deviation, kurtosis and skewness statistics of corn yields for each management zone (MZ) in Field 1 as influenced by percent of recommended N applied. Productivity zones that did not have observed samples are presented as not available (na).

Delineation technique	MZ	N applied	Average yield	Standard Deviation	Kurtosis	Skewness	Number of samples
		---%---	------kg ha^{-1}------				
SCMZ†	Low	0	11024	2540	-0.12	-0.36	654
	Medium	0	na				
	High	0	na				
SCMZ	Low	50	13631	2086	4.20	-1.86	585
	Medium	50	na				
	High	50	na				
SCMZ	Low	100	14482	2594	7.61	-2.54	710
	Medium	100	na				
	High	100	na				
EC_aMZ‡	Low	0	11092	2090	0.63	-0.26	416
	Medium	0	9307	2603	-1.40	0.14	74
	High	0	12391	2375	-1.23	-0.61	112
EC_aMZ	Low	50	14044	2062	7.58	-2.62	442
	Medium	50	11916	1056	2.44	-1.12	87
	High	50	12381	1554	1.04	-1.45	13
EC_aMZ	Low	100	14623	2964	6.99	-2.62	328
	Medium	100	13689	2077	1.22	-1.08	174
	High	100	15486	600	-0.38	0.04	149
YBMZ§	Low	0	10445	1831	-0.12	-0.16	432
	Medium	0	11659	1391	1.32	-0.54	170
	High	0	na				
YBMZ	Low	50	13674	2056	4.58	-1.91	567
	Medium	50	na				
	High	50	na				
YBMZ	Low	100	14198	2516	2.32	-1.23	329
	Medium	100	15112	1321	8.11	-1.70	364
	High	100	na				
RCMZ¶	Low	0	10480	1375	0.59	1.11	271
	Medium	0	11447	3050	-0.37	-0.78	375
	High	0	na				
RCMZ	Low	50	13982	1309	4.03	-1.78	104
	Medium	50	13336	2458	2.03	-1.43	357
	High	50	14122	668	-0.82	-0.11	111
RCMZ	Low	100	15214	1193	0.36	-0.57	346
	Medium	100	13900	3178	3.81	-2.02	394
	High	100	na				

† Soil color management zone delineation technique.
‡ Apparent electrical conductivity management zone delineation technique.
§ Yield based management zone delineation technque.
¶ Remotely sensed data and cluster sampling management zone delineation technique.

Table 5.9 Average, standard deviation, kurtosis and skewness statistics of corn yields for each management zone (MZ) in Field 2 as influenced by percent of recommended N applied. Productivity zones that did not have observed samples are presented as not available (na).

Delineation technique	MZ	N applied	Average yield	Standard deviation	Kurtosis	Skewness	Number of samples
		---%---	------kg ha^{-1}------				
SCMZ†	Low	0	8462	922	-0.80	0.01	96
	Medium	0	9418	1594	-0.43	0.30	317
	High	0	11009	670	-0.45	-0.26	110
SCMZ	Low	50	11886	1113	-0.46	-0.79	88
	Medium	50	9185	1893	-1.08	0.05	216
	High	50	8949	1650	-1.08	-0.24	97
SCMZ	Low	100	na				
	Medium	100	10310	1799	-0.43	-0.41	277
	High	100	9141	1543	-0.73	-0.28	253
EC_aMZ‡	Low	0	9049	1351	-0.55	0.17	449
	Medium	0	11152	881	-0.21	0.33	104
	High	0	na				
EC_aMZ	Low	50	9581	2129	-0.51	-0.53	409
	Medium	50	10922	1340	-1.05	-0.01	15
	High	50	na				
EC_aMZ	Low	100	9432	1798	-0.77	-0.16	477
	Medium	100	10505	10505	-0.60	0.40	92
	High	100	na				
YBMZ§	Low	0	9980	1195	-0.62	-0.22	106
	Medium	0	11234	882	-0.33	0.22	108
	High	0	8878	1326	-0.57	0.22	328
YBMZ	Low	50	9825	1232	-0.32	-0.61	65
	Medium	50	9011	501	-0.14	-0.11	28
	High	50	9832	2397	-0.83	-0.45	368
YBMZ	Low	100	11680	1333	0.66	-0.98	93
	Medium	100	10208	741	-0.87	0.04	75
	High	100	9037	1631	-0.81	-0.25	382
RCMZ¶	Low	0	9393	1874	-0.85	0.40	188
	Medium	0	9243	1209	-0.30	0.19	277
	High	0	11051	686	-0.48	-0.31	110
RCMZ	Low	50	9184	2244	-0.83	-0.20	316
	Medium	50	11621	1367	-0.24	-1.01	69
	High	50	9965	942	-0.67	-0.16	87
RCMZ	Low	100	9122	1700	-0.83	-0.19	331
	Medium	100	10368	1826	-0.83	-0.14	130
	High	100	10459	831	-0.78	-0.07	101

† Soil color management zone delineation technique.
‡ Apparent electrical conductivity management zone delineation technique.
§ Yield based management zone delineation technque.
¶ Remotely sensed data and cluster sampling management zone delineation technique.

Table 5.10 Average, standard deviation, kurtosis and skewness statistics of corn yields for each management zone (MZ) in Field 3 as influenced by percent of recommended N applied.

Delineation technique	MZ	N applied	Average yield	Standard deviation	Kurtosis	Skewness	Number of samples
		---%---	------kg ha^{-1}------				
SCMZ†	Low	0	6787	521	-0.70	0.19	86
	Medium	0	8119	1346	-0.02	0.42	399
	High	0	9070	1740	-0.17	-0.16	558
SCMZ	Low	50	9780	960	-0.23	0.34	93
	Medium	50	11233	1378	0.61	0.22	426
	High	50	12401	1099	0.38	0.26	377
SCMZ	Low	100	10978	1114	-0.39	0.04	385
	Medium	100	12047	1344	1.50	-0.36	1091
	High	100	12732	1193	-0.31	0.01	682
EC_aMZ‡	Low	0	6698	657	-0.05	-0.07	200
	Medium	0	8874	1468	0.10	-0.24	766
	High	0	12003	1035	-0.36	0.65	31
EC_aMZ	Low	50	10428	1429	1.31	0.49	135
	Medium	50	11731	1327	0.46	0.16	863
	High	50	11130	1004	-0.95	-0.10	22
EC_aMZ	Low	100	11248	1199	0.17	-0.41	627
	Medium	100	11989	1286	1.29	-0.14	1369
	High	100	13391	926	-0.47	0.22	139
YBMZ§	Low	0	7387	1160	0.59	0.18	247
	Medium	0	7559	1106	-0.19	0.58	178
	High	0	9264	1297	0.40	0.46	691
YBMZ	Low	50	11643	1043	-0.29	-0.06	225
	Medium	50	10255	1123	-0.27	0.05	188
	High	50	11912	1385	1.18	0.52	704
YBMZ	Low	100	11678	1210	0.89	-0.27	618
	Medium	100	11641	1626	0.30	-0.52	238
	High	100	12433	1276	1.05	-0.12	1434
RCMZ¶	Low	0	7879	1427	0.04	0.21	230
	Medium	0	8426	1662	1.12	0.81	618
	High	0	9780	1055	-0.09	-0.33	144
RCMZ	Low	50	10685	1366	0.97	0.88	366
	Medium	50	12046	1035	-0.10	-0.02	432
	High	50	12061	1575	2.58	-0.58	196
RCMZ	Low	100	11441	1154	0.39	-0.13	626
	Medium	100	11992	1348	0.26	-0.14	617
	High	100	12441	1275	1.27	-0.54	705

† Soil color management zone delineation technique.
‡ Apparent electrical conductivity management zone delineation technique.
§ Yield based management zone delineation technque.
¶ Remotely sensed data and cluster sampling management zone delineation technique.

Table 5.11 The ANOVA and Tukey's HSD test on 30 randomly selected corn grain yields from each production management zone (MZ) delineated by the EC_aMZ technique for the 0, 50, and 100% recommended N treatments on Field 1.

0%	Source	df	SS	MS	*F*	*p*-value
	MZ	2	1.57E+08	7.83E+07	14.46	<0.001
	Error	87	4.71E+08	5.42E+06		
	Total	89	6.28E+08			

MZ	Average	Tukey Intervals
	--kg ha^{-1}--	
Low†	11580	(1289,4153)^{LxM*}
Medium	8859	(1438,4302)^{MxH*}
High	11729	(-1283,1581)^{HxL}

50%	Source	df	SS	MS	*F*	*p*-value
	MZ	2	8.91E+07	4.46E+07	12.38	<0.001
	Error	87	3.13E+08	3.60E+06		
	Total	89	4.02E+08			

MZ	Average	Tukey Intervals
	--kg ha^{-1}--	
Low	14025	(1131,3466)^{LxM*}
Medium	11726	(-721,1614)^{MxH}
High	12172	(-3020,-685)^{HxL*}

100%	Source	df	SS	MS	*F*	*p*-value
	MZ	2	6.57E+07	3.29E+07	7.74	0.001
	Error	87	3.69E+08	4.25E+06		
	Total	89	4.35E+08			

MZ	Average	Tukey Intervals
	--kg ha^{-1}--	
Low	14617	(110,2645)^{LxM*}
Medium	13239	(786,3322)^{MxH*}
High	15293	(-591,1945)^{HxL}

† The management zone comparison is indicated by superscript letters and the null hypothesis of equal sample means was rejected at $\alpha \leq 0.05$ and is indicated with an asterisk (*). Two treatment means are declared unequal when the interval does not cover 0.

Table 5.12 The ANOVA and Tukey's HSD test on 30 randomly selected corn grain yields from each production management zone (MZ) delineated by the YBMZ technique for the 0 and 100% recommended N treatments on Field 1.

0%	Source	df	SS	MS	*F*	*p*-value
	MZ	1	4.70E+07	4.70E+07	12.96	0.001
	Error	58	2.10E+08	3.63E+06		
	Total	59	2.57E+08			

MZ	Average	Tukey Intervals
	--kg ha^{-1}--	
Low†	9945	(-2754,-786)^{LxM*}
Medium	11715	

100%	Source	df	SS	MS	*F*	*p*-value
	MZ	1	1.15E+08	1.15E+08	11.48	0.001
	Error	58	5.83E+08	1.00E+07		
	Total	59	6.98E+08			

MZ	Average	Tukey Intervals
	--kg ha^{-1}--	
Low	12408	(-4411,-1135)^{LxM*}
Medium	15181	

† The management zone comparison is indicated by superscript letters and the null hypothesis of equal sample means was rejected at $\alpha \leq 0.05$ and is indicated with an asterisk (*). Two treatment means are declared unequal when the interval does not cover 0.

Table 5.13 The ANOVA and Tukey's HSD test on 30 randomly selected corn grain yields from each production management zone (MZ) delineated by the RCMZ technique for the 0, 50, and 100% recommended N treatments on Field 1.

0%	Source	df	SS	MS	*F*	*p*-value
	MZ	1	2.86E+06	2.86E+06	0.56	0.456
	Error	58	2.94E+08	5.08E+06		
	Total	59	2.97E+08			

MZ	Average
	--kg ha^{-1}--
Low†	10493
Medium	10930

50%	Source	df	SS	MS	*F*	*p*-value
	MZ	2	1.73E+07	8.67E+06	3.84	0.025
	Error	87	1.96E+08	2.26E+06		
	Total	89	2.14E+08			

MZ	Average	Tukey Intervals
	--kg ha^{-1}--	
Low	14124	$(29,1878)^{LxM*}$
Medium	13171	$(-17,1831)^{MxH}$
High	14077	$(-971,878)^{HxL}$

100%	Source	df	SS	MS	*F*	*p*-value
	MZ	1	3.30E+06	3.30E+06	1.48	0.229
	Error	58	1.30E+08	2.23E+06		
	Total	59	1.33E+08			

MZ	Average
	--kg ha^{-1}--
Low	15172
Medium	14702

† The management zone comparison is indicated by superscript letters and the null hypothesis of equal sample means was rejected at $\alpha \leq 0.05$ and is indicated with an asterisk (*). Two treatment means are declared unequal when the interval does not cover 0.

Table 5.14 The ANOVA and Tukey's HSD test on 30 randomly selected corn grain yields from each production management zone (MZ) delineated by the SCMZ technique for the 0, 50, and 100% recommended N treatments on Field 2.

0%	Source	df	SS	MS	*F*	*p*-value
	MZ	2	8.34E+07	4.17E+07	44.22	<0.001
	Error	87	8.20E+07	9.43E+05		
	Total	89	1.65E+08			

MZ	Average	Tukey Intervals
	--kg ha^{-1}--	
Low†	8742	(-1351,-156)^{LxM*}
Medium	9496	(961,2156)^{MxH*}
High	11054	(1714,2909)^{HxL*}

50%	Source	df	SS	MS	*F*	*p*-value
	MZ	2	9.03E+07	4.51E+07	13.86	<0.001
	Error	87	2.83E+08	3.26E+06		
	Total	89	3.74E+08			

MZ	Average	Tukey Intervals
	--kg ha^{-1}--	
Low	11222	(768,2989)^{LxM*}
Medium	9343	(-1538,683)^{MxH}
High	8916	(-3416,-1196)^{HxL*}

100%	Source	df	SS	MS	*F*	*p*-value
	MZ	1	4.91E+07	4.91E+07	16.15	<0.001
	Error	58	1.76E+08	3.04E+06		
	Total	59	2.25E+08			

MZ	Average	Tukey Intervals
	--kg ha^{-1}--	
Medium	10654	(-2709,-908)^{MxH*}
High	8846	

† The management zone comparison is indicated by superscript letters and the null hypothesis of equal sample means was rejected at $\alpha \leq 0.05$ and is indicated with an asterisk (*). Two treatment means are declared unequal when the interval does not cover 0.

Table 5.15 The ANOVA and Tukey's HSD test on 30 randomly selected corn grain yields from each production management zone (MZ) delineated by the EC_aMZ technique for the 0, 50, and 100% recommended N treatments on Field 2.

0%	Source	df	SS	MS	*F*	*p*-value
	MZ	1	5.02E+07	5.02E+07	35.51	<0.001
	Error	58	8.20E+07	1.41E+06		
	Total	59	1.32E+08			

MZ	Average	Tukey Intervals
	--kg ha^{-1}--	
Low†	9327	$(-2445,-1215)^{LxM*}$
Medium	11157	

50%	Source	df	SS	MS	*F*	*p*-value
	MZ	1	1.22E+07	1.22E+07	6.04	0.017
	Error	58	1.17E+08	2.02E+06		
	Total	59	1.29E+08			

MZ	Average	Tukey Intervals
	--kg ha^{-1}--	
Low	10066	$(-1635,-167)^{LxM*}$
Medium	10967	

100%	Source	df	SS	MS	*F*	*p*-value
	MZ	1	8.75E+06	8.75E+06	4.07	0.048
	Error	58	1.25E+08	2.15E+06		
	Total	59	1.33E+08			

MZ	Average	Tukey Intervals
	--kg ha^{-1}--	
Low	9516	$(-1522,-6)^{LxM*}$
Medium	10280	

† The management zone comparison is indicated by superscript letters and the null hypothesis of equal sample means was rejected at $\alpha \leq 0.05$ and is indicated with an asterisk (*). Two treatment means are declared unequal when the interval does not cover 0.

Table 5.16 The ANOVA and Tukey's HSD test on 30 randomly selected corn grain yields from each production management zone (MZ) delineated by the YBMZ technique for the 0, 50, and 100% recommended N treatments on Field 2.

0%	Source	df	SS	MS	*F*	*p*-value
	MZ	2	9.32E+07	4.66E+07	35.12	<0.001
	Error	87	1.15E+08	1.33E+06		
	Total	89	2.09E+08			

MZ	Average	Tukey Intervals
	--kg ha^{-1}--	
Low†	9914	(-2013,-595)^{LxM*}
Medium	11218	(-3201,-1783)^{MxH*}
High	8726	(-1897,-479)^{HxL*}

50%	Source	df	SS	MS	*F*	*p*-value
	MZ	2	2.93E+07	1.47E+07	9.29	<0.001
	Error	87	1.37E+08	1.58E+06		
	Total	89	1.67E+08			

MZ	Average	Tukey Intervals
	--kg ha^{-1}--	
Low	9848	(80,1626)^{LxM*}
Medium	8996	(613,2159)^{MxH*}
High	10382	(-240,1306)^{HxL}

100%	Source	df	SS	MS	*F*	*p*-value
	MZ	2	1.06E+08	5.31E+07	27.56	<0.001
	Error	87	1.68E+08	1.93E+06		
	Total	89	2.74E+08			

MZ	Average	Tukey Intervals
	--kg ha^{-1}--	
Low	11732	(580,2288)^{LxM*}
Medium	10298	(-2077,-369)^{MxH*}
High	9075	(-3511,-1803)^{HxL*}

† The management zone comparison is indicated by superscript letters and the null hypothesis of equal sample means was rejected at $\alpha \leq 0.05$ and is indicated with an asterisk (*). Two treatment means are declared unequal when the interval does not cover 0.

Table 5.17 The ANOVA and Tukey's HSD test on 30 randomly selected corn grain yields from each production management zone (MZ) delineated by the RCMZ technique for the 0, 50, and 100% recommended N treatments on Field 2.

0%	Source	df	SS	MS	*F*	*p*-value
	MZ	2	5.38E+07	2.69E+07	17.15	<0.001
	Error	87	1.37E+08	1.57E+06		
	Total	89	1.90E+08			

MZ	Average	Tukey Intervals
	--kg ha^{-1}--	
Low†	9760	(-133,1408)^{LxM}
Medium	9123	(1093,2634)^{MxH*}
High	10986	(455,1997)^{HxL*}

50%	Source	df	SS	MS	*F*	*p*-value
	MZ	2	1.65E+08	8.24E+07	26.44	<0.001
	Error	87	2.71E+08	3.12E+06		
	Total	89	4.36E+08			

MZ	Average	Tukey Intervals
	--kg ha^{-1}--	
Low	8730	(-4381,-2208)^{LxM*}
Medium	12024	(-3055,-882)^{MxH*}
High	10055	(239,2412)^{HxL*}

100%	Source	df	SS	MS	*F*	*p*-value
	MZ	2	3.82E+07	1.91E+07	10.89	<0.001
	Error	87	1.52E+08	1.75E+06		
	Total	89	1.91E+08			

MZ	Average	Tukey Intervals
	--kg ha^{-1}--	
Low	9327	(-2134,-505)^{LxM*}
Medium	10646	(-697,932)^{MxH}
High	10763	(622,2251)^{HxL*}

† The management zone comparison is indicated by superscript letters and the null hypothesis of equal sample means was rejected at $\alpha \leq 0.05$ and is indicated with an asterisk (*). Two treatment means are declared unequal when the interval does not cover 0.

Table 5.18 The ANOVA and Tukey's HSD test on 30 randomly selected corn grain yields from each production management zone (MZ) delineated by the EC_aMZ technique for the 0, 50, and 100% recommended N treatments on Field 3.

0%	Source	df	SS	MS	*F*	*p*-value
	MZ	2	3.93E+08	1.97E+08	166.85	<0.001
	Error	87	1.03E+08	1.18E+06		
	Total	89	4.96E+08			

MZ	Average	Tukey Intervals
	--kg ha^{-1}--	
Low†	6943	$(-2656,-1320)^{LxM*}$
Medium	8931	$(2425,3761)^{MxH*}$
High	12024	$(4413,5750)^{HxL*}$

50%	Source	df	SS	MS	*F*	*p*-value
	MZ	2	1.41E+07	7.04E+06	4.01	0.022
	Error	87	1.53E+08	7.04E+06		
	Total	89	1.67E+08			

MZ	Average	Tukey Intervals
	--kg ha^{-1}--	
Low	10578	$(-1741,-110)^{LxM*}$
Medium	11504	$(-1526,105)^{MxH}$
High	10793	$(-600,1030)^{HxL*}$

100%	Source	df	SS	MS	*F*	*p*-value
	MZ	2	2.81E+07	1.41E+07	11.06	<0.001
	Error	87	1.11E+08	1.27E+06		
	Total	89	1.39E+08			

MZ	Average	Tukey Intervals
	--kg ha^{-1}--	
Low	11957	$(-1566,-178)^{LxM*}$
Medium	12829	$(-215,1172)^{MxH}$
High	13307	$(657,2045)^{HxL*}$

† The management zone comparison is indicated by superscript letters and the null hypothesis of equal sample means was rejected at $\alpha \leq 0.05$ and is indicated with an asterisk (*). Two treatment means are declared unequal when the interval does not cover 0.

Table 5.19 The ANOVA and Tukey's HSD test on 30 randomly selected corn grain yields from each production management zone (MZ) delineated by the SCMZ technique for the 0, 50, and 100% recommended N treatments on Field 3.

0%	Source	df	SS	MS	*F*	*p*-value
	MZ	2	6.13E+07	3.06E+07	25.5	<0.001
	Error	87	1.05E+08	1.20E+06		
	Total	89	1.66E+08			

MZ	Average	Tukey Intervals
	--kg ha^{-1}--	
Low†	6773	(-2022,-673)^{LxM*}
Medium	8120	(-43,1306)^{MxH}
High	8751	(1304,2653)^{HxL*}

50%	Source	df	SS	MS	*F*	*p*-value
	MZ	2	1.02E+08	5.11E+07	47.8	<0.001
	Error	87	9.30E+07	1.07E+06		
	Total	89	1.95E+08			

MZ	Average	Tukey Intervals
	--kg ha^{-1}--	
Low	9877	(-1965,-693)^{LxM*}
Medium	11206	(644,1916)^{MxH*}
High	12486	(1973,3245)^{HxL*}

100%	Source	df	SS	MS	*F*	*p*-value
	MZ	2	6.20E+07	3.10E+07	21.09	<0.001
	Error	87	1.28E+08	1.47E+06		
	Total	89	1.90E+08			

MZ	Average	Tukey Intervals
	--kg ha^{-1}--	
Low	11414	(-2058,-566)^{LxM*}
Medium	12727	(-57,1435)^{MxH}
High	13416	(1255,2748)^{HxL*}

† The management zone comparison is indicated by superscript letters and the null hypothesis of equal sample means was rejected at $\alpha \leq 0.05$ and is indicated with an asterisk (*). Two treatment means are declared unequal when the interval does not cover 0.

Table 5.20 The ANOVA and Tukey's HSD test on 30 randomly selected corn grain yields from each production management zone (MZ) delineated by the YBMZ technique for the 0, 50, and 100% recommended N treatments on Field 3.

0%	Source	df	SS	MS	*F*	*p*-value
	MZ	2	7.14E+07	3.57E+07	33.89	<0.001
	Error	87	9.17E+07	1.05E+06		
	Total	89	1.63E+08			

MZ	Average	Tukey Intervals
	--kg ha^{-1}--	
Low†	7690	$(-153,1110)^{LxM}$
Medium	7212	$(1451,2715)^{MxH*}$
High	9295	$(973,2236)^{HxL*}$

50%	Source	df	SS	MS	*F*	*p*-value
	MZ	2	5.92E+07	2.96E+07	24.25	<0.001
	Error	87	1.06E+08	1.22E+06		
	Total	89	1.65E+08			

MZ	Average	Tukey Intervals
	--kg ha^{-1}--	
Low	11752	$(742,2102)^{LxM*}$
Medium	10330	$(1233,2593)^{MxH*}$
High	12243	$(-189,1171)^{HxL}$

100%	Source	df	SS	MS	*F*	*p*-value
	MZ	2	2.12E+07	1.06E+07	5.37	0.006
	Error	87	1.72E+08	1.97E+06		
	Total	89	1.93E+08			

MZ	Average	Tukey Intervals
	--kg ha^{-1}--	
Low	11818	$(-1819,-90)^{LxM*}$
Medium	12772	$(-728,1001)^{MxH}$
High	12909	$(226,1956)^{HxL*}$

† The management zone comparison is indicated by superscript letters and the null hypothesis of equal sample means was rejected at $\alpha \leq 0.05$ and is indicated with an asterisk (*). Two treatment means are declared unequal when the interval does not cover 0.

Table 5.21 The ANOVA and Tukey's HSD test on 30 randomly selected corn grain yields from each production management zone (MZ) delineated by the RCMZ technique for the 0, 50, and 100% recommended N treatments on Field 3.

0%	Source	df	SS	MS	*F*	*p*-value
	MZ	2	4.83E+07	2.42E+07	12.12	<0.001
	Error	87	1.73E+08	2.42E+07		
	Total	89	2.22E+08			

MZ	Average	Tukey Intervals
	--kg ha^{-1}--	
Low†	7801	$(-1673,65)^{LxM}$
Medium	8605	$(119,1857)^{MxH*}$
High	9593	$(923,2661)^{HxL*}$

50%	Source	df	SS	MS	*F*	*p*-value
	MZ	2	4.45E+07	2.22E+07	11.97	<0.001
	Error	87	1.62E+08	1.86E+06		
	Total	89	2.06E+08			

MZ	Average	Tukey Intervals
	--kg ha^{-1}--	
Low	10518	$(-2381,-704)^{LxM*}$
Medium	12061	$(-948,729)^{MxH}$
High	11951	$(595,2272)^{HxL*}$

100%	Source	df	SS	MS	*F*	*p*-value
	MZ	2	5.60E+07	2.80E+07	17.72	<0.001
	Error	87	1.38E+08	1.58E+06		
	Total	89	1.94E+08			

MZ	Average	Tukey Intervals
	--kg ha^{-1}--	
Low	11236	$(-1995,-408)^{LxM*}$
Medium	12418	$(-40,1507)^{MxH}$
High	13151	$(1141,2689)^{HxL*}$

† The management zone comparison is indicated by superscript letters and the null hypothesis of equal sample means was rejected at $\alpha \leq 0.05$ and is indicated with an asterisk (*). Two treatment means are declared unequal when the interval does not cover 0.

Table 5.22 Summary of *p*-values for *S*-statistic analysis. Values are partitioned by field, percent of recommended N applied, and MZ delineation technique. A minimum of two MZ per treatment is required for *S*-statistic analysis. Treatments with only one MZ are presented as not available (na).

	N applied	SCMZ†	EC_aMZ‡	YBMZ§	RCMZ¶
	---%---				
Field 1	0	na	0.010	<0.001	0.260
	50	na	<0.001	na	0.143
	100	na	<0.001	<0.001	0.142
Field 2	0	<0.001	<0.001	<0.001	<0.001
	50	<0.001	0.221	<0.001	<0.001
	100	<0.001	0.107	<0.001	<0.001
Field 3	0	<0.001	<0.001	<0.001	<0.001
	50	<0.001	0.024	<0.001	<0.001
	100	<0.001	0.002	0.001	<0.001

† Soil color management zone delineation technique.

‡ Apparent electrical conductivity management zone delineation technique.

§ Yield based management zone delineation technque.

¶ Remotely sensed data and cluster sampling management zone delineation technique.

Table 5.23 The agreement between yield classification (high, medium, or low) using the cluster approach for 3 fertilizer treatments and four production management zone delineation techniques for Field 1 as evaluated with the Chi-square goodness-of-fit test. Values are percent.

		Delineation technique											
		SCMZ†			EC_aMZ‡			YBMZ§			RCMZ¶		
		Management Zone											
N treatment	Yield	Low	Medium	High	Low	Medium	High	Low	Medium	High	Low	Medium	High
0% N	Low	10	0	50	5	38	5	13	4	na	3	16	na
	Medium	50	100	25	58	35	30	47	56	na	80	27	na
	High	40	0	25	36	27	65	40	40	na	17	57	na
	Overall#	**11****			**21****			**26****			**17****		
50% N	Low	7	na	na	7	6	0	6	33	na	3	9	na
	Medium	28	na	na	14	75	65	27	33	na	17	34	na
	High	66	na	na	79	19	35	67	33	na	79	57	na
	Overall	**7^{ns}**			**21****			**7****			**22****		
100% N	Low	5	0	4	7	6	0	11	1	0	1	9	na
	Medium	19	31	29	15	42	4	21	18	33	21	20	na
	High	75	69	68	78	52	96	68	81	67	79	71	na
	Overall	**9^{ns}**			**37****			**17****			**10****		

† Soil color management zone delineation technique.

‡ Apparent electrical conductivity management zone delineation technique.

§ Yield based management zone delineation technque.

¶ Remotely sensed data and cluster sampling management zone delineation technique.

Overall accuracy values with ** indicate p-value <0.05; ns=not significant. Treatments without observed samples are denoted not available (na).

Table 5.24 The agreement between yield classification (high, medium, or low) using the non-parametric approach for 3 fertilizer treatments and four production management zone delineation techniques for Field 1 as evaluated with the Chi-square goodness-of-fit test. Values are percent.

		Delineation technique											
		SCMZ†			EC_aMZ‡			YBMZ§			RCMZ¶		
		Management Zone											
N treatment	Yield	Low	Medium	High	Low	Medium	High	Low	Medium	High	Low	Medium	High
0% N	Low	33	20	50	33	50	23	41	15	na	40	28	na
	Medium	32	80	25	37	28	15	24	51	na	47	20	na
	High	35	0	25	30	22	62	35	34	na	13	51	na
	Overall#	**34^{ns}**			**37****			**44****			**29****		
50% N	Low	33	na	na	20	79	61	32	67	na	18	41	na
	Medium	33	na	na	36	17	39	33	33	na	54	20	na
	High	34	na	na	44	4	0	35	0	na	27	39	na
	Overall	**33^{ns}**	**ns**		**18****			**32****			**19****		
100% N	Low	32	48	43	29	55	13	39	26	48	29	36	na
	Medium	32	41	25	28	27	49	34	30	41	31	34	na
	High	36	10	32	43	18	38	27	44	11	40	30	na
	Overall	**32^{ns}**			**30****			**34****			**31****		

† Soil color management zone delineation technique.

‡ Apparent electrical conductivity management zone delineation technique.

§ Yield based management zone delineation technque.

¶ Remotely sensed data and cluster sampling management zone delineation technique.

Overall accuracy values with ** indicate p-value <0.05; ns=not significant. Treatments without observed samples are denoted not available (na).

Table 5.25 The agreement between yield classification (high, medium, or low) using the subjective approach for 3 fertilizer treatments and four production management zone delineation techniques for Field 1 as evaluated with the Chi-square goodness-of-fit test. Values are percent.

		Delineation technique											
		SCMZ†			EC_aMZ‡			YBMZ§			RCMZ¶		
		Management Zone											
N treatment	Yield	Low	Medium	High	Low	Medium	High	Low	Medium	High	Low	Medium	High
0% N	Low	12	0	50	7	40	6	15	4	na	4	17	na
	Medium	46	80	25	55	27	30	43	53	na	76	23	na
	High	43	20	25	38	33	64	42	43	na	20	59	na
	Overall#	**12^{ns}**			**20****			**26****			**15****		
50% N	Low	9	na	na	8	15	0	8	33	na	5	12	na
	Medium	45	na	na	34	79	100	45	61	na	51	42	na
	High	46	na	na	58	6	0	47	6	na	44	46	na
	Overall	**9^{ns}**			**21****			**10****			**28****		
100% N	Low	8	0	7	8	14	0	17	1	0	1	14	na
	Medium	50	90	57	43	66	55	51	50	89	53	51	na
	High	41	10	36	49	20	45	32	49	11	46	35	na
	Overall	**12****			**33****			**34****			**27****		

† Soil color management zone delineation technique.

‡ Apparent electrical conductivity management zone delineation technique.

§ Yield based management zone delineation technque.

¶ Remotely sensed data and cluster sampling management zone delineation technique.

Overall accuracy values with ** indicate p-value <0.05; ns=not significant. Treatments without observed samples are denoted not available (na).

Table 5.26 The agreement between yield classification (high, medium, or low) using the cluster approach for 3 fertilizer treatments and four production management zone delineation techniques for Field 2 as evaluated with the Chi-square goodness-of-fit test. Values are percent.

		Delineation technique											
		SCMZ†			EC_aMZ‡			YBMZ§			RCMZ¶		
		Management Zone											
N treatment	Yield	Low	Medium	High	Low	Medium	High	Low	Medium	High	Low	Medium	High
0% N	Low	45	30	2	34	2	0	18	2	39	41	28	2
	Medium	54	45	35	48	30	62	44	33	49	32	58	32
	High	1	25	63	19	68	38	38	65	12	27	15	65
	Overall#	**50****			**33****			**18****			**54****		
50% N	Low	0	24	31	21	13	na	14	19	22	28	3	9
	Medium	24	43	50	40	46	na	53	79	34	39	20	62
	High	76	33	19	39	40	na	33	2	44	33	77	29
	Overall	**28****			**24**^{ns}			**42****			**27****		
100% N	Low	na	15	32	27	1	na	10	1	31	33	10	11
	Medium	na	39	50	42	57	na	12	70	49	44	33	57
	High	na	45	18	30	42	na	78	29	20	24	57	32
	Overall	**29****			**32****			**24****			**33****		

† Soil color management zone delineation technique.

‡ Apparent electrical conductivity management zone delineation technique.

§ Yield based management zone delineation technque.

¶ Remotely sensed data and cluster sampling management zone delineation technique.

Overall accuracy values with ** indicate p-value <0.05; ns=not significant. Treatments without observed samples are denoted not available (na).

Table 5.27 The agreement between yield classification (high, medium, or low) using the non-parametric approach for 3 fertilizer treatments and four production management zone delineation techniques for Field 2 as evaluated with the Chi-square goodness-of-fit test. Values are percent.

		Delineation technique											
		SCMZ†			EC_aMZ‡			YBMZ§			RCMZ¶		
		Management Zone											
N treatment	Yield	Low	Medium	High	Low	Medium	High	Low	Medium	High	Low	Medium	High
0% N	Low	56	36	4	32	31	8	22	3	48	45	38	3
	Medium	39	36	21	31	63	31	39	20	37	27	44	20
	High	4	27	75	37	6	62	39	77	15	28	18	77
	Overall#	**50****			**37****			**18****			**52****		
50% N	Low	0	42	43	32	38	na	26	33	35	43	11	16
	Medium	27	31	42	34	21	na	49	64	26	30	11	62
	High	73	27	15	33	40	na	25	2	39	27	77	21
	Overall	**20****			**31**^{ns}			**39****			**34****		
100% N	Low	na	25	43	39	4	na	11	5	46	44	25	15
	Medium	na	27	37	29	47	na	11	58	33	31	18	48
	High	na	48	20	32	48	na	78	36	21	25	58	37
	Overall	**23****			**41****			**24****			**38****		

† Soil color management zone delineation technique.

‡ Apparent electrical conductivity management zone delineation technique.

§ Yield based management zone delineation technque.

¶ Remotely sensed data and cluster sampling management zone delineation technique.

Overall accuracy values with ** indicate p-value <0.05; ns=not significant. Treatments without observed samples are denoted not available (na).

Table 5.28 The agreement between yield classification (high, medium, or low) using the subjective approach for 3 fertilizer treatments and four production management zone delineation techniques for Field 2 as evaluated with the Chi-square goodness-of-fit test. Values are percent.

		Delineation technique											
		SCMZ†			EC_aMZ‡			YBMZ§			RCMZ¶		
		Management Zone											
N treatment	Yield	Low	Medium	High	Low	Medium	High	Low	Medium	High	Low	Medium	High
0% N	Low	15	14	1	15	1	0	4	1	18	23	9	1
	Medium	77	55	21	61	18	38	52	20	64	47	69	19
	High	8	31	78	25	81	62	44	79	18	30	22	80
	Overall#	**54****			**16****			**16****			**57****		
50% N	Low	0	22	30	20	13	na	11	17	21	27	0	8
	Medium	21	41	44	36	46	na	44	71	32	37	23	50
	High	79	36	27	44	40	na	44	12	47	36	77	42
	Overall	**29****			**22**^{ns}			**43****			**29****		
100% N	Low	na	10	20	17	0	na	4	0	20	21	6	4
	Medium	na	33	51	42	39	na	13	47	49	45	28	45
	High	na	57	29	41	61	na	83	53	31	34	66	51
	Overall	**31****			**20****			**28****			**29****		

† Soil color management zone delineation technique.

‡ Apparent electrical conductivity management zone delineation technique.

§ Yield based management zone delineation technque.

¶ Remotely sensed data and cluster sampling management zone delineation technique.

Overall accuracy values with ** indicate p-value <0.05; ns=not significant. Treatments without observed samples are denoted not available (na).

Table 5.29 The agreement between yield classification (high, medium, or low) using the cluster approach for 3 fertilizer treatments and four production management zone delineation techniques for Field 3 as evaluated with the Chi-square goodness-of-fit test. Values are percent.

		Delineation technique											
		SCMZ†			EC_aMZ‡			YBMZ§			RCMZ¶		
		Management Zone											
N treatment	Yield	Low	Medium	High	Low	Medium	High	Low	Medium	High	Low	Medium	High
0% N	Low	27	45	73	61	36	40	38	66	33	56	33	30
	Medium	62	47	27	35	54	46	54	30	56	37	58	57
	High	11	9	1	4	10	14	7	3	11	7	10	13
	Overall#	**34****			**54****			**21****			**48****		
50% N	Low	24	34	62	46	31	na	37	52	28	43	30	27
	Medium	58	54	31	44	56	na	49	38	59	48	55	57
	High	18	12	8	10	14	na	15	10	13	10	15	16
	Overall	**40****			**53****			**23****			**39****		
100% N	Low	9	20	33	25	19	6	31	13	13	35	20	13
	Medium	52	51	51	55	49	53	52	49	51	47	55	49
	High	39	29	16	20	32	41	16	38	36	18	25	38
	Overall	**28****			**40****			**35****			**44****		

† Soil color management zone delineation technique.

‡ Apparent electrical conductivity management zone delineation technique.

§ Yield based management zone delineation technque.

¶ Remotely sensed data and cluster sampling management zone delineation technique.

Overall accuracy values with ** indicate p-value <0.05; ns=not significant. Treatments without observed samples are denoted not available (na).

Table 5.30 The agreement between yield classification (high, medium, or low) using the non-parametric approach for 3 fertilizer treatments and four production management zone delineation techniques for Field 3 as evaluated with the Chi-square goodness-of-fit test. Values are percent.

		Delineation technique											
		SCMZ†			EC_aMZ‡			YBMZ§			RCMZ¶		
		Management Zone											
N treatment	Yield	Low	Medium	High	Low	Medium	High	Low	Medium	High	Low	Medium	High
0% N	Low	20	37	67	56	28	34	31	57	26	49	26	23
	Medium	29	37	26	25	34	26	36	27	33	35	30	35
	High	51	26	7	20	37	40	34	16	41	16	44	42
	Overall#	**27****			**38****			**36****			**39****		
50% N	Low	22	32	61	44	29	na	35	51	26	41	28	25
	Medium	35	35	24	32	34	na	36	28	34	34	34	32
	High	43	33	15	24	37	na	29	21	40	25	38	43
	Overall	**29****			**37****			**36****			**40****		
100% N	Low	18	33	50	43	30	15	48	36	23	46	37	22
	Medium	38	34	30	34	33	40	32	24	36	33	34	35
	High	44	33	20	23	37	45	20	40	41	21	29	43
	Overall	**25****			**38****			**43****			**40****		

† Soil color management zone delineation technique.

‡ Apparent electrical conductivity management zone delineation technique.

§ Yield based management zone delineation technque.

¶ Remotely sensed data and cluster sampling management zone delineation technique.

Overall accuracy values with ** indicate p-value <0.05; ns=not significant. Treatments without observed samples are denoted not available (na).

Table 5.31 The agreement between yield classification (high, medium, or low) using the subjective approach for 3 fertilizer treatments and four production management zone delineation techniques for Field 3 as evaluated with the Chi-square goodness-of-fit test. Values are percent.

		Delineation technique											
		SCMZ†			EC_aMZ‡			YBMZ§			RCMZ¶		
		Management Zone											
N treatment	Yield	Low	Medium	High	Low	Medium	High	Low	Medium	High	Low	Medium	High
0% N	Low	5	15	36	27	10	11	10	29	9	22	8	9
	Medium	36	52	54	47	45	46	50	52	42	57	40	38
	High	59	33	10	26	45	43	40	19	49	21	52	53
	Overall#	**29****			**42****			**41****			**36****		
50% N	Low	7	10	34	19	10	na	10	26	8	16	11	8
	Medium	40	49	43	50	44	na	53	44	44	52	42	39
	High	54	41	23	31	47	na	37	30	48	33	47	53
	Overall	**34****			**36****			**40****			**33****		
100% N	Low	4	10	19	11	11	4	17	2	7	17	9	9
	Medium	50	55	60	64	50	50	62	56	50	61	60	47
	High	46	35	21	25	39	46	21	42	43	22	31	44
	Overall	**29****			**37****			**34****			**46****		

† Soil color management zone delineation technique.

‡ Apparent electrical conductivity management zone delineation technique.

§ Yield based management zone delineation technque.

¶ Remotely sensed data and cluster sampling management zone delineation technique.

Overall accuracy values with ** indicate p-value <0.05; ns=not significant. Treatments without observed samples are denoted not available (na).

Table 5.32 The Kappa statistics (κ) of each field for the percent of recommended N applied, production management zone delineation technique, and yield classification technique.

		Delineation technique											
	N	SCMZ†			EC_aMZ‡			YBMZ§			RCMZ¶		
	applied	cl#	np	su	cl	np	su	cl	np	su	cl	np	su
	---%---												
Field 1	0	0.001	0.004	0.000	-0.012	0.056	-0.027	0.048	0.169	0.053	-0.241	-0.056	-0.238
	50	0.000	0.000	0.000	0.088	-0.217	0.039	-0.007	-0.015	-0.003	0.034	-0.202	-0.056
	100	0.005	-0.010	0.018	0.159	-0.041	0.069	0.019	0.014	0.030	-0.031	-0.016	-0.055
Field 2	0	0.198	0.249	0.225	0.042	0.051	-0.054	-0.215	-0.248	-0.315	0.292	0.276	0.331
	50	-0.127	-0.192	-0.097	0.017	-0.026	0.019	0.091	0.082	0.064	-0.002	0.012	0.035
	100	-0.155	-0.197	-0.197	0.072	-0.026	0.020	-0.116	-0.151	-0.163	0.050	0.063	0.045
Field 3	0	-0.145	-0.093	-0.050	0.124	0.083	0.035	-0.038	0.031	0.080	0.155	0.086	0.042
	50	-0.042	-0.071	-0.031	0.107	0.057	0.009	-0.035	0.038	0.044	0.081	0.094	0.049
	100	-0.108	-0.128	-0.083	0.030	0.067	-0.010	0.115	0.149	0.098	0.126	0.096	0.120

† Soil color management zone delineation technique.

‡ Apparent electrical conductivity management zone delineation technique.

§ Yield based management zone delineation technque.

¶ Remotely sensed data and cluster sampling management zone delineation technique.

Yield values were classified by cluster technique (cl), non-parametric technique (np), and subjective technique (su).

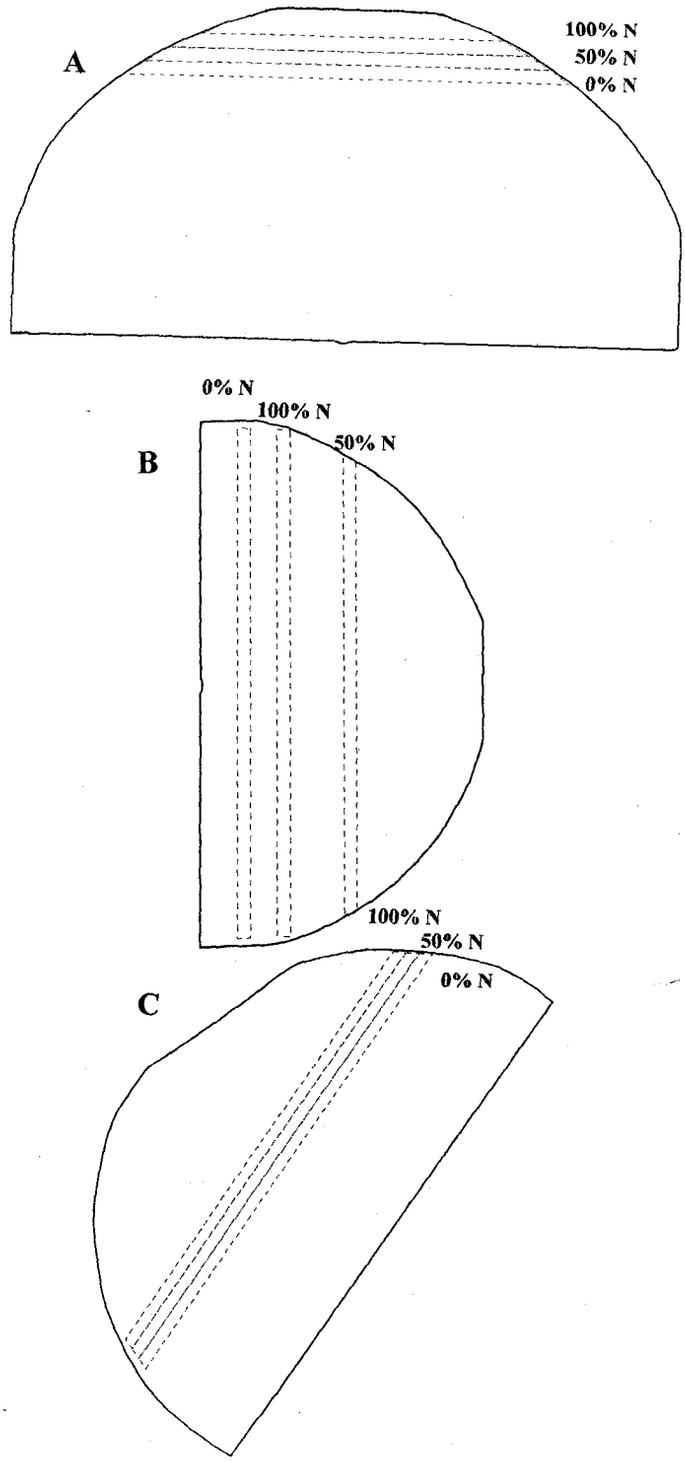

Figure 5.1 Strip-plot layout for Fields 1 (A), 2 (B) and 3 (C). The displayed N rates indicate percent of recommended N applied.

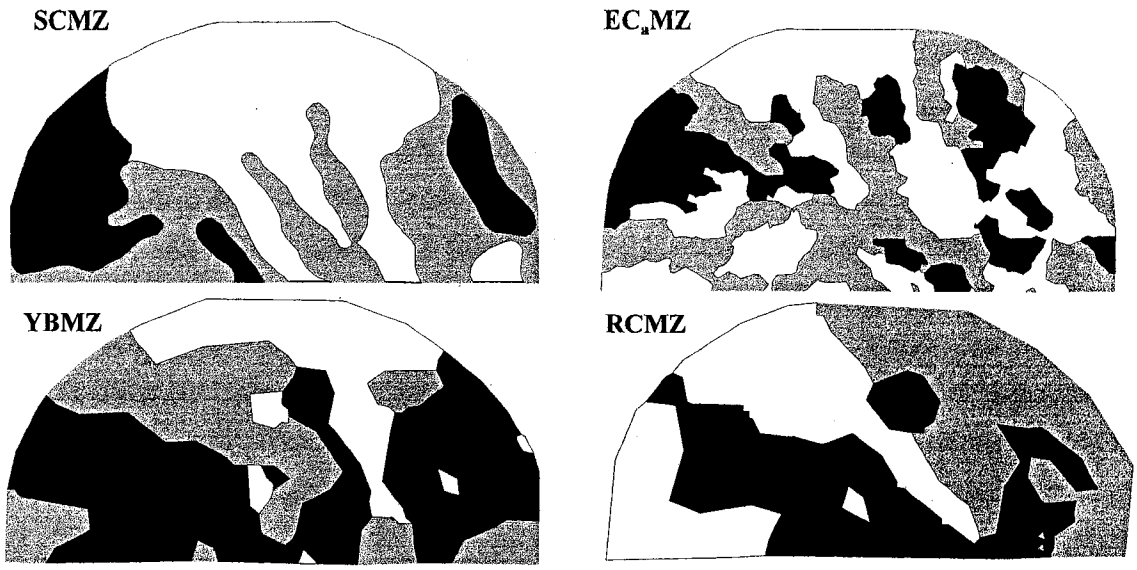

Figure 5.2 Management zone delineation on Field 1 for soil color management zone technique (SCMZ), apparent soil electrical conductivity technique (EC_aMZ), yield based management zone technique (YBMZ), and remotely sensed data and cluster sampling technique (RCMZ). Low productivity zone is white, Medium productivity zone is gray, and High productivity zone is black.

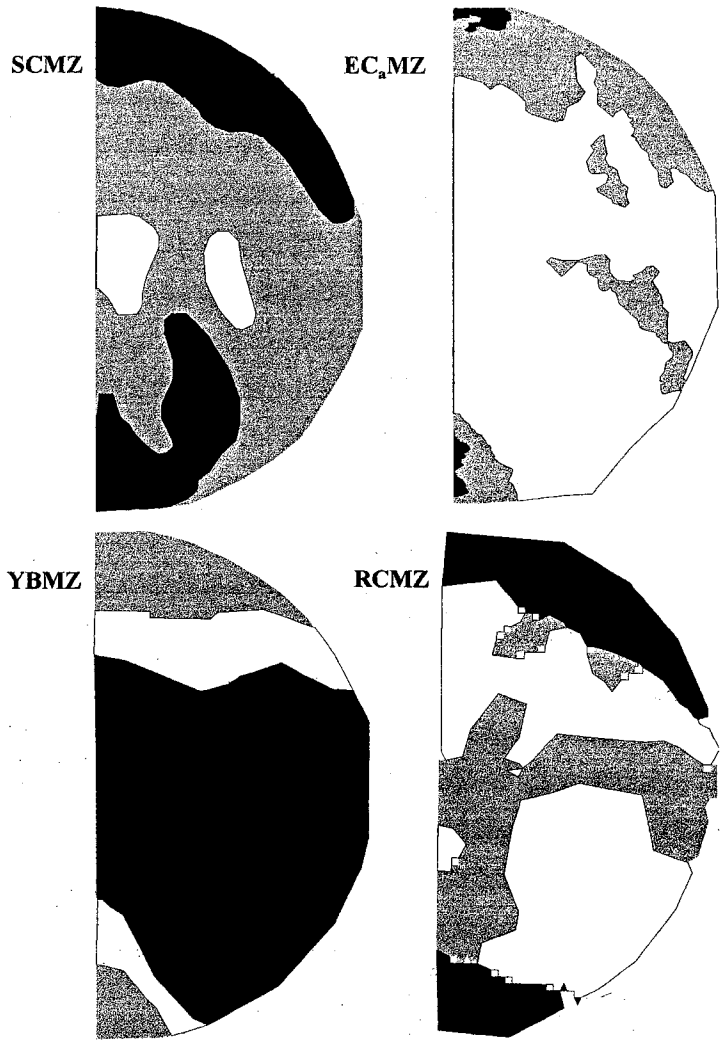

Figure 5.3 Management zone delineation on Field 2 for soil color management zone technique (SCMZ), apparent soil electrical conductivity technique (EC_aMZ), yield based management zone technique (YBMZ), and remotely sensed data and cluster sampling technique (RCMZ). Low productivity zone is white, medium productivity zone is gray, and High productivity zone is black.

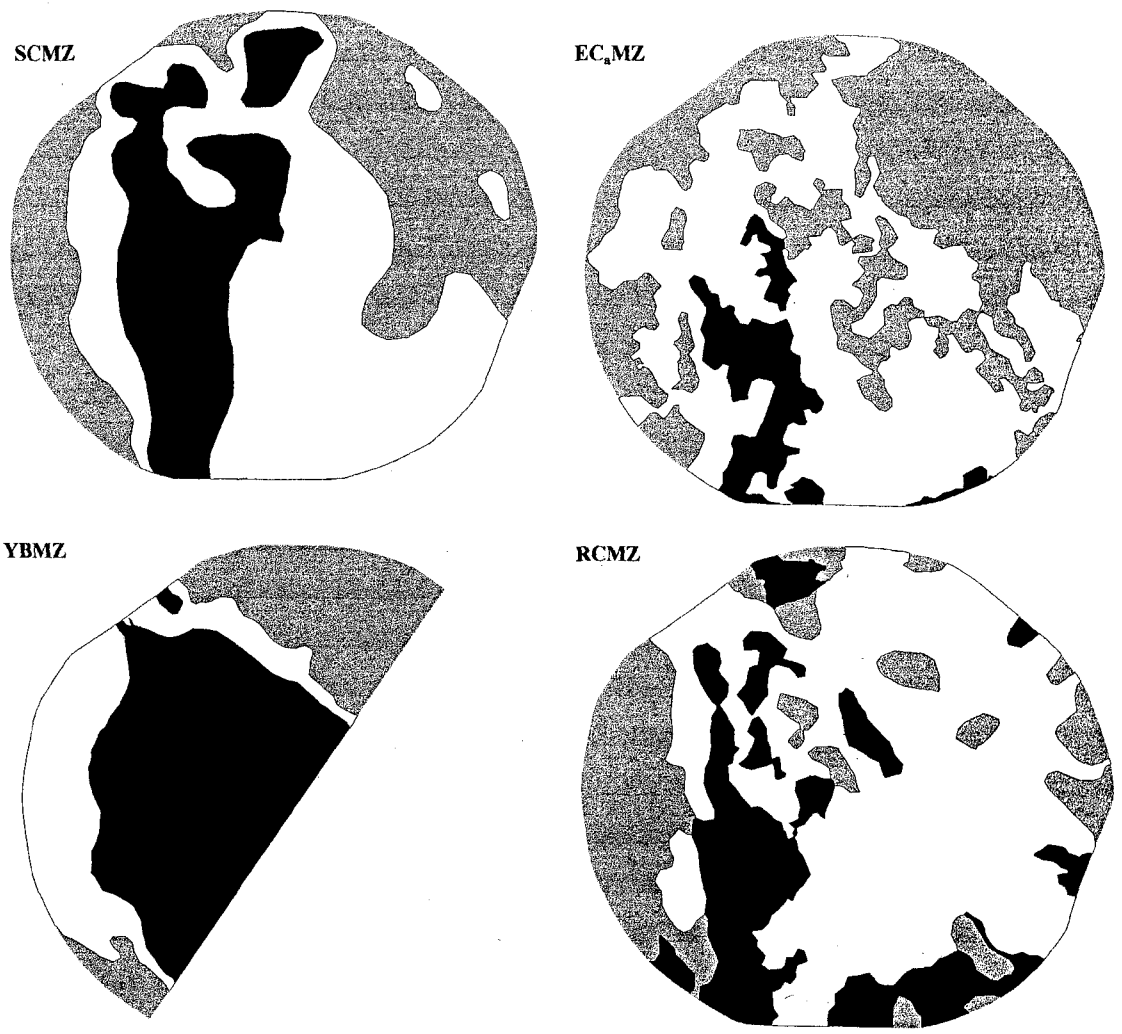

Figure 5.4 Management zone delineation on Field 3 for soil color management zone technique (SCMZ), apparent soil electrical conductivity technique (EC_aMZ), yield based management zone technique (YBMZ), and remotely sensed data and cluster sampling technique (RCMZ). Low productivity zone is white, medium productivity zone is gray, and High productivity zone is black.

APPENDIX A

Surface maps for interpolated soil properties.

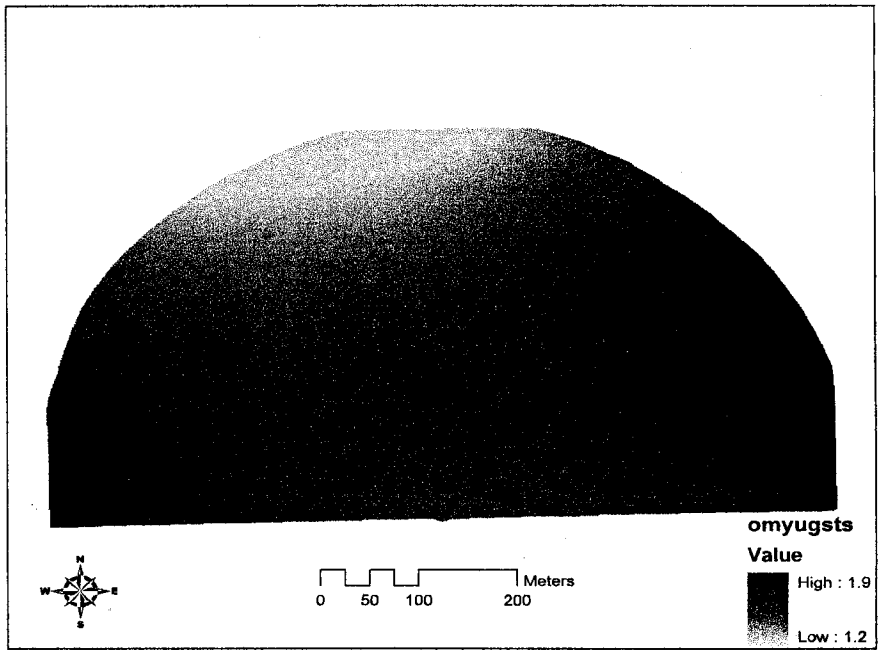

Figure A.1 Distribution of organic matter (OM; %) across Field 1. Soil samples were collected using a standard grid approach. Data were interpolated with a trend surface model.

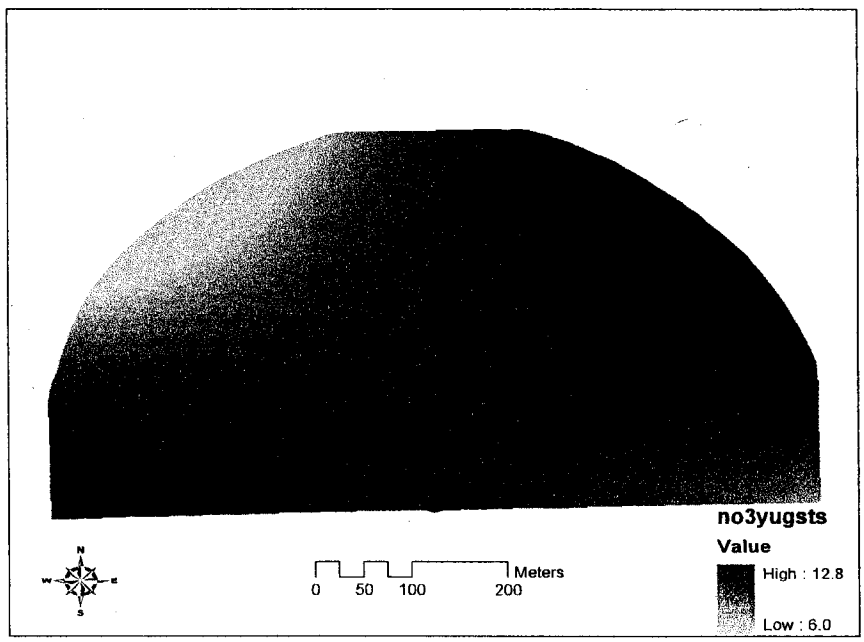

Figure A.2 Distribution of nitrate-N (NO_3-N; mg kg^{-1}) across Field 1. Soil samples were collected using a standard grid approach. Data were interpolated with a trend surface model.

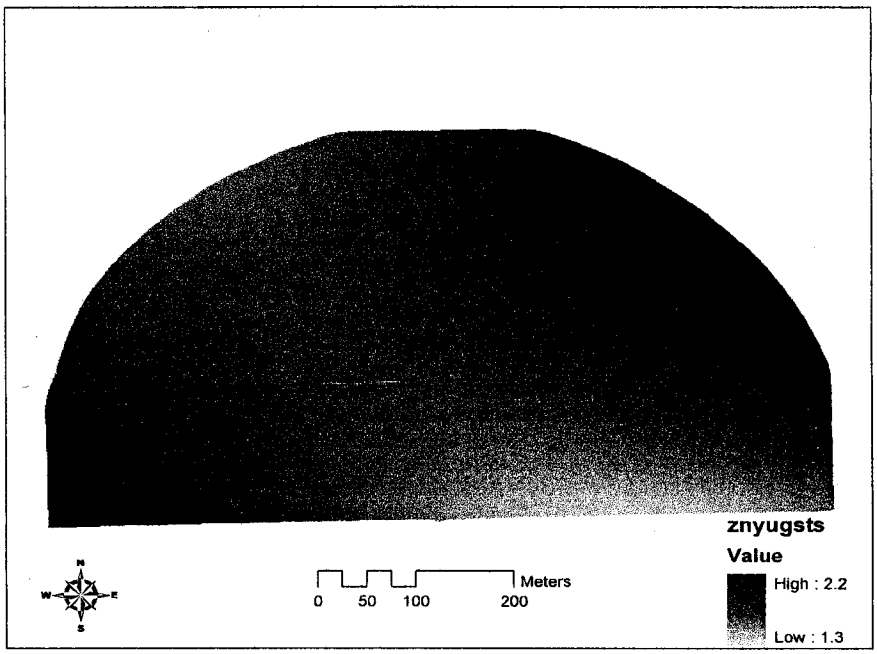

Figure A.3 Distribution of zinc (Zn; mg kg^{-1}) across Field 1. Soil samples were collected using a standard grid approach. Data were interpolated with a trend surface model.

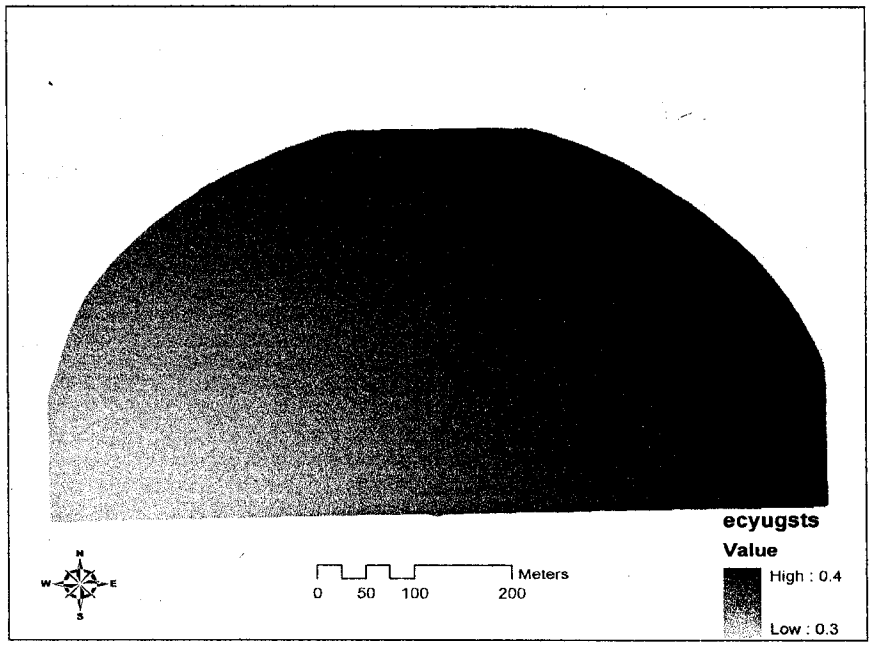

Figure A.4 Distribution of electrical conductivity (EC; mmhos cm^{-1}) across Field 1. Soil samples were collected using a standard grid approach. Data were interpolated with a trend surface model.

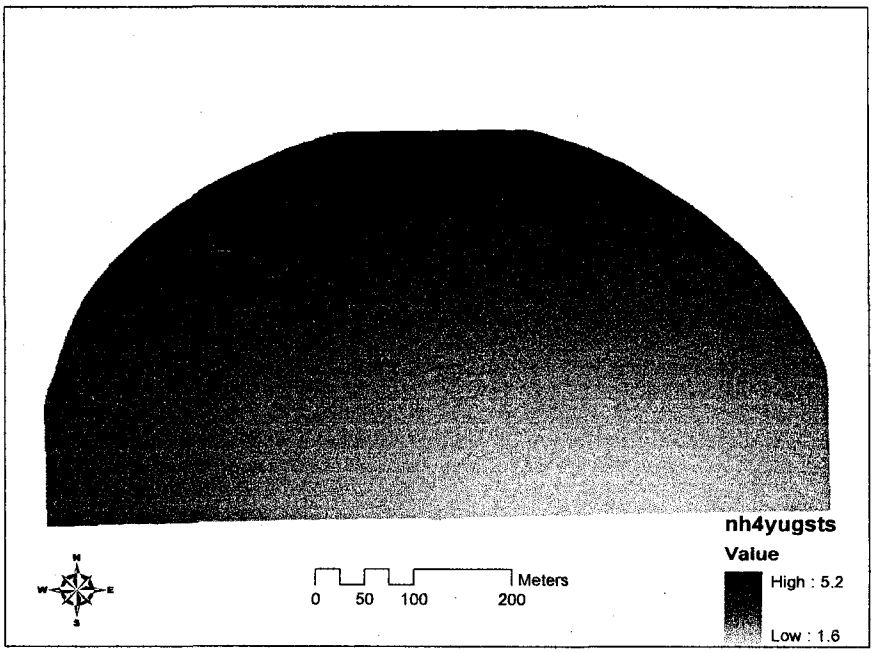

Figure A.5 Distribution of ammonium-N (NH_4-N; mg kg^{-1}) across Field 1. Soil samples were collected using a standard grid approach. Data were interpolated with a trend surface model.

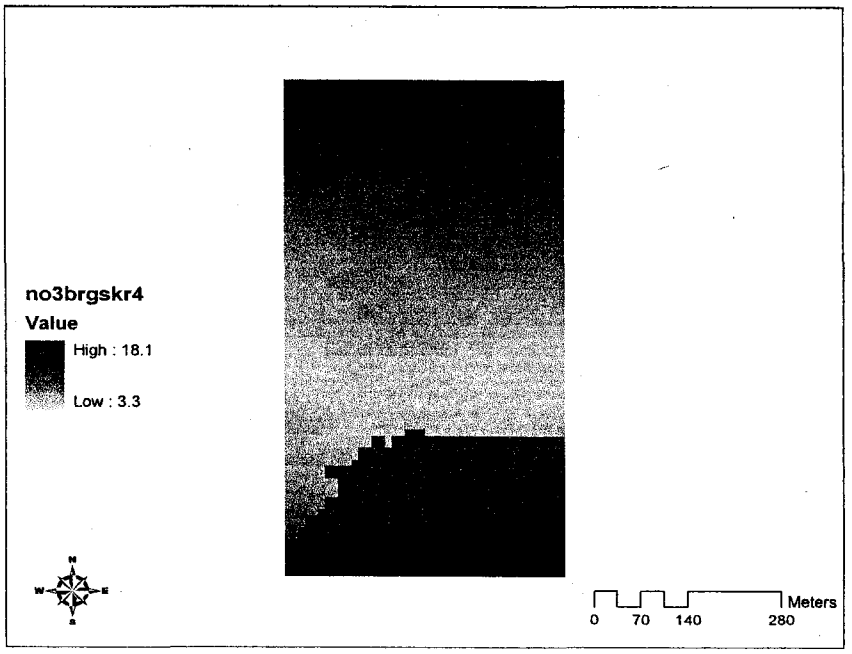

Figure A.6 Distribution of nitrate-N (NO_3-N; mg kg^{-1}) across Field 2. Soil samples were collected using a standard grid approach. Data were first interpolated with a trend surface model; residuals from the trend surface model were modeled using ordinary kriging. Final NO_3-N surface was calculated as the sum of trend surface and ordinary kriging surface.

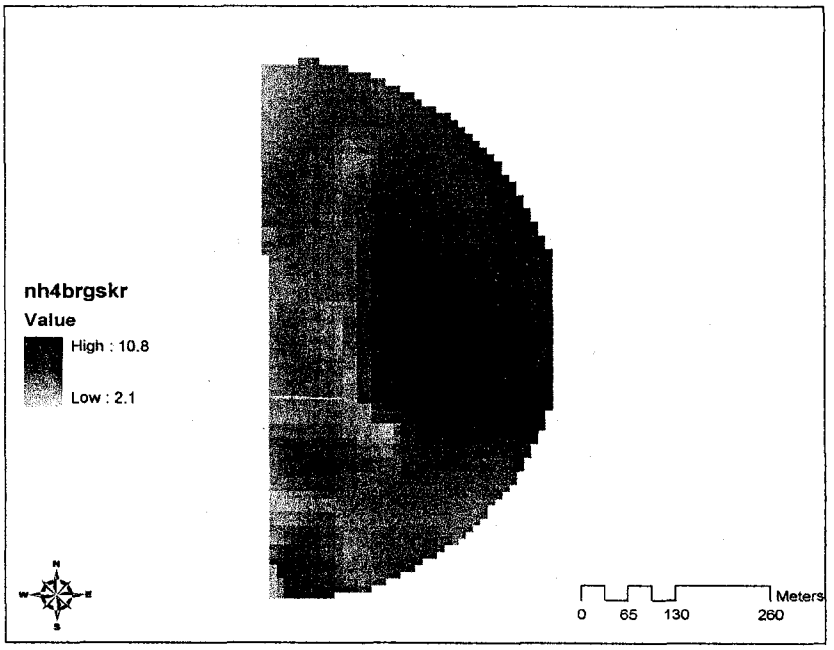

Figure A.7 Distribution of ammonium-N (NH_4-N; mg kg^{-1}) across Field 2. Soil samples were collected using a standard grid approach. Data were first interpolated with a trend surface model; residuals from the trend surface model were modeled using ordinary kriging. Final NH_4-N surface was calculated as the sum of trend surface and ordinary kriging surface.

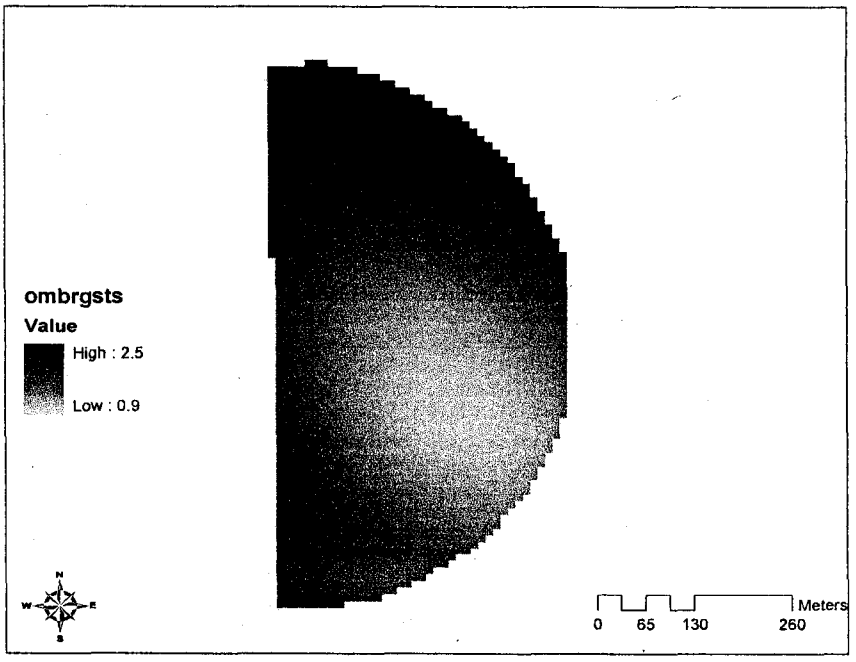

Figure A.8 Distribution of organic matter (OM; %) across Field 2. Soil samples were collected using a standard grid approach. Data were interpolated with a trend surface model.

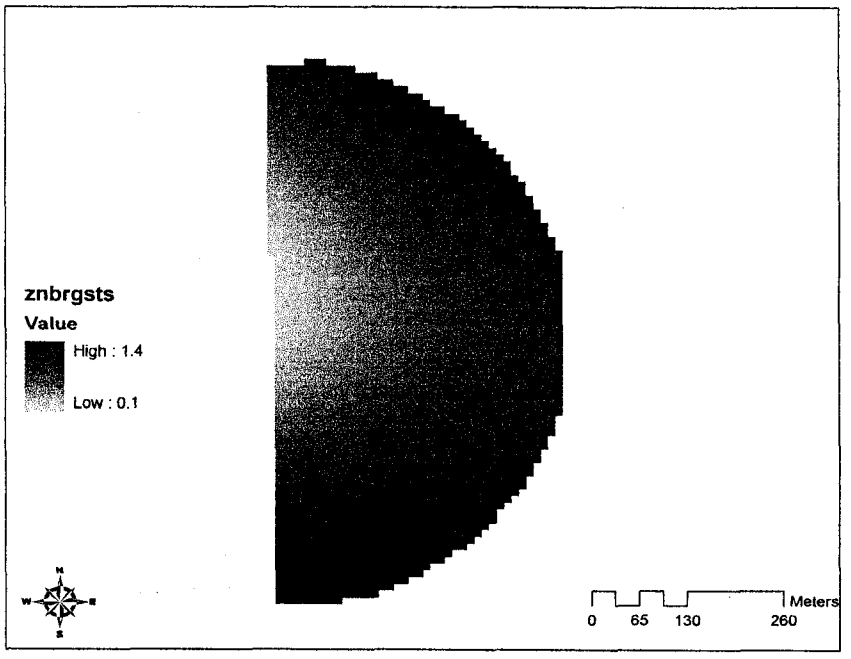

Figure A.9 Distribution of zinc (Zn; mg kg^{-1}) across Field 2. Soil samples were collected using a standard grid approach. Data were interpolated with a trend surface model.

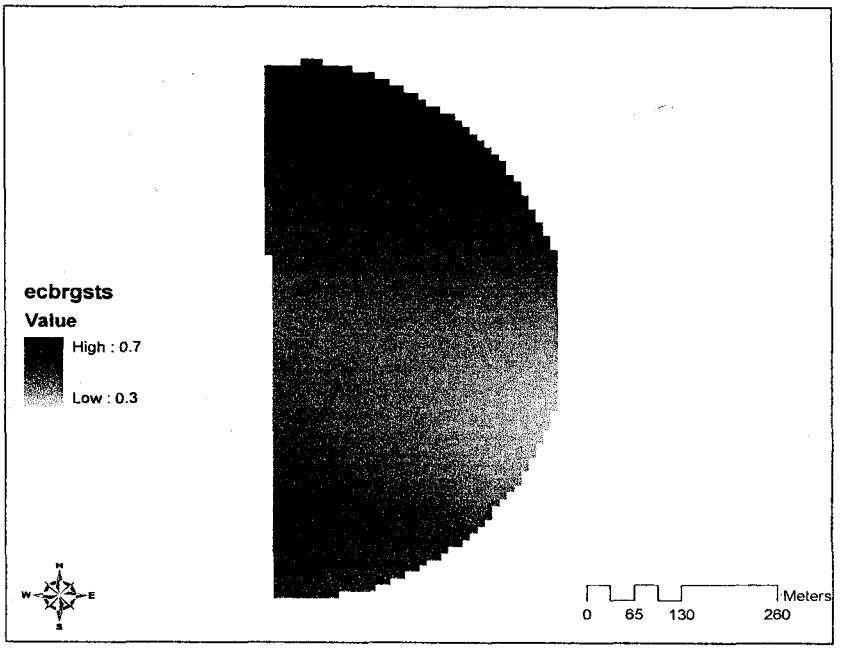

Figure A.10 Distribution of electrical conductivity (EC; mmhos cm^{-1}) across Field 2. Soil samples were collected using a standard grid approach. Data were interpolated with a trend surface model.

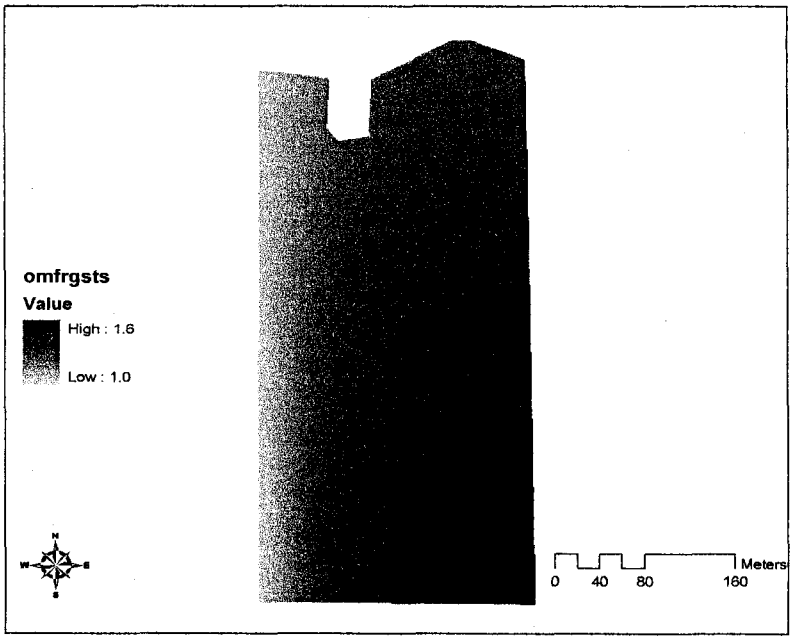

Figure A.11 Distribution of organic matter (OM; %) across Field 3. Soil samples were collected using a standard grid approach. Data were interpolated with a trend surface model.

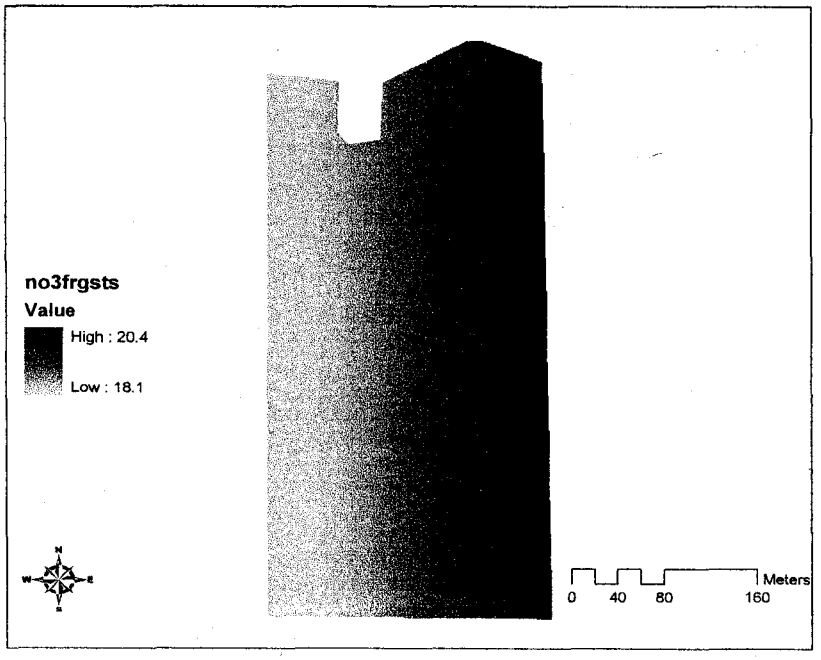

Figure A.12 Distribution of nitrate-N (NO_3-N; mg kg^{-1}) across Field 3. Soil samples were collected using a standard grid approach. Data were interpolated with a trend surface model.

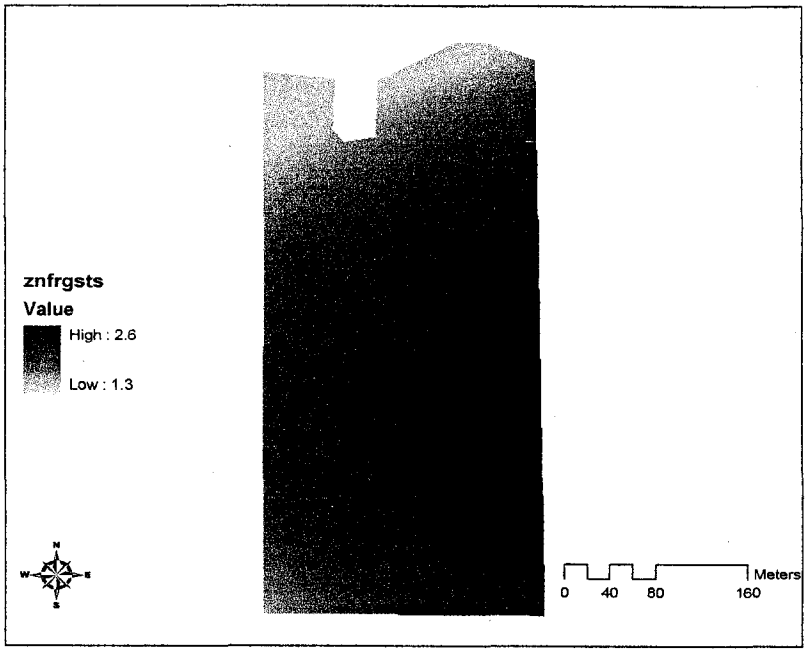

Figure A.13 Distribution of zinc (Zn; mg kg^{-1}) across Field 3. Soil samples were collected using a standard grid approach. Data were interpolated with a trend surface model.

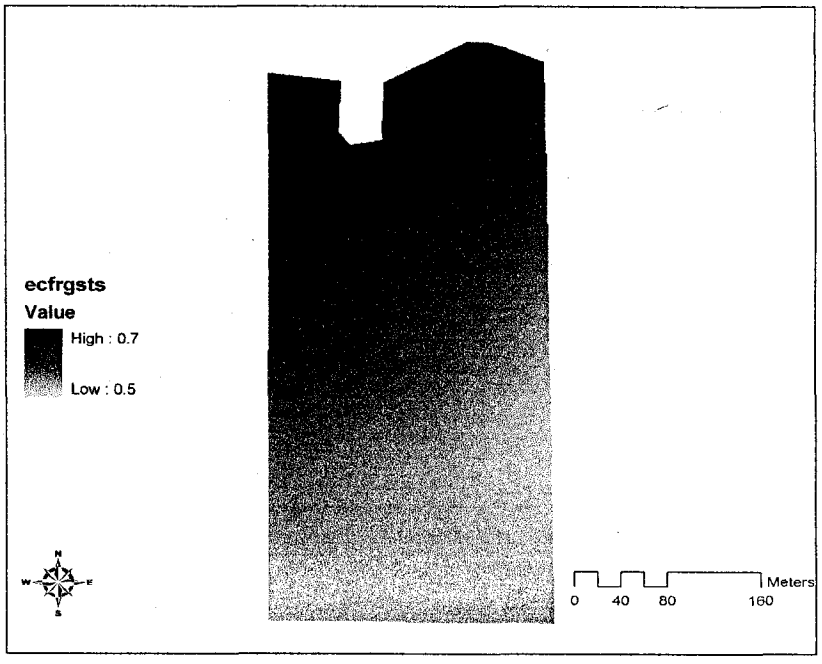

Figure A.14 Distribution of electrical conductivity (EC; mmhos cm^{-1}) across Field 3. Soil samples were collected using a standard grid approach. Data were interpolated with a trend surface model.

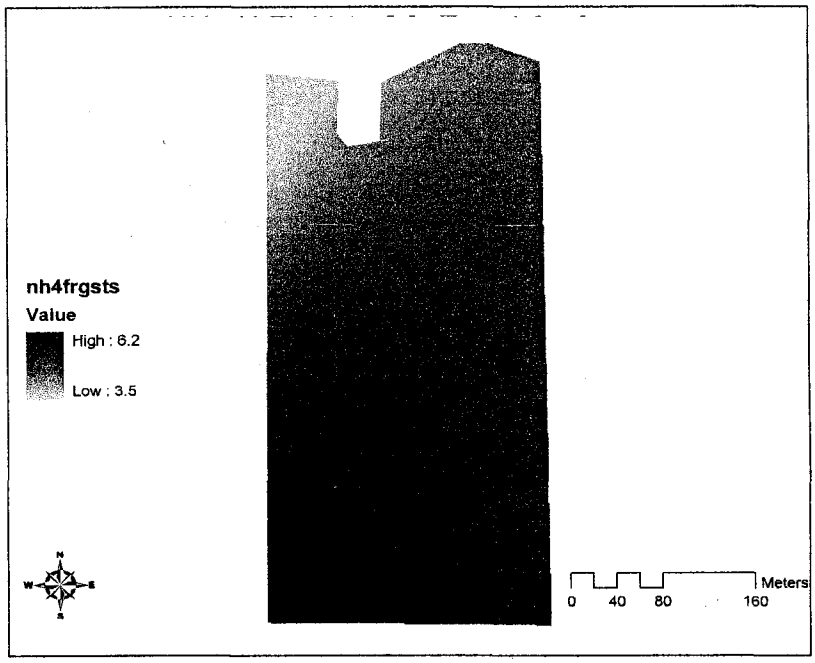

Figure A.15 Distribution of ammonium-N (NH_4-N; mg kg^{-1}) across Field 3. Soil samples were collected using a standard grid approach. Data were interpolated with a trend surface model.

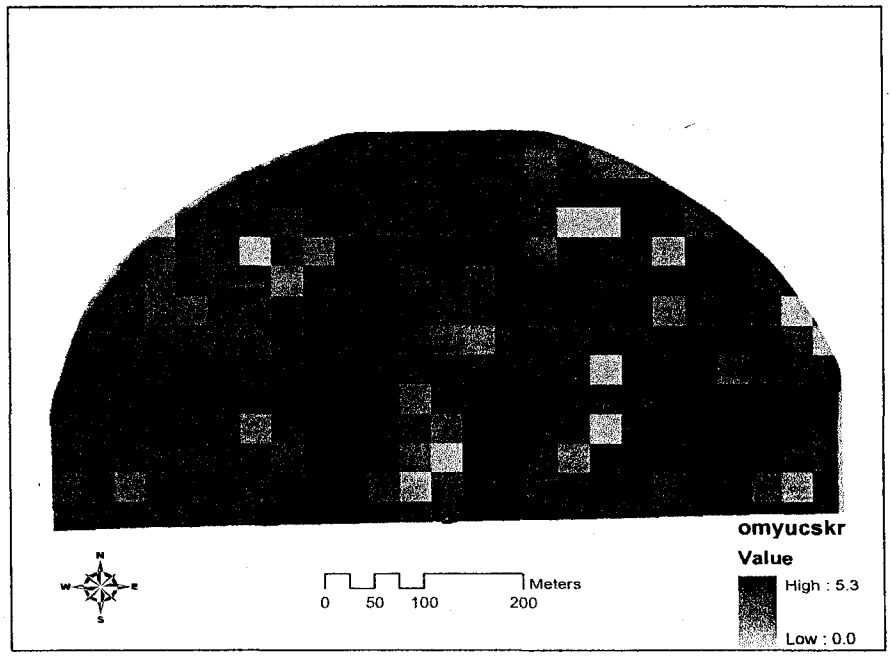

Figure A.16 Distribution of organic matter (OM; %) across Field 1. Soil samples were collected using a cluster approach. Data were first interpolated with a trend surface model; residuals from the trend surface model were modeled using ordinary kriging. Final OM surface was calculated as the sum of trend surface and ordinary kriging surface.

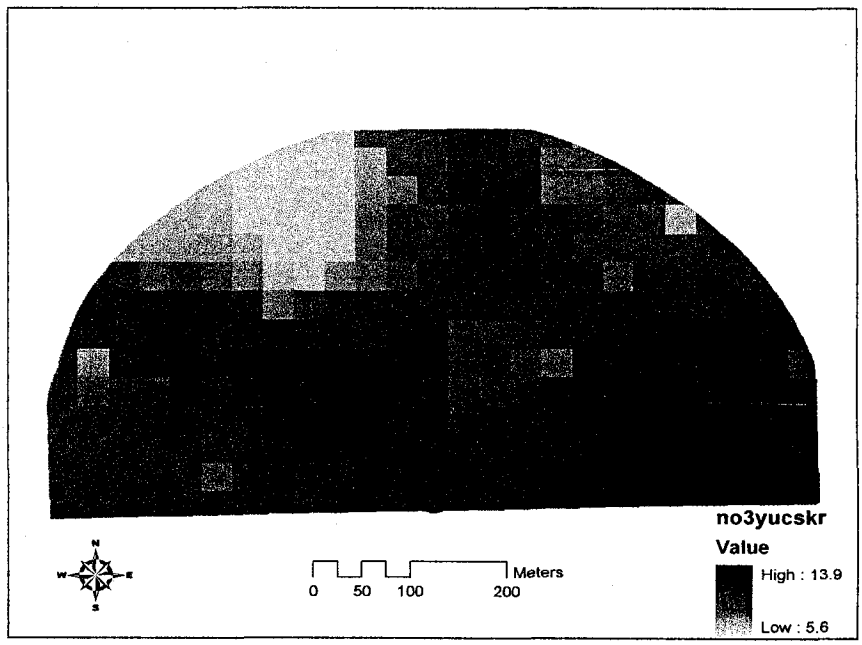

Figure A.17 Distribution of nitrate-N (NO_3-N; mg kg^{-1}) across Field 1. Soil samples were collected using a cluster approach. Data were first interpolated with a trend surface model; residuals from the trend surface model were modeled using ordinary kriging. Final NO_3-N surface was calculated as the sum of trend surface and ordinary kriging surface.

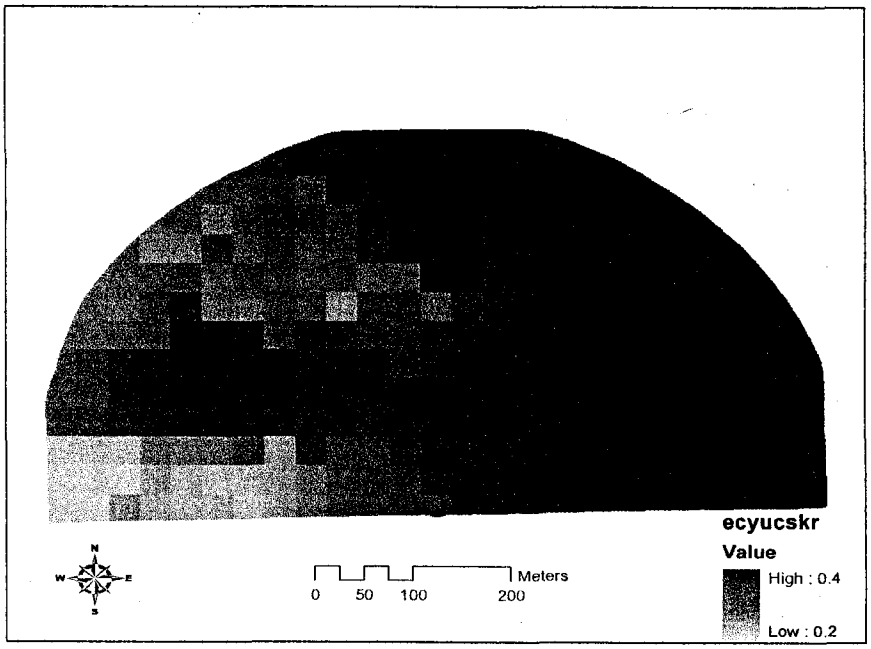

Figure A.18 Distribution of electrical conductivity (EC; mmhos cm^{-1}) across Field 1. Soil samples were collected using a cluster approach. Data were first interpolated with a trend surface model; residuals from the trend surface model were modeled using ordinary kriging. Final EC surface was calculated as the sum of trend surface and ordinary kriging surface.

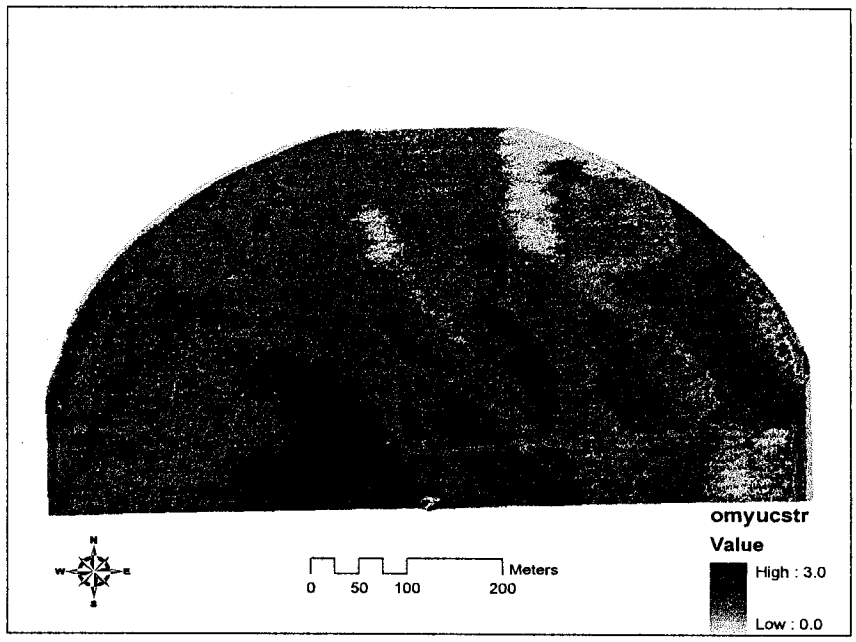

Figure A.19 Distribution of organic matter (OM; %) across Field 1. Soil samples were collected using a cluster approach. Data were first interpolated with a trend surface model; residuals from the trend surface model were modeled using regression tree analysis. Final OM surface was calculated as the sum of trend surface and ordinary kriging surface.

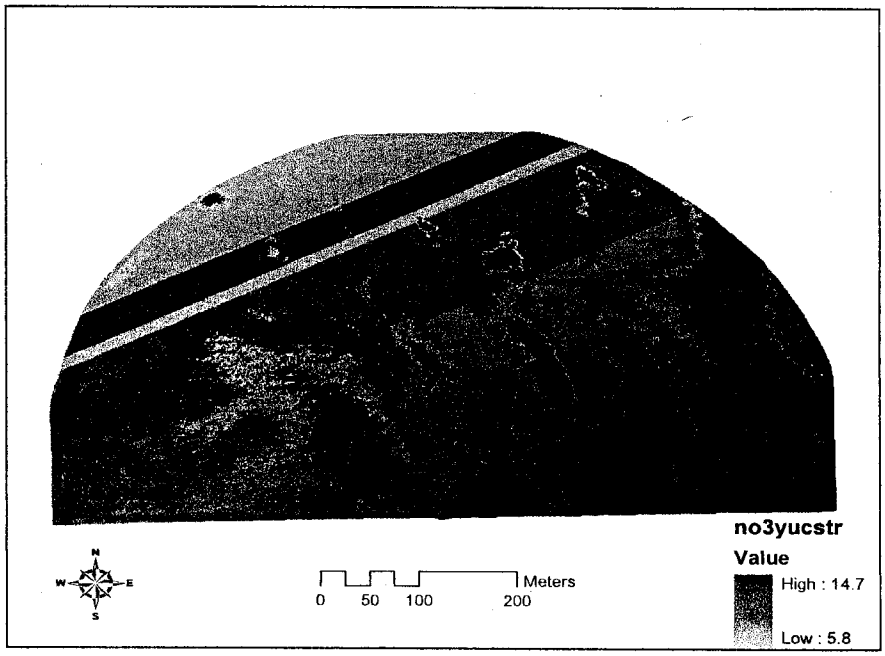

Figure A.20 Distribution of nitrate-N (NO_3-N; mg kg^{-1}) across Field 1. Soil samples were collected using a cluster approach. Data were first interpolated with a trend surface model; residuals from the trend surface model were modeled using regression tree analysis. Final NO_3-N surface was calculated as the sum of trend surface and regression tree surface.

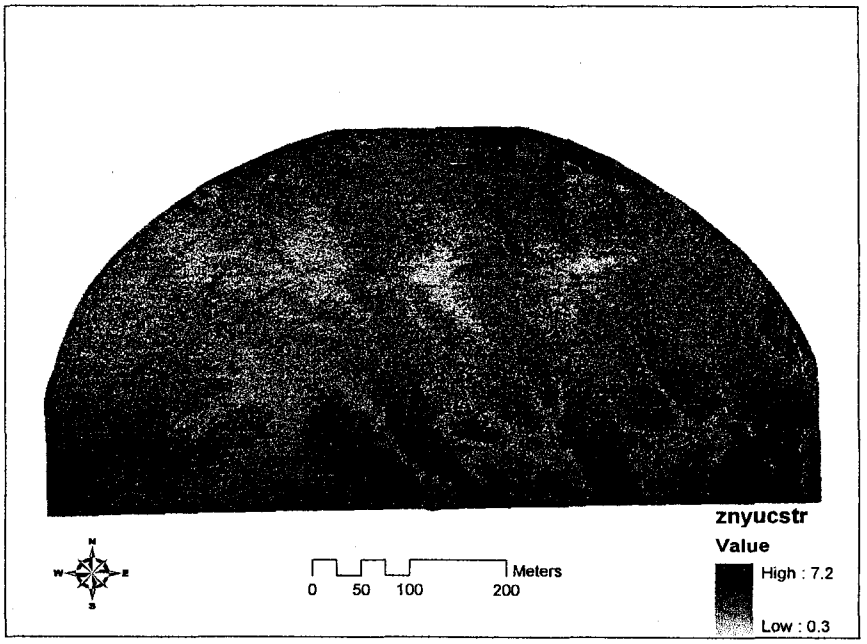

Figure A.21 Distribution of zinc (Zn; mg kg^{-1}) across Field 1. Soil samples were collected using a cluster approach. Data were first interpolated with a trend surface model; residuals from the trend surface model were modeled using regression tree analysis. Final Zn surface was calculated as the sum of trend surface and regression tree surface.

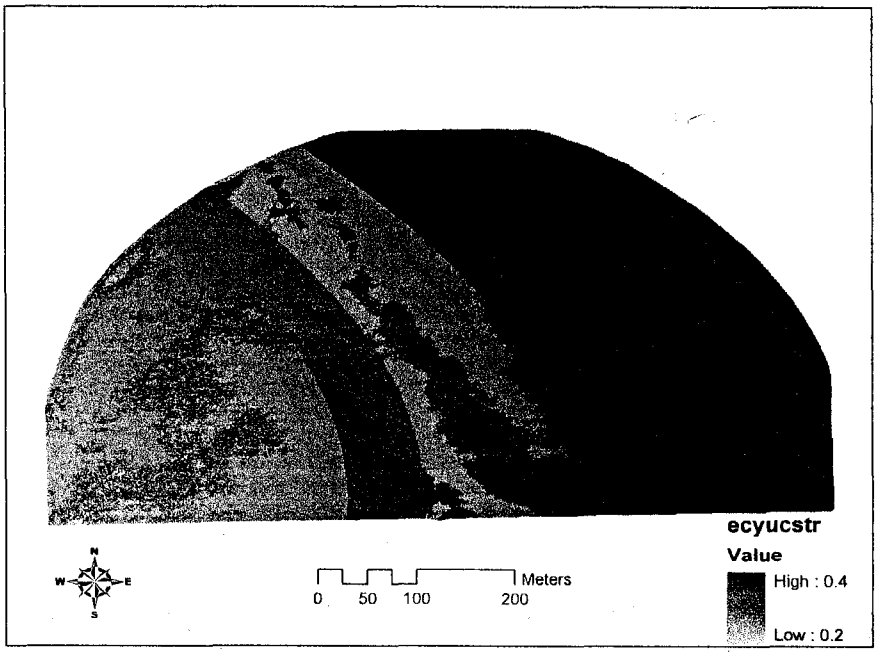

Figure A.22 Distribution of electrical conductivity (EC; mmhos cm^{-1}) across Field 1. Soil samples were collected using a cluster approach. Data were first interpolated with a trend surface model; residuals from the trend surface model were modeled using regression tree analysis.

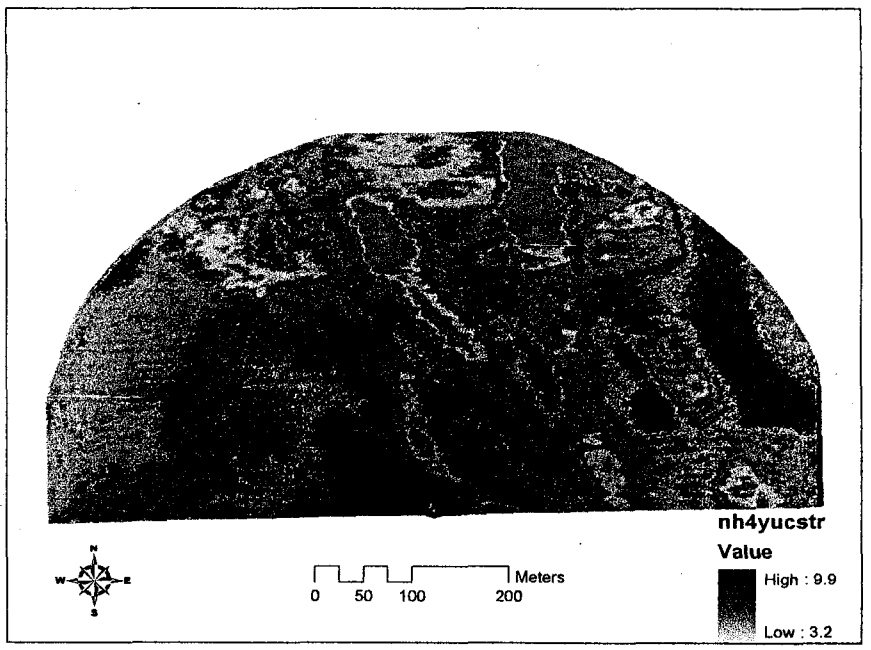

Figure A.23 Distribution of ammonium-N (NH_4-N; mg kg^{-1}) across Field 1. Soil samples were collected using a cluster approach. Data were first interpolated with a trend surface model; residuals from the trend surface model were modeled with regression tree analysis. Final NH_4-N surface was calculated as the sum of trend surface and regression tree surface.

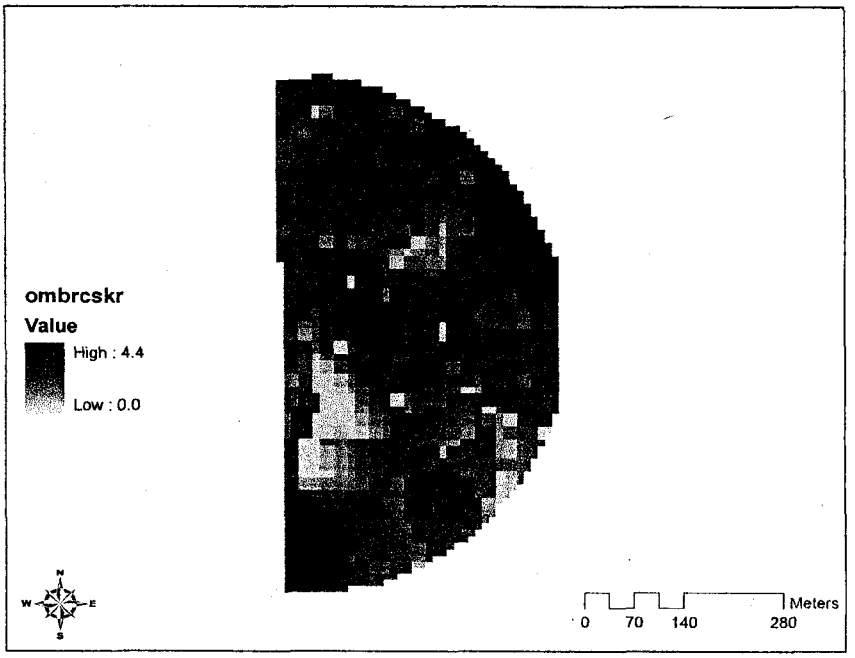

Figure A.24 Distribution of organic matter (OM; %) across Field 2. Soil samples were collected using a cluster approach. Data were first interpolated with a trend surface model; residuals from the trend surface model were modeled using ordinary kriging. Final OM surface was calculated as the sum of trend surface and ordinary kriging surface.

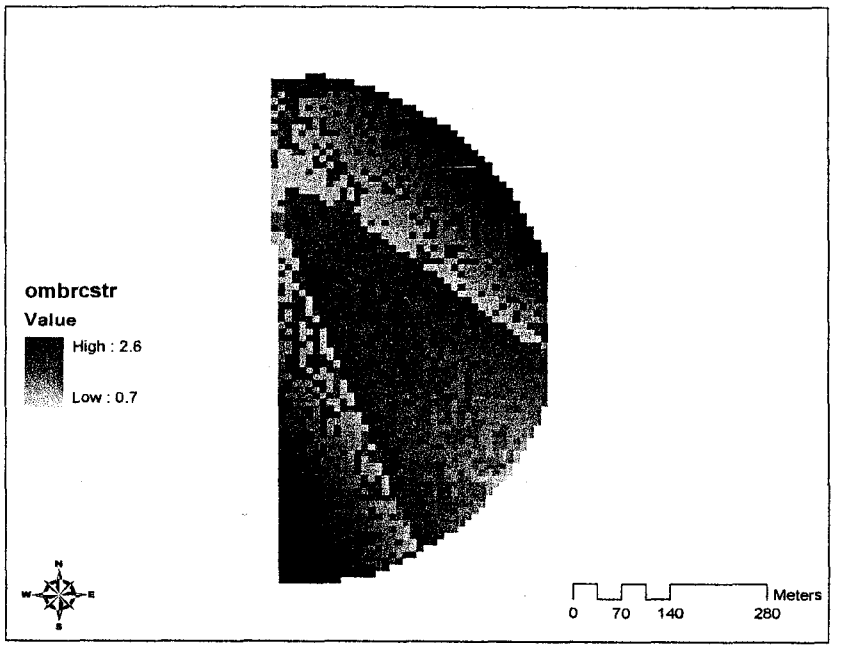

Figure A.25 Distribution of organic matter (OM; %) across Field 2. Soil samples were collected using a cluster approach. Data were first interpolated with a trend surface model; residuals from the trend surface model were modeled using regression tree analysis. Final OM surface was calculated as the sum of trend surface and regression tree surface.

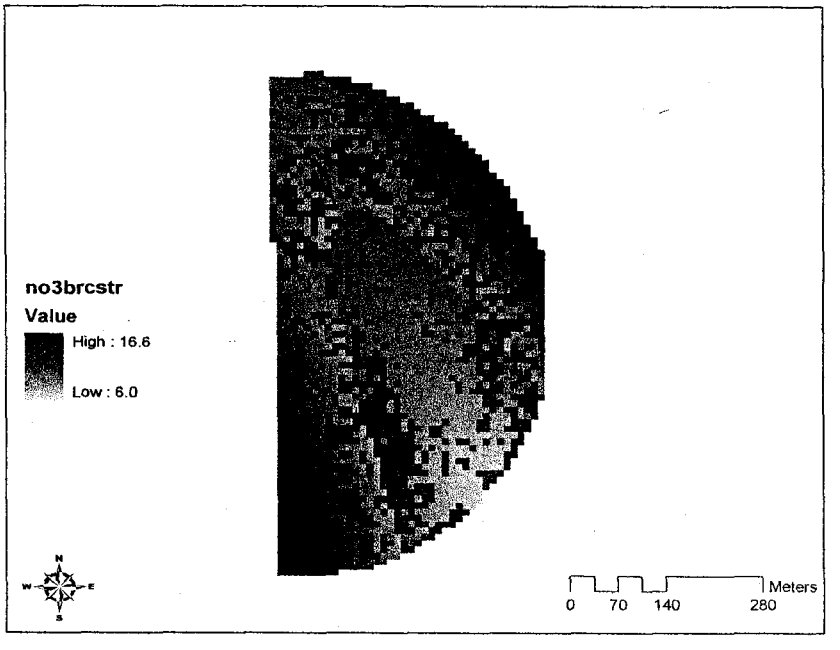

Figure A.26 Distribution of nitrate-N (NO3-N; mg kg-1) across Field 2. Soil samples were collected using a cluster approach. Data were first interpolated with a trend surface model; residuals from the trend surface model were modeled using regression tree analysis. Final NO_3-N surface was calculated as the sum of trend surface and regression tree surface.

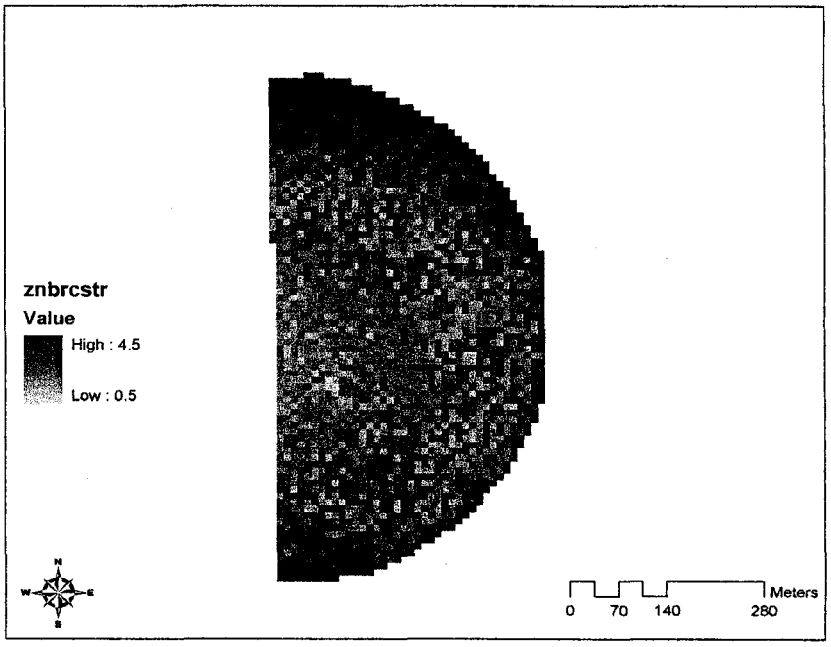

Figure A.27 Distribution of zinc (Zn; mg kg^{-1}) across Field 2. Soil samples were collected using a cluster approach. Data were first interpolated with a trend surface model; residuals from the trend surface model were modeled using regression tree analysis. Final Zn surface was calculated as the sum of trend surface and regression tree surface.

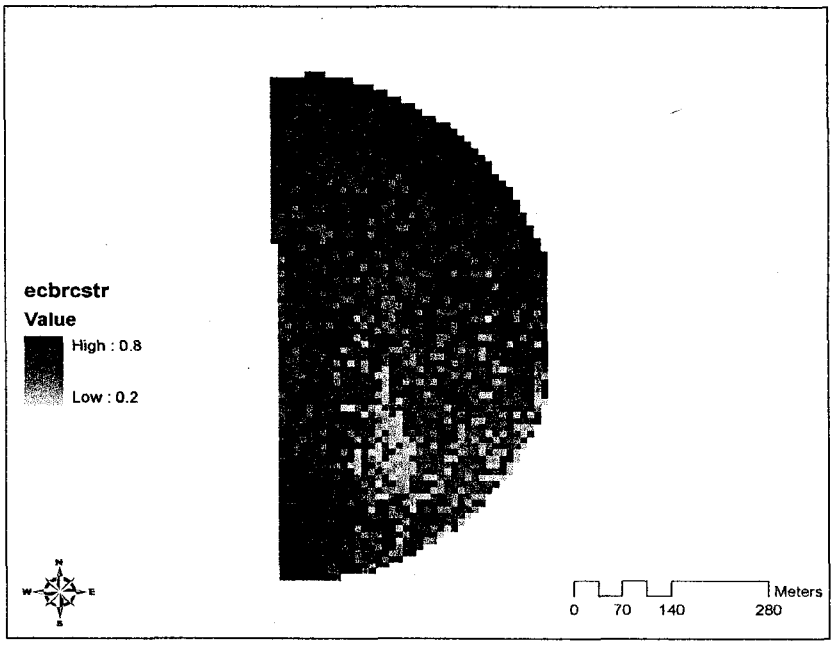

Figure A.28 Distribution of electrical conductivity (EC; mmhos cm^{-1}) across Field 2. Soil samples were collected using a cluster approach. Data were first interpolated with a trend surface model; residuals from the trend surface model were modeled using regression tree analysis. Final EC surface was calculated as the sum of trend surface and regression tree surface.

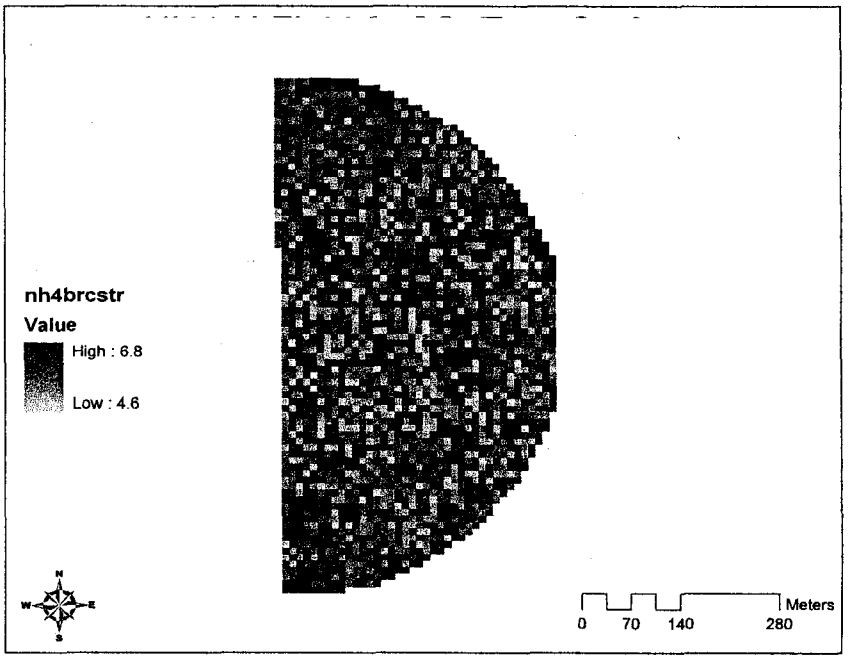

Figure A.29 Distribution of ammonium-N (NH_4-N; mg kg^{-1}) across Field 2. Soil samples were collected using a cluster approach. Data were first interpolated with a trend surface model ; residuals from the trend surface model were modeled using regression tree analysis. Final NH_4-N surface was calculated as the sum of trend surface and regression tree surface.

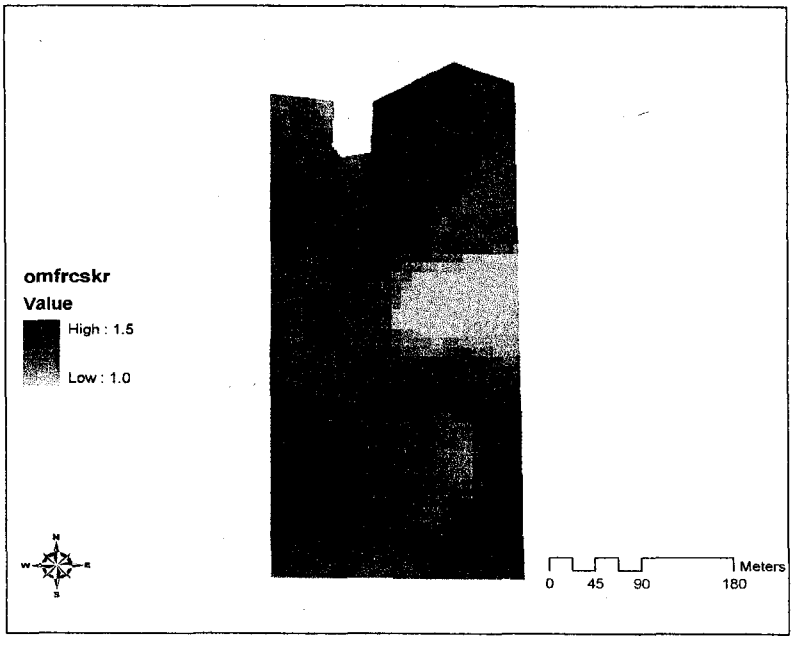

Figure A.30 Distribution of organic matter (OM; %) across Field 3. Soil samples were collected using a cluster approach. Data were first interpolated with a trend surface model; residuals from the trend surface were modeled using ordinary kriging. Final OM surface was calculated as the sum of trend surface and ordinary kriging surface.

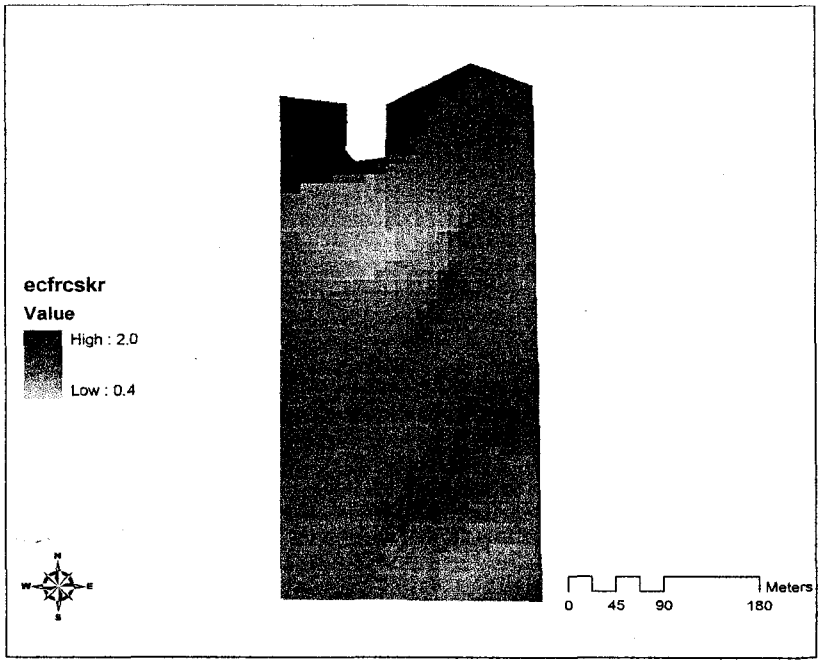

Figure A.31 Distribution of electrical conductivity (EC; mmhos cm^{-1}) across Field 3. Soil samples were collected using a cluster approach. Data were first interpolated with a trend surface model; residuals from the trend surface model were modeled using ordinary kriging. Final EC surface was calculated as the sum of trend surface and ordinary kriging surface.

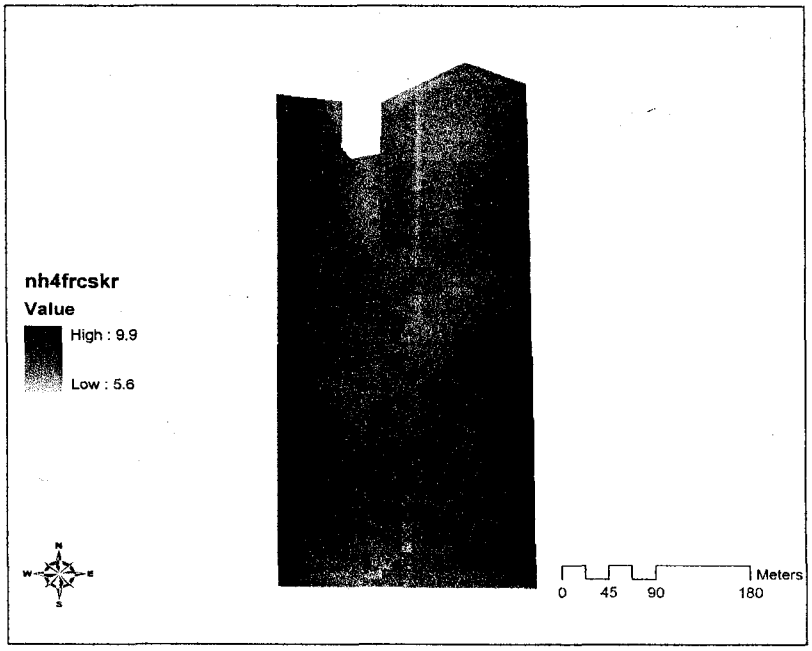

Figure A.32 Distribution of ammonium-N (NH_4-N; mg kg^{-1}) across Field 3. Soil samples were collected using a cluster approach. Data were first interpolated with a trend surface model; residuals from the trend surface model were modeled using ordinary kriging. Final NH_4-N surface was calculated as the sum of trend surface and ordinary kringing surface.

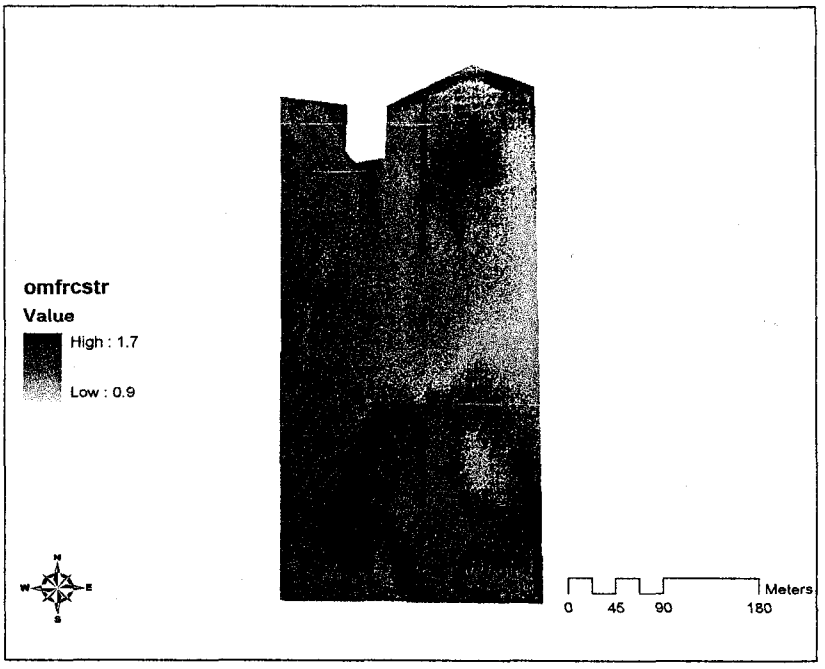

Figure A.33 Distribution of organic matter (OM; %) across Field 3. Soil samples were collected using a cluster approach. Data were first interpolated with a trend surface model; residuals from the trend surface model were modeled using regression tree analysis. Final OM surface was calculated as the sum of trend surface and regression tree surface.

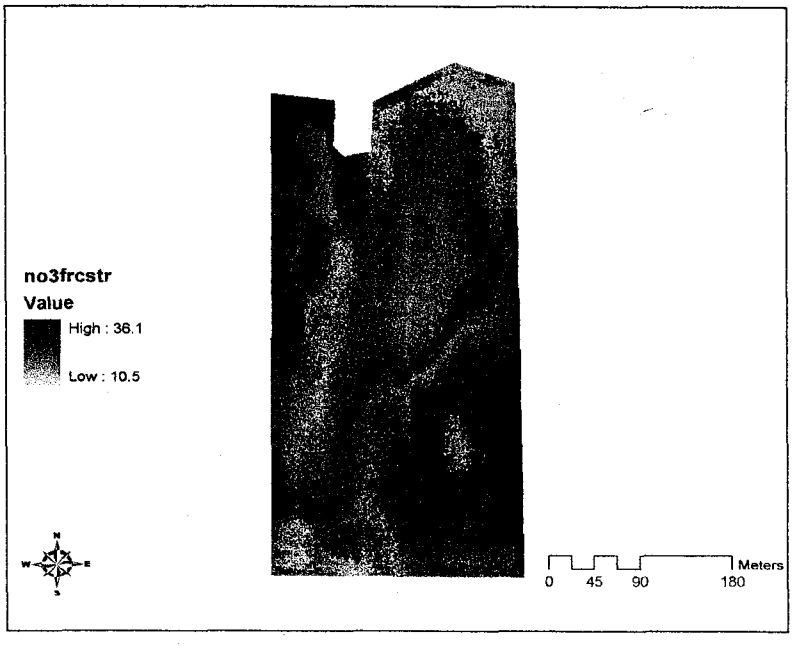

Figure A.34 Distribution of nitrate-N (NO_3-N; mg kg^{-1}) across Field 3. Soil samples were collected using a cluster approach. Data were first interpolated with a trend surface model; residuals from the trend surface model were modeled using regression tree analysis. Final NO_3-N surface was calculated as the sum of trend surface and regression tree surface.

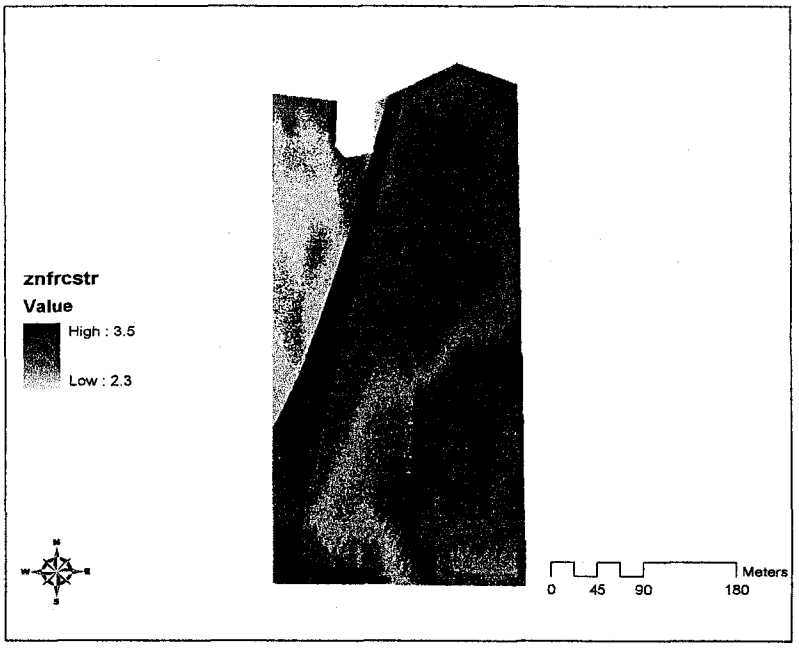

Figure A.35 Distribution of zinc (Zn; mg kg^{-1}) across Field 3. Soil samples were collected using a cluster approach. Data were first interpolated with a trend surface model; residuals from the trend surface model were modeled using regression tree analysis. Final Zn surface was calculated as the sum of trend surface and regression tree surface.

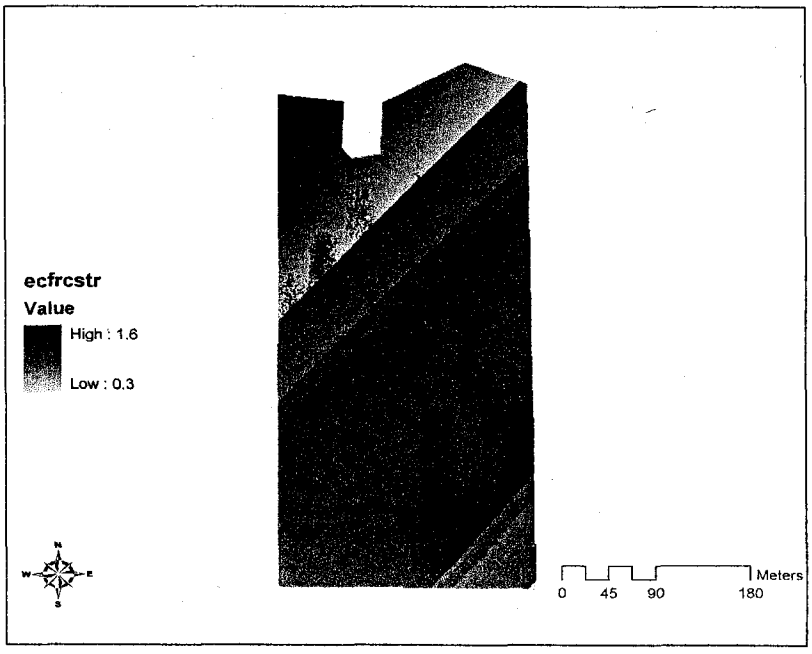

Figure A.36 Distribution of electrical conductivity (EC; mmhos cm^{-1}) across Field 3. Soil samples were collected using a cluster approach. Data were first interpolated with a trend surface model; residuals from the trend surface model were modeled using regression tree analysis. Final EC surface was calculated as the sum of trend surface and regression tree surface.

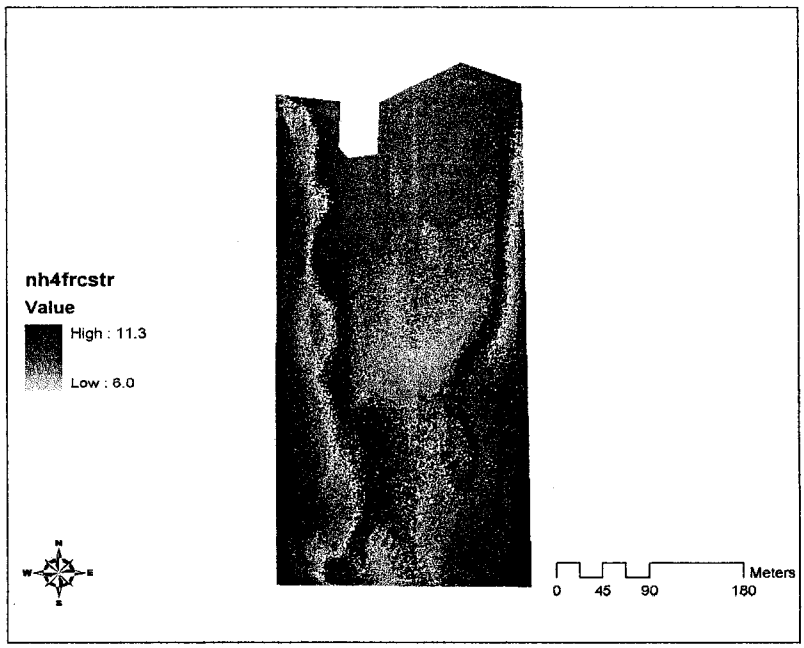

Figure A.37 Distribution of ammonium-N (NH_4-N; mg kg^{-1}) across Field 3. Soil samples were collected using a cluster approach. Data were first interpolated with a trend surface model; residuals from the trend surface model were modeled using regression tree analysis. Final NH_4-N surface was calculated as the sum of trend surface and regression tree surface.

APPENDIX B

Histograms of residual distributions from 10-fold cross-validation procedure.

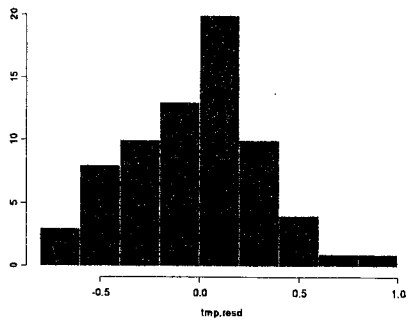

Figure B.1 Histogram of residuals distribution from 10-fold cross-validation procedure for OM trend surface model from Field 1; standard grid approach.

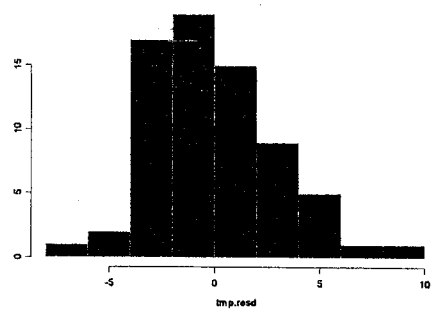

Figure B.2 Histogram of residuals distribution from 10-fold cross-validation procedure for NO_3-N trend surface model from Field 1; standard grid approach.

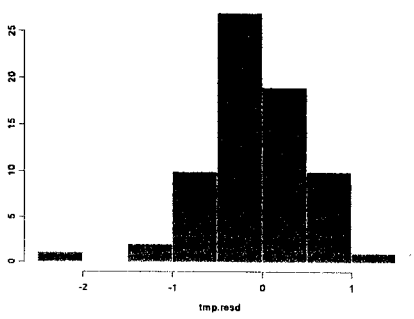

Figure B.3 Histogram of residuals distribution from 10-fold cross-validation procedure for Zn trend surface model from Field 1; standard grid approach.

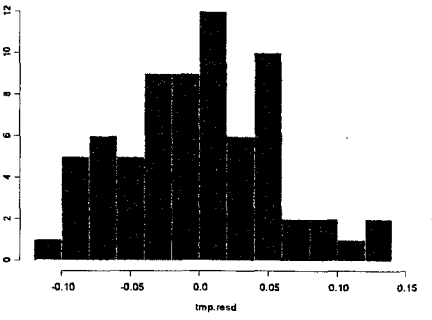

Figure B.4 Histogram of residuals distribution from 10-fold cross-validation procedure for EC trend surface model from Field 1; standard grid approach.

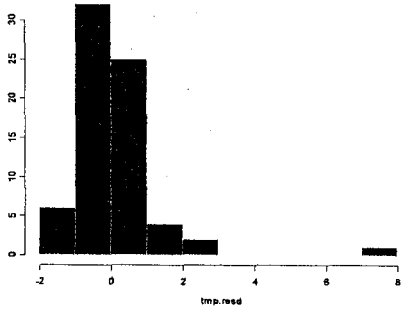

Figure B.5 Histogram of residuals distribution from 10-fold cross-validation procedure for NH_4-N trend surface model from Field 1; standard grid approach.

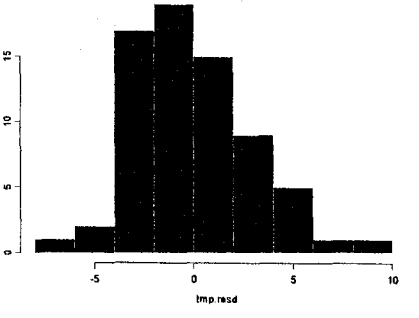

Figure B.6 Histogram of residuals distribution from 10-fold cross-validation procedure for NO_3-N kriging model from Field 2; standard grid approach.

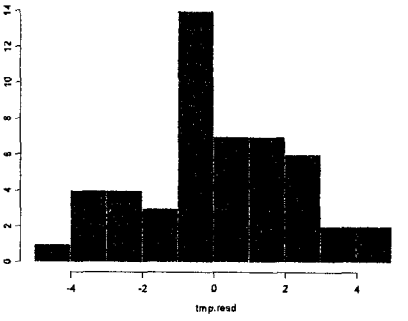

Figure B.7 Histogram of residuals distribution from 10-fold cross-validation procedure for NH_4-N kriging model from Field 2; standard grid approach.

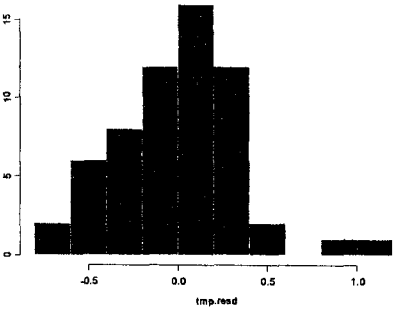

Figure B.8 Histogram of residuals distribution from 10-fold cross-validation procedure for OM trend surface model from Field 2; standard grid approach.

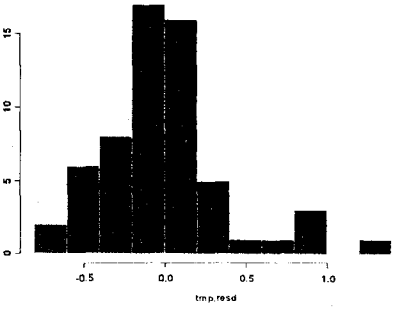

Figure B.9 Histogram of residuals distribution from 10-fold cross-validation procedure for Zn trend surface model from Field 2; standard grid approach.

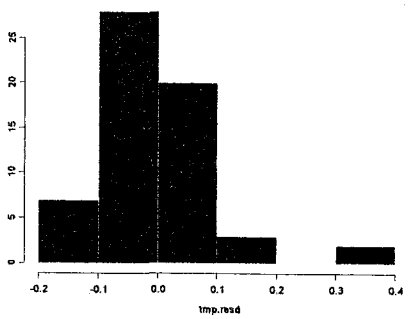

Figure B.10 Histogram of residuals distribution from 10-fold cross-validation procedure for EC trend surface model from Field 2; standard grid approach.

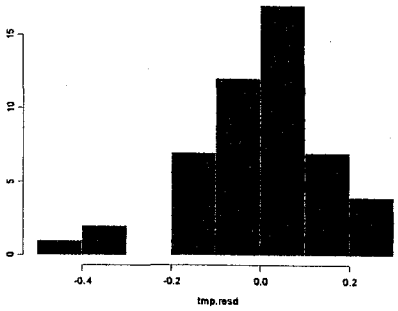

Figure B.11 Histogram of residuals distribution from 10-fold cross-validation procedure for OM trend surface model from Field 3; standard grid approach.

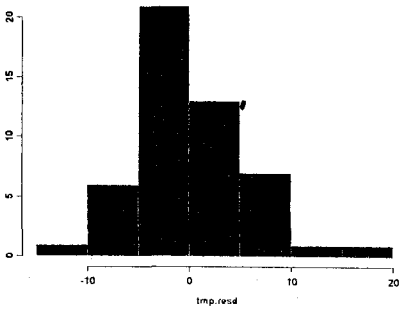

Figure B.12 Histogram of residuals distribution from 10-fold cross-validation procedure for NO_3-N trend surface model from Field 3; standard grid approach.

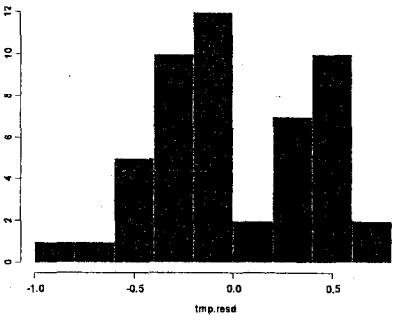

Figure B.13 Histogram of residuals distribution from 10-fold cross-validation procedure for Zn trend surface model from Field 3; standard grid approach.

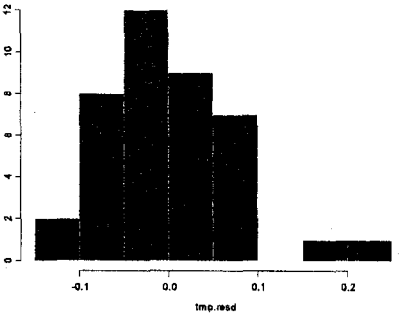

Figure B.14 Histogram of residuals distribution from 10-fold cross-validation procedure for EC trend surface model from Field 3; standard grid approach.

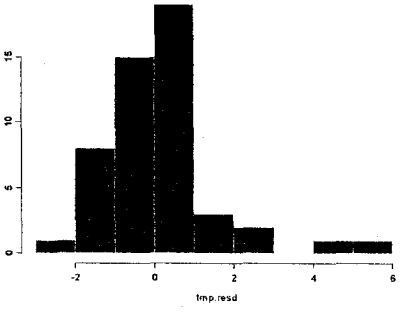

Figure B.15 Histogram of residuals distribution from 10-fold cross-validation procedure for NH_4-N trend surface model from Field 3; standard grid approach.

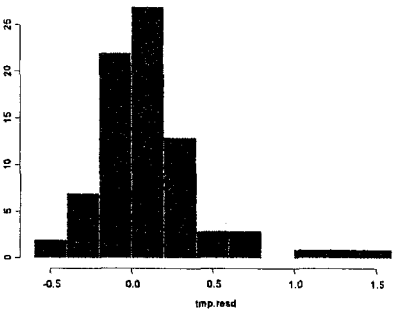

Figure B.16 Histogram of residuals distribution from 10-fold cross-validation procedure for OM kriging model from Field 1; cluster sampling approach.

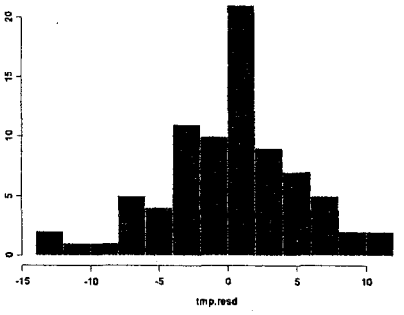

Figure B.17 Histogram of residuals distribution from 10-fold cross-validation procedure for NO_3-N kriging model from Field 1; cluster sampling approach.

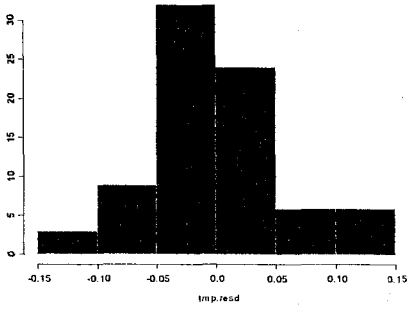

Figure B.18 Histogram of residuals distribution from 10-fold cross-validation procedure for EC kriging model from Field 1; cluster sampling approach.

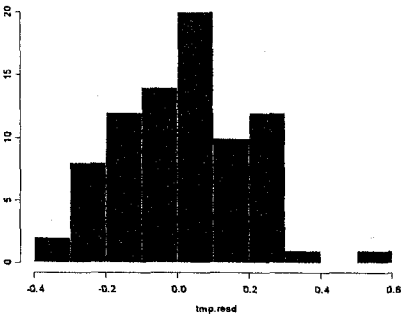

Figure B.19 Histogram of residuals distribution from 10-fold cross-validation procedure for OM regression tree model from Field 1; cluster sampling approach.

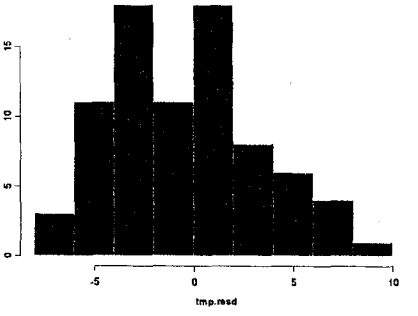

Figure B.20 Histogram of residuals distribution from 10-fold cross-validation procedure for NO_3-N regression tree model from Field 1; cluster sampling approach.

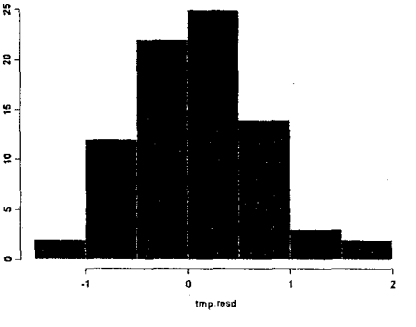

Figure B.21 Histogram of residuals distribution from 10-fold cross-validation procedure for Zn regression tree model from Field 1; cluster sampling approach.

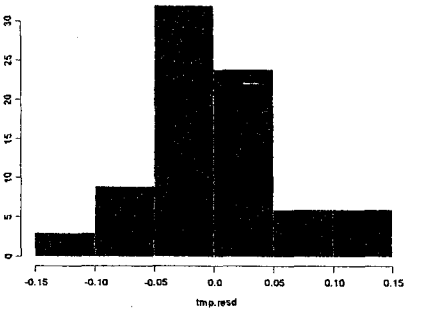

Figure B.22 Histogram of residuals distribution from 10-fold cross-validation procedure for EC regression tree model from Field 1; cluster sampling approach.

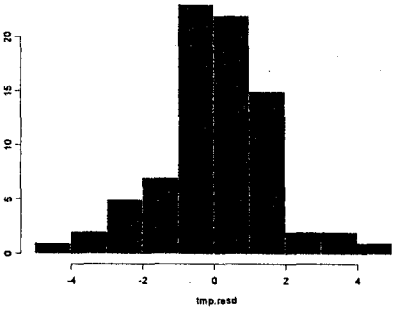

Figure B.23 Histogram of residuals distribution from 10-fold cross-validation procedure for NH_4-N regression tree model from Field 1; cluster sampling approach.

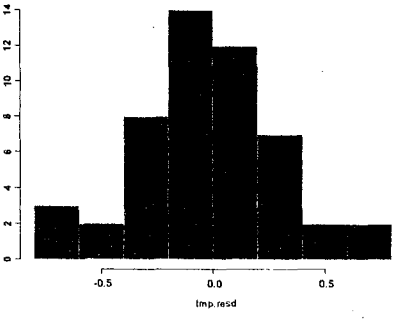

Figure B.24 Histogram of residuals distribution from 10-fold cross-validation procedure for OM kriging model from Field 2; cluster sampling approach.

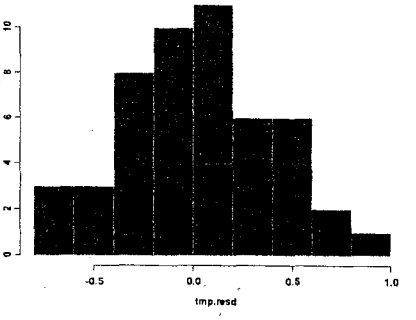

Figure B.25 Histogram of residuals distribution from 10-fold cross-validation procedure for OM regression tree model from Field 2; cluster sampling approach.

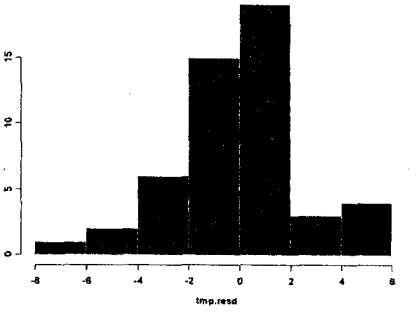

Figure B.26 Histogram of residuals distribution from 10-fold cross-validation procedure for NO_3-N regression tree model from Field 2; cluster sampling approach.

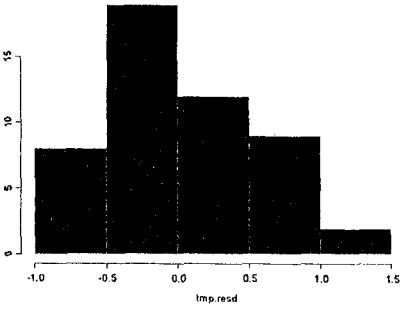

Figure B.27 Histogram of residuals distribution from 10-fold cross-validation procedure for Zn regression tree model from Field 2; cluster sampling approach.

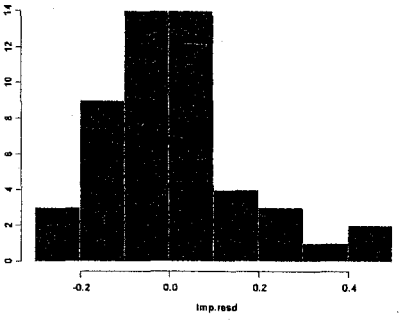

Figure B.28 Histogram of residuals distribution from 10-fold cross-validation procedure for EC regression tree model from Field 2; cluster sampling approach.

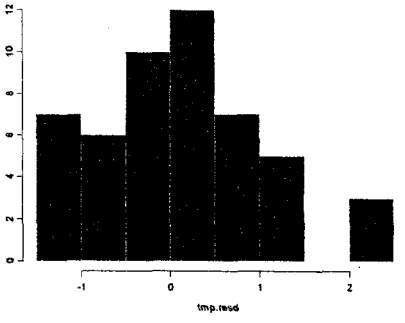

Figure B.29 Histogram of residuals distribution from 10-fold cross-validation procedure for NH_4-N regression tree model from Field 2; cluster sampling approach.

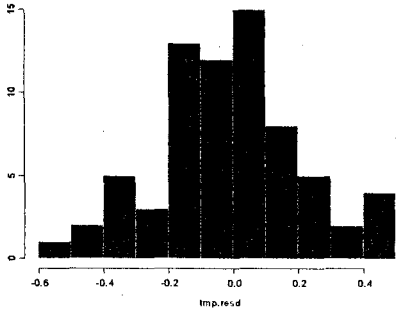

Figure B.30 Histogram of residuals distribution from 10-fold cross-validation procedure for OM kriging model from Field 3; cluster sampling approach.

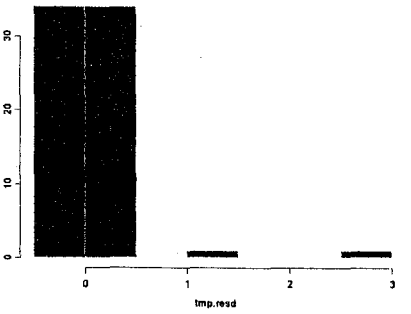

Figure B.31 Histogram of residuals distribution from 10-fold cross-validation procedure for EC kriging model from Field 3; cluster sampling approach.

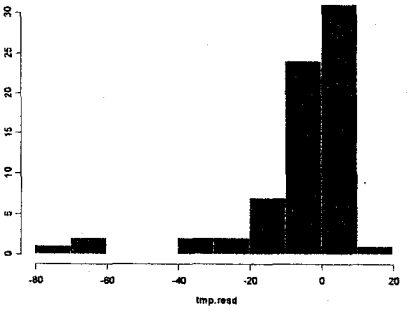

Figure B.32 Histogram of residuals distribution from 10-fold cross-validation procedure for NH_4-N kriging model from Field 3; cluster sampling approach.

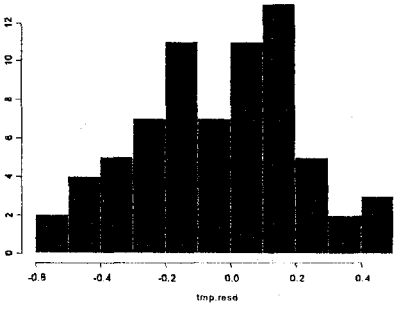

Figure B.33 Histogram of residuals distribution from 10-fold cross-validation procedure for OM regression tree model from Field 3; cluster sampling approach.

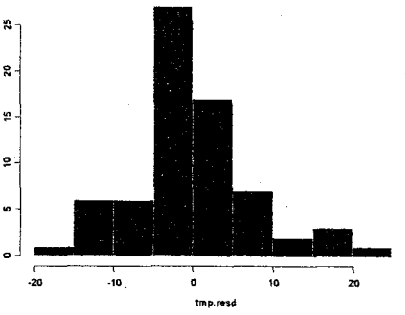

Figure B.34 Histogram of residuals distribution from 10-fold cross-validation procedure for NO_3-N regression tree model from Field 3; cluster sampling approach.

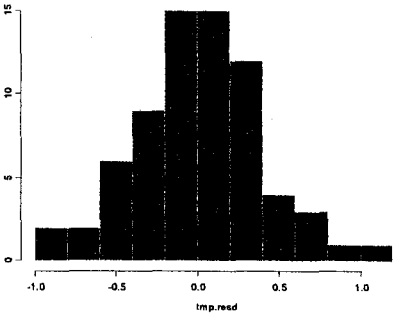

Figure B.35 Histogram of residuals distribution from 10-fold cross-validation procedure for Zn regression tree model from Field 3; cluster sampling approach.

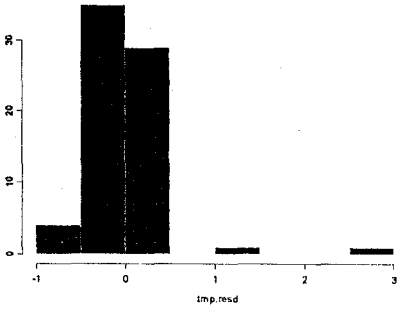

Figure B.36 Histogram of residuals distribution from 10-fold cross-validation procedure for EC regression tree model from Field 3; cluster sampling approach.

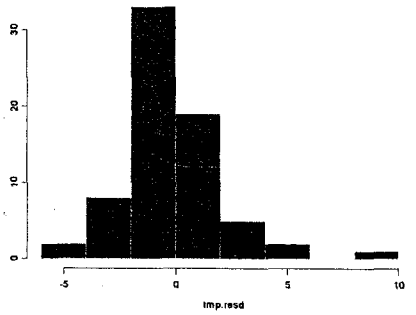

Figure B.37 Histogram of residuals distribution from 10-fold cross-validation procedure for NH4-N regression tree model from Field 3; cluster sampling approach.

APPENDIX C

Details of one-way analysis of variance procedure.

The model under consideration was a completely randomized design (CRD) with one factor (i.e. management zone) and alternative response model of the form:

$$y_{ij} = \mu_i + e_{ij},\ e_{ij} \sim N(0, \sigma^2) \qquad [C.1]$$

where y_{ij} is the response variable (i.e. yield value) for replicate $j=1,2,...,r$ of treatment $i=1,2,...,t$, μ_i is the population mean (cell mean) for treatment i, and e_{ij} is experimental error. The e_{ij} are assumed to have mean 0 and be normally distributed. The measure of variation under the alternative response model is estimated as:

$$SSE_f = \sum_{i=1}^{t}\sum_{j=1}^{r}\left(y_{ij} - \bar{y}_{i\bullet}\right)^2 \qquad [C.2]$$

where SSE_f is the error under the full (i.e. alternative) model and $\bar{y}_{i\bullet}$ is the mean of individuals in the i^{th} treatment. The SSE_f is considered the unexplainable error in the alternative model and has $rt-t$ degrees of freedom. The null response model has the form:

$$y_{ij} = \mu + e_{ij},\ e_{ij} \sim N(0, \sigma^2) \qquad [C.3]$$

where y_{ij} is the response variable (i.e. yield value) for replicate $j=1,2,...,r$ of treatment $i=1,2,...,t$, μ is the population mean common to all treatments, and e_{ij} is experimental error. The e_{ij} are assumed to have mean 0 and be normally distributed. The null hypothesis was that all sample means were equal (i.e. $\bar{y}_1 = \bar{y}_2 = \bar{y}_3$). The measure of variation under the null response model is estimated as:

$$SSE_r = \sum_{i=1}^{t}\sum_{j=1}^{r}\left(y_{ij} - y_{\bullet\bullet}\right)^2 \qquad [C.4]$$

where SSE_r is the error under the reduced (i.e. null) model and $\bar{y}_{\bullet\bullet}$ is the mean of all individuals summed over i and j. The SSE_r is considered the sums of squares total error

and has *rt-1* degrees of freedom. The measure of variation attributable to the imposed treatments is estimated as:

$$SST = \sum_{i=1}^{t}\sum_{j=1}^{r}(\bar{y}_{i\bullet} - \bar{y}_{\bullet\bullet})^2 \qquad [C.5]$$

This partitioning of variation components allows determination of the significance of the imposed experimental design with the *F* statistic. The experimental *F* statistic is calculated as:

$$F = \frac{SST}{t-1}\frac{t(r-1)}{SSE_f} \qquad [C.6]$$

The experimental *F* is compared to ideally distributed *F* values with *t-1* numerator degrees of freedom and *N-t* denominator degrees of freedom at the desired α level, where *N* is the total number of experimental units. Tables of *F* distributions are readily available in most introductory statistics texts. In this study, the *p*-value generated by computer software was used to test the null hypothesis with α level of 0.05. Significant models were considered to have at least one $\neq \bar{y}_t$.